MUNI
FACULTY
OF SCIENCE

Periodic stellar variability among A-F spectral type stars

Marek Skarka

Habilitation thesis

2026

MUNI

Abstract

This Habilitation thesis is a compilation of my most distinct publications regarding stellar variability among stars with temperatures between 6500 and 10000 K. The goal of all these efforts has been to identify common features and correlations between the observational characteristics of variable stars, improve their classification, and reveal the underlying causes of their behaviour. A better understanding of stellar pulsations, processes in stellar atmospheres, and stellar multiplicity is essential because it impacts many applications of variable stars in astrophysics, for example, distance determination. The thesis comprises my research on main-sequence, as well as on horizontal-branch stars, represented by seven first- and one second-author papers. Apart from that, I have participated in general studies dedicated to stellar variability, research focused on exoplanets, instrumentation and collaboration with citizen astronomers. According to the NASA ADS database, my efforts have resulted in the publication of 152 papers and conference proceedings (38 of them as the first author) with almost 1800 citations (without self-citations). Only about two-thirds of these are listed in WoS and/or SCOPUS databases.

The thesis begins with a brief introduction and is followed by my investigations of large samples of RR Lyrae stars in the Galactic bulge and the Galactic field to study the modulation (the Blazhko effect) and binarity of these old, radially pulsating stars. We discovered a gap in the modulation-period distribution at around 1000 days, which we named the Blazhko valley. We sorted Blazhko stars into six groups, considering the shapes of their modulation envelopes, and showed that there are basically no differences between Blazhko and non-Blazhko stars. On the example of Z CVn, we showed that spectroscopic confirmation of binary candidates with an RR Lyr component is an absolute necessity. The third chapter of the thesis is dedicated to chemically peculiar (CP) stars in binary systems. We studied a tight binary system HD 99458 that may contain the first magnetic CP star which pulsates as a δ Sct pulsator. Magnetism, δ Sct pulsations and binarity are not expected to work together in such configuration. The other presented system is 50 Dra, which consists of two slowly-rotating metallic chemically peculiar components that most likely show high-order g-mode oscillations. In the fourth chapter of the thesis, I present my results on stellar variability classification based on *TESS* space-mission data, where I thoroughly discuss shortcomings in classification and reveal substantial discrepancies between classification in various catalogues. I conclude and provide future prospects in the last chapter.

List of included papers

1. **SKARKA, M.*(corresponding author)***, J. LISKA, R. F. AUER, Z. PRUDIL, A. JURANOVA and A. SODOR. The SERMON project: 48 new field Blazhko stars and an investigation of modulation-period distribution. Astronomy&Astrophysics [online]. 2016, 592(Article A144). ISSN 1432-0746. Available at: doi:10.1051/0004-6361/201628855

   I managed the team, developed the methodology, taught others how to analyse data, partly performed the analysis, prepared figures and wrote most of the paper.

2. PRUDIL, Z. and **M. SKARKA**. "Blazhko effect in the Galactic bulge fundamental mode RR Lyrae stars - I. Incidence rate and differences between modulated and non-modulated stars". Monthly Notices of the Royal Astronomical Society [online]. 2017, 466(3), 2602–2613. ISSN 1365-2966. Available at: doi:10.1093/mnras/stw3231

   Paper with a MSc student. I developed methodology, supervised analysis, and partially interpreted the results. The work on the paper writing and preparation of figures was shared equally between the authors.

3. **SKARKA, M.*(corresponding author)***, J. LISKA, R. DREVENY, E. GUGGENBERGER, A. SODOR, T. G. BARNES and K. KOLENBERG. "A cautionary tale of interpreting O-C diagrams: period instability in a classical RR Lyr Star Z CVn mimicking as a distant companion". Monthly Notices of the Royal Astronomical Society [online]. 2018, 474(1), 824–837. ISSN 1365-2966. Available at: doi:10.1093/mnras/stx2737

   I managed the team and observations, developed methodology, analysed photometric data and the Blazhko effect, calculated a Bondi-Hoyle-Lyttleton accretion, produced most of the figures and wrote most of the paper.

4. **SKARKA, M.*(corresponding author)***, P. KABATH, E. PAUNZEN, M. FEDURCO, J. BUDAJ, D. DUPKALA, J. KRTICKA, A. HATZES, T. PRIBULLA, S. PARIMUCHA, Z. MIKULASEK, E. GUENTHER, S. SABOTTA, M. BLAZEK, J. DVORAKOVA, L. HAMBALEK, T. KLOCOVA, V. KOLLAR, E. KUNDRA, M. SLECHTA and M. VANKO. "HD 99458: First time ever Ap-type star as a S Scuti pulsator in a short period eclipsing binary?". Monthly Notices of the Royal Astronomical Society [online]. 2019, 487(3), 4230–4237. ISSN 1365-2966. Available at: doi:10.1093/mnras/stz1478

   I managed the team and observations, reduced spectroscopic data, wrote most of the paper, and produced the majority of the figures.

5. **SKARKA, M.*(corresponding author)***, Z. PRUDIL and J. JURCSIK. "Blazhko effect in the Galactic bulge fundamental mode RR Lyrae stars - II. Modulation shapes, amplitudes, and periods". Monthly Notices of the Royal Astronomical Society [online]. 2020, 494(1), 1237–1249. ISSN 1365-2966. Available at: doi:10.1093/mnras/staa673

   I managed the team, performed most of the analysis and interpretation, wrote most of the paper and produced most of the figures.

6. **SKARKA, M.*(corresponding author)***, J. ZAK, M. FEDURCO, E. PAUNZEN, Z. HENZL, M. MASEK, R. KARJALAINEN, J. P. Sanchez ARIAS, A. SODOR, R. F. AUER, P. KABATH, M. KARJALAINEN, J. LISKA and D. STEGNER. "Periodic variable A-F spectral type stars in the northern TESS continuous viewing zone I. Identification and classification". Astronomy&Astrophysics [online]. 2022, 666(Article A142). ISSN 1432-0746. Available at: doi:10.1051/0004-6361/202244037

   I managed the team, developed methodology, downloaded and prepared data, reduced and analysed spectroscopic observations, supervised and participated in the classification, prepared figures and wrote most of the paper.

7. **SKARKA, M.*(corresponding author)*** and Z. HENZL. "Periodic variable A-F spectral type stars in the southern TESS continuous viewing zone". Astronomy&Astrophysics [online]. 2024, 688(Article A25). ISSN 1432-0746. Available at: doi:10.1051/0004-6361/202450711

   I performed the vast majority of all necessary work on the paper including data preparation, analysis, interpretation of the results and manuscript writing.

8. **SKARKA, M.*(corresponding author)***, J. LIPTAK, E. NIEMCZURA, Z. MIKULASEK, M. CABEZAS, M. VITKOVA, R. KARJALAINEN and P. KABATH. "50 Dra: Am-type twins with additional variability in a non-eclipsing system". Astronomy&Astrophysics [online]. 2025, 698(Article A48). ISSN 1432-0746. Available at: doi:10.1051/0004-6361/202452341

   I managed the team and observations, reduced the spectroscopic observations, downloaded, prepared, and partially analysed the photometric observations, analysed circularisation of the orbit and synchronisation of the rotation. Further, I interpreted the results, wrote the majority of the paper, and produced most of the figures.

Acknowledgements

I cannot express my gratitude to my wife, Helena, who has strongly supported and accompanied me on my astronomical journey. Thank you, my beloved! I would not be where I am without my teachers and advisors, colleagues, students and friends. First, I would like to thank Zdeněk Mikulášek, my former teacher and mentor, for many fruitful discussions we have had over the years about stellar variability. I thank Jiří Liška, with whom I began my scientific journey and started exploring the secrets of scientific investigation, for his brilliant ideas, support, and enthusiasm. Special thanks go to Ádam Sódor, my advising colleague during my postdoc stay at Konkoly Observatory in Budapest, from whom I learned a lot about space data and spectra reduction. Further, I am grateful to Petr Kabáth, one of the most inspiring men I have ever met. He has provided me with a significantly different view of how scientific work can be done, revealed to me that everything is possible and opened many doors to me. I also thank my former students, Zdeněk Prudil, Jiří Žák and Ema Šipková for their open minds and for giving me the chance to help them grow. Thank you, my Czech and foreign colleagues and collaborators, all my students and citizen observers for sharing your curiosity and enthusiasm, which helped me to become a better investigator. I would also like to express my gratitude to Marie Novosadová Šípková, Jana Nguyen Baluchová and Michaela Švestková for their help in preparing the necessary documents for the habilitation. Thank you all and many others whom I have not mentioned!

Hereby, I certify that the thesis was fully prepared by me, without any help from AI, except for grammar corrections by the free version of Grammarly. The text fully reflects my personal knowledge, language and stylistic skills.

In Ondřejov, January 20, 2026

Contents

CHAPTER 1

Introduction

Stars evolve and experience many physical processes that make them vary in brightness on timescales observable by humans. Such stars, which often also change their spectral characteristics, are called variable stars, or shortly variables. Since the variations reflect real physical processes, variables represent unique objects that help us better understand stars, their atmospheres and interiors, and indirectly the whole Universe (for example, formation history of galaxies, distances using standard candles, etc.). This Habilitation thesis is a compilation of my studies focused on observational aspects of periodic A-F spectral type variable stars, particularly, research of long-term (quasi)periodic variations, chemical peculiarity and classification of these objects. As such, the thesis reflects my scientific development since my PhD, and evolution from highly specialised phenomena in RR Lyrae stars (RRLs) to general questions connected with the origin of the variations and their classification.

I start with RRLs, one of the most important classes of variables that comprises hundreds of thousands of catalogised examples (Watson et al., 2006; Gaia Collaboration et al., 2019). These old, helium-core-burning pulsating stars with characteristic fast rise and slow decay of brightness obey period-luminosity-metallicity relations and serve as important distance indicators (e.g., Drake et al., 2013; Ngeow et al., 2022). They help us map and investigate the evolutionary past of the Milky Way Galaxy (e.g. Kunder et al., 2025; Prudil et al., 2025), understand the late stellar evolutionary phases, and mass loss on the red-giant branch that precedes the horizontal-branch evolution (e.g. Caloi & D'Antona, 2008; Tailo et al., 2025).

In Chapter 2, I elaborate on our findings of RRLs with the light curve modulation known as the Blazhko effect (papers 1, 2, and 5 from the list of publications, Skarka et al., 2016; Prudil & Skarka, 2017; Skarka et al., 2020) and discuss the long-term period variations originally assumed to be connected with binarity. This issue is demonstrated on an RRL star Z CVn (publication 3 from the list of included papers, Skarka et al., 2018). Our investigation on statistically large samples of RRLs revealed correlations in modulation periods, modulation shapes and amplitudes. In the case of Z CVn, we showed that the long-term cyclic pulsation-period variations usually considered as a consequence of binarity (e.g. Liška et al., 2016; Hajdu et al., 2021) might be wrong, at least in some RRLs.

In contrast to Z CVn, main-sequence stars HD 99458 and 50 Dra are in binary systems for sure. Stars in both systems show peculiar chemical composition, classifying them as chemically peculiar (CP) stars. For some reason, the presence of stars in tight binary systems prevents strong magnetic fields from appearing. Thus, the existence of magnetic CP stars (mCP, alternatively Ap stars) in tight binary systems is still a matter of debate, and only a few candidates have been identified (Paunzen, 2020). On the other hand, binarity is one of the important conditions allowing chemical peculiarity of the metallic-type stars (Am stars). HD 99458 was identified as one of the very few candidates of an Ap star in a short-period binary system (paper 4 from the list of publications Skarka et al., 2019). The star 50 Dra (paper 8 from the list of publications Skarka et al., 2025) shows very interesting additional variability that is difficult to explain. Both systems are discussed in Chapter 3.

Both stars mentioned in the previous paragraph show a combination of variability that would be detectable from the ground with a great difficulty. With the advent of space missions, such as *CoRoT* (Auvergne et al., 2009), *Kepler* (Borucki et al., 2010) and *TESS* (Ricker et al.,

2015), and their enhanced precision, effects in the mmag regime become significant. Thus, space missions triggered the need to explain various phenomena under various, previously unexpected and undetected, physical conditions. In addition, ultra-precise space observations have shown the need for a better-defined multi-parametric classification, which is rapidly evolving with the evolution of machine learning methods. In Chapter 4, we discuss manual classification of thousands of bright stars observed by the space mission *TESS* which is based on results in papers 6 and 7 from the list of publications (Skarka et al., 2022; Skarka & Henzl, 2024). We revealed serious issues in the classification of variable stars when using space data and demonstrated how poor the classification can be when using low-quality ground-based data.

CHAPTER 2

Period changes and other variations in RR Lyrae stars

As mentioned in Chapter 1, RRL stars are considered old ($> 10\,\mathrm{Gyr}$) and evolved horizontal branch stars that fuse helium in their cores (Catelan & Smith, 2015). The main source of their light variations is radial stellar pulsations generated by variations in opacity – the κ mechanism (Eddington, 1926). RRLs show three basic types of period variations that differ in nature and time scales. First, very slow evolutionary period changes in both directions appear due to changes in the internal structure of stars (typically in the order of about $\pm 0.1\,\mathrm{d\,Myr^{-1}}$, e.g., Lee, 1991; Le Borgne et al., 2007). Second, quasi-periodic variations in the order of days to decades, that are induced by dynamical effects connected with pulsations, are observed in a large portion of RRLs (the Blazhko effect, Blažko, 1907; Jurcsik et al., 2009; Smolec, 2016; Molnár et al., 2022). The third type of period variations observed in RRLs is strictly periodic with cycle periods in the order of years or decades (Liška et al., 2016; Prudil et al., 2019; Hajdu et al., 2021). These variations are assumed to be connected with binarity. However, in some cases they might be caused by an unknown phenomenon intrinsic to the stars that is likely connected with pulsations and evolution of the stars (see Skarka et al., 2018, and Sect.2.2). In addition to these three types of period variations, some stars were reported to show erratic period changes likely connected with evolutionary instabilities (e.g., Le Borgne et al., 2007).

2.1 Blazhko effect in RR Lyrae stars

Already a few years after the discovery of RRLs, Blažko (1907) noticed regular period instability of RW Dra, while Shapley (1916) reported pulsation period and amplitude variations of RR Lyrae itself. The nature of these amplitude and period/phase modulations, which we call the Blazhko effect[1] now, has not been fully explained yet. This effect is common among RRLs, and it affects the mean luminosity (Jurcsik, 2019). Since RRLs serve as distance indicators, it is important to understand the background of this phenomenon. In addition to RRLs, modulation similar to the Blazhko effect also appears among other pulsators, for example, Cepheids (e.g. Molnár & Szabados, 2014; Smolec, 2017; Rathour et al., 2021).

A huge progress in the Blazhko effect investigation has been made in the last 15 years, mainly due to the advent of space missions *Kepler* (Borucki et al., 2010) and *TESS*, and ground-based surveys such as OGLE (Udalski et al., 1992; Soszyński et al., 2014). Long-term monitoring and precise observations are crucial because the manifestations of the Blazhko effect become more apparent in long-time-span and high-quality data sets. The light curves of Blazhko RRLs show a typical modulation pattern. An example is shown in the top and bottom left panels of Fig. 2.1.

The brightness variations in amplitude are always accompanied by period/phase and mean-magnitude variations (e.g., Szeidl et al., 2012). The modulation is not always apparent visually from the light curve. However, it can be efficiently detected in Fourier spectra from the presence

[1] Kurtz (2022) suggests to call the modulation Tseraskaya–Blazhko effect since it was Lidiya Petrovna Tseraskaya who actually first noticed the variations in RW Dra.

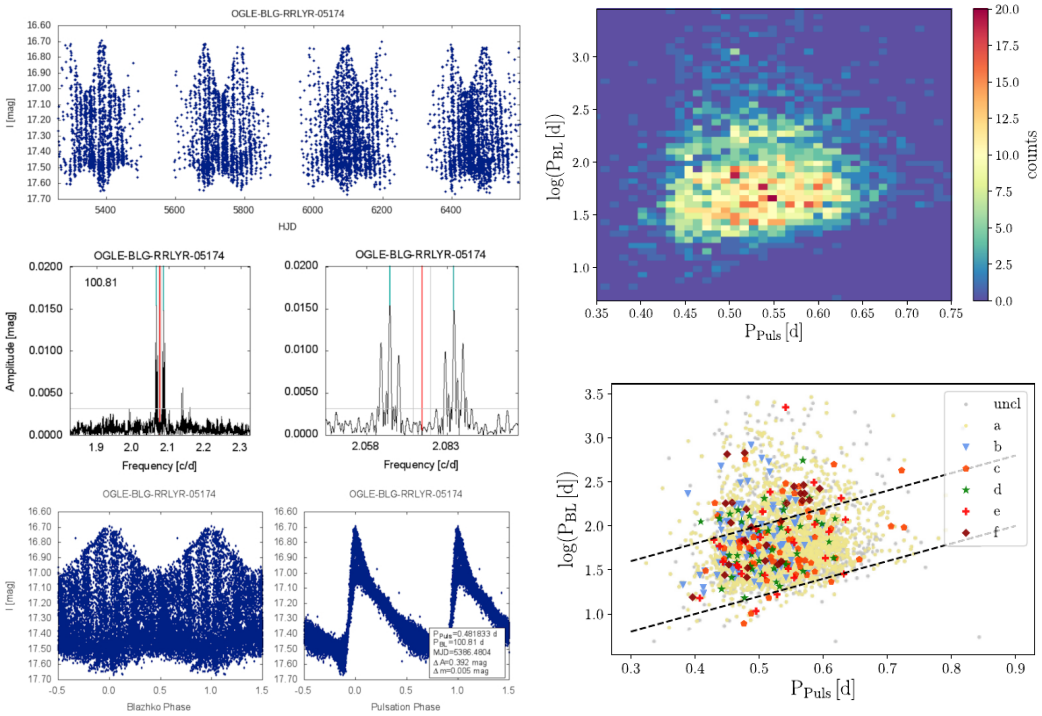

Figure 2.1: *left panels:* Example of a star that shows the Blazhko effect. The top panel shows the light curve (magnitude versus Julian date), while the bottom panels show data phase-folded with the modulation frequency (left) and pulsation frequency (right). The middle panels show the frequency spectra close to the pulsation frequency (the red vertical line) with the equidistant peaks (cyan lines) produced by modulation. *right panels:* Blazhko period versus the pulsation period as a density map (top panel) and a classical plot (bottom panel) with different modulation types shown. Figures from Skarka et al. (2020).

of a characteristic equidistant pattern close to the main pulsation frequency f_0 and its harmonics kf_0 (k being an integer number) that are products of the modulation (Benkő et al., 2011; Szeidl et al., 2012). The frequency difference between the peaks in this pattern is equal to the modulation frequency f_m.

In 2015, we established the SERMON project (SEarch for Rr Lyrae stars with MOdulatioN, Skarka et al., 2016, publication 1 from the list of publications) in cooperation with students and enthusiastic citizen astronomers, to search for modulated stars in survey data and describe their characteristics on a statistical basis. Additionally, a master project dedicated to RRL stars in the Galactic bulge under my supervision started in the same year (student Zdeněk Prudil). We manually searched for modulated fundamental mode RR Lyrae stars (RRab) by investigating frequency spectra and light curves from the ASAS (1234 Galactic field stars, Skarka et al., 2016) and OGLE survey data (8282 Galactic bulge stars Prudil & Skarka, 2017, publication 2 from the list of publications).

In Skarka et al. (2016), we identified 87 Blazhko stars, of which 48 were new detections. Back in 2016, the new identifications constituted almost 20 % of all known Blazhko stars from the Galactic field. The detected portion of modulated stars in the ASAS data was 12 %, which was about two times higher than that detected by Szczygieł & Fabrycky (2007), who used semi-automated routines applied to the ASAS data. Our approach demonstrated the efficiency of individual manual investigation. However, the detection efficiency depends on data quality, sampling and time span of the data. We showed that modulation with periods as long as two-thirds of the time span of the data can be reliably detected.

In the Galactic bulge stars, the percentage of Blazhko stars was at least 40.3 %. We identified

3341 Blazhko stars[2] out of 8282 investigated fundamental-mode RRLs (RRab) (Prudil & Skarka, 2017, publication 2 from the list of included papers). The actual percentage remains a matter of debate. Kovacs (2018) identified modulation in 91 % of stars from the *K2* mission, while Molnár et al. (2022) found that up to 72 % of RRab stars are modulated (based on *TESS* data). This is in line with the most recent study by Kovacs (2025)[3] who corrected the modulation distributions for noise and time span of the data and found the underlying occurrence rate at least 75 %. In any case, the modulation is widespread among RRLs. Nevertheless, what determines whether the star shows the Blazhko effect? Why do some RRLs show modulation and others not?

We used our large samples of RRLs to investigate differences between modulated and non-modulated stars, and to describe the modulation characteristics based on the light curves. In Prudil & Skarka (2017), we performed a Fourier decomposition of the light curves and investigated the so-called Fourier amplitude and phase parameters (ratios of the i-th and the first amplitude $R_{i1} = A_i/A_1$ and phase differences between i-th and the first ($\varphi_{i1} = \varphi_i - \varphi_1$) sine components). The interrelations of the Fourier parameters allowed us to define empirical relations that are powerful in the identification of modulated stars.

In combination with the fact that the Fourier parameters are connected with metallicity [Fe/H] (Jurcsik & Kovacs, 1996), which is in turn connected with luminosity (e.g., Lee et al., 1990), we were also able to estimate the spatial distribution of modulated and non-modulated stars in the Galactic bulge. We found no differences in the spatial distribution of non- and modulated stars, their mean dereddened colours, absolute magnitudes, and metallicity (see table 2 and figs. 11, 12, 13 in Prudil & Skarka, 2017). This was the first time that such a comparison was made on a statistically large and homogeneous sample of stars. Our results suggest that the modulation is only a temporary episode in the life of RRL stars, which is supported also by other authors who reported diminishing/reappearance of modulation in some RRL stars (e.g. Sódor et al., 2007; Soszyński et al., 2014; Jurcsik, 2019).

All the characteristics of the mean light curves, including amplitudes and phase Fourier parameters, as well as the pulsation periods, are lower for modulated stars than for regular RRL stars Prudil & Skarka (2017). This means that the Blazhko effect suppresses the pulsation amplitude, which has been demonstrated in fig. 7 in Prudil & Skarka (2017) and fig. 10 in Skarka et al. (2020, publication 5 from the list of included papers). The shorter pulsation periods of Blazhko stars are given by the fact that the modulation does not appear among RRLs with periods longer than about 0.65 days.

Our studies on amplitudes, shapes and periods of modulation led to a definition of six basic morphological types, with the majority of modulated stars (90 %) showing symmetric and sinusoidal modulation envelopes (Skarka et al., 2020, 2021). We were able to quantify limits of modulation amplitudes and periods regarding the pulsation period. We clearly confirmed previous assumptions that long-pulsation-period Blazhko stars have small modulation amplitudes and their modulation periods are longer than in their short-pulsation-period counterparts (Skarka et al., 2020). We discovered that the distribution of the modulation periods is log-normal (Skarka et al., 2016) and bimodal, separated with a well-defined gap in the modulation versus pulsation period plane (see the right-hand panels of Fig. 2.1). We named this less populated region 'The Blazhko valley' (Skarka et al., 2020). The signs of this region have been apparent already in Skarka et al. (2016) but clearly proven with the OGLE data in Skarka et al. (2020).

A big step toward explaining the Blazhko effect has been made in infrared wavelengths when Jurcsik et al. (2018) discovered that the modulation is mainly driven by temperature variations, while the radius variations are marginal. From many theories that have been proposed (see Smolec, 2016; Kolláth, 2018), the model involving non-linear resonance 9:2 between the fundamental and the 9th pulsation overtone seems to be the most likely one to explain the Blazhko effect and period doubling discovered in the *Kepler* data (Kolláth et al., 2011; Kolláth, 2018). Space observations also revealed that modulated stars almost exclusively show additional

[2]about 10 times more than all known modulated Galactic field RRLs known in 2017 and 10 % more than previous estimates for the Galactic bulge.

[3]The study largely uses our results from Prudil & Skarka (2017) and Skarka et al. (2020).

pulsation modes (e.g., Molnár et al., 2022, and references therein). Our contribution to the research of the Blazhko effect is in a detailed light-curve investigation of a large number of modulated stars, providing reliable statistical RRL characteristics that have not been available before.

2.2 Binarity or other effects

Together with the Blazhko effect, a lack of RRL stars in binary systems is the most intriguing mystery of these old stars. Only TU UMa, a single example, has been directly proven to reside in a binary system via radial velocity observations (Wade et al., 1999; Liška et al., 2016; Kervella et al., 2019a). No other candidate has been unambiguously proven. A few tens of candidates have been identified by their common proper motion in the Gaia DR2 catalogue (Kervella et al., 2019a,b). An additional few tens of RRLs have been reported to show a cyclic pulsation period variations (Le Borgne et al., 2007; Liška et al., 2016; Prudil et al., 2019; Hajdu et al., 2021)[4], that can be linked with binarity and the Light-Travel-Time Effect, shortly LTTE (e.g. Irwin, 1952; Sterken, 2005; Liska & Skarka, 2015). The origin of the LTTE is in the finite speed of light and orbital motion around a common centre of mass. Observations of the pulsation timings in the most distant point of the orbit from the observer would appear later than calculated, while they would appear earlier in the closest point of the orbit, resulting in apparent cyclic period variations.

It seems that classical RRLs can only arise in wide systems with large orbital separations, where the mass transfer does not trigger another evolutionary path of a star, creating objects of different types, for example, a blue horizontal branch star. Hajdu et al. (2021) studied the largest sample of RRLs showing cyclic pulsation period variations. They discovered that the population of RRLs in such systems increases towards systems with periods between 3000 and 4000 days. Most of their candidate systems have high eccentricities. The distribution of their mass function suggests trimodality, which can be associated with three groups of companions - white dwarfs, low-mass main-sequence stars and Brown dwarfs.

Within my collaboration with citizen astronomers, we started monitoring a Blazhko star Z CVn to describe its modulation (Skarka et al., 2018, article 3 from the list of included papers). However, already shortly after our observations, it appeared that the star is far more interesting even beyond its modulation since it shows spectacular long-term cyclic pulsation period variations (see the top panel of Fig. 2.2). The full amplitude of the Observer-Calculated (O-C) variations is approximately 0.6 days, and the period is about 78 years. If the assumption of binarity was true, Z CVn would orbit around a black hole with a mass of about 56 $M_\odot$. We used available radial velocity observations and showed that the binary scenario cannot be true since the observed radial velocities do not follow the orbital model values at all (bottom panel of Fig. 2.2). Thus, we discovered an unknown effect that produces pulsation period changes in RR Lyrae stars and mimics LTTE.

There have been objects similar to Z CVn reported in the literature. The common characteristics of these objects are large amplitudes of their O-C diagrams and high companion masses. For example, in Liška et al. (2016), we identified two possible systems with a black hole (AQ Lyr and AE Peg, assumed companion masses of 6-9 and 18.6 $M_\odot$). Furthermore, we detected O-C variations consistent with an 8-solar-mass companion of KIC 2831097 (Sódor et al., 2017). Derekas et al. (2004) detected O-C variations in the pulsation period of BE Dor that would assume a companion with the mass of about 60 $M_\odot$. However, later spectroscopic observations, together with new photometric observations, ruled out the binary scenario of BE Dor. Derekas et al. (2021) and Li et al. (2022) revealed that the pulsation period variations of BE Dor are abrupt and quasi-periodic and radial-velocity observations do not show the expected variations.

[4]Binary candidates known before 2019 are listed in the online RRL bincan database https://rrlyrbincan.physics.muni.cz/ (Liska & Skarka, 2016).

Our results (Skarka et al., 2018), together with results on BE Dor (Derekas et al., 2021; Li et al., 2022) move all the RRLs showing cyclic pulsation period variations to a candidate class unless confirmed by spectroscopic observations.

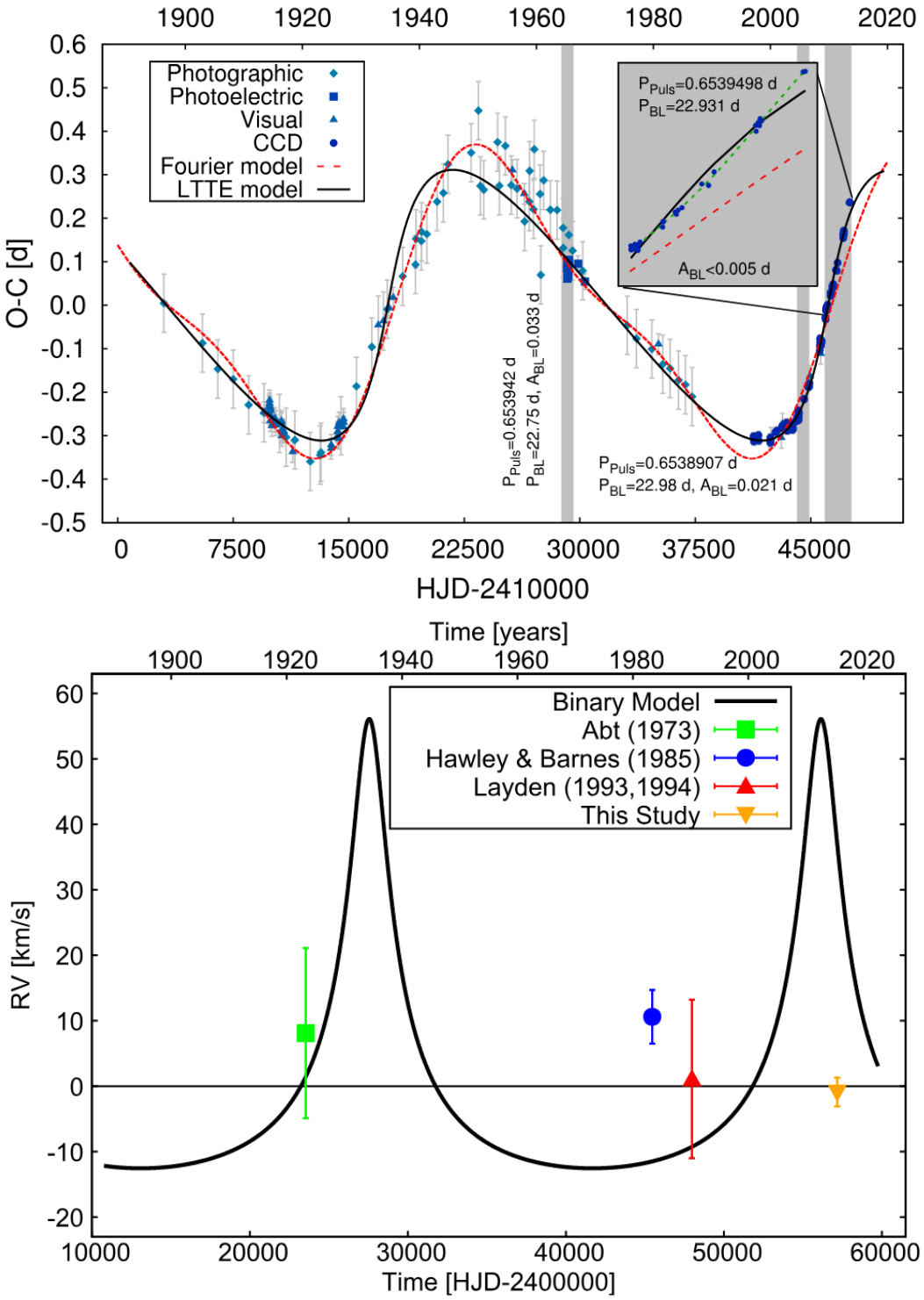

Figure 2.2: The top panel shows the LTTE effect and variations of the pulsation period. The bottom panel shows the expected radial velocities (full line) and available observations (points). Figures from Skarka et al. (2018).

CHAPTER 3

Chemical peculiarity in tight binary systems

In stars hotter than about 7000 K, slow to moderate rotation of $<\approx 100$ km/s and radiative transfer of energy in their envelopes can result in their chemical peculiarity[1]. In these stars, rotational mixing is weak, and elements with large cross-sections (typically rare-earth elements) are radiatively levitated to the stellar surface, while other elements (e.g. He) gravitationally settle down (Michaud et al., 1976; Abt & Morrell, 1995). Stars that have strong globally-organised magnetic fields (300 G to several tens of kG, Paunzen, 2020) with over-abundances of metals such as Sr, Cr, Eu, and Si are labelled as CP2 stars (Preston, 1974). The magnetic field, which is assumed to be of fossil nature in CP2 stars, sustains long-living stable chemical spots producing periodic brightness modulation. These variations are connected with the rotation that itself can be variable (both decelerating or accelerating, Mikulášek et al., 2011).

Although the binary fraction of wide, long-period systems with CP2 stars is up to 50 % (Paunzen, 2020), only very few binary systems with periods below 50 days have been discovered, with a complete lack of binaries with periods below 1.5 days (e.g. Abt & Snowden, 1973; Carrier et al., 2002; Paunzen, 2020). As a result of the Binarity and Magnetic Interactions in various classes of Stars (BinaMIcS) survey, (Alecian et al., 2015) found that the incidence rate of close binary systems hosting a main-sequence star with a strong magnetic field is only about 2 %. It is about three to five times lower incidence rate of strong magnetic fields occurrence than among single massive main-sequence stars.

We still know very little about the role of binarity in CP2 stars. It seems that there is some interplay between binarity and magnetism that prevents CP2 stars from appearing in tight binary systems (Abt & Snowden, 1973; Budaj, 1999). The rarity of magnetic CP stars in tight binaries is likely related to the formation mechanism of fossil magnetic fields of these objects. The three basic theories of magnetic-field formation are listed by Shultz et al. (2019). During the formation process, strong magnetic fields might inhibit the cloud fragmentation and prevent the formation of a binary system (Commerçon et al., 2011). In already formed close binaries, turbulent tidal flows may lead to a rapid decay of the fossil magnetic field (Vidal et al., 2019). A fossil magnetic field may also appear after merger of two stars (Ferrario et al., 2009; Tutukov & Fedorova, 2010; Schneider et al., 2016).

Contrary to CP2 stars, only weak magnetic fields with a strength of up to tenths of Gauss were reported in CP1 stars (e.g., Petit et al., 2011; Blazère et al., 2016). CP1 stars are deficient in He, Ca and/or Sr and overabundant in iron-group and rare-earth elements (Preston, 1974). Thus, CP1 stars are also called metallic stars, shortly AmFm stars. CP1 stars were not expected to host spots nor to show rotational modulation. However, in space photometry from the *Kepler* and *TESS* satellites, it was discovered that most of Am stars show some kind of variability that may be related to rotation (Balona, 2013; Balona et al., 2015; Henriksen et al., 2023a). However, the origin of the rotational variability is still a matter of debate (Henriksen et al.,

[1]There are also examples of fast-rotating magnetic chemically peculiar stars, for example, HD 60431 (Mikulášek et al., 2022).

2023b), although there is evidence that spots might be formed in CP1 stars (Antoci et al., 2025).

About 70 % of CP1 stars are bound in binary systems, with the majority of those with orbital periods shorter than 20 days (peaking at about 5 days), where tidal effects slow down the stars' rotation rate (Abt, 1961, 1985; Carquillat & Prieur, 2007). Thus, in CP1 stars, binarity plays a crucial role in slowing down the rotation through tides and allowing the chemical peculiarity to emerge.

Although helium is gravitationally settled down in CP1 stars and the role of the classical κ mechanism is suppressed, they can still pulsate in low-overtone pressure modes (δ Sct type pulsations with periods between minutes and hours). The κ mechanism may be reinforced by other mechanisms to drive the pulsations, such as turbulent pressure in the hydrogen ionisation zone (Antoci et al., 2014; Smalley et al., 2017) and bump in Rosseland mean opacity resulting from the discontinuous H-ionisation edge in bound-free opacity (Murphy et al., 2020). Thus, we know δ Sct pulsators among CP1 stars (Balona et al., 2015; Smalley et al., 2017; Dürfeldt-Pedros et al., 2024). CP1 stars can also pulsate in high-order gravity modes, as was found recently by Dürfeldt-Pedros et al. (2024). In case of CP2 stars, the strong magnetic field suppresses the low-overtone pressure and high-order gravity modes (Saio, 2005; Murphy et al., 2020), explaining why δ Sct and γ Dor[2] pulsators are not commonly observed among CP2 stars, although some exceptions exist (Murphy et al., 2020).

3.1 HD 99458 - The first Ap star in a short-period binary?

We observed HD 99458 spectroscopically in 2017 and 2018 to confirm the proposed exoplanetary nature of its transits detected in the *K2* mission data (Howell et al., 2014; Barros et al., 2016). The radial-velocity analysis (see Fig. 3.1) showed that the primary star with the mass of $M_1 = 2.15\,\mathrm{M}_\odot$ and temperature of $T_1 = 7600\,\mathrm{K}$ is accompanied by a small, cool dwarf star ($M_2 = 0.45\,\mathrm{M}_\odot$) on a circular orbit, not by an exoplanet. However, a more interesting discovery emerged from the abundance analysis that showed that the primary component of the HD 99458 system is likely a CP2 star with an overabundance of Fe, Si, Mn, Ni, and other elements typical for CP2 stars. Thus, HD 99458 with an orbital period of 2.7 days was identified as an additional item to the list of a very few CP2 known candidates in short-period binary systems.

The other candidates for binaries with CP2 component are HD 62658 (Shultz et al., 2019), HD 66051 (Kochukhov et al., 2018), V772 Cas (Gandet, 2008), and non-eclipsing HD 200405 (Carrier et al., 2002). The assumption of the CP2 nature of our star was further reinforced by the shape of the light curve from the *K2* mission (right-hand panel of Fig. 3.1), which could be described assuming two spots which are also typical for CP2 stars.

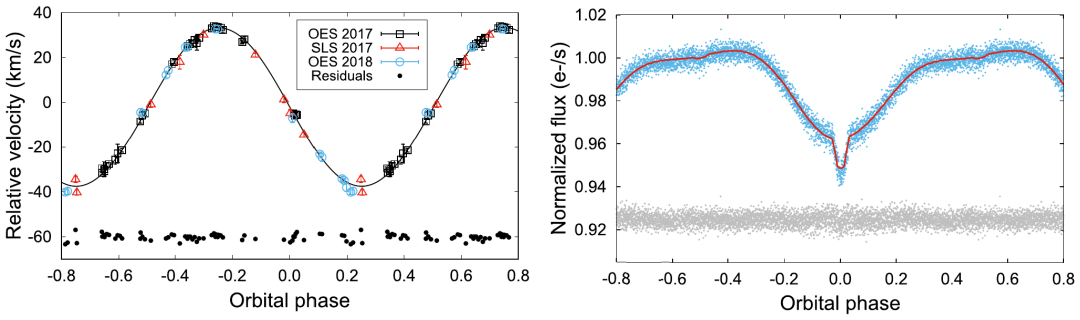

Figure 3.1: Radial-velocity curve (left) and light curve (right) of HD 99458. Figures from Skarka et al. (2019).

The last surprise came with the analysis of the residual light curve after the binary model was subtracted from the *K2* data. The star shows δ Sct type pulsations (Fig. 3.2). Due to the

[2] g-mode pulsators with periods typically between 0.3 and 3 days.

30-minute cadence of the *K2* data, the amplitudes of the fast pulsations were suppressed due to averaging, and we were only able to search frequencies up to 24 c/d (cycles per day), that is, the Nyquist frequency for the data with a 30-minute cadence. New observations from the *TESS* satellite showed that the original frequencies identified in the *K2* data were only Nyquist reflections of the real frequencies (black frequency spectrum in Fig. 3.2). In any case, HD 99458 looked like a very promising and unique object that showed characteristics not expected to be present among CP2 stars.

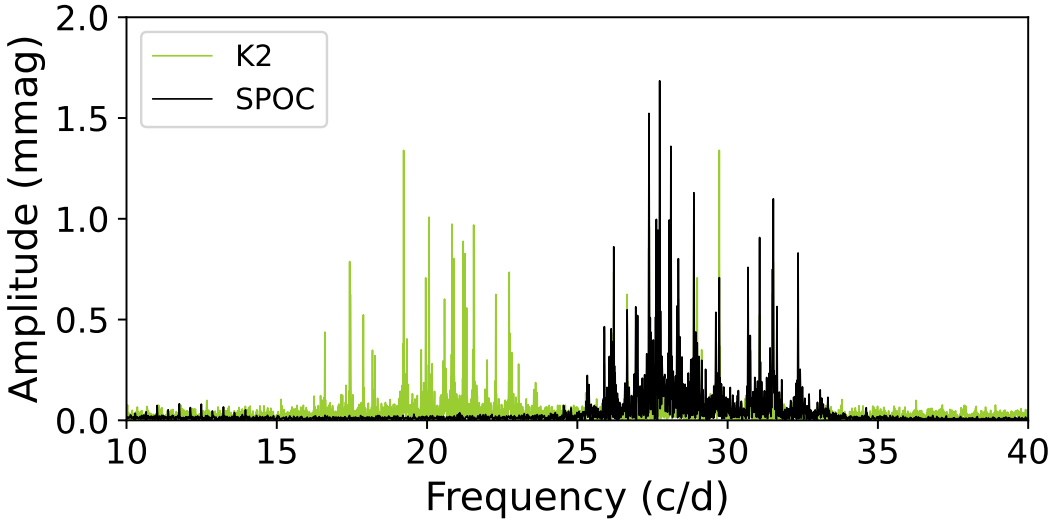

Figure 3.2: A comparison of frequency spectra of HD 99458 from *K2* (30-minutes cadence) and *TESS* (SPOC 2-minutes cadence data) missions after prewhitening with two dominant rotational frequencies.

Unfortunately, at the time of publication of the study of HD 99458, we did not have spectropolarimetric observations that would prove a strong magnetic field and CP2 nature of HD 99458. Such observations were gathered afterwards with the 3.6m CFHT in Hawai and the 6m telescope in Russia. Both observations showed very weak or no magnetic field, which disqualifies HD 99458 from being of CP2 type (Semenko et al., in prep.). Thus, it seems that HD 99458 is more likely a CP1 star because the abundance pattern of CP1 and CP2 may be similar and difficult to distinguish in some cases. In addition, CP1 nature would easily explain binarity, but also the presence of δ Sct pulsations since they have been observed among CP1 stars (e.g. Dürfeldt-Pedros et al., 2024). Alternative explanation proposed by Semenko et al. (in prep.) would be that HD 99458 is an intrinsically metal-poor Population I star.

Similar troubles with a proper identification of the peculiarity type were experienced with the other mentioned candidates. First, HD 66051 was assumed to be a HgMn star (CP3 type, Niemczura et al., 2017). Subsequently, it was found that the chemical pattern is closer to CP2 stars (Kochukhov et al., 2018). Two years later, Paunzen et al. (2020) speculated that HD 66051 is likely a CP1 star. The same situation occurred with another CP2 candidate in an eclipsing binary, V772 Cas. Gandet (2008) assumed this star to be a CP2 candidate, while a detailed investigation by Kochukhov et al. (2021) showed that it is actually a CP3 star. These examples, together with HD 99458, show that the investigation of CP stars might be difficult and sometimes ambiguous. The out-of-transit variations of HD 99458, which we linked with spots back in 2019, likely originate from the effects of close binarity such as tidal deformation, Doppler beaming and reflection. In addition, photometric observations taken after our study suggest that the system is actually triple and contains an additional component that can impact the light curve. Detailed analysis of HD 99458 with new data is expected in the near future (Semenko et al., in prep.).

3.2 50 Dra - hot CP1 twins in a non-eclipsing system

During our classification of stars close to the northern ecliptic pole (see Chapter 4 Skarka et al., 2022), we noticed that 50 Dra shows a double-wave light curve in TESS data that might be a signature of either spots or proximity effects in a close binary system. The fact that 50 Dra has been known to be a spectroscopic binary (Harper, 1919) suggests that the latter might be the correct explanation. However, it appeared that 50 Dra is a very interesting system of two hot CP1 stars showing additional low-amplitude variability.

We obtained 20 spectra with the OES spectrograph installed at the 2m Perek telescope in Ondrejov, covering the whole orbital phase in 2022. Further, we used 440 thousand 2-minute photometric observations from 28 sectors gathered by *TESS* for the analysis. After refining the orbital period based on modelling the light curve, we were able to model the orbit and disentangle spectra with Korel (Hadrava, 1995) and fully describe the system by modelling in Phoebe (Prša et al., 2016; Conroy et al., 2020).

Our analysis showed that 50 Dra consists of two almost identically big ($R_{1,2} \approx 2\,\mathrm{R}_\odot$) and massive stars ($M_{1,2} \approx 2\,\mathrm{M}_\odot$) with temperatures of $T_{\mathrm{eff},1} = 9800\,\mathrm{K}$ and $T_{\mathrm{eff},2} = 9200\,\mathrm{K}$. We showed that the stars have synchronised rotation and orbit the common centre of mass at almost perfectly circular orbits ($e = 0.002$) with a period of 4.117 d. The abundance analysis of the disentangled spectra revealed that both components are metallic chemically peculiar stars (CP1) having an underabundance of Sc and overabundance of iron-peak and rare-earth elements. The abundances of 50 Dra components are typical for CP1 stars, as can be seen from Fig. 3.3, which makes them great representatives of this class of stars. What makes 50 Dra special regarding its chemical peculiarity is the high temperature of both components. CP1 peculiarity is typically observed among stars with temperatures between 7200 and 8200 K, with a peak at 7750 K (based on LAMOST spectroscopic observations of more than 9000 stars, Qin et al., 2019). Only a very small fraction of CP1 stars have temperatures above 9000 K (Catanzaro et al., 2019; Qin et al., 2019).

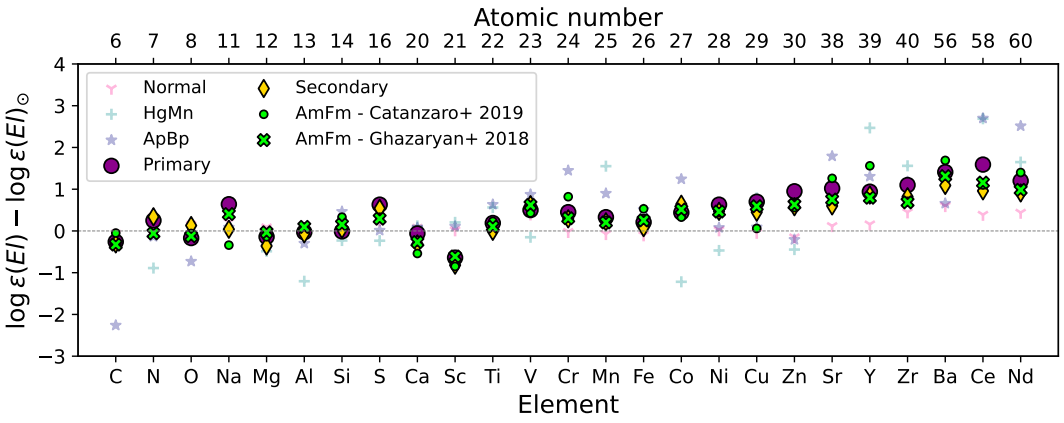

Figure 3.3: Abundances of 50 Dra components compared to abundances of catalogued CP1 stars. Figure from Skarka et al. (2025).

In recent years, thanks to the data from space-based observatories, it was discovered that stars hotter than about 6000 K might also show rotational variability even though they do not have strong large-scale magnetic fields usually required to stabilise chemical spots (Sikora et al., 2019; Kochukhov et al., 2021; Trust et al., 2020). This type of variability is less regular in normal A-type and CP1 stars than in CP2 stars and resembles longitudinal differential rotation and spot evolution in cool stars (e.g. Balona, 2013; Sikora et al., 2019). As such, this kind of rotational modulation manifests itself as a group of unresolved peaks that might be approximated with a Gaussian centred at the rotational frequency. This group of peaks is usually called 'spike'. Only recently, Antoci et al. (2025) demonstrated that these variations

are really connected with spots, which are induced by local magnetic fields. These magnetic fields are dynamo-generated by the subsurface convection layers, rather than by the g-modes resonantly induced by the overstable convective modes in the core as suggested by Lee & Saio (2020) and Lee (2021).

The spike feature, which has been identified in many A-type stars, is usually accompanied by another group of peaks that is called 'hump' (Balona, 2013; Balona et al., 2015; Saio et al., 2018; Henriksen et al., 2023a,b). Saio et al. (2018) explained the hump either as a product of prograde g-modes or Rossby modes mechanically excited by deviated flows caused by stellar spots or mass outbursts, and by non-synchronous tidal forces. In the case of prograde g-modes, the hump has a higher frequency than the spike. 50 Dra shows a group of unresolved peaks at frequency around 0.275 c/d that is slightly higher than the orbital period.

We proved that the components of 50 Dra show synchronised rotation with the orbital period. The frequencies calculated from the observed $v \sin i$, radii and inclination derived from binary modelling are consistent with the orbital frequency. Therefore, we can safely assume that the spike, if present, would be at the position of the orbital frequency peak in the Fourier spectrum. The group of unresolved peaks with higher frequency could then be explained as prograde g-mode pulsations. On the other hand, we cannot rule out the so-called anti-solar rotation when the polar regions rotate faster than the equator, which could explain rotational modulation with higher frequencies. However, the anti-solar rotation has not been commonly observed (see the discussion in e.g. Rüdiger et al., 2019), preferring prograde g-modes as the more likely explanation of the additional variations observed in 50 Dra.

The system of 50 Dra represents a very complex laboratory showing many interesting features. It can serve as an ideal example of typical Am stars regarding their abundances, but at high temperatures, which are, on the other hand, unusual. In addition, 50 Dra shows prograde g-modes and can be used for investigating the co-existence of chemical peculiarity, tidal interactions, and internal oscillations and rotation. In that sense, 50 Dra is a unique object.

CHAPTER 4

Classification of variable stars

Each study of a variable star starts with an estimation of the nature of its variations. The proper classification not only allows description of the observed variations with an appropriate model, but also enables performing statistical studies on large samples of stars and defining limits of the physical processes. Brightness variations can be intrinsic to the stars, meaning that the physical conditions on the surface or close surrounding of the stars change. The second channel of variations is extrinsic, which means that the overall flux of the star (or stars in a system) is more or less constant, and the change of geometry of observations causes the variations.

The current catalogues contain a few million variable stars detected mainly in the last few years. The increase in the number of known variable stars can be demonstrated by the number of stars in the Variable Star Index (VSX, Watson et al., 2006), the most used and one of the largest variable star catalogues. In 2009, VSX contained 178 thousand stars, while in July 2025, there were about 10.2 million variable stars. Another gigantic catalogue has been released once the analysis of millions sources from the *Gaia* satellite was finished. The *Gaia* DR3 variable star catalogue contains 12.4 million variable sources (Rimoldini et al., 2023).

The stars are classified based on their common features. Mostly it is the similarity in shape of their light curves together with periods and amplitudes of variations. An example of such a classification scheme of variable stars, that has been adopted by the *Gaia* mission researchers (Gaia Collaboration et al., 2019), is shown in Fig. 4.1. This logical sorting system has evolved through decades from the General Catalogue of Variable Stars (GCVS, Samus et al., 2017) first established already in forties of 20th century (Samus et al., 2001).

As can be seen, the classification becomes more and more detailed with lots of variability types, especially among pulsating stars. This is the consequence of accurate data produced by space missions and long-term surveys that allow the detection of subtle variations. Subgroups are named after the first or most distinct member of the class. However, the classification often becomes ambiguous, and the borders between different types are not well defined. In addition, different physical effects may produce variations with similar amplitudes and can combine. For example, rotation can be observed together with pulsations.

The problem with classification is most distinct among main-sequence A-F spectral type stars (region approximately corresponding to the green colour-coded stars in Fig.4.2). This part of the Hertzsprung-Russell (H-R) diagram is extremely interesting. It is a region where the energy transfer via convection becomes inefficient in the upper layers, and energy transfer through radiation starts to dominate (e.g. Kraft, 1967; Cantiello & Braithwaite, 2019; Beyer & White, 2024). The transition of energy transfer is correlated with the transition from slow to fast rotation (e.g. Royer et al., 2007; Nielsen et al., 2013; McQuillan et al., 2014; Beyer & White, 2024). These effects go hand in hand with the dominance of dynamo-generated and fossil large-scale magnetic fields in cool stars and hot stars, respectively (e.g. Donati & Landstreet, 2009; Cantiello & Braithwaite, 2019; David-Uraz et al., 2019).

The above-mentioned implies that we can expect signatures of rotational variability induced by both temperature and chemical spots, and signatures of pulsations that are either stochastic, classical p-modes, or g-modes. In addition, binarity and the combination of all the discussed effects can be observed simultaneously. Thus, it is not surprising that the percentage of variable

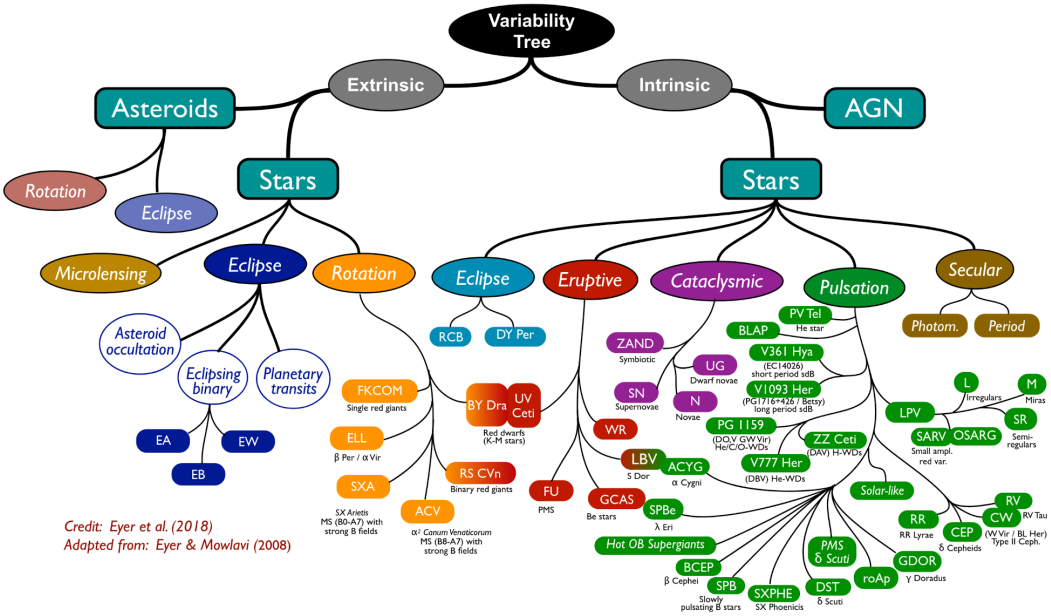

Figure 4.1: Variability tree (Gaia Collaboration et al., 2019).

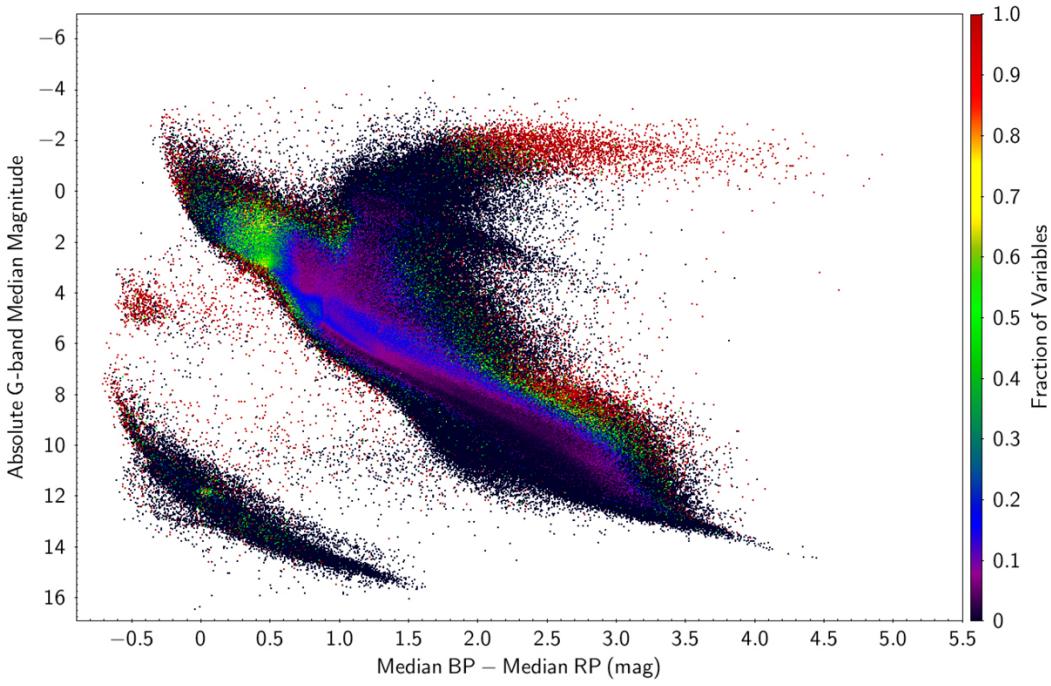

Figure 4.2: The Hertzsprung-Russel diagram showing the incidence rate of variable stars (Gaia Collaboration et al., 2019).

stars among intermediate stars of A to F spectral types is high (see Fig. 4.2). As complex variables, stars of A-F spectral types can help us better understand many physical effects and their interplay. For example, studying stellar pulsations (e.g. Aerts, 2021; Kurtz, 2022) can help us better understand the angular-momentum transport and rotation of the inner and outer parts of the stars (e.g. Aerts et al., 2019; Mombarg, 2023; Aerts & Tkachenko, 2024; Aerts et al., 2025). The intermediate stars also offer a way to study the interplay between magnetism, chemical peculiarity and pulsations (e.g. Quentin & Tout, 2018; Thomson-Paressant et al., 2024; Dürfeldt-Pedros et al., 2024).

As an addition to physical variability, instrumental effects, data processing and low-angular resolution of the photometric missions started to play a significant role, introducing artificial signals to the data (e.g. Jenkins et al., 2016; Higgins & Bell, 2023). Keeping all the above-mentioned in mind, the proper classification and disentanglement of all observable effects might be a true challenge.

4.1 Variable stars of A-F spectral types in the *TESS* continuous viewing zones

In Skarka et al. (2022) and Skarka & Henzl (2024) (papers 6 and 7 from the list of included papers), we took advantage of the availability of quasi-continuous data produced by the *Transiting Exoplanet Space Satellite*, shortly *TESS* (Ricker et al., 2015). We performed a detailed and careful visual investigation of thousands of light curves of stars brighter than 11 and 9 mag, respectively, around both ecliptic poles to provide a reliable classification.

In our studies, we found and emphasized that different available data products (SPOC and QLP, Jenkins et al., 2016; Huang et al., 2020a,b) with different cadences can provide significantly different light curves that may lead to wrong classification. For example, there might be unexpected instrumental trends in different data products, data with a 30-minute cadence are not suitable for the investigation of fast variations (for instance, in δ Sct stars). In (Skarka et al., 2022), we pointed out that there are no firmly defined classification criteria in the literature. Thus, we provided a detailed description of the variability types that we used, together with examples of light curves and Fourier spectra.

By careful visual inspection of every particular star, we classified them into three rotational classes (ROTM, ROTS, ROT), four classes of binary stars (EA, EB, EW, ELL), and two pulsation classes (DSCT, GDOR). In cases where we were unable to decide about the dominant variability type, we just put a note that the star is variable (VAR). Studies around both ecliptic poles give a consistent incidence rate of variable stars of approximately 51 %. This percentage is in great agreement with the percentage of variable stars identified in *Gaia* (see the green points in Fig. 4.2, Gaia Collaboration et al., 2019).

The distribution of variability types is shown in Fig. 4.3. There are small differences in the methodology and nomenclature between studies from 2022 and 2024. There is a larger fraction of pulsating stars in the northern continuous viewing zone (CVZ, 65 %) than in the southern CVZ (43 %). The difference is too high to be caused by some instrumental effects. Perhaps different stellar population characteristics could account for this discrepancy between northern and southern CVZs.

There are small differences between the two studies in the methodology and nomenclature. In Skarka & Henzl (2024), the 'Uncertain' class also contains the VAR class, the BIN contains all binary types, and we do not distinguish between ROTM and ELL. This is because it is impossible to distinguish between a single star with stable spots and a non-eclipsing binary with tidally deformed components, as we discussed in (Skarka et al., 2022). This problem was subsequently studied and elaborated under my supervision as an MSc project by Ema Šipková, who spectroscopically monitored 35 stars with sinusoidal photometric variability in *TESS* data (MSc thesis, Šipková, 2025; Šipková et al., 2025, accepted in A&A). The classification was possible in 75 % of the studied stars. Šipková et al. (2025) found that at least half of the studied stars are binary stars. In addition to that, in about 25 % of the stars, the radial velocity variations did not show any apparent trend. Thus, there might also be ELL stars with low

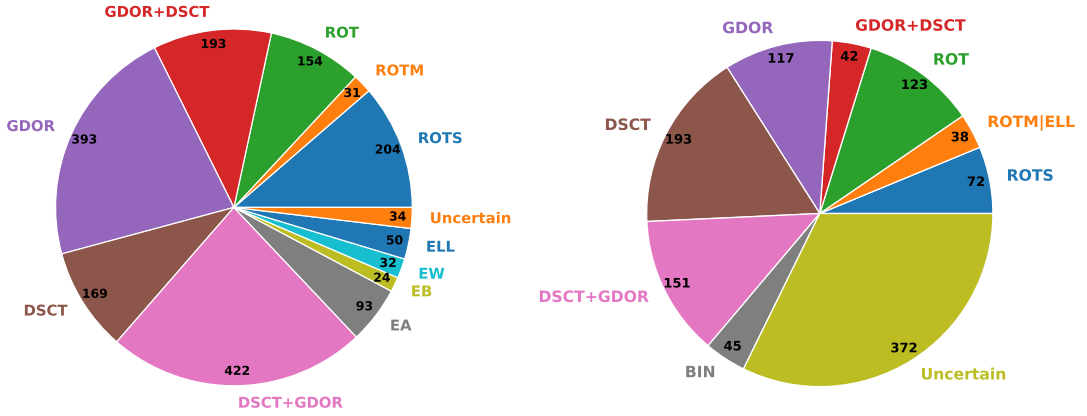

Figure 4.3: Statistics of the variability types identified in the northern (left, Skarka et al., 2022) and southern (right, Skarka & Henzl, 2024) *TESS* CVZ, respectively.

inclination angles among these stars, and even spectroscopic time series are not much helpful to differentiate between spotted stars and binaries. Except for the light curves generated for spotted stars and binary systems in Skarka et al. (2022) and the thorough discussion in the same study, the results by Šipková et al. (2025) clearly demonstrate the impossibility of reliable classification of such stars based purely on single-channel photometry provided by *TESS*.

When we plot all pulsating variables from both CVZs into H-R diagrams (Fig. 4.4), we realise that GDOR stars cluster within the ZAMS in the theoretical instability strip (the violet-shaded area, Dupret et al., 2005) and that DSCT stars and DSCT-GDOR hybrids are mainly located near the red edge of the DSCT instability strip that has been empirically determined by Murphy et al. (2019). Similar preference for the red edge has been observed by Dürfeldt-Pedros et al. (2024) among metallic (Am) DSCT stars. These are important results that will allow us to better understand the excitation mechanisms in DSCT and GDOR stars. In chemically peculiar Am stars, the classical κ mechanism in the HeII zone is suppressed, and the turbulent pressure mechanism likely becomes more efficient (Antoci et al., 2014, 2019).

As can be seen, there are also pulsating stars outside the instability strips. This has been noticed already by other authors (e.g. Murphy et al., 2019). In the case of GDOR, it can be likely due to misclassification with rotating spotted solar-like stars (ROTS type), as they may look very similar (as we discussed in Skarka et al., 2022). For DSCT, there might be a few reasons for the strange position in the HRD: 1) Poorly determined temperature, 2) poorly known physical limits of excitations (loosely defined limits of the instability strip), 3) missclassification of the star as DSCT due to contamination. The latter option has been investigated by Václav Chmelař as a BSc project at Masaryk University (Chmelař, 2025) under my supervision. The student investigated ten DSCT stars with the lowest temperatures from the sample of DSCT stars in Skarka et al. (2022).

After performing a detailed investigation of the *TESS* data using LIGHTCURVE (Lightkurve Collaboration et al., 2018) and TESS-LOCALIZE (Higgins & Bell, 2023), and new ground-based photometry with higher angular resolution, we now know that all the DSCT candidates with low temperatures were false positives. They were stars contaminated by nearby faint DSCT stars or by binary stars. As was already shown in Skarka & Henzl (2024), the light can be contaminated even by surprisingly faint stars a few pixels away from the target stars. If the light curves of such stars are symmetric, the highest frequency apparent in the contaminated light can be a harmonic of a real frequency that is above the 5 c/d (the limit for DSCT pulsations). Thus, it only mimics this kind of pulsation. Further troubles can be caused by red giant and red clump stars that show a characteristic pattern of their stochastic p-modes. In case of these types of stars, the pattern can be located in the DSCT and GDOR frequency ranges.

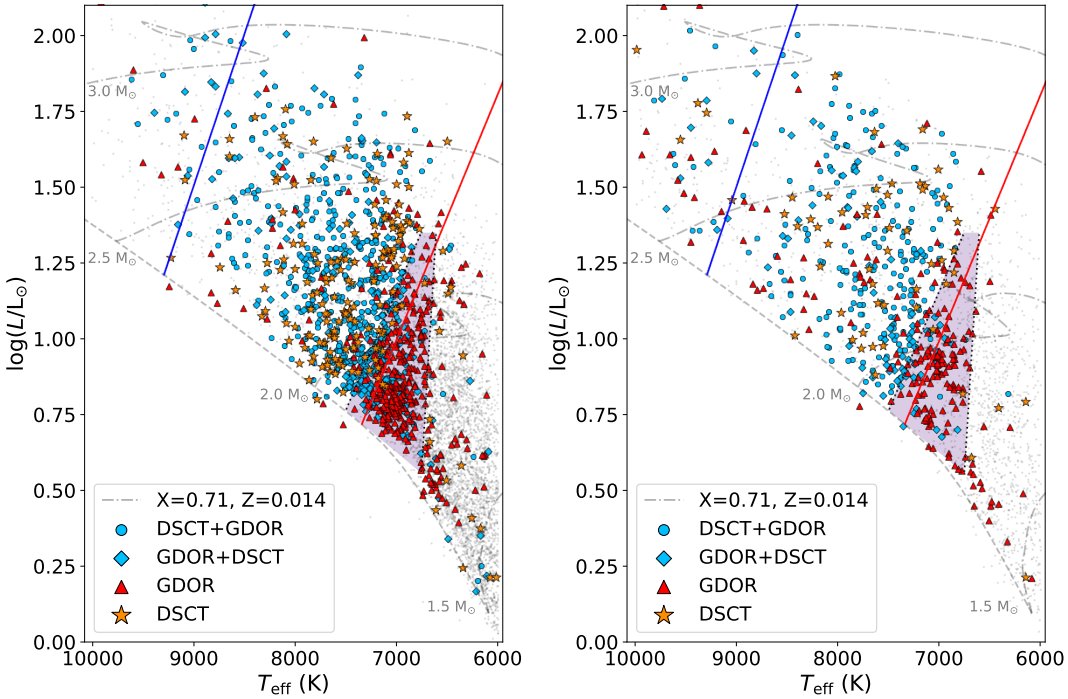

Figure 4.4: Pulsating stars in the HRD from the northern (left, Skarka et al., 2022) and southern (right, Skarka & Henzl, 2024) *TESS* CVZ, respectively.

Our classification of variable stars based on *TESS* data shows significant differences when compared with previous studies of available catalogues. In Skarka et al. (2022), we performed a new analysis of data from the *Kepler* satellite using our methodology and compared the classification with previous studies. The main discrepancies were found between GDOR and rotating variables. For example, among stars classified as rotating variables by Balona (2013), we identified GDOR variability. On the other hand, we were in total agreement with the GDOR classification with Balona (2013). In the crossmatch with classifications provided by general catalogues, such as VSX (Watson et al., 2006) or *Gaia* variability catalogue (Rimoldini et al., 2023), we got significant discrepancies reaching mostly tens of per cent. This may point towards the need for a detailed contamination analysis and revision of catalogues. It is appropriate to note that we did not perform detailed contamination analysis and only provided the numbers of contaminating stars with the magnitude difference of 5 mag from the target star as a kind of proxy for the contamination warning.

CHAPTER 5

Conclusions and future prospects

The investigation of stellar variability has become an integral part of stellar research because it is a natural outcome of physical processes in stars. This compilation contains studies focused on interesting targets, trying to expand our knowledge on RR Lyrae stars and intermediate-mass stars on the main sequence. As was demonstrated, the classification of variable stars becomes difficult with the availability of precise data that spans many years. Such data reveal details that were previously hidden or were not observable at a given moment due to unstable nature of the processes. It becomes obvious that the effects of rotation and pulsations are commonly detectable in single stars, making a proper classification difficult in some cases. The community would benefit from a general agreement on classification criteria and a common system reflecting the multi-variable character of stars. In the case of HD 99458 (Sect. 3.1), we have seen that long-term monitoring is vital for understanding stellar variability. By analysing short time series, although precise, it may happen that we only get a snapshot of a full movie and get misleading results.

Regarding the topics noted in this compilation, we can expect large developments in all aspects of stellar variability research in future. The current and near-future instruments will enable us to employ all possible techniques, including multi-wavelength photometry, spectroscopy, and astrometry, both from the ground and from space. The ongoing photometric surveys, such as OGLE (Udalski et al., 1992, 2015; Soszyński, 2024) and *TESS* (Ricker et al., 2015), will be complemented by the Vera Rubin observatory (in operation since 2025, Ivezić et al., 2019) and PLATO mission (launch in January 2027, Rauer et al., 2024). The Vera Rubin Observatory will provide us with precise observations of faint targets across almost the whole sky (valuable mostly for distant RR Lyrae stars), while PLATO will produce uninterrupted long-term observations of brighter targets with high precision and cadence (valuable for asteroseismology, chemical peculiarity, stellar activity). The optical observations will be complemented with already available infra-red observations (e.g. VISTA Dalton et al., 2006; Emerson et al., 2006) and future ultraviolet space observations from ULTRASAT (launch in 2027-2028, Shvartzvald et al., 2024) and QUVIK (launch 2028-2029, Werner et al., 2024; Krtička et al., 2024) satellites.

Spectroscopic surveys and instruments will make a further step towards a better understanding of stellar variability. The ongoing LAMOST (Zhao et al., 2012; Yan et al., 2022), APOGEE (Majewski et al., 2017), WEAVE (Jin et al., 2024) and other spectroscopic projects will be complemented in the near future with 4MOST (de Jong et al., 2019), and *Gaia* DR4 and DR5 releases (Brown, 2025). We will have a truly outstanding set of data, allowing us to study the ages and populations of stars and model various physical processes in detail, everything possible by means of statistical studies on large samples of stars. Small telescopes with versatile spectrographs such as OES (Kabáth et al., 2020) or PLATOSpec (Kabáth et al., 2025) will allow dedicated studies through the available observing time. The amount of data and stellar parameters together with the development of classification techniques will allow accurate automatic variability classification through machine learning methods (e.g. Audenaert, 2025; Wang et al., 2025).

My personal journey will continue mostly with studies of intermediate-mass stars and the relation between chemical peculiarity, rotation, and pulsations. An integral part of my future

research will be the classification of variable stars because only properly classified stars can provide reliable results. In particular, this will be essential for the preparation of training samples for automated routines that enable the reliable preparation of a catalogue of variable stars in the LOPS2 field of the PLATO mission. I will continue my work within Czech and international teams, in cooperation with professionals, and citizen astronomers. Last, but not least, I will do my best to introduce the interesting topics covered by stellar variability to enthusiastic students and the public. The future is not bright, nor faint. It is variable!

Bibliography

Abt, H. A. 1961, ApJS, 6, 37. doi:10.1086/190060

Abt, H. A. & Snowden, M. S. 1973, ApJS, 25, 137. doi:10.1086/190265

Abt, H. A. 1985, ApJS, 6, 37. doi:10.1086/190060

Abt, H. A. & Morrell, N. I. 1995, ApJS, 99, 135. doi:10.1086/192182

Aerts, C., Mathis, S., & Rogers, T. M. 2019, Annual Review of Astronomy and Astrophysics, 57, 35. doi:10.1146/annurev-astro-091918-104359

Aerts, C. 2021, Reviews of Modern Physics, 93, 015001. doi:10.1103/RevModPhys.93.015001

Aerts, C. & Tkachenko, A. 2024, A&A, 692, R1. doi:10.1051/0004-6361/202348575

Aerts, C., Van Reeth, T., Mombarg, J. S. G., et al. 2025, A&A, 695, A214. doi:10.1051/0004-6361/202452691

Alecian, E., Neiner, C., Wade, G. A., et al. 2015, New Windows on Massive Stars, 307, 330. doi:10.1017/S1743921314007030

Antoci, V., Cunha, M., Houdek, G., et al. 2014, ApJ, 796, 118. doi:10.1088/0004-637X/796/2/118

Antoci, V., Cunha, M. S., Bowman, D. M., et al. 2019, MNRAS, 490, 4040. doi:10.1093/mnras/stz2787

Antoci, V., Cantiello, M., Khalack, V., et al. 2025, arXiv:2502.11879. doi:10.48550/arXiv.2502.11879

Audenaert, J. 2025, ApJSS, 370, 7, 72. doi:10.1007/s10509-025-04460-5

Auvergne, M., Bodin, P., Boisnard, L., et al. 2009, A&A, 506, 1, 411. doi:10.1051/0004-6361/200810860

Balona, L. A. 2013, MNRAS, 431, 2240. doi:10.1093/mnras/stt322

Balona, L. A., Catanzaro, G., Abedigamba, O. P., et al. 2015, MNRAS, 448, 1378. doi:10.1093/mnras/stv076

Barragán, O., Armstrong, D. J., Gandolfi, D., et al. 2022, MNRAS, 514, 1606. doi:10.1093/mnras/stac638

Barros, S. C. C., Demangeon, O., & Deleuil, M. 2016, A&A, 594, A100. doi:10.1051/0004-6361/201628902

Benkő, J. M., Szabó, R., & Paparó, M. 2011, MNRAS, 417, 974. doi:10.1111/j.1365-2966.2011.19313.x

Beyer, A. C. & White, R. J. 2024, ApJ, 973, 1, 28. doi:10.3847/1538-4357/ad6b0d

Blazère, A., Petit, P., Lignières, F., et al. 2016, A&A, 586, A97. doi:10.1051/0004-6361/201527556

Blažko, S. 1907, Astronomische Nachrichten, 175, 325. doi:10.1002/asna.19071752002

Borucki, W. J., Koch, D., Basri, G., et al. 2010, Science, 327, 977. doi:10.1126/science.1185402

Breger, M. 2010, Variable Stars, the Galactic halo and Galaxy Formation, 95. doi:10.48550/arXiv.1001.4443

Brown, A. G. A. 2025, , arXiv:2503.01533. doi:10.48550/arXiv.2503.01533

Budaj, J. 1999, MNRAS, 310, 419. doi:10.1046/j.1365-8711.1999.02985.x

Caloi, V. & D'Antona, F. 2008, ApJ, 673, 2, 847. doi:10.1086/523346

Cantiello, M. & Braithwaite, J. 2019, ApJ, 883, 1, 106. doi:10.3847/1538-4357/ab3924

Carquillat, J.-M. & Prieur, J.-L. 2007, MNRAS, 380, 1064. doi:10.1111/j.1365-2966.2007.12143.x

Carrier, F., North, P., Udry, S., et al. 2002, A&A, 394, 151. doi:10.1051/0004-6361:20021122

Catanzaro, G., Busà, I., Gangi, M., et al. 2019, MNRAS, 484, 2530. doi:10.1093/mnras/stz080

Catelan, M. & Smith, H. A. 2015, Pulsating Stars (Wiley-VCH), 2015

Chmelař, V. 2025, Masaryk University, https://is.muni.cz/auth/th/s5uff/Bakalarska_prace_Vaclav_Chmelar.pdf, BSc thesis

Commerçon, B., Hennebelle, P., & Henning, T. 2011, ApJL, 742, L9. doi:10.1088/2041-8205/742/1/L9

Conroy, K. E., Kochoska, A., Hey, D., et al. 2020, ApJS, 250, 34. doi:10.3847/1538-4365/abb4e2

Cunha, M. S., Antoci, V., Holdsworth, D. L., et al. 2019, MNRAS, 487, 3523. doi:10.1093/mnras/stz1332

Dalton, G. B., Caldwell, M., Ward, A. K., et al. 2006, SPIE, 6269, 62690X. doi:10.1117/12.670018

David-Uraz, A., Neiner, C., Sikora, J., et al. 2019, MNRAS, 487, 1, 304. doi:10.1093/mnras/stz1181

de Jong, R. S., Agertz, O., Berbel, A. A., et al. 2019, The Messenger, 175, 3. doi:10.18727/0722-6691/5117

Derekas, A., Kiss, L. L., Udalski, A., et al. 2004, MNRAS, 354, 3, 821. doi:10.1111/j.1365-2966.2004.08242.x

Derekas, A., Thompson, I. B., Bokon, A., et al. 2021, Posters from the TESS Science Conference II (TSC2), 53. doi:10.5281/zenodo.5123547

Donati, J.-F. & Landstreet, J. D. 2009, Annual Review of Astronomy and Astrophysics, 47, 1, 333. doi:10.1146/annurev-astro-082708-101833

Drake, A. J., Catelan, M., Djorgovski, S. G., et al. 2013, ApJ, 765, 2, 154. doi:10.1088/0004-637X/765/2/154

Dupret, M.-A., Grigahcène, A., Garrido, R., et al. 2005, A&A, 435, 3, 927. doi:10.1051/0004-6361:20041817

Dürfeldt-Pedros, O., Antoci, V., Smalley, B., et al. 2024, A&A, Variability and stellar pulsation incidence in Am and Fm stars using TESS and Gaia data, 690, A104. doi:10.1051/0004-6361/202349076

Eddington, A. S. 1926, The Internal Constitution of the Stars, Cambridge: Cambridge University Press, 1926. ISBN 9780521337083.

Emerson, J., McPherson, A., & Sutherland, W. 2006, The Messenger, 126, 41.

Ferrario, L., Pringle, J. E., Tout, C. A., et al. 2009, MNRAS, 400, L71. doi:10.1111/j.1745-3933.2009.00765.x

Gaia Collaboration, Eyer, L., Rimoldini, L., et al. 2019, A&A, 623, A110. doi:10.1051/0004-6361/201833304

Gandet, T. L. 2008, Information Bulletin on Variable Stars, 5848, 1

Hadrava, P. 1995, A&AS, 114, 393

Hajdu, G., Pietrzyński, G., Jurcsik, J., et al. 2021, ApJ, 915, 50. doi:10.3847/1538-4357/abff4b

Harper, W. E. 1919, JRASC, 13, 236.

Henriksen, A. I., Antoci, V., Saio, H., et al. 2023, MNRAS, 524, 4196. doi:10.1093/mnras/stad1971

Henriksen, A. I., Antoci, V., Saio, H., et al. 2023, MNRAS, 520, 216. doi:10.1093/mnras/stad153

Higgins, M. E. & Bell, K. J. 2023, AJ, 165, 4, 141. doi:10.3847/1538-3881/acb20c

Howell, S. B., Sobeck, C., Haas, M., et al. 2014, PASP, 126, 938, 398. doi:10.1086/676406

Huang, C. X., Vanderburg, A., Pál, A., et al. 2020, Research Notes of the American Astronomical Society, 4, 11, 204. doi:10.3847/2515-5172/abca2e

Huang, C. X., Vanderburg, A., Pál, A., et al. 2020, Research Notes of the American Astronomical Society, 4, 11, 206. doi:10.3847/2515-5172/abca2d

Irwin, J. B. 1952, ApJ, 116, 211. doi:10.1086/145604

Ivezić, Ž., Kahn, S. M., Tyson, J. A., et al. 2019, ApJ, 873, 2, 111. doi:10.3847/1538-4357/ab042c

Jenkins, J. M., Twicken, J. D., McCauliff, S., et al. 2016, SPIE, 9913, 99133E. doi:10.1117/12.2233418

Jin, S., Trager, S. C., Dalton, G. B., et al. 2024, MNRAS, 530, 3, 2688. doi:10.1093/mnras/stad557

Jurcsik, J. & Kovacs, G. 1996, A&A, 312, 111

Jurcsik, J., Sódor, Á., Szeidl, B., et al. 2009, MNRAS, 400, 1006. doi:10.1111/j.1365-2966.2009.15515.x

Jurcsik, J., Hajdu, G., Dékány, I., et al. 2018, MNRAS, 475, 4208. doi:10.1093/mnras/sty112

Jurcsik, J. 2019, MNRAS, 490, 80. doi:10.1093/mnras/stz2498

Kabáth, P., Skarka, M., Sabotta, S., et al. 2020, PASP, 132, 035002. doi:10.1088/1538-3873/ab6752

Kabáth, P., Chaturvedi, P., MacQueen, P. J., et al. 2022, MNRAS, 513, 5955. doi:10.1093/mnras/stac1254

Kabáth, P., Skarka, M., Hatzes, A., et al. 2025, , arXiv:2510.11961. doi:10.48550/arXiv.2510.11961

Kervella, P., Gallenne, A., Evans, N. R., et al. 2019, A&A, 623, A117. doi:10.1051/0004-6361/201834211

Kervella, P., Gallenne, A., Remage Evans, N., et al. 2019, A&A, 623, A116. doi:10.1051/0004-6361/201834210

Kochukhov, O., Johnston, C., Alecian, E., et al. 2018, MNRAS, 478, 1749. doi:10.1093/mnras/sty1118

Kochukhov, O., Johnston, C., Labadie-Bartz, J., et al. 2021, MNRAS, 500, 2577. doi:10.1093/mnras/staa3472

Kolláth, Z., Molnár, L., & Szabó, R. 2011, MNRAS, 414, 1111. doi:10.1111/j.1365-2966.2011.18451.x

Kolláth, Z. 2018, The RR Lyrae 2017 Conference. Revival of the Classical Pulsators: from Galactic Structure to Stellar Interior Diagnostics, 6, 137

Kovacs, G. 2018, A&A, 614, L4. doi:10.1051/0004-6361/201833181

Kovacs, G. 2025, A&A, 699, A20. doi:10.1051/0004-6361/202555264

Kraft, R. P. 1967, ApJ, Studies of Stellar Rotation. V. The Dependence of Rotation on Age among Solar-Type Stars, 150, 551. doi:10.1086/149359

Krtička, J., Benáček, J., Budaj, J., et al. 2024, Space Science Reviews, 220, 2, 24. doi:10.1007/s11214-024-01058-1

Kunder, A., Prudil, Z., Monachesi, A., et al. 2025, AJ, 170, 3, 173. doi:10.3847/1538-3881

Kurtz, D. W. 2022, Annual Review of Astronomy and Astrophysics, 60, 31. doi:10.1146/annurev-astro-052920-094232

Lampens, P., Frémat, Y., Vermeylen, L., et al. 2018, A&A, 610, A17. doi:10.1051/0004-6361/201730694

Le Borgne, J. F., Paschke, A., Vandenbroere, J., et al. 2007, A&A, 476, 307. doi:10.1051/0004-6361:20077957

Lee, Y.-W., Demarque, P., & Zinn, R. 1990, ApJ, 350, 155. doi:10.1086/168370

Lee, Y.-W. 1991, ApJ, 367, 524. doi:10.1086/169649

Lee, U. & Saio, H. 2020, MNRAS, 497, 4117. doi:10.1093/mnras/staa2250

Lee, U. 2021, MNRAS, 505, 1495. doi:10.1093/mnras/stab1433

Lemasle, B., Lala, H. N., Kovtyukh, V., et al. 2022, A&A, 668, A40. doi:10.1051/0004-6361/202243273

Li, L.-J., Qian, S.-B., & Zhu, L.-Y. 2022, MNRAS, 510, 4, 6050. doi:10.1093/mnras/stab3808

Lightkurve Collaboration, Cardoso, J. V. de M., Hedges, C., et al. 2018, Astrophysics Source Code Library. ascl:1812.013

Liska, J. & Skarka, M. 2015, Open European Journal on Variable Stars, 169, 38.

Liška, J., Skarka, M., Mikulášek, Z., et al. 2016, A&A, 589, A94. doi:10.1051/0004-6361/201525870

Liška, J., Skarka, M., Zejda, M., et al. 2016, MNRAS, 459, 4360. doi:10.1093/mnras/stw851

Liska, J. & Skarka, M. 2016, Commmunications of the Konkoly Observatory Hungary, 105, 209

Lipták, J., Skarka, M., Guenther, E., et al. 2024, arXiv:2408.06897. doi:10.48550/arXiv.2408.06897

Majewski, S. R., Schiavon, R. P., Frinchaboy, P. M., et al. 2017, AJ, 154, 3, 94. doi:10.3847/1538-3881/aa784d

Maxted, P. F. L., Gaulme, P., Graczyk, D., et al. 2020, MNRAS, 498, 332. doi:10.1093/mnras/staa1662

McQuillan, A., Mazeh, T., & Aigrain, S. 2014, ApJS, Rotation Periods of 34,030 Kepler Main-sequence Stars: The Full Autocorrelation Sample, 211, 2, 24. doi:10.1088/0067-0049/211/2/24

Michaud, G., Charland, Y., Vauclair, S., et al. 1976, ApJ, 210, 447. doi:10.1086/154848

Mikulášek, Z., Krtička, J., Henry, G. W., et al. 2011, A&A, 534, L5. doi:10.1051/0004-6361/201117784

Mikulášek, Z., Semenko, E., Paunzen, E., et al. 2022, A&A, 668, A159. doi:10.1051/0004-6361/202243622

Molnár, L. & Szabados, L. 2014, MNRAS, 442, 3222. doi:10.1093/mnras/stu1091

Molnár, L., Bódi, A., Pál, A., et al. 2022, ApJS, 258, 8. doi:10.3847/1538-4365/ac2ee2

Mombarg, J. S. G. 2023, A&A, 677, A63. doi:10.1051/0004-6361/202345956

Murphy, S. J., Hey, D., Van Reeth, T., et al. 2019, MNRAS, 485, 2, 2380. doi:10.1093/mnras/stz590

Murphy, S. J., Saio, H., Takada-Hidai, M., et al. 2020, MNRAS, 498, 4272. doi:10.1093/mnras/staa2667

Ngeow, C.-C., Bhardwaj, A., Dekany, R., et al. 2022, AJ, 163, 5, 239. doi:10.3847/1538-3881/ac617e

Nielsen, M. B., Gizon, L., Schunker, H., et al. 2013, A&A, Rotation periods of 12 000 main-sequence Kepler stars: Dependence on stellar spectral type and comparison with v sin i observations, 557, L10. doi:10.1051/0004-6361/201321912

Niemczura, E., Hümmerich, S., Castelli, F., et al. 2017, Scientific Reports, 7, 5906. doi:10.1038/s41598-017-05987-6

Paunzen, E. 2020, Contributions of the Astronomical Observatory Skalnate Pleso, 50, 570. doi:10.31577/caosp.2020.50.2.570

Paunzen, E., Niemczura, E., Kołaczek-Szymański, P. A., et al. 2020, Contributions of the Astronomical Observatory Skalnate Pleso, 50, 621. doi:10.31577/caosp.2020.50.2.621

Petit, P., Lignières, F., Aurière, M., et al. 2011, A&A, 532, L13. doi:10.1051/0004-6361/201117573

Preston, G. W. 1974, Annual Rev. Astron. Astrophys., 12, 257. doi:10.1146/annurev.aa.12.090174.001353

Prša, A., Conroy, K. E., Horvat, M., et al. 2016, ApjS, 227, 2, 29. doi:10.3847/1538-4365/227/2/29

Prudil, Z. & Skarka, M. 2017, MNRAS, 466, 2602. doi:10.1093/mnras/stw3231

Prudil, Z., Skarka, M., Liška, J., et al. 2019, MNRAS, 487, L1. doi:10.1093/mnrasl/slz069

Prudil, Z., Hanke, M., Lemasle, B., et al. 2021, A&A, 648, A78. doi:10.1051/0004-6361/202140422

Prudil, Z., Debattista, V. P., Beraldo e Silva, L., et al. 2025, A&A, 699, A349. doi:10.1051/0004-6361/202554819

Quentin, L. G. & Tout, C. A. 2018, MNRAS, 477, 2, 2298. doi:10.1093/mnras/sty770

Qin, L., Luo, A.-L., Hou, W., et al. 2019, ApJS, 242, 13. doi:10.3847/1538-4365/ab17d8

Rauer, H., Aerts, C., Cabrera, J., et al. 2024, arXiv:2406.05447. doi:10.48550/arXiv.2406.05447

Rathour, R. S., Smolec, R., & Netzel, H. 2021, MNRAS, 505, 4, 5412. doi:10.1093/mnras/stab1603

Ricker, G. R., Winn, J. N., Vanderspek, R., et al. 2015, Journal of Astronomical Telescopes, Instruments, and Systems, 1, 014003. doi:10.1117/1.JATIS.1.1.014003

Riess, A. G., Casertano, S., Yuan, W., et al. 2021, ApJL, 908, L6. doi:10.3847/2041-8213/abdbaf

Rimoldini, L., Holl, B., Gavras, P., et al. 2023, A&A, 674, A14. doi:10.1051/0004-6361/202245591

Royer, F., Zorec, J., & Gómez, A. E. 2007, A&A, Rotational velocities of A-type stars. III. Velocity distributions, 463, 2, 671. doi:10.1051/0004-6361:20065224

Rüdiger, G., Küker, M., Käpylä, P. J., et al. 2019, A&A, 630, A109. doi:10.1051/0004-6361/201935280

Saio, H. 2005, MNRAS, 360, 1022. doi:10.1111/j.1365-2966.2005.09091.x

Saio, H., Kurtz, D. W., Murphy, S. J., et al. 2018, MNRAS, 474, 2774. doi:10.1093/mnras/stx2962

Samus, N. N., Kazarovets, E. V., & Durlevich, O. V. 2001, Odessa Astronomical Publications, 14, 266.

Samus', N. N., Kazarovets, E. V., Durlevich, O. V., et al. 2017, Astronomy Reports, General catalogue of variable stars: Version GCVS 5.1, 61, 1, 80. doi:10.1134/S1063772917010085

Shapley, H. 1916, ApJ, 43, 217. doi:10.1086/142246

Shultz, M. E., Johnston, C., Labadie-Bartz, J., et al. 2019, MNRAS, 490, 4154. doi:10.1093/mnras/stz2846

Shvartzvald, Y., Waxman, E., Gal-Yam, A., et al. 2024, ApJ, 964, 1, 74. doi:10.3847/1538-4357/ad2704

Schneider, F. R. N., Podsiadlowski, P., Langer, N., et al. 2016, MNRAS, 457, 2355. doi:10.1093/mnras/stw148

Sikora, J., David-Uraz, A., Chowdhury, S., et al. 2019, MNRAS, 487, 4695. doi:10.1093/mnras/stz1581

Šipková, E. 2025, Masaryk University, https://is.muni.cz/auth/th/md355/thesis.pdf, MSc thesis

Šipková, E., Skarka, M., Vaňko, M., et al. 2025, , arXiv:2512.22341. doi:10.48550/arXiv.2512.22341

Skarka, M. 2013, A&A, 549, A101. doi:10.1051/0004-6361/201220398

Skarka, M., Liška, J., Auer, R. F., et al. 2016, A&A, 592, A144. doi:10.1051/0004-6361/201628855

Skarka, M. & Cagas, P. 2017, Information Bulletin on Variable Stars, 6229, 1. doi:10.22444/IBVS.6229

Skarka, M., Liška, J., Dřevěný, R., et al. 2018, MNRAS, 474, 824. doi:10.1093/mnras/stx2737

Skarka, M., Kabáth, P., Paunzen, E., et al. 2019, MNRAS, 487, 4230. doi:10.1093/mnras/stz1478

Skarka, M., Prudil, Z., & Jurcsik, J. 2020, MNRAS, 494, 1237. doi:10.1093/mnras/staa673

Skarka, M., Prudil, Z., & Jurcsik, J. 2021, RR Lyrae/Cepheid 2019: Frontiers of Classical Pulsators, 529, 130

Skarka, M., Žák, J., Fedurco, M., et al. 2022, A&A, 666, A142. doi:10.1051/0004-6361/202244037

Skarka, M. & Henzl, Z. 2024, A&A, 688, A25. doi:10.1051/0004-6361/202450711

Skarka, M., Lipták, J., Niemczura, E., et al. 2025, A&A, 698, A48. doi:10.1051/0004-6361/202452341

Smalley, B., Antoci, V., Holdsworth, D. L., et al. 2017, MNRAS, 465, 2662. doi:10.1093/mnras/stw2903

Smolec, R. 2016, 37th Meeting of the Polish Astronomical Society, 3, 22. doi:10.48550/arXiv.1603.01252

Smolec, R. 2017, MNRAS, 468, 4299. doi:10.1093/mnras/stx679

Sódor, Á., Szeidl, B., & Jurcsik, J. 2007, A&A, 469, 1033. doi:10.1051/0004-6361:20066886

Sódor, Á., Skarka, M., Liška, J., et al. 2017, MNRAS, 465, 1, L1. doi:10.1093/mnrasl/slw194

Soszyński, I., Udalski, A., Szymański, M. K., et al. 2014, AcA, 64, 177. doi:10.48550/arXiv.1410.1542

Soszyński, I. 2024, Contributions of the Astronomical Observatory Skalnate Pleso, 54, 2, 234. doi:10.31577/caosp.2024.54.2.234

Sterken, C. 2005, The Light-Time Effect in Astrophysics: Causes and cures of the O-C diagram, 335, 3

Szczygieł, D. M. & Fabrycky, D. C. 2007, MNRAS, 377, 1263. doi:10.1111/j.1365-2966.2007.11678.x

Szeidl, B., Jurcsik, J., Sódor, Á., et al. 2012, MNRAS, 424, 3094. doi:10.1111/j.1365-2966.2012.21461.x

Tailo, M., Milone, A. P., Marino, A. F., et al. 2025, A&A, 695, A274. doi:10.1051/0004-6361/202452660

Thomson-Paressant, K., Neiner, C., & Labadie-Bartz, J. 2024, A&A, 689, A208. doi:10.1051/0004-6361/202450651

Trust, O., Jurua, E., De Cat, P., et al. 2020, MNRAS, 492, 3143. doi:10.1093/mnras/stz3623

Tutukov, A. V. & Fedorova, A. V. 2010, Astronomy Reports, 54, 156. doi:10.1134/S1063772910020083

Udalski, A., Szymanski, M., Kaluzny, J., et al. 1992, AcA, 42, 253

Udalski, A., Szymański, M. K., & Szymański, G. 2015, AcA, 65, 1, 1. doi:10.48550/arXiv.1504.05966

Van Reeth, T., De Cat, P., Van Beeck, J., et al. 2022, A&A, 662, A58. doi:10.1051/0004-6361/202142921

Vida, K., Oláh, K., Kővári, Z., et al. 2019, ApJ, 884, 160. doi:10.3847/1538-4357/ab41f5

Vidal, J., Cébron, D., ud-Doula, A., et al. 2019, A&A, 629, A142. doi:10.1051/0004-6361/201935658

Wade, R. A., Donley, J., Fried, R., et al. 1999, AJ, 118, 2442. doi:10.1086/301109

Wang, J., Shi, J., Fu, J., et al. 2024, ApJS, 272, 2, 31. doi:10.3847/1538-4365/ad43d5

Wang, K., Bu, Y., Zhang, Y., et al. 2025, ApJS, 280, 1, 37. doi:10.3847/1538-4365/adf2a0

Watson, C. L., Henden, A. A., & Price, A. 2006, Society for Astronomical Sciences Annual Symposium, 25, 47

Werner, N., Řípa, J., Thöne, C., et al. 2024, Space Science Reviews, 220, 1, 11. doi:10.1007/s11214-024-01048-3

Yan, H., Li, H., Wang, S., et al. 2022, The Innovation, 3, 100224. doi:10.1016/j.xinn.2022.100224

Zhao, G., Zhao, Y.-H., Chu, Y.-Q., et al. 2012, Research in Astronomy and Astrophysics, 12, 7, 723. doi:10.1088/1674-4527/12/7/002

Reprints of articles

Paper 1

The SERMON project: 48 new field Blazhko stars and an investigation of modulation-period distribution

A&A 592, A144 (2016)
DOI: 10.1051/0004-6361/201628855

Astronomy & Astrophysics

The SERMON project: 48 new field Blazhko stars and an investigation of modulation-period distribution

M. Skarka[1,2,3], J. Liška[2,3], R. F. Auer[3], Z. Prudil[2], A. Juráňová[2], and Á. Sódor[1]

[1] Konkoly Observatory, MTA Research Centre for Astronomy and Earth Sciences, Konkoly Thege Miklós út 15−17, 1121 Budapest, Hungary
e-mail: marek.skarka@csfk.mta.hu
[2] Department of Theoretical Physics and Astrophysics, Masaryk University, Kotlářská 2, 611 37 Brno, Czech Republic
[3] Variable Star and Exoplanet Section of the Czech Astronomical Society, Valašské Meziříčí, Vsetínská 78, 757 01 Valašské Meziříčí, Czech Republic

Received 4 May 2016 / Accepted 13 June 2016

ABSTRACT

Aims. We investigated 1234 fundamental mode RR Lyrae stars observed by the All Sky Automated Survey (ASAS) to identify the Blazhko (BL) effect. A sample of 1547 BL stars from the literature was collected to compare the modulation-period distribution with stars newly identified in our sample.
Methods. A classical frequency spectra analysis was performed using PERIOD04 software. Data points from each star from the ASAS database were analysed individually to avoid confusion with artificial peaks and aliases. Statistical methods were used in the investigation of the modulation-period distribution.
Results. Altogether we identified 87 BL stars (48 new detections), 7 candidate stars, and 22 stars showing long-term period variations. The distribution of modulation periods of newly identified BL stars corresponds well to the distribution of modulation periods of stars located in the Galactic field, Galactic bulge, Large Magellanic Cloud, and globular cluster M5 collected from the literature. As a very important by-product of this comparison, we found that pulsation periods of BL stars follow Gaussian distribution with the mean period of 0.54 ± 0.07 d, while the modulation periods show log-normal distribution with centre at $\log(P_{\rm m}\ [{\rm d}]) = 1.78 \pm 0.30$ dex. This means that 99.7% of all known modulated stars have BL periods between 7.6 and 478 days. We discuss the identification of long modulation periods and show, that a significant percentage of stars showing long-term period variations could be classified as BL stars.

Key words. stars: variables: RR Lyrae – stars: horizontal-branch – methods: statistical

1. Introduction

Together with ultra-precise space measurements from the *Kepler* and CoRoT telescopes, the large-scale surveys play crucial role in investigation of long-term amplitude and frequency (phase) modulation in RR Lyrae stars known as the Blazhko (BL) effect (Blažko 1907). Accurate space data helped uncover various dynamical processes present only in modulated stars (for example, period doubling (Szabó et al. 2010; Kolláth et al. 2011) and additional radial and non-radial modes Benkő et al. 2014; Szabó et al. 2014). Data from the ground-based surveys, on the other hand, are very useful for studying large samples statistically and investigating general and common characteristics of modulated stars (e.g. Alcock et al. 2003; Soszyński et al. 2011).

Both approaches are important in their own way because the nature of the BL effect has not been fully explained yet. The true percentage of modulated stars is still unknown (see e.g. Jurcsik et al. 2009; Kovács 2016). Even more interestingly, it is not clear why some stars show modulation and some with very similar physical properties do not (e.g. Skarka 2014b). Knowledge about characteristics of the BL effect is still insufficient to give a reliable answer to the question of if and how the pulsation period is connected with the length and amplitude of the modulation. Jurcsik et al. (2005a) showed that the modulation amplitude of short-pulsation-period RR Lyrae stars can be higher than for long-period stars. Benkő et al. (2014) and Benkő & Szabó (2015) suggest a monotonic dependence between the strength of amplitude modulation and the period of the BL cycle (the longer the cycle, the larger the amplitude). While the upper limit of the modulation length is still unclear, the bottom limit is probably defined by the upper limit of the rotational velocity of a star. RR Lyrae stars with short pulsation periods can have short modulation periods, while long-pulsation-period stars can only have a BL cycle that is longer than about 20 d (Jurcsik et al. 2005b).

Several studies report on the mode switching and (or) disappearing (reappearing) of the BL effect, suggesting that the phenomenon could be of temporal nature (see e.g. Szeidl 1976; Sódor et al. 2007; Goranskij et al. 2010; Jurcsik et al. 2012; Plachy et al. 2014). Many stars also show variations of their modulation cycles (see e.g. Guggenberger et al. 2012; Benkő et al. 2014; Szabó et al. 2014). In some BL stars, for example in RR Lyrae itself, the modulation reappears cyclically during an additional four-year cycle (Detre & Szeidl 1973; Le Borgne et al. 2014; Poretti et al. 2016). There are many more interesting features of the BL effect. Extensive reviews of the BL effect are provided in recent overviews by Szabó (2014), Kovács (2016), and Smolec (2016).

In his study based on the brightest RRab stars observed by the All Sky Automated Survey (ASAS; e.g. Pojmański 1997, 2001) and the Super Wide Angle Search for Planets

(SuperWASP; Pollacco et al. 2006), Skarka (2014a) revealed the shortcomings of current automated procedures dedicated for the search for the BL effect and the need for permanent supervision of all steps when analysing noisy ground-based data dominated by various aliases. His study also showed that there are many undiscovered modulated stars even in previously studied data sets. Because frequency analysis and searching for the manifestations of the BL effect in many targets individually is a very time-consuming task, we establish a new group involving professionals, students, and amateur astronomers that aim to analyse data from various surveys. The project was called SERMON which is the abbreviation of SEarch for Rr lyraes with MOdulatioN.

In this paper we focus on RRab stars observed by ASAS that are brighter than 13.5 mag in maximum light to investigate their frequency spectra trying to reveal the BL effect. Because the ASAS data have special characteristics and need special handling, we describe these data in detail in Sect. 2. We also describe the sample selection in this section. Analysis, criteria for the detection of the BL effect and discussion about the sample stars are described in Sect. 3. In Sect. 4 we investigate the distribution of modulation periods. The results are discussed in Sect. 5, the content of the paper is summarized in Sect. 6.

2. The ASAS data

The ASAS-3 survey is performed by small-aperture telescopes that are primarily dedicated to search for new variables among stars with declination below +28° (technical details can be found in Pojmański 2001). The telescopes regularly scan the sky, and typically observe a particular object once per a few days with a three-minute exposure in *V* filter.

The publicly available data typically contain several hundreds of data points, which are marked with flags from A (the best quality) to D (the worst quality). The photometry often consists of several blocks in the data files because each star is usually observed in a few different fields. Magnitudes with errors are provided in five apertures with diameter between 2 and 6 pixels. The time span of the data is about 3300 days in most cases.

The philosophy of the survey has a deep impact on data characteristics. Low sampling rate causes the frequency spectra to be strongly dominated by daily aliases (Fig. 1). Because the angular resolution of the ASAS instruments is very low (about 15 arcsec/pixel), even with the smallest aperture the light of the target star could be influenced by neighbouring star(s), which is (are) closer than 30 arcsec. This fact could seriously bias the data. We discuss this problem in detail in Appendix A. An extensive overview of the ASAS data characteristics can be found in Pigulski (2014).

2.1. The sample selection and data cleaning

This paper represents the extension of the study by Skarka (2014a) with fainter stars and stars with more scattered data. To some extend it complements the analysis by Szczygieł & Fabrycky (2007) who performed an automatic search on the full sample of all types of RR Lyrae stars in the ASAS Catalogue of Variable Stars (ACVS).

The selection process started with the International Variable Star indeX catalogue (VSX; Watson et al. 2006, version from 27th October, 2014), in which 1760 stars of RRab type with maximum light brighter than 13.5 mag and declination below +28° were listed. The declination limit is given by the observational

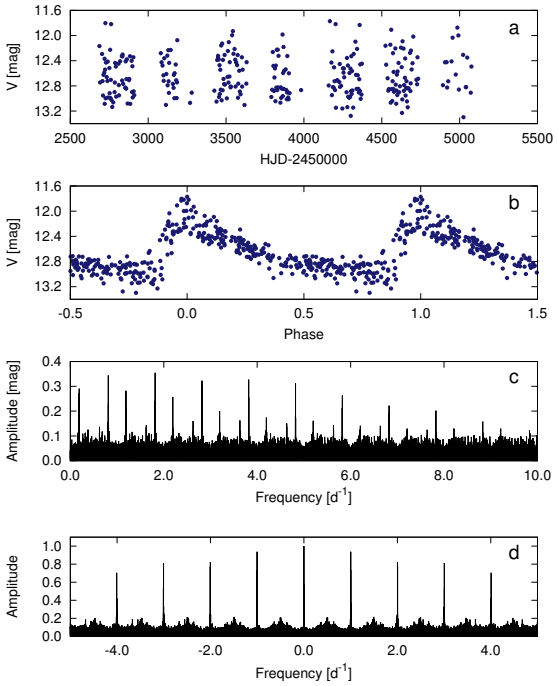

Fig. 1. Typical ASAS data demonstrated on V1124 Her. Panels **a)** and **b)** show the data distribution and data phased with the basic pulsation period. Panel **c)** shows corresponding frequency spectrum; panel **d)** shows the spectral window.

constraints of the ASAS survey. The magnitude limit was chosen according to several tests as the most limiting for reliable analysis because the scatter steeply increases with decreasing brightness. The corresponding photometric error of a data point at 13.5 mag is about 0.15 mag (Pojmański 2002).

Stars analysed by Skarka (2014a) were ignored. Then we checked for the availability of the data via the online VSX tools. This resulted in 1435 stars that were observed by ASAS. After downloading the data, we obtained a basic idea about the quality of the data, checked for possible blends in the area with diameter of 30 arcsec, and made a note (col. Blend in Tables 1, B.4, B.5, and col. Rem in Table 2). We used only data with flags A and B in aperture with the smallest average photometry error. Possible shifts in the mean magnitude between blocks were ignored because of the poor data sampling and problems with blends. All points that differed more than 1.5 mag from the median value were automatically removed. No other automatic procedure was applied for improving the data to avoid possible misinterpretation because, for example, scatter caused by modulation could be very easily confused with observational scatter.

In the next step, all stars with less than 150 points were discarded. Then we performed a visual inspection of all light curves again, and searched for the basic pulsation period in stars where the value given in VSX was not reliable. In stars where suitable period was found (or was available in VSX) obvious outliers were manually deleted. Stars with extremely scattered data were removed from the sample. This kind of pre-analysis gave us an idea about some peculiarities in the objects and allowed us to identify duplicates (Sect. 3.4) and stars of different variable types (Sect. 3.5). Together with these peculiar objects the sample for further analysis contained 1234 stars.

Table 1. Stars identified as modulated for the first time.

ID	$P_{\rm Puls}$ [d]	$P_{\rm m}$ [d]	*S/N*	Blend	*N*	*TS* [d]	Rem
ASAS J103622-3722.1	0.468036(2)	86.2(4)	4.8		553	3289	
CH Aps	0.509710(7)	730(40)	3.9		616	3176	
ASAS J211737+0011.8	0.489135(4)	43.59(14)	4.0	+	295	3235	
OW Aqr	0.655187(2)	172(2)	4.3		404	3254	
V0356 Aqr	0.554594(2)	41.65(6)	4.7		440	3219	
V0522 Cen	0.623662(2)	2100(240)	3.9		582	3187	
V0570 Cen	0.604507(8)	65.35(32)	3.6		470	3170	
BW CMa	0.526804(2)	45.89(12)	6.7	+	530	3299	
ASAS J112830-2429.7	0.678271(2)	11.37(2)	3.9	+	840	3172	
NSV 1888	0.458739(2)	980(60)	4.2		708	3248	
RT Equ	0.444761(10)	106.8(8)	4.2		366	2921	+
BE Eri	0.579536(4)	57.38(12)	6.5		380	3214	
WZ Gru	0.536766(4)	27.35(4)	4.7		360	3261	
ASAS J175143+1708.4	0.435601(4)	6.67(2)	3.8	+	610	2404	
V1332 Her	0.522353(4)	21.59(4)	3.9		435	2404	
ASAS J023020-5908.1	0.572857(4)	29.85(4)	5.3		714	3279	
UW Hor	0.662156(14)	300(8)	5.2		560	3297	
ASAS J094115-1348.8	0.467569(8)	101.0(6)	4.7	+	295	3141	
ASAS J104924-2812.5	0.574553(4)	93.3(6)	5.1		571	3299	
ASAS J110733-2944.1	0.526282(4)	63.48(20)	5.1		592	3154	
ASAS J145702-2642.6	0.586273(8)	75.26(36)	4.2	+	419	3170	
NSV 14546	0.349662(2)	1070(60)	4.4		733	3294	
ASAS J151317-1445.9	0.613006(4)	43.33(8)	6.8	+	588	2965	
CU Lib	0.506956(6)	121.6(8)	4.6	+	473	3175	+
AC Men	0.553409(4)	120.2(8)	4.5	+	380	3288	
ASAS J055109-7219.4	0.558809(4)	168.3(16)	4.4		634	3296	
ASAS J095835-8311.7	0.543469(2)	243(2)	8.4		1344	3294	
BN Oct	0.508267(2)	23.93(4)	5.2		580	3275	
EE Oct	0.444320(2)	175.9(16)	4.5		750	3293	
XZ Oct	0.473867(2)	26.00(4)	4.9		739	3251	
CSS J165728.3+055825	0.592147(2)	406(8)	5.9		343	2959	
FU Pav	0.454554(6)	206(4)	4.0		280	3215	
GV Pav	0.575562(4)	109.4(6)	5.2		481	3215	
NSVS 11726192	0.576882(8)	31.61(6)	4.1		388	3239	
SS Pic	0.494099(2)	61.86(14)	5.9		621	3287	
RR Pyx	0.491078(4)	30.17(4)	5.2	+	878	3295	
AK Scl	0.494987(2)	94.2(6)	5.5		558	3283	
CN Scl	0.585871(4)	1270(80)	4.2		600	3286	+
V0484 Ser	0.511390(4)	119(1)	3.6		324	2946	
ASAS J181510-3545.7	0.579472(4)	127.7(6)	5.2	+	1200	3174	
ASAS J193321-2517.6	0.507410(2)	55.7(2)	4.4	+	438	3132	+
V1069 Sgr	0.478929(6)	206(2)	5.3	+	501	3067	
V2281 Sgr	0.479455(6)	180(2)	3.8	+	360	3271	
ASAS J185332-5133.3	0.611209(8)	432(10)	3.9		466	3155	
ASAS J162246-6723.5	0.543464(2)	85.7(4)	4.7	+	909	3181	
UX Tuc	0.509089(8)	50.25(16)	4.2	+	288	3254	
V0420 Vel	0.605077(2)	66.38(10)	10.2	+	598	3299	
ASAS J073358-6508.1	0.538119(6)	113.2(8)	3.9	+	510	3299	

Notes. Columns $P_{\rm Puls}$ and $P_{\rm m}$ give pulsation and modulation periods and corresponding 2σ errors in the last digits; Col. *S/N* gives the signal-to-noise ratio; Col. Blend gives information about nearby stars; Cols. *N* and *TS* give the number of data points and the time span of the data. Stars denoted with "+" in Col. Rem are suspected of multiple modulation or additional long-period variation.

3. Analysis and identification of the BL stars

A mathematical description of simultaneous amplitude and phase (frequency) modulation suggests the rise of an additional peak with modulation frequency ($f_{\rm m}$) and equidistant peaks near the basic pulsation frequency components ($kf_0 \pm f_{\rm m}$; for details see Benkő et al. 2011; Szeidl et al. 2012). This equidistant spacing is equivalent to $f_{\rm m}$. Because the presence of the side peaks in the frequency spectra is the most distinct and convincing evidence of the BL effect, which is also detectable in scattered data, we searched for this feature using PERIOD04 software (Lenz & Breger 2005). Owing to the characteristics of the data, it was necessary to pay special attention to properly identify correct peaks and avoid possible confusion with aliases.

It is likely that variable contamination with parasite light from nearby stars entering the aperture could resemble the amplitude modulation in some of the sample stars. In such cases, the mean magnitude and total amplitude of the light variations varies in time and produces conspicuous peak in the low-frequency range of the frequency spectrum. A visual check of the data itself would not help much because of large scatter and poor sampling, and statistics fails too for the same reasons. Therefore, the only way to reveal this issue is to identify the false modulation peak. No such peak was observed in any of the sample stars, however, we cannot exclude that some of the stars could be influenced by this problem. This is one of the reasons why we give the information about blends in the tables.

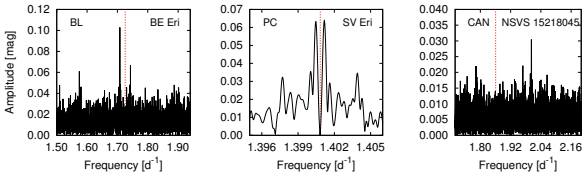

Fig. 2. Typical frequency spectra after prewhitening with the basic pulsation components for BL stars, PC, and candidate stars (from *left to the right*). The position of the basic pulsation frequency is shown with the red dashed line.

A star was marked as a BL star when a peak with $S/N > 3.5$ in the interval of $f_0 \pm 0.2$ c/d was identified. It was found by Nagy & Kovács (2006) that in stars with frequency separation of less than $1.5/TS$ (periods longer than $2/3TS$), where TS is the time span of the data, it is impossible to distinguish unambiguously between BL modulation and long-term continuous period change (instability) of the main pulsation period (i.e. period-change stars, PC class, as described in the next paragraph). Therefore, only peaks with separation larger than $1.5/TS$ were considered a consequence of the BL effect. An example of the frequency spectrum for a BL star is shown in the left-hand panel of Fig. 2, where an equidistant triplet is seen.

The second category that we adopted is a PC group. Stars assigned to this group are usually those showing either unresolved peaks (peaks with frequency distance lower than $1/TS$), or it is impossible to prewhiten the peaks in a few consecutive steps (Alcock et al. 2000; Nagy & Kovács 2006). Following our period limit for BL stars, each star with frequency separation lower than $1.5/TS$ was assigned to PC class as well. However, it is sometimes difficult to properly decide about BL/PC category, thus, we adopted these conservative criteria to make sure that PC stars do not contaminate significantly our BL sample (see also the discussion in Sect. 5). A typical frequency spectrum of a PC star is shown in the middle panel of Fig. 2.

Finally, we use candidate category for stars that would belong to the BL group, but the peaks have amplitudes under the detection limit or very close to integer daily frequencies (1 c/d, 2 c/d etc., the right-hand panel of Fig. 2).

3.1. Stars with the BL effect

An online version of the BlaSGalF database[1] containing Galactic field RR Lyrae stars with the BL effect reported in literature contains 58 stars from our sample (version from 29th February, 2016, Skarka 2013). We detected the side peak in only 39 of these stars (see Table B.4). One of these 58 stars belongs to our candidate category, one was found to be of different variability type, and one star is a PC star. In remaining 16 stars we did not detect any peak possibly related to modulation (see Table B.1).

Although we cannot be sure in 100 percent of the stars, we assume, that the nondetection of the BL effect is a consequence of the data characteristics rather then the result of absence of the BL effect. We found two reasons for that. First, the noise level of the residuals after removing significant frequencies is typically between 0.01 and 0.02 mag, which means that sometimes side peaks with amplitude below ~0.07 mag do not fulfil $S/N > 3.5$. Second, some of the stars surely showed large-amplitude BL effect at the times when ASAS gathered the data. For example, Jurcsik et al. (2009) easily detected the modulation in the frequency spectra of AQ Lyr and UZ Vir using high-quality photometric observations gathered with a 60-cm telescope between 2004 and 2009. They also did not detect any clear sign of modulation in ASAS and NSVS data that is confirmed by our analysis. In any case, the nondetection of the BL effect in ASAS data should not be considered as a proof of the absence of the modulation.

In 48 stars the BL effect was detected for the first time (see Table 1). In addition to the information about pulsation and modulation periods resulting from our analysis (Cols. 2 and 3) and corresponding errors in the last digits in parentheses, we give information about nearby stars closer than 30 arcsec (18 objects with "+" in col. 5 named Blend), and about the number of data points and the time span of the data (Cols. 6 N and 7 TS). Four stars denoted with "+" in the last column Rem, in which we detected additional, either unresolved, or unique peaks close to kf_0, are suspected of multiple modulation (category νM from Alcock et al. 2003 and MC from Nagy & Kovács 2006), or additional long-period variation. Instead of amplitudes of the side peaks, which could be influenced by nearby stars, we give S/N in the fourth column. Errors of periods (in all tables) are 2σ formal uncertainties from the least-squares fitting method.

All data of newly identified modulated stars phased with the modulation periods from Table 1 are shown in Fig. 3. In most of the stars the modulation envelope is well apparent. This figure also shows a variety of envelope shapes and modulation amplitudes. Some of the stars, for example ASAS J181510-3545.7 and V0420 Vel, have very small total amplitudes compared to the other stars, which is most likely a result of blends with nearby stars.

3.2. Stars with unresolved peaks

Our 22 PC stars are listed in Table 2. The modulation periods suggested by the frequency spacing range from 1900 d in BK Eri to 4000 d in SV Eri. The latter is a star with the most rapid period

Table 2. Stars showing close, unresolved peaks near f_0 that were marked as PC.

ID	$P_{\rm Puls}$ [d]	$P_{\rm m}$ [d]	S/N	N	TS [d]	Rem
DI Aps	0.519187(6)	2700(300)	7.7	509	3212	
ASAS J204705-0919.2	0.508809(6)	2500(200)	6.7	369	3146	+
ASAS J083815-6025.9	0.465751(5)	2400(400)	5.9	550	3293	b
QZ Cen	0.502052(6)	2200(200)	6.1	634	3188	b
V0584 Cen	0.459032(2)	3200(600)	5.0	418	3153	
RS Crv	0.536834(6)	2200(200)	6.0	727	3169	
BK Eri	0.548148(4)	1900(100)	4.9	363	3243	+
SV Eri	0.713861(4)	2800(100)	10.0	536	3296	
NSV 14009	0.563985(6)	3000(200)	6.4	585	3256	
ASAS J054843-1627.0*	0.376709(4)	3000(200)	7.9	544	3299	b
PS Lup	0.471878(2)	3200(400)	5.7	663	3191	+
V0898 Mon	0.541493(12)	2200(200)	5.0	316	3078	b
ASAS J160612-4319.2	0.356944(2)	2800(200)	8.0	639	3194	b
ASAS J165834-8458.6	0.549312(6)	3200(500)	5.1	561	3241	
V0455 Oph	0.453893(2)	2200(400)	3.6	377	2586	b
KV Pav	0.527929(6)	4000(600)	6.9	528	3289	
V0338 Pav	0.530827(6)	2600(400)	4.4	330	3273	b
ASAS J075127-4136.3	0.335716(2)	3000(300)	6.8	610	3296	b
V0687 Pup	0.575194(8)	2500(300)	5.8	483	3246	b
ASAS J200147-2153.8	0.546631(14)	2500(400)	4.3	562	3144	b
ASAS J190713-5205.7	0.526724(2)	3100(600)	4.0	725	3173	
GR Tel	0.611916(4)	2900(400)	4.9	696	3134	b

Notes. The notation of the columns is the same as in Table 1. The star with "*" is known to the literature as a BL star. Blended stars are marked with "b" and stars with additional peaks are marked with "+" in the column Rem.

[1] http://physics.muni.cz/~blasgalf/

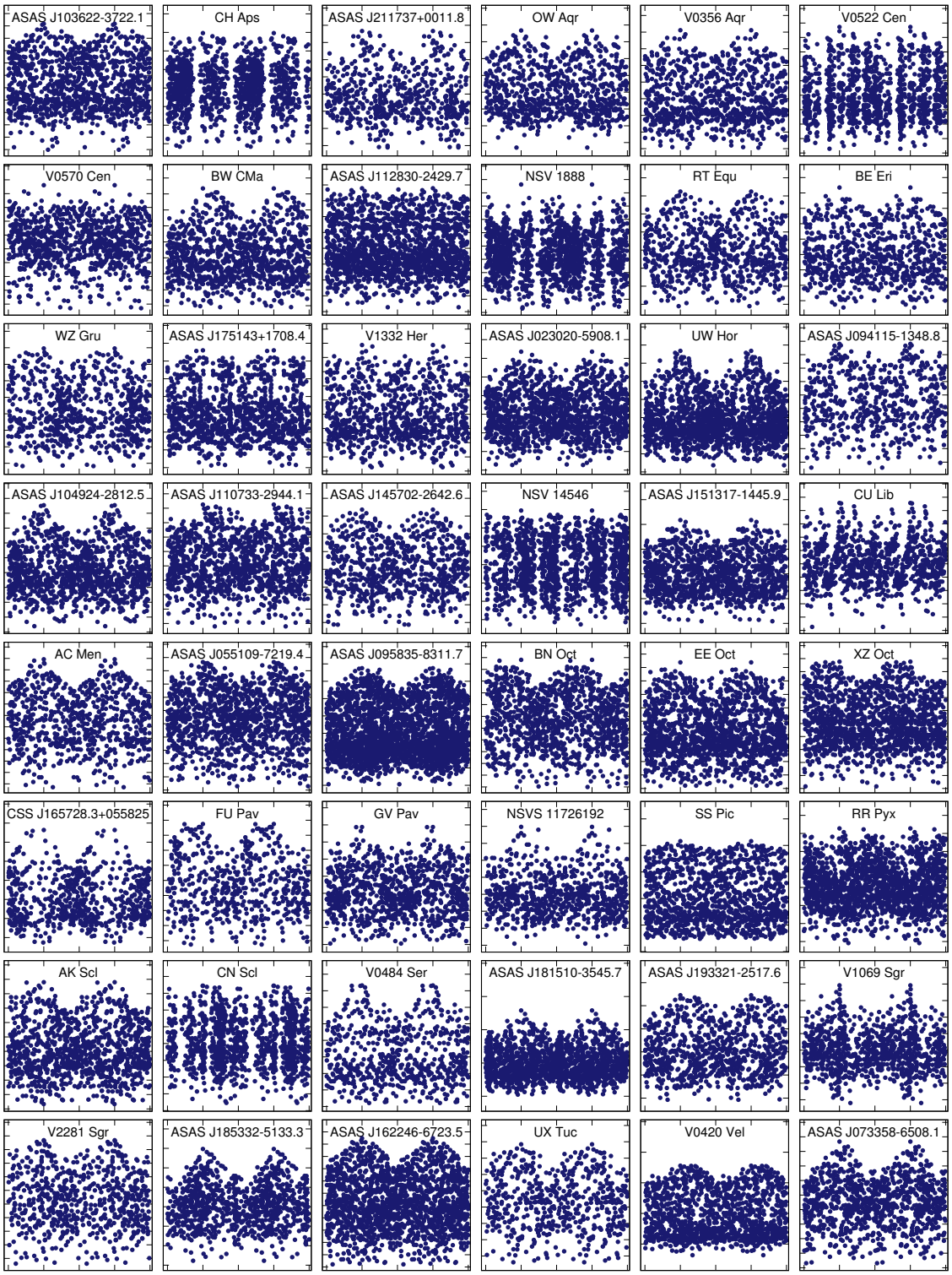

Fig. 3. BL stars phased with modulation periods from Table 1. As the zero epoch we simply took HJD of the brightest data point. Ticks at the ordinate show interval of 0.2 mag, at abscissa the interval is 0.5 in BL phase.

change known among RR Lyrae stars so far (Poretti et al. 2016). When the data are phased with the suggested modulation periods, DI Aps, QZ Cen, V0584 Cen, NSVS 14009, V0898 Mon, and V0687 Pup show apparent amplitude changes. It may be possible that in a data set with long enough time span, these stars will turn out to be classical BL stars with very long modulation periods (see also Sect. 5 and Fig. 7.)

Short pulsation periods of ASASJ 054843-1627.0, J160612-4319.2 and their low amplitude and phase Fourier coefficients (transformed to I-band filter) suggest that they are of RRc type when compared to characteristics of Galactic bulge RR Lyrae parameters provided by Soszyński et al. (2011).

3.3. Candidates for BL stars

In seven stars we noticed peaks within $f_0 \pm 0.2$ c/d, but we mark them as candidates from the reasons discussed previously. In YZ Aps, NSVS 15218045 (see Fig. 2), ASAS J054238-2557.3, and V1211 Sgr, the suspicious peaks were very close to integer multiples of 1 c/d, which is always problematic. In ASAS J081549-0732.9 and ASAS J194745-4539.7 only peaks with $S/N < 3.5$ were detected.

3.4. Duplicates

During our analysis we identified three stars as duplicates because a star with a different ID is located almost at the same coordinates and it has similar pulsation (variability) properties. Actually, this was a trigger to perform a detail analysis of this problem regarding the total VSX catalogue (Liška et al. 2015). Our duplicates are given in Table B.3.

3.5. Stars with different variable type

In 24 stars (Table B.2 in Appendix B) we detected no signs of variability, 19 other stars are probably not RRab stars, but we suspect that they are of different variability type (Table B.5, Fig. B.1). We give suggested variability types that were estimated on the basis of period, light-curve shape, and $B - V$ (Table B.5, Fig. B.1).

3.6. Characteristics of sample BL stars

The percentage of all BL stars in our sample (both known + new detections) is very low, at slightly less than 7%. The reason is a large scatter that could hider the modulation, rather than a real lack of modulated stars among faint stars. Therefore, this number has nothing to do with the real amount of modulated stars, but only gives information about the detectability of modulation in the data set. Our assumption is reinforced by the look of the magnitude distribution of the sample stars shown in Fig. 4 (see the percentages above bins). The highest number of BL stars was detected between 12.5 and 13.0 mag [2] and decreases steeply in the most populated area with faint stars with scattered data.

In the majority of the new BL stars the modulation is very apparent causing large amplitude changes (e.g. BW CMa, V0484 Ser), while in some of the stars the modulation in amplitude is barely seen (e.g. NSV 14546, SS Pic, see Fig. 3). Even in scattered ASAS data, a wide palette of the shapes of modulation envelopes is apparent. In this sense, one of the most interesting examples is UW Hor, which seems to show non-sinusoidal amplitude modulation. On the other hand, BN Oct and ASAS J162246-6723.5 show nearly sinusoidal variations in amplitude. The BL peak f_m itself was detected only in BL Col, a known BL star. In four new BL stars and three PC stars we detected additional peaks, which could be interpreted as additional modulation, or signs of additional period change. Unfortunately, the low quality of the data does not allow us to investigate these peculiarities in detail.

[2] The percentage is not the highest in this magnitude range.

4. Modulation-period distribution

To get an idea about the new BL stars, we collected a sample of 1547 fundamental mode stars with estimated modulation period from the literature. This sample contains RRab stars from the Galactic field (246 stars from the BlaSGalF database; Skarka 2013), the LMC (731 stars; Alcock et al. 2003), the Galactic bulge (19+526 stars; Moskalik & Poretti 2003; Collinge et al. 2006), and globular cluster M5 (25 stars; Jurcsik et al. 2011). We considered all periods in stars with multiple modulation. For example, from RS Boo we have three values on our list. Together with our new detections (48), it amounts 1628 entries, which is, to our knowledge, the most extended sample of modulation periods investigated so far.

The modulation periods of newly identified BL stars (black circles in the top panel of Fig. 5) match the distribution very well, and no sample star has extreme modulation period[3]. Two of our stars with the shortest modulation period, ASAS J175143+1708.4 and ASAS J112830-2429.7, however, seem to significantly differ from the general trend. The BL effect in these two stars should be proved independently. Light curve shape, pulsation period of only about 0.35 d, and its Fourier parameters suggest that NSV 14546 could be an RRc-type rather than RRab-type star.

To test the similarity of our sample with the sample of stars from literature, we performed the two-sample Kolmogorov-Smirnov test. The result is, that the agreement between the two populations cannot be ruled out with probability of 7%. Thus we can conclude that our sample stars have a similar distribution of modulation periods as BL stars from literature (see the cumulative-distribution functions in the right-hand panel of Fig. 6).

However, the modulation-period distribution in Fig. 5 itself is far more interesting than the distribution of new BL stars[4]. While pulsation periods show a distribution close to the normal Gaussian distribution (the bottom part of the top panel in Fig. 5), modulation periods follow the log-normal distribution. In other words, they show normal distribution when the BL periods are plotted in logarithmic scale, which is nicely seen from the bottom panel of Fig. 5 and histograms in the left-hand panel of Fig. 6. The mean pulsation period of BL stars is 0.54 ± 0.07 d, and the mean modulation period based on the log-normal distribution is 1.78 ± 0.30 dex. This means that 99.7% (3σ interval) of all BL stars have modulation periods between 7.6 and 478 days.

5. Discussion

The log-normal distribution commonly appears in measured quantities that cannot be negative. Many of natural, social, and

[3] The shortest BL period was detected in ASAS J175143+1708.4 (6.67 d), the longest in V0522 Cen (2100 d), which is exactly the limit for BL stars that we adopted (2/3TS).

[4] From here on we do not distinguish between new and known BL stars; all stars create one sample.

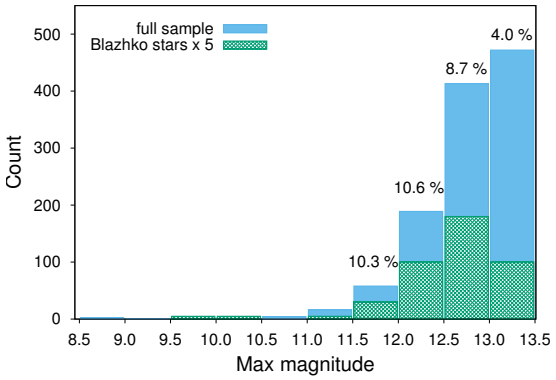

Fig. 4. Magnitude distribution of all sample stars (blue) and BL stars (green grid). The distribution of modulated stars was enlarged five times for better visibility.

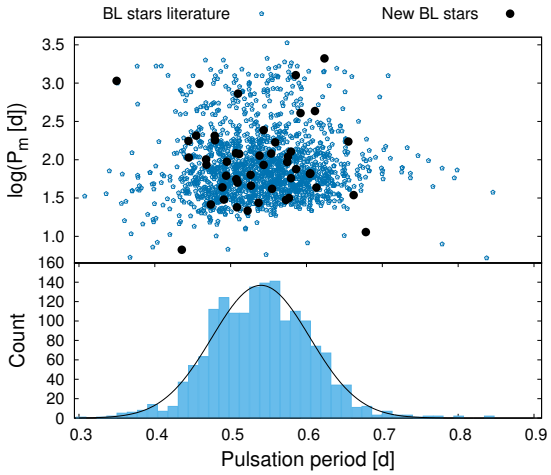

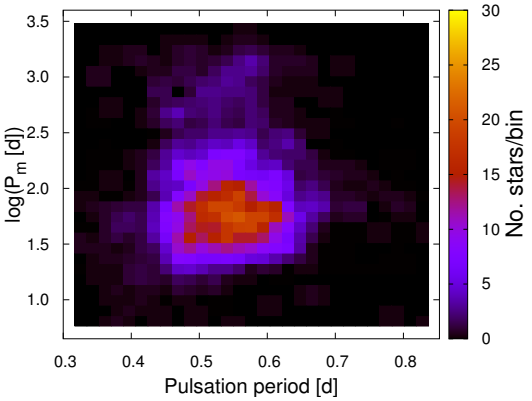

Fig. 5. BL period as a function of the pulsation period for known and new modulated stars (*top*), and corresponding density plot (*bottom*). The bottom part of the *top panel* shows the distribution of pulsation periods.

technical systems and quantities show such distribution, for example the length of a latent infection (from infection to burst of the disease), species abundance, age of marriage, and probability of failure of mechanical devices (nice examples across the disciplines can be found in Limpert et al. 2001). The question is why the pulsation periods have Gaussian distribution, while modulation periods show log-normal distribution. Why do the majority of BL stars have modulation periods between 30 and 120 days (1σ interval)? At the present time, it is impossible to answer this question because no correlation between any of the physical characteristics and the length of the modulation period has been found.

The selection effects only have minor impact on the distribution, if any. The majority of used BL stars come from the data sets with time span that is several years long, where the modulation periods of several hundreds of days should be safely detectable. Yearly aliases cause problems with identification only in a very small part of the distribution (see the gap around 350 d in the top insert in the left-hand panel of Fig. 6). Thus we are convinced that the log-normal distribution is real. The very good agreement between the cumulative-distribution function for the periods in this interval and the normal distribution with the same parameters also confirms our assumption (the insert in the right-hand panel of Fig. 6).

It seems that the log-normal distribution only represents the short-period part of the modulation period distribution well (0−400 d), which has a long tail towards longer modulation periods. However, the distribution of the longest BL periods, which is probably much more numerous than our collection shows, is somewhat uncertain from several reasons. First, the entire sample is sharply cut at BL periods of about $\log P_{\rm m} \sim 3.5$ (~3300 d). This limit is given by the extension of the longest data used for modulation period estimation (the ASAS-3 data with maximum time span of about 3300 days). Data from MACHO survey has time span of about 7.5 yrs. It can be naturally expected that the distribution continues to even longer modulation periods because we do not know the upper limit. What is probably the longest BL effect with period longer than 25 yrs is reported by Jurcsik & Smitola (2016) in V144 in globular cluster M3.

Recent observational investigations (e.g. Benkő et al. 2014) showed that the BL stars always show both amplitude and phase variations. The BL stars could then be identified through the variations in amplitude even when the modulation period is comparable with *TS*, or longer. For example, V0898 Mon and V0687 Pup from our sample (top panels of Fig. 7) show significant amplitude changes with suggested periods that are a bit longer than 2/3*TS*. Although the modulation periods are only very roughly estimated in these stars, the BL-phased light curves suggest, that they could safely be considered BL stars.

Another uncertainty relies in the problems with the BL/PC classification. Although secular period changes and nonstationarity in pulsation period are quite common among RR Lyrae stars (see e.g. Le Borgne et al. 2007), we can expect a significant number of PC stars to be classified as BL stars in long-enough data sets. This is, for example, the case of OGLE-BLG-RRLYR-07697 and OGLE-BLG-RRLYR-06232. These two stars were classified as pure PC stars by Collinge et al. (2006) on the basis of the four-year-long OGLE-II data. In OGLE-III data (Soszyński et al. 2011), with a time span of about 12 yrs, these two stars appeared to be clear BL stars showing significant amplitude modulation with periods of 1300 and 2200 d (the middle panels of Fig. 7). In OGLE-BLG-RRLYR-07697 the side peaks were easily prewhitenable[5]. In OGLE-BLG-RRLYR-06232 we detected additional, unresolved structures very close

[5] The star shows additional BL modulation with period of 36.48 d.

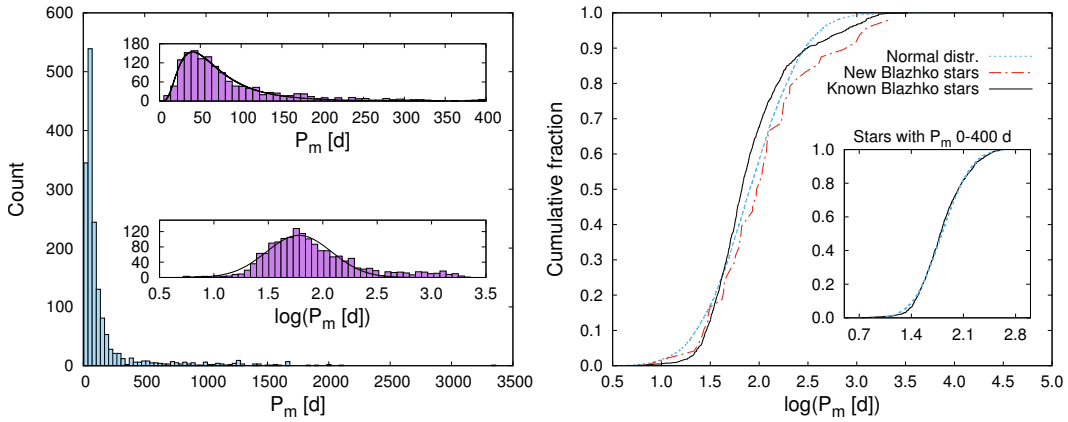

Fig. 6. Distribution of modulation periods (*left-hand panel*) and cumulative distribution functions (*right-hand panel*). It is apparent that the overall distribution follows the log-normal distribution. The agreement with the normal distribution for stars with modulation periods between 0 and 400 days shown in the insert in the right-hand panel is very good.

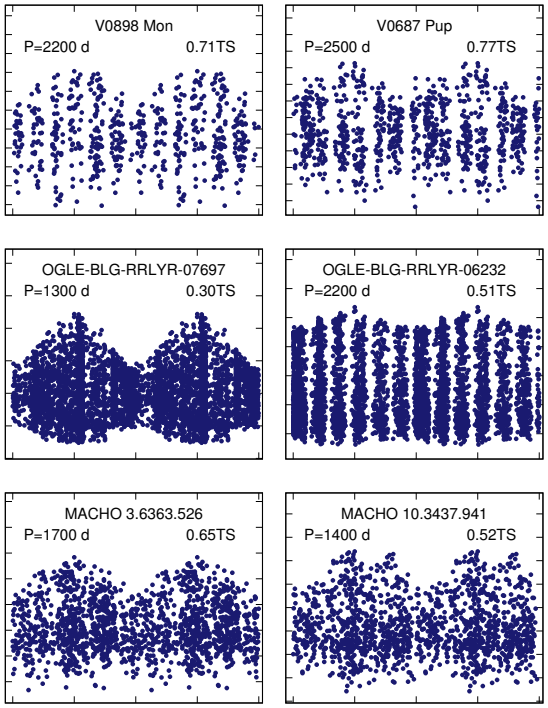

Fig. 7. Stars originally classified as pure PC. There are stars from our sample in the *top panels*. The *middle panels* show OGLE-III data demonstrating that in long-enough data sets (original classification comes from OGLE-II data with three-times shorter time span) the stars could be classified as BL stars, not pure PC stars. The *bottom panels* show two stars that clearly show amplitude modulation with periods shorter than $2/3TS$ suggesting classification as BL+PC, not pure PC. The scales of the axes are the same as in Fig. 3.

to f_0, which cannot be fully eliminated, thus, suggesting some additional period variations. According to the criteria adopted in Sect. 3, this star should be classified as both BL and PC star.

Further, we also suppose that stars showing dense patterns close to f_0, which cannot be prewhitened in a few steps, do not necessarily exclude the possibility of being BL stars. In the bottom panel of Fig. 7 we see two stars identified as pure PC stars on the basis of MACHO data (Alcock et al. 2003). Both of these stars clearly show large amplitude modulation with periods shorter than $2/3TS$. Thus, there is no reason why we do not assign them to the BL class with a possible additional PC component. It would be advisable to strictly distinguish between unresolved peaks close to f_0, which could mean instability of the main pulsation period, and other unresolved peaks near the side peaks, which in turn could mean the nonstationarity of the modulation itself, additional modulation, or some artificially generated periodicity in the data. In such cases the star should be classified as BL star with additional PC, rather then pure PC.

As many previous investigations show (LaCluyzé et al. 2004; Sódor et al. 2007; Detre & Szeidl 1973; Szeidl 1976; Le Borgne et al. 2014; Guggenberger et al. 2012), the BL modulation itself can change on year-long time scale. Although the ASAS and MACHO data sets span rather long time bases, they typically do not contain sufficient number of data points to investigate such details. Therefore, many stars with changing BL modulation might remain undetected or classified as PC stars. These very few examples show that the distribution of modulation periods that are longer than ~1000 d is certainly more populated than we see in Fig. 6.

6. Summary and conclusions

We performed an in-depth study of frequency spectra of 1234 fundamental RR Lyrae stars observed by the ASAS survey, placing emphasis on proper identification of possible modulation. Therefore, we investigated each target individually within a new project SERMON employing professionals, amateurs, and students. We omitted stars with a low number of points (<150) and scattered light curves with insufficient quality for period analysis. The limiting magnitude was set to 13.5 in maximum light because of large scatter of the data in faint stars.

The criteria for accepting a star as modulated were purely on the basis of the appearance of the frequency spectra. In this sense we establish three groups: (i) BL stars: stars with peak with $S/N > 3.5$ in the vicinity of f_0, no closer than $1/TS$, but closer than 0.2 c/d; (ii) BL candidates: stars with one suspicious peak at integer daily frequencies, or with peaks close to f_0 with

$S/N < 3.5$; and (iii) PC: stars with unresolved side peaks or with a separation of the peaks suggesting modulation periods that are longer than $2/3TS$. Altogether we detected 87 BL stars, 48 of these stars for the first time. Even in low-cadence ASAS data with large scatter we observed a variety of possible shapes of modulation envelopes (Fig. 3). We also detected 7 candidates and 22 PC stars. When we put together stars from the ASAS-3 survey analysed by Skarka (2014a) with the sample analysed in this study, the detection efficiency of individual approach is about 12% in ASAS data, which is more than two times better than in Szczygieł & Fabrycky (2007)[6].

For the comparison of newly identified BL stars, we collected a sample comprising 1547 stars with known BL periods from literature. The distribution of modulation periods of newly identified stars corresponds well to the distribution of periods of known BL stars. As a by-product of this analysis, we noticed that the pulsation periods of BL stars follow Gaussian distribution (mean 0.54 ± 0.07 d), while the modulation periods are distributed log-normally with mean $\log P_{\rm m}[{\rm d}] = 1.78 \pm 0.30$ dex. Especially modulation periods in range 0–400 d follow the log-normal distribution well.

Behind its log-normal part ($P_{\rm m} > 480$ d), the distribution shows an almost constant number of stars per bin, however, this could be simply observational bias caused by the lack of suitable data with long-enough time span. Additional ambiguity comes from the difficulties in properly assigning a star to the PC or BL class. From our discussion about long-term modulation, it follows that stars showing amplitude modulation with period shorter than $2/3TS$ can be safely classified as BL stars, no matter whether there are additional peaks that cannot be prewhitened. These unresolved peaks simply mean that some additional non-stationarity is present in the star, not that the star is unmodulated. Therefore, the classification criteria for PC stars could be revised and summarized in two simple points: (i) the separation of the side peaks and f_0 is lower than $1.5/TS$, whether or not the peaks are prewhitenable and (ii) the star shows no apparent amplitude changes. Combined data sets, for example OGLE-III and OGLE-IV, could shed more light on the problem with PC stars and allow us to establish more firm criteria.

The reasons standing behind the log-normal distribution are, unfortunately, unclear. Could there be any connection between the length of modulation period and evolutionary stadium, metallicity, and Oosterhoff groups? These questions would need a deep-in detailed investigation, which is out of scope of our study.

Acknowledgements. We are very grateful to Johanna Jurcsik and Géza Kovács for their very useful comments on the first version of the manuscript. We also thank the referee for his/her useful suggestions. The financial support of the Hungarian National Research, Development and Innovation Office – NKFIH K-115709 is acknowledged. M.S. acknowledges the support of the postdoctoral fellowship programme of the Hungarian Academy of Sciences at the Konkoly Observatory as a host institution. In addition to the mentioned grant, Á.S. acknowledges financial support of the OTKA K-113117 grants, and the János Bolyai Research Scholarship of the Hungarian Academy of Sciences. This research has made use of the International Variable Star Index (VSX) database, operated at AAVSO, Cambridge, Massachusetts, USA, SIMBAD and VizieR catalogue databases, operated at CDS, Strasbourg, France, and NASA's Astrophysics Data System Bibliographic Services.

References

Alcock, C., Allsman, R., Alves, D. R., et al. 2000, ApJ, 542, 257
Alcock, C., Alves, D. R., Becker, A., et al. 2003, ApJ, 598, 597
Benkő, J. M., & Szabó, R. 2015, Eur. Phys. J. Web Conf., 101, 06008
Benkő, J. M., Szabó, R., & Paparó, M. 2011, MNRAS, 417, 974
Benkő, J. M., Plachy, E., Szabó, R., Molnár, L., & Kolláth, Z. 2014, ApJS, 213, 31
Blažko, S. 1907, Astron. Nachr., 175, 325
Bonnardeau, M., & Hambsch, F.-J. 2015, Information Bulletin on Variable Stars, 6132, 1
Bramich, D. M., Alsubai, K. A., Arellano Ferro, A., et al. 2014, Information Bulletin on Variable Stars, 6106, 1
Chadid, M., Benkő, J. M., Szabó, R., et al. 2010, A&A, 510, A39
Collinge, M. J., Sumi, T., & Fabrycky, D. 2006, ApJ, 651, 197
de Ponthière, P., Hambsch, F.-J., Krajci, T., Menzies, K., & Wils, P. 2013, J. American Association of Variable Star Observers (JAAVSO), 41, 58
de Ponthière, P., Hambsch, F.-J., Menzies, K., & Sabo, R. 2014, J. American Association of Variable Star Observers (JAAVSO), 42, 298
Detre, L., & Szeidl, B. 1973, Information Bulletin on Variable Stars, 764, 1
Goranskij, V., Clement, C. M., & Thompson, M. 2010, in Variable Stars, the Galactic Halo and Galaxy Formation, eds. C. Sterken, N. Samus, & L. Szabados (Moscow: Sternberg Astronomical Institute of Moscow Univ.), 115
Guggenberger, E., Kolenberg, K., Nemec, J. M., et al. 2012, MNRAS, 424, 649
Hajdu, G., Catelan, M., Jurcsik, J., et al. 2015, MNRAS, 449, L113
Jurcsik, J., & Smitola, P. 2016, Commmunications of the Konkoly Observatory Hungary, 105, 167
Jurcsik, J., Sódor, Á, & Váradi, M. 2005a, Information Bulletin on Variable Stars, 5666, 1
Jurcsik, J., Szeidl, B., Nagy, A., & Sódor, Á 2005b, Acta Astron., 55, 303
Jurcsik, J., Sódor, Á., Szeidl, B., et al. 2009, MNRAS, 400, 1006
Jurcsik, J., Szeidl, B., Clement, C., Hurta, Z., & Lovas, M. 2011, MNRAS, 411, 1763
Jurcsik, J., Hajdu, G., Szeidl, B., et al. 2012, MNRAS, 419, 2173
Jurcsik, J., Smitola, P., Hajdu, G., & Nuspl, J. 2014, ApJ, 797, L3
Khruslov, A. V. 2011, Peremennye Zvezdy Prilozhenie, 11
Kolláth, Z., Molnár, L., & Szabó, R. 2011, MNRAS, 414, 1111
Kocián, R., Liška, J., Skarka, M., et al. 2012, Open Eur. J. Variable Stars, 154, 1
Kovács, G. 2005, A&A, 438, 227
Kovács, G. 2016, Communications from the Konkoly Observatory, 105, 61
LaCluyzé, A., Smith, H. A., Gill, E.-M., et al. 2004, AJ, 127, 1653
Le Borgne, J. F., Paschke, A., Vandenbroere, J., et al. 2007, A&A, 476, 307
Le Borgne, J. F., Poretti, E., Klotz, A., et al. 2014, MNRAS, 441, 1435
Lenz, P., & Breger, M. 2005, Comm. Asteroseismol., 146, 53
Liška, J., Skarka, M., Auer, R. F., Prudil, Z., & Juráňová, A. 2015, Open Eur. J. Variable Stars, 170, 1
Limpert, E., Stahel, W. A., Abbt, M. 2001, BioScience, 51, 5
Moskalik, P., & Poretti, E. 2003, A&A, 398, 213
Nagy, A., & Kovács, G. 2006, A&A, 454, 257
Pigulski, A. 2014, Precision Asteroseismology, 301, 31
Plachy, E., Benkő, J. M., Kolláth, Z., Molnár, L., & Szabó, R. 2014, MNRAS, 445, 2810
Pojmański, G. 1997, AcA, 47, 467
Pojmański, G. 2001, IAU Colloq. 183: Small Telescope Astronomy on Global Scales, 246, 53
Pojmański, G. 2002, Acta Astron., 52, 397
Pollacco, D. L., Skillen, I., Collier Cameron, A., et al. 2006, PASP, 118, 1407
Poretti, E., Le Borgne, J.-F., Klotz, A., Audejean, M., & Hirosawa, K. 2016, Commmunications of the Konkoly Observatory Hungary, 105, 73
Skarka, M. 2013, A&A, 549, A101
Skarka, M. 2014a, A&A, 562, A90
Skarka, M. 2014b, MNRAS, 445, 1584
Smolec, R. 2016, ArXiv e-print [arXiv:1603.01252]
Sódor, Á., Szeidl, B., & Jurcsik, J. 2007, A&A, 469, 1033
Sódor, Á., Hajdu, G., Jurcsik, J., et al. 2012, MNRAS, 427, 1517
Soszyński, I., Dziembowski, W. A., Udalski, A., et al. 2011, Acta Astron., 61, 1
Szabó, R. 2014, IAU Symp., 301, 241
Szabó, R., Kolláth, Z., Molnár, L., et al. 2010, MNRAS, 409, 1244
Szabó, R., Benkő, J. M., Paparó, M., et al. 2014, A&A, 570, A100
Szczygieł, D. M., & Fabrycky, D. C. 2007, MNRAS, 377, 1263
Szeidl, B. 1976, IAU Colloq. 29: Multiple Periodic Variable Stars, 60, 133
Szeidl, B., Hurta, Zs., Jurcsik, J., Clement, C., & Lovas, M. 2011, MNRAS, 411, 1744
Szeidl, B., Jurcsik, J., Sódor, Á., Hajdu, G., & Smitola, P. 2012, MNRAS, 424, 3094
Walker, A. R., & Nemec, J. M. 1996, AJ, 112, 2026
Watson, C. L., Henden, A. A., & Price, A. 2006, 25th Annual Symp., The Society for Astronomical Sciences, 47
Wils, P., & Sódor, Á. 2005, Information Bulletin on Variable Stars, 5655, 1
Wils, P., Lloyd, C., & Bernhard, K. 2006, MNRAS, 368, 1757
Zacharias, N., Finch, C. T., Girard, T. M., et al. 2013, AJ, 145, 44

[6] It is worth noting that they analysed data with a time span two years shorter than our data sample.

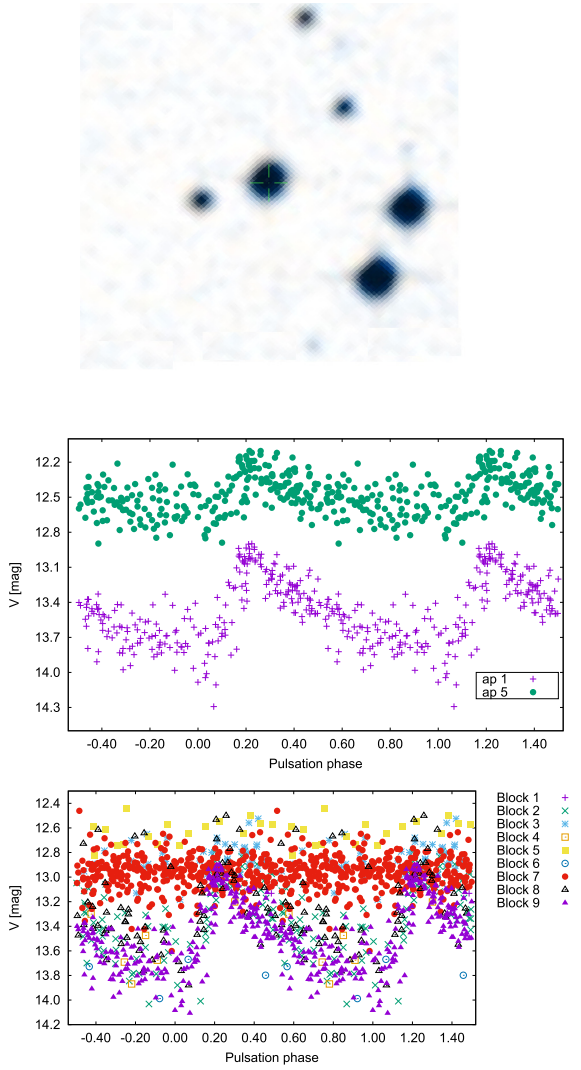

Fig. A.1. ASAS data of CSS J054243.2-114742 (star in the centre of the *top panel*) phased with elements given in VSX. The *middle panel* demonstrates problems caused by large aperture, the *bottom panel* shows confusing the target with nearby stars in different fields (blocks of data).

Appendix A: Blend troubles

We demonstrate the problem with blends on CSS J054243.2-114742, where three similarly bright stars and three additional fainter stars are present within area with diameter of 1.5 arcmin = 6 pixels in ASAS (the top panel of Fig. A.1). The data set of this star comprises nine blocks of data points in ASAS-3 database. The middle panel of Fig. A.1 shows how the data from block 9 differs in apertures 1 and 5. It is obvious that in the largest aperture the light contribution of all neighbouring stars is taken into account. This results in higher brightness and lower pulsation amplitude in aperture 5 (6 pixels) than in aperture 1 (2 pixels).

An additional problem caused by close stars could arise from the combination of different fields. The bottom panel of Fig. A.1 shows the measurements in aperture 1 for different blocks of the data set. It is apparent that in different fields (blocks 3, 5, 7) the variable star was mistaken for one of the close nonvariable stars. Only blocks 2 and 9 probably show the data for the target star exclusively.

Appendix B: Additional tables and figures

Table B.1. Known BL stars where we did not detect the modulation.

ID	$P_{\rm Puls}$ [d]	*S/N*	$P_{\rm literature}$ [d]	Ref.
AL Eri	0.656947(4)	3.3	–	K05
ASAS J030534-3116.1	0.496453(2)	3.2	6.67	SF07
V0461 Her	0.513006(6)	3.0	–	B14
V1162 Her	0.547929(6)	3.3	–	B14
GL Hya	0.505932(4)	3.4	157	B14
V0487 Hya	0.561482(6)	3.2	64.4	B14
ASAS J101200+1921.9	0.482830(10)	3.3	1141.03	SF07
MS Lib	0.441446(8)	3.1	105	B14
AQ Lyr	0.356809(4)	3.2	64.9	J09
V0829 Oph	0.569222(8)	3.1	165	Wa06
V2683 Oph	0.597012(4)	2.9	26.28	SF07
V0606 Peg	0.529658(4)	2.9	26.7	B14
FI Psc	0.531285(6)	3.2	>170	B14
CzeV0245	0.513328(4)	3.0	–	K12
UZ Vir	0.459394(4)	3.3	68.24	J09, S12
ASAS J194502+2434.2	0.845945(22)	3.2	37.56	SF07

Notes. The column *S/N* gives information about *S/N* of the highest peak detected after removing significant pulsation components in the vicinity of $f_0 \pm 0.2$ c/d. Ref: K05 – Kovács (2005); SF07 – Szczygieł & Fabrycky (2007); B14 – Bramich et al. (2014); J09 – Jurcsik et al. (2009); Wa06 – Watson et al. (2006); K12 – Kocián et al. (2012); S12 – Sódor et al. (2012).

Table B.2. Stars in which we cannot find any sign of variability or detect any period.

ID	ID
2MASS J06533015+1531072	NSVS 9525696
CSS J163942.1+223202	V0429 Ori
CSS J102417.2+161949	CSS J225023.1+171307
CSS J150035.2-165444	ASAS J004535+0526.1
CSS J150917.1-170252	MM Pup
CSS J153512.2-145339	NSVS 19123091
NSVS 12552884	NSVS 19168136
NSVS 15305366	V0713 Sco
CSS J164808.5+012515	ASAS J185602-1934.6
OGLE BLG-RRLYR-00252	NSVS 19562915
V0771 Oph	OGLE BLG-RRLYR-16496
CSS J053340.7-021532	V0701 Sgr

Table B.3. Stars with duplicate occurrence in VSX (the same coordinates and pulsation properties).

ID	Coord. (J2000)
ASAS J165728+0558.4	16 57 28.42 +05 58 25.5
CSS J165728.3+055825	16 57 28.39 +05 58 25.7
CSS J160717.1-063352	16 07 17.12 −06 33 53.0
V0681 Oph	16 07 15.33 −06 34 18.1
CSS J213502.5+195641	21 35 02.59 +19 56 41.7
ASAS J213502+1956.7	21 35 02.61 +19 56 41.0

Table B.4. Known BL stars from literature detected in our ASAS sample.

ID	$P_{\rm Puls}$ [d]	$P_{\rm m}$ [d]	*S/N*	Blend	*N*	*TS* [d]	$P_{\rm literature}$ [d]	Ref.
CK Aps	0.623640(5)	56.4(2)	3.9	+	887	3205	–	K05
KM Aql	0.438191(4)	192(2)	4.7		384	3162	192.2	SF07
PQ Aqr	0.512292(4)	120.3(9)	4.5		362	3144	–	B14
V0354 Aqr	0.529555(6)	182(1)	6.2		398	3291	181.2	SF07
ASAS J172721-5305.9	0.435434(2)	58.5(2)	4.8		615	3171	58.66	SF07
ASAS J123812-4422.5	0.523543(6)	1540(120)	6.6	+	534	3162	1307.7	SF07
ASAS J135813-4215.1	0.523179(3)	145(1)	5.3	+	492	3197	146.01	SF07
GW Cet	0.516652(4)	84.2(4)	4.1		462	3278	84.99	SF07
ASAS J053830-3554.4 = BL Col	0.590761(4)	40.53(6)	6.3		583	3289	40.05	K11
AI Crt	0.502901(4)	63.0(2)	5.8		622	3176	63	WS05
V0365 Her	0.613178(10)	40.8(1)	4.5	+	224	2396	40	W06
V1124 Her	0.551018(4)	38.92(6)	6.4	+	296	2388	38.8	B14
RV Hor	0.572496(4)	79.7(3)	5.8	+	512	3264	79.81	SF07
ASAS J093731-1816.2	0.520920(8)	87.7(3)	6.0		320	3294	87.73	SF07
ASAS J141025-2244.8	0.639874(4)	1700(100)	7.3		567	3186	1556.66	SF07
V0430 Hya	0.496828(2)	58.5(3)	4.6		363	3109	56.6	B14
V0486 Hya	0.508644(4)	53.4(2)	4.0		405	3286	18.5	B14
V0543 Hya	0.598263(6)	58.8(2)	5.2		668	3299	59	B14
CZ Ind	0.605147(4)	133(1)	4.1		462	3257	133.38	SF07
V0550 Peg	0.493047(13)	21.98(4)	4.0		219	3235	348.58	SF07
V1820 Ori	0.479040(6)	27.95(2)	6.5		364	2625	27.917	dP13
ASAS J185719-6321.4	0.412008(2)	63.0(2)	4.6		496	3149	61.39	SF07
CS Phe	0.484395(4)	61.2(2)	5.9		530	3287	62.5	WS05
NSV 0539 = DR Dor	0.460421(2)	40.10(4)	7.0		515	3256	40.17	SF07
AL Pic	0.548618(6)	34.13(6)	5.0	+	404	3287	34.07	dP14
NSV 1856	0.516080(2)	742(14)	8.4		1018	3248	786.91	SF07
FR Psc	0.455680(4)	51.47(8)	5.8		305	3240	51.31	dp14
NSV 3331 = V0714 Pup	0.494182(2)	119.4(7)	7.2		893	3272	116.96	SF07
BT Sco	0.548718(4)	39.11(8)	4.6		508	3167	78	WS05
AR Ser	0.575213(8)	1325(60)	6.3		463	3167	109	WS05
V5659 Sgr	0.379706(4)	45.58(8)	5.9	+	488	3134	45.7	WS05
ASAS J153830-6906.4	0.622472(6)	117.9(6)	5.9	+	660	3209	1702.13	SF07
EP Tuc	0.615003(6)	63.0(2)	4.0		451	3274	63	WS05
BQ Vir	0.637027(4)	50.8(1)	4.4		805	3160	–	K05
V0354 Vir	0.595045(8)	49.0(2)	4.0		407	3168	59	W06
V0551 Vir	0.446854(8)	53.0(2)	4.6	+	289	2941	48	W06
V0574 Vir	0.474391(8)	25.71(4)	4.1	+	227	3099	26.3	B14
V0585 Vir	0.601611(4)	94.1(5)	4.7	+	574	3183	93.8	B14
V0586 Vir	0.682773(4)	134(1)	4.0	+	517	3174	132	B14

References. The notation of the columns is the same as in Table 1. Ref: K05 – Kovács (2005); SF07 – Szczygieł & Fabrycky (2007); B14 – Bramich et al. (2014); W06 – Wils et al. (2006); K11 – Khruslov (2011); WS05 – Wils & Sodor (2005); dP13 – de Ponthière et al. (2013); dP14 – de Ponthière et al. (2014); BH15 – Bonnardeau & Hambsch (2015).

Table B.5. Stars of different variability type originally classified as RRab stars in VSX.

ID	P [d]	Type	Blend	$B-V$ [mag]	N	TS [d]	Remarks
NSVS 14248877	0.99842(4)	E:	+	1.2	344	2939	
ASAS J134527-3616.8	4.77429(10)	CEP		1.1	164	1008	
ASAS J142204-3404.3	0.773789(6)	CEP		1.0	141	998	
ASAS J020345-1729.1	4.089(12)	CEP		1.1	455	3296	
NSVS 15925156	1.06135(4)	CEP		1.1	580	3293	jump in amplitude at 2 453 500
ASAS J205934+1812.7	3.24610(4)	CEP	+	1.2	491	2422	
ASAS J040615-3050.0	1.32465(4)	CEP		0.9	593	3300	
ASAS J144908-1150.8	119.907(2)	M	+	1.6	494	3174	
CSS J153535.3-155042	0.121131(8)	DSCT		0.9	499	2966	amplitude only 0.1 mag
ASAS J202746-2850.5	0.408462(4)	RRC/EW		0.2	701	3250	additional period with 90 d
ASAS J053552-0508.2	2.82362(4)	CEP		1.2	754	3298	
ASAS J183333-6654.0	1.924273(4)	CEP	+	1.0	1066	3162	
CSS J222816.3+192154	0.140082(14)	DSCT		0.4	292	2366	amplitude only 0.1 mag
ASAS J085816-3022.1	1.90949(4)	ELL	+	1.8	598	3291	amplitude only 0.1 mag
NSVS 19229378	318(6)	LPV	+	0.7	447	3092	
AK Sct	189(4)	LPV	+	0.8	348	3119	
NSVS 19501853	319(2)	M	+	1.4	1476	3191	
ASAS J135447-1640.8	0.37225(4)	EW		0.8	480	3183	
ASAS J195215+1943.2	0.6169(6)	E:	+	0.5	277	2386	

Notes. Colour index is a rough value taken from Zacharias et al. (2013).

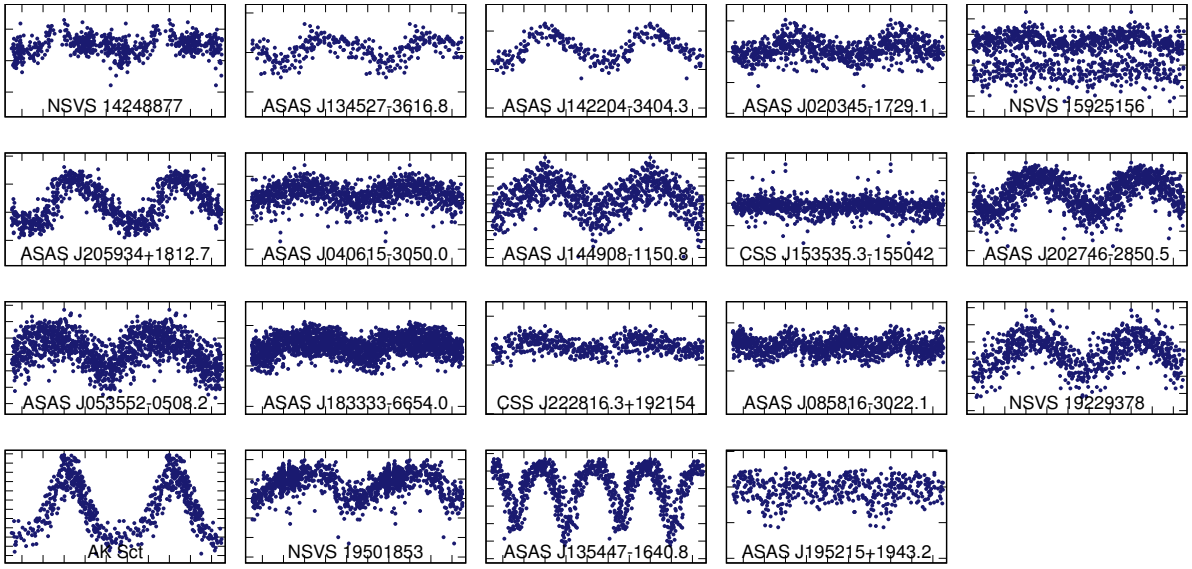

Fig. B.1. Stars misclassified as RRab stars in VSX identified in our sample. Data are phased with periods from Table B.5. The scales of axes are the same as in Fig. 3.

Paper 2

Blazhko effect in the Galactic bulge fundamental mode RR Lyrae stars I. Incidence rate and differences between modulated and non-modulated stars

Monthly Notices
of the
ROYAL ASTRONOMICAL SOCIETY

MNRAS **466,** 2602–2613 (2017) doi:10.1093/mnras/stw3231

Blazhko effect in the Galactic bulge fundamental mode RR Lyrae stars – I. Incidence rate and differences between modulated and non-modulated stars

Z. Prudil[1,2]★ and M. Skarka[3]

[1]*Department of Theoretical Physics and Astrophysics, Masaryk University, Kotlářská 2, 611 37 Brno, Czech Republic*
[2]*Astronomisches Rechen-Institut, Zentrum für Astronomie der Universität, Heidelberg, Mönchhofstr. 12-14, D-69120 Heidelberg, Germany*
[3]*Konkoly Observatory, Research Centre for Astronomy and Earth Sciences, Hungarian Academy of Sciences, Konkoly Thege Miklós út 15-17, H-1121 Budapest, Hungary*

Accepted 2016 December 8. Received 2016 December 6; in original form 2016 October 27

ABSTRACT

We present the first paper of a series focused on the Blazhko effect in RR Lyrae type stars pulsating in the fundamental mode that are located in the Galactic bulge. A comprehensive overview of the incidence rate and light-curve characteristics of the Blazhko stars is given. We analysed 8282 stars having the best quality data in the OGLE-IV survey, and found that at least 40.3 per cent of the stars show modulation of their light curves. The number of Blazhko stars we identified is 3341, which is the largest sample ever studied, implying that these are the most relevant statistical results currently available. Using combined data sets with OGLE-III observations, we found that 50 per cent of the stars that show unresolved peaks close to the main component in OGLE-IV are actually Blazhko stars with extremely long periods. Blazhko stars with modulation occur preferentially among RR Lyrae stars with shorter pulsation periods in the Galactic bulge. Fourier amplitude and phase coefficients based on the mean light curves appear to be substantially lower for Blazhko stars than for stars with an unmodulated light curve on average. We derived new relations for the compatibility parameter D_m in the I passband and relations that allow for differentiating modulated and non-modulated stars easily based on R_{31}, ϕ_{21} and ϕ_{31}. Photometric metallicities, intrinsic colours and absolute magnitudes computed using empirical relations are the same for Blazhko and non-modulated stars in the Galactic bulge, suggesting there is no correlation between the occurrence of the Blazhko effect and these parameters.

Key words: Methods: data analysis – methods: statistical – techniques: photometric – stars: horizontal branch – stars: variables: RR Lyrae.

1 INTRODUCTION

Horizontal-branch stars, which cross the classical instability strip, are known as RR Lyrae (RRL) stars. These radially pulsating stars have applications in many astrophysical fields (e.g. distance indicators, Catelan & Cortés 2008) and constitute the most numerous class of catalogued pulsating stars in our Galaxy and close galactic systems (e.g. Soszyński et al. 2014, 2016). Usually they are sorted according to their light-curve shapes, which result from the mode in which they pulsate, into three basic historical groups: RRab (asymmetric light curve, fundamental mode), RRc (more symmetric light curve, first-overtone mode) and RRd (fuzzy light curve, simultaneous fundamental and first-overtone mode pulsations).

A substantial portion of the RRab stars show amplitude and phase modulation of their light curves from days to thousands of days, which is known as the Blazhko (BL) effect (Blažko 1907). The mechanism behind the BL effect is still under discussion. Recent discoveries of dynamical phenomena (such as period doubling, e.g. Szabó et al. 2010) suggest that resonances between low- and high-order radial modes could play an important role in explaining the BL effect (Kolláth, Molnár & Szabó 2011; Buchler & Kolláth 2011). In addition, it seems that only modulated RRab stars show additional radial and non-radial pulsational modes (Benkő et al. 2014; Szabó et al. 2014).

However, we are still at the beginning of understanding the BL effect, and no connection between the physical characteristics of RRL stars and modulation has been reported so far. Simply, it is not known why some RRL stars show modulation and others with similar parameters do not. In addition, there is some indication that

★ E-mail: prudilz@ari.uni-heidelberg.de

the BL effect could actually be a temporary episodic phase in RRL life (e.g. Sódor, Szeidl & Jurcsik 2007; Jurcsik et al. 2012).

Estimates of the incidence rate of BL stars depend strongly on the data quality and time span of the data and the number of stars investigated, and they also differ for different stellar systems (see table 1 in Kovács 2016). For Galactic field RRLs, recent estimates are between 35 and 60 per cent (based on precise space data, Benkő et al. 2014; Szabó et al. 2014). This discrepancy shows that these estimates could be somewhat misleading due to the small number of stars available for the statistics.

There are many other unanswered questions surrounding the Blazhko phenomenon. Alcock et al. (2003), Jurcsik et al. (2011) and Skarka (2014a) reported slightly shorter pulsation periods of BL stars in comparison with non-BL stars, while Moskalik & Poretti (2003) found no difference. Some studies showed that modulated stars are slightly less luminous (Jurcsik et al. 2011; Skarka 2014a), but some show the opposite (e.g. Arellano Ferro et al. 2012). Contradictory results are also reported for metallicity estimates: Moskalik & Poretti (2003) suggested that the occurrence rate of BL stars increases with increasing metallicity, while Smolec (2005) and Skarka (2014a) found no metallicity dependence. However, the mentioned studies are based on various numbers of stars with different numbers of observations with different quality, in addition, they are for diverse stellar systems, which could intrinsically differ. Any comparison is, therefore, somewhat questionable. It is clear that for reliable statistics of any kind, a large and homogeneous sample of stars with good quality data is desired to reduce the selection effects and reasonably describe the overall characteristics of BL stars for a particular stellar system.

We utilized high-quality measurements of more than 8000 RRL stars from the Galactic bulge (GB) provided by the fourth generation of the Optical Gravitational Lensing Experiment (OGLE-IV, Udalski, Szymański & Szymański 2015), and searched for modulation. This data set is almost perfect for securing reliable statistical results on the BL effect: the observations are homogeneous (gathered with the same telescope and through a single filter), have very good quality, sufficient time span (4 + 12 yr from OGLE-II and OGLE-III if needed in some targets), and all observed stars belong to one, essentially homogeneous group of stars. After identifying the BL stars, we compared their periods and light curve characteristics with those of non-BL stars.

Note that in this study we have only identified BL stars and have not performed a detailed analysis of the modulation properties. Modulation periods, amplitudes and the relations between them will be elaborated in the second paper of the series by Skarka et al. (in preparation).

The article is organized as follows. Section 2 describes the data and sample selection criteria used in this investigation. Methods for analysing the observations are detailed in Section 3. The results for the occurrence rate and differences between BL and non-modulated stars are presented in Section 4. The results and future prospects are summarized in Section 5.

2 SAMPLE SELECTION

The OGLE survey is an ongoing long-term experiment managed by the University of Warsaw, Poland.[1] Since its beginning in the early 1990s, it has undergone a few substantial upgrades defining different phases of the survey (Udalski et al. 1992; Udalski, Kubiak & Szymanski 1997; Udalski 2003; Udalski et al. 2015). The present phase of the project, OGLE-IV, started in 2010 at Las Campanas in Chile. A 1.3-m telescope equipped with a 262.5 megapixel 32-chip mosaic CCD camera (*V* and *I* photometric filters) was recently used to observe the Large Magellanic Cloud (LMC), Small Magellanic Cloud, GB and Galactic disc (Udalski et al. 2015).

In 2014, the first data gathered by OGLE-IV for more than 38 000 RRL type stars (27 258 of RRab type) located in the GB were publicly released. Together with photometric data, Soszyński et al. (2014) published a complete catalogue with light ephemerides, mean brightness, peak-to-peak amplitudes and Fourier coefficients, which we adopted for further analysis.[2]

Not all of the available observations were suitable for our purposes. Because we aimed to search for the BL effect on a sufficiently large sample of stars, we had to take into account the quality of the observations and the number of points for a particular star, secure a sufficient number of stars to get reliable statistics and use only stars located in the GB. The following criteria were the most convenient for all our requirements:

(i) We used only measurements in the *I* band because they contain substantially more data points than observations in the *V* passband, and have much better quality.
(ii) Stars with Galactic latitude below $b = -8^\circ$ were ignored (due to possible membership of the Sagittarius tidal stream).
(iii) Stars from globular clusters were omitted.
(iv) Stars identified by Hajdu et al. (2015) as binary candidates were removed from the sample.
(v) We did not use RRL stars listed in the `remarks.txt` file (stored at the FTP mirror), which contains RRLs with uncertain identification.
(vi) After visual inspection, we decided to use only stars brighter than 18 mag in *I* because of their acceptable scatter.
(vii) Stars with suspicious light curves that are probably misclassified as RRab were ignored.
(viii) Only stars with more than 420 points (data file size of 10 kB) were used.

Our final sample contains 8282 stars that have between 420 and 8334 data points (median 1016). The left-hand panel of Fig. 1 shows the distribution of observations per star. The discrete pattern of the histogram is because some fields were observed more often than the others. We can see that the majority of stars have less than about 1200 data points. The right-hand panel of the same figure shows the distribution of main magnitudes of the sample stars. Because we did not remove any of the bright stars from the sample, it is likely that a very few of the brightest stars are actually foreground Galactic field RRLs.

The mean photometric error of a single point for stars with mean $I < 15.5$ mag is 4 mmag. For faint stars with $I \sim 18$ mag, it is about 20 mmag. The time span (T_S) of the observations is similar for all stars: from 1100 to 1400 d (median 1334 d).

3 SEARCHING FOR THE BL EFFECT

First, we plotted raw observations and phase curves (using pulsation periods determined by Soszyński et al. 2014) and visually inspected all light curves. Although very subjective and time-consuming, this approach gave a basic idea about the data and allowed us to assign each star to one of the three preliminary categories (clear BL effect,

[1] http://ogle.astrouw.edu.pl/

[2] ftp://ftp.astrouw.edu.pl/ogle/ogle4/OCVS/blg/rrlyr/

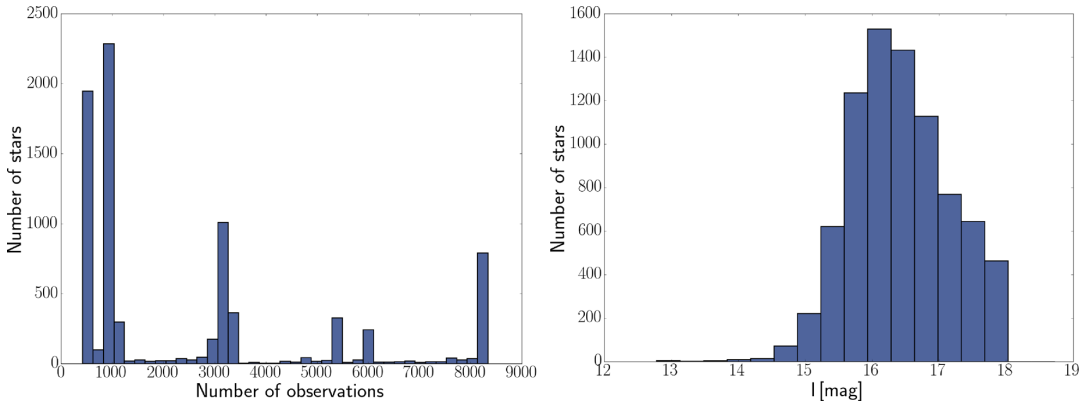

Figure 1. Distribution of stars according to the number of observations (left-hand panel) and the mean magnitude (right-hand panel).

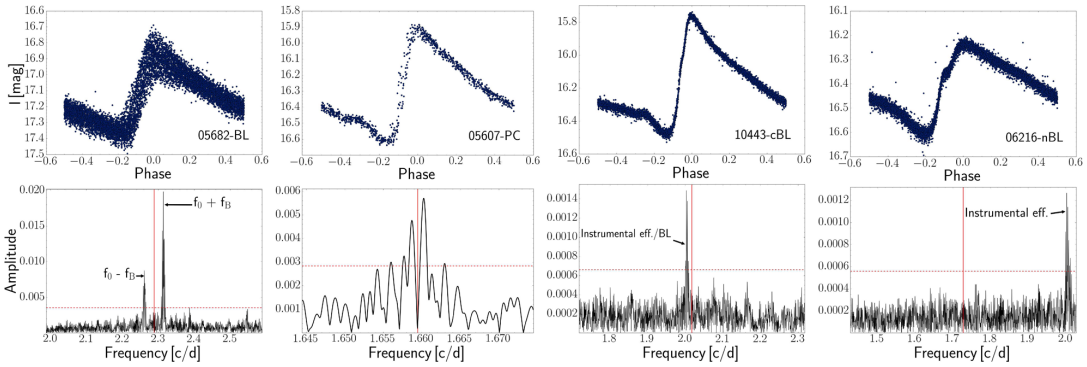

Figure 2. Examples of phase curves and frequency spectra around the main pulsation frequency after pre-whitening with 10 pulsation harmonics. BL, PC, candidate and unmodulated stars are shown from left to right. The horizontal dotted lines show the average $S/N = 3.5$ limit and the red vertical lines mark the position of the main pulsation frequency.

candidate or non-modulated star). It also helped us to identify special cases (for example, the discovery of peculiar pulsation modes in several RRLs, Smolec et al. 2016; Prudil et al. 2017) and stars showing distinct seasonal changes and secular trends in the mean magnitude suggesting blends. It should be borne in mind that this procedure was only informative, having no influence on the further analysis and the decision about the presence of the BL effect. After the visual inspection, we decided not to remove any of the light-curve outliers because their number was generally low and their separation from the mean light curve was mostly negligible (see Fig. 2).

Because the most prominent signs of modulation, which is detectable also in scattered data, are the side peaks close to the basic pulsation frequency (f_0) and its multiples (kf_0, for details see Szeidl & Jurcsik 2009; Szeidl et al. 2011), we searched for the BL effect in the frequency spectra of the time series. The distance between a side peak and the pulsation frequency defines the modulation frequency.

The side peaks are most easily and quickly identified using fully automatic procedures employing classical Fourier pre-whitening techniques. Although this approach would be very comfortable and save a lot of time, we must remember that the BL effect may be very complex, and that OGLE is a ground-based single-side survey producing data affected by various instrumental effects resulting in various aliases and false peaks in the frequency spectrum [typically the frequency at ∼2.005 c/d, which is the frequency corresponding to twice the sidereal day (see Fig. 2); frequencies at integer multiples of 1/day; higher noise in the low-frequency range, etc.]. Proper identification of the modulation is, therefore, not a straightforward task. The advantages and efficiency of individual analysis against fully automated procedures were demonstrated well by Skarka (2014b) and Skarka et al. (2016).

However, owing to the number of stars for analysis and the time necessary for each individual analysis, it would be extremely time-consuming to perform a manual step-by-step pre-whitening. Thus, we chose the way of the golden mean. We automatically pre-whitened the frequency spectrum of each of the sample stars with the first 10 pulsation harmonics using non-linear least-squares methods, and then searched manually for the side peaks near f_0 and $2f_0$ in residuals using PERIOD04 software (Lenz & Breger 2004). Because our goal was only to identify the BL effect, the manual (non)identification of the side peaks was quite fast. We considered a side peak as significant when it had signal-to-noise ratio (S/N) larger than 3.5.[3]

[3] S/N is simply defined as the ratio of the amplitude of the measured peak and the average of the amplitudes of peaks in the ±1 c/d vicinity of the measured peak.

We adopted similar criteria as introduced in Skarka et al. (2016) for assigning the stars to individual categories. Regarding the (non)detection of the side peaks and their characteristics, our categories are as follows:

(i) *BL stars* – These are stars with detectable side peak(s) within $f_0 \pm 0.3$ c/d, but no closer than $1.5/T_S$ (Nagy & Kovács 2006; Skarka et al. 2016). As a BL star, we also considered stars that showed unambiguous secular amplitude variations with side peaks indicating a modulation period longer than $2/3\ T_S$. An example of a frequency spectrum of a BL star after pre-whitening with 10 pulsation harmonics in the vicinity of f_0 is shown in the leftmost panel of Fig. 2.

(ii) *Stars with long-term/irregular period changes (PC)* – The detected side peak(s) were closer than $1.5/T_S$, with no apparent amplitude variations in the light curve (the middle-left panel of Fig. 2).

(iii) *Candidates (cBL)* – These are stars that have close side peak(s) with $S/N < 3.5$, or side peaks with $S/N > 3.5$ near integer multiples of cycles per day within our limits for BL stars, or showing many peaks near the $S/N \sim 3.5$ limit where we were unable to decide which peak could be the consequence of the modulation. Candidate stars are typically stars with periods close to 0.5 d where possible BL peaks interfere with instrumental peaks (middle-right panel of Fig. 2).

(iv) *Non-modulated (nBL)* – Signs of modulation were undetectable (Fig. 2, right-hand panel).

We searched for additional data in the OGLE-III survey for stars that showed side peaks closer than $1.5/T_S$ to decide unambiguously the PC/BL membership. Because OGLE-III observations usually contain significantly less points than OGLE-IV, we combined both data sets, which is allowed by the close similarity of the data (Soszyński et al. 2014). First, we determined zero-points for both data sets by applying a six-order Fourier fit. Then we shifted and combined the data sets, pre-whitened six basic pulsation harmonics and analysed the residuals. With the combined data set, we were able to determine BL periods safely up to a length of 3000 d, and in some stars up to 4000 d. In a few cases, the amplitudes were significantly different for the OGLE-IV and OGLE-III data. These stars were not analysed and remained in the PC class. An example of this procedure is shown in Fig. 3, which shows a BL star with an extremely long BL effect.

Finally, the light curves of all BL and candidate stars were visually inspected once again to reveal secular or seasonal changes suggesting possible blends, or instrumental problems. Additional light from a close star would change the amplitude and the mean magnitude of the target star mimicking the BL effect (for example, due to variable seeing). Such stars would show a distinct peak in the low-frequency range with higher amplitude than possible side peaks. We searched for such peaks in the range between 0 and 0.2 c/d in all BL and candidate stars and identified possible problems with blends in 21 stars (including visually identified and non-modulated stars, marked with 'b' in the remarks column of Table 1).

4 RESULTS

We used only BL and nBL stars for comparison between BL and non-modulated stars. Candidate and PC stars were omitted from the investigation. Thus, all statistics and figures are based purely on BL and non-modulated stars.

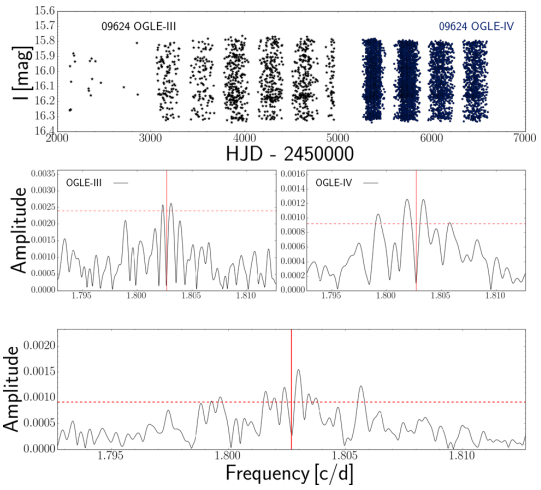

Figure 3. Combined OGLE-III and OGLE-IV data set (top panel) and corresponding frequency spectra (bottom panel). Based purely on the OGLE-IV observations (middle right-hand panel), the BL nature, represented by a tiny amplitude variation, is very hardly revealed. Dashed red horizontal lines show the average $S/N = 3.5$ limit. The vertical red lines mark the position of the main pulsation frequency.

4.1 Incidence rate of the BL stars

The identification of the sample stars into one of the four groups is shown in Table 1. We identified the BL effect in 3341 of the target stars. This is almost twice as many as all catalogued BL stars identified in all stellar systems together so far. For 29 objects ('a' in the remarks column of Table 1), we detected a doublet in the vicinity of f_0 (it was not detected close to the other harmonic frequencies). Besides these objects, all of the stars identified as modulated can be considered as firm BL stars because at least two side peaks with equidistant spacing from kf_0 were detected in their frequency spectra. An unambiguous secular amplitude change is apparent in 29 stars with extremely long modulation (marked with 'lm' in the last column of Table 1).

Only 26 stars were assigned to the candidate group ('cBL' in Table 1). Another 53 stars were identified as PC stars ('PC' in Table 1). For the remaining stars, no signs of modulation were detected ('nBL' in the second column of Table 1). From the analysis of the combined data sets (i.e. OGLE-III and IV), we find that 50 per cent of stars identified as PC in the 4-yr-long OGLE-IV data are actually BL stars with extremely long modulation periods. This finding could have a large impact on incidence rates that are estimated based only on short data sets.

The percentage of modulated stars is 40.3 per cent, and 40.0 per cent when we omit stars with only one detected side peak. The true portion and completeness of the BL identification is extraordinary difficult to estimate because the amplitudes of the side peaks depend on the strength of the modulation, in both amplitude and frequency/phase, which can be very diverse. In addition, the detectability of the side peaks depends on the noise level, which is unique for each star and data set. Also, the human factor and methods used could play role. Thus, some of the BL stars could be missed or misclassified.

Fig. 4 shows the noise level around the basic pulsation frequency for stars from our sample that we identified as non-modulated as

Table 1. Sample of the full online table, which lists the membership to one of our groups: non-modulated star (nBL), candidate star (cBL), BL star (BL) and PC star (PC), and observability in Kepler K2 campaigns 9 and 11 (0 – not on silicon, 1 – near silicon, 2 – on silicon). The name of a star is in the form OGLE-BLG-RRLYR-ID. The 'a' in the remarks column means that only one side peak was detected, 'b' means a possible blend, 'lm' means that the modulation period is longer than 2/3 T_S, 'h' is when the side peaks were identified in higher pulsation harmonics first, and letters 'c' and 'm' mean that stars are present in Collinge, Sumi & Fabrycky (2006) or Moskalik & Poretti (2003), respectively. Furthermore, we included the rise time (RT), together with the calculated metallicity, $(V-I)_0$ and absolute magnitude in the I band. Additional information about pulsation periods, amplitudes and Fourier coefficients can be found in Soszyński et al. (2014). The full table is available as supplementary material to this paper. The amplitudes of the side peaks and modulation periods will be given in Skarka et al. (in preparation).

ID	Group	K2-9	K2-11	Remarks	RT	[Fe/H]	$(V-I)_0$ [mag]	M_I [mag]
00162	BL	0	2	–	0.176	−1.09	0.467	0.183
01983	PC	0	0	–	0.178	−0.86	0.419	0.297
01994	nBL	0	0	–	0.145	−0.57	0.441	0.375
08688	cBL	2	0	b	0.123	−0.98	0.406	0.274
...	...	...	...	...	...	...	...	...

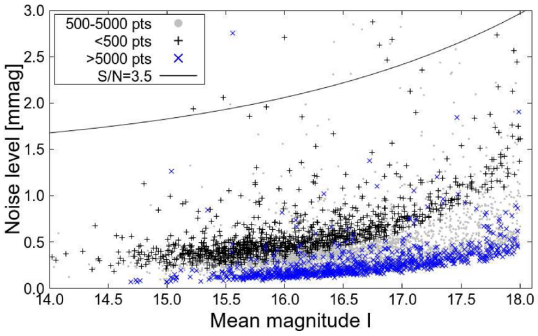

Figure 4. Noise level in Fourier amplitude spectra of non-Blazhko stars from our sample as a function of the mean magnitude. Stars with less than 500 data points are shown with black crosses. Stars with more than 5000 points are plotted with blue crosses to highlight the influence of the number of points on the noise level. The solid line shows the $S/N = 3.5$ limit for stars with less than 500 observations.

a function of the mean magnitude. It is seen that the noise level increases with increasing mean magnitude, which could be naturally expected due to the increasing scatter. The noise is also higher for stars with a low number of points (black crosses). The solid line is an exponential fit of the noise level of stars with less than 500 observations multiplied by 3.5, which shows the $S/N = 3.5$ limit for the stars with the noisiest Fourier spectra.

In the sample of BL stars observed by the *Kepler* space telescope, 1/4 of the modulated stars have side peaks with Fourier amplitudes lower than 1 mmag (Benkő et al. 2014). There are 1320 non-modulated stars that have the $S/N = 3.5$ limit larger than 0.001 mag in our sample. Possibly all of these stars are actually BL stars for which the modulation was undetectable. If this were true, then these 1320 stars would constitute 28 per cent of all BL stars, and the full percentage of modulated stars in the GB would be 56 per cent. However, this is a huge simplification and a very strong assumption that stands only on a very limited sample of BL stars in the *Kepler* field.

40 per cent is a high incidence rate in comparison with previous studies of the GB. Moskalik & Poretti (2003) estimated the percentage of modulated stars as 23 per cent (OGLE-I), Mizerski (2003) found 25 per cent of stars to be modulated (OGLE-II), Collinge et al. (2006) reported 28 per cent (OGLE-II) and Soszyński et al. (2011) gives that 30 per cent of RRab type stars exhibit the BL effect (OGLE-II + OGLE-III). The rising tendency of the estimates with longer and higher cadence and better quality data sets is obvious. The current estimates by Jurcsik et al. (2009, 47 per cent), Sódor et al. (2012, 43 per cent), Nemec et al. (2013, 43 per cent) and Szabó et al. (2014) and Benkő et al. (2016, 47 per cent) show that the occurrence rate is a bit higher for Galactic field stars than for GB stars. On one hand, the lower percentage of GB BL stars could be a natural property of this Galactic subsystem. Confirmation of this possibility is of high importance because it is still not known what physical processes rule the occurrence of the BL effect. On the other hand, the different result for the GB could be due to selection effects possibly caused by different quality data with different time spans. Former studies used only a low number of stars (maximally several tens), which could also distort the statistics. Unfortunately, we do not know which possibility is more likely because no other study with a similarly large and good quality sample of stars has been available so far.

A more reliable picture of the efficiency of the detection of the BL effect and its incidence rate in GB will be available when the data gathered by mission *K2* (Howell et al. 2014) campaigns 9 and 11 are analysed. More than 2000 of our sample stars fall on the silicon (1293 non-modulated stars, 910 BL stars, 13 PC stars and nine candidates with flag '2', see Table 1). However, due to time-limited observations, this will tell us something only about BL stars with a short modulation cycle.

4.2 Pulsation period

Fig. 6 shows the distribution of the BL star population according to the pulsation period in 0.05-d bins. It is seen that the highest incidence rate of BL stars (about 48 per cent) appears in stars with a pulsation period of 0.5 d. Below 0.625 d, the average percentage is almost 44 per cent, while above this limit it drastically falls to 20 per cent. The same behaviour was observed by Smolec (2005) in stars from the GB and LMC, by Szczygieł & Fabrycky (2007) and Skarka (2014a) in stars from the Galactic field and by Jurcsik et al. (2011) in globular cluster M5. All this evidence suggests that the rare occurrence of the BL stars in RRLs with periods longer than 0.65 d is real and has general plausibility regardless of the investigated stellar system, its metal abundance or age.

Because the pulsation period roughly relates to the mean density, the mass and size of an RRL star could be the factors that determine the occurrence of the modulation more than other physical

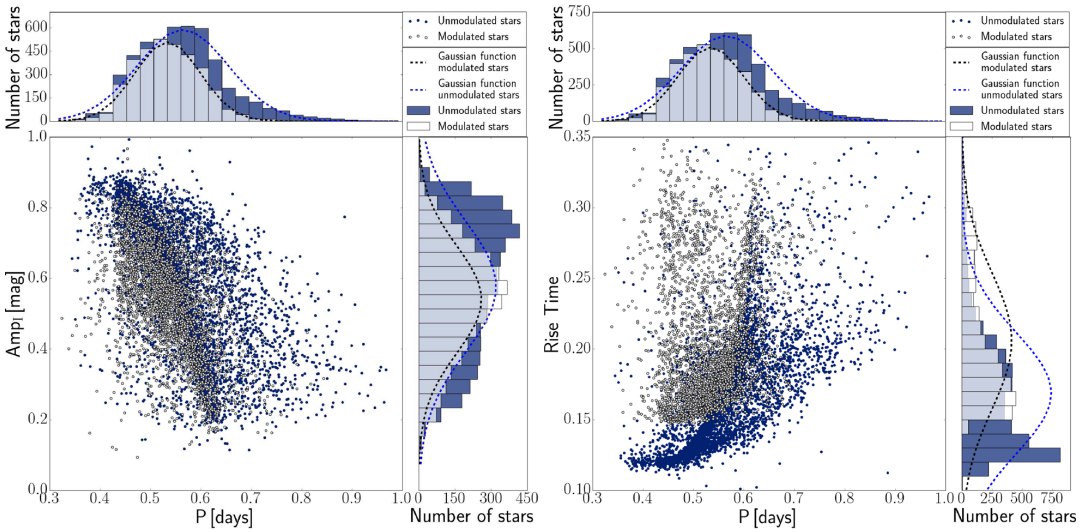

Figure 5. Period–amplitude (Bailey) diagram together with pulsation-period distribution and distribution of pulsational amplitudes (left-hand panels) and plots showing the distribution of the rise time. Normal distributions with the same mean and standard deviation are plotted with lines in the histograms for comparison.

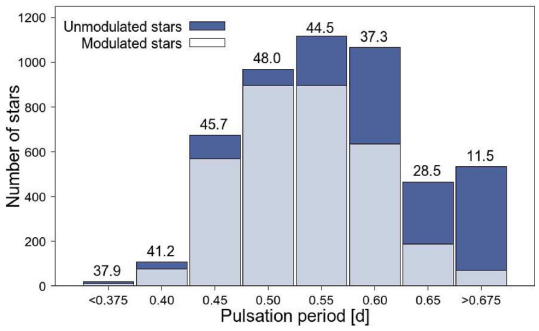

Figure 6. Distribution of the BL stars according to the pulsation period. The number above each bin shows the corresponding percentage of BL stars in the given range.

parameters.[4] During its evolution, the size and density of an RRL star gradually change and could be tuned to the right values, allowing the modulation to rise. The mass–size parameter space for BL stars is probably somewhat limited, preventing the modulation from being present in long-pulsation-period RRL stars, which generally have a lower density.

The lack of modulated stars among long-pulsation-period RRLs is the reason why the mean pulsation period of BL stars is shorter than for nBL stars: 0.533 ± 0.001 d versus 0.564 ± 0.001 d. The difference of 0.031 d corresponds well to what was found by Jurcsik et al. (2011) and Alcock et al. (2003).

4.3 Amplitudes of the light curves

Because the properties of the BL modulation have not been investigated in this study, we are unable to investigate light-curve amplitudes during the maximum BL phase, nor the amplitudes of modulation-free light curves. We can only investigate the amplitudes of the mean light curves for BL stars.

Although there are some exceptions from a general trend (as was shown e.g. by Jurcsik & Smitola 2016), it is generally accepted that for a given period most of the light curves of modulated stars have amplitudes comparable to single-period RRLs only near their maximum-amplitude BL phase; see fig. 3 in Szeidl (1988) and fig. 1 in Jurcsik & Smitola (2016), which display the amplitudes of RRLs in M3. Therefore, we can expect that for a given period, the mean light curves of BL stars will have a smaller peak-to-peak amplitude (from minimum to maximum light) than their non-modulated counterparts.

This is to some extent apparent from the left-hand panel of Fig. 5, but it is obvious without a doubt from Fig. 7, where the difference between the mean amplitudes of the light curves of single-period RRLs and BL stars in 32 bins is plotted as a function of the period.[5] To be more precise, we simply computed the average value of amplitudes for non-modulated stars in a given period bin and we did the same for BL stars, and then we subtracted these two values. The amplitude difference shown in Fig. 7 linearly decreases with increasing period as

$$\Delta A_I = 0.434(46) - 0.643(86)P, \quad \sigma = 0.045. \tag{1}$$

Because the larger the amplitude of the BL modulation, the lower usually is the total pulsation amplitude of a BL-star light curve, and because we see the largest difference in short-pulsation-period

[4] Computed metallicity, intrinsic colour and absolute magnitude are the same for BL and non-modulated stars; see the following sections.

[5] The shortest- and longest-period regions were omitted from the calculations because of the low number of stars.

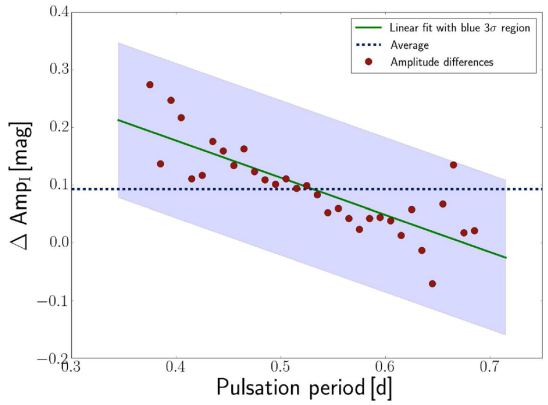

Figure 7. Difference in pulsation amplitudes of BL and single-period stars computed in 32 period bins as $\Delta\mathrm{Amp_I} = \mathrm{Amp}^{\mathrm{nBL}}_{\mathrm{median\,I}} - \mathrm{Amp}^{\mathrm{BL}}_{\mathrm{median\,I}}$. The straight line shows the linear fit.

RRLs, our result supports the finding by Jurcsik, Sodor & Varadi (2005). They proposed that short-pulsation-period BL stars can have both small and large modulation amplitudes, while long-period BL stars can have only small modulation amplitudes (resulting in a smaller difference between BL and single-period RRLs).

4.4 Rise time

From the mean light curves, we also estimated the rise time (RT), which is the phase difference between maximum and minimum light. Modulated stars have generally less skewed, more symmetric mean light curves with smaller amplitudes, thus, we can expect a larger RT for BL stars. This is really observed: the mean RT of the BL stars is 0.2048(8), while nBL stars have mean RT = 0.1690(4). The difference is clearly seen in the right-hand panels of Fig. 5. The RT of BL stars is never less than approximately 0.16, while the majority of non-modulated RRLs have RT lower than 0.16. This finding could be used for the first rough identification of BL stars in future classifications.

4.5 Low-order Fourier coefficients

The mean values of the Fourier parameters[6] are systematically lower for BL stars than for stars with a non-modulated light curve (see Table 2), which is naturally expected with the same reasons for why RT is larger.[7] The lower values for BL stars are clearly apparent in all panels of Fig. 8.

The Fourier parameters are correlated, which means that one parameter can be expressed as a linear combination of the others. The agreement between computed and observed values can serve as a criterion for testing whether a particular light curve is similar for the majority of RRL stars or not. The mean light curves of BL stars can, especially when strong modulation is present, significantly differ from those of single-period stars. Jurcsik & Kovacs (1996) introduced the so-called deviation parameter D_F, which reflects the normality of the light curve in the V passband. In addition, the value of this parameter indicates whether an empirical equation for determination of metallicity can be used for a particular star or not.

We followed their approach and determined new linear interrelations between Fourier amplitudes and phases in the I filter. We used only 2260 non-modulated stars that are between 15 and 17 mag, have more than 900 observations, and do not have pulsation periods between 0.49 and 0.51 d to secure good quality light curves with homogeneous phase coverage. From the pre-whitening procedure, we have a Fourier decomposition into 10 sine harmonics that we used for this purpose.[8]

For each amplitude and phase up to the sixth order, we performed linear fits with various combinations of the other parameters. Because the Fourier coefficients are correlated, by using different combinations of parameters one can get very similar results. An additional problem is that the more parameters are used, the better is the fit. Because classical decisive criteria (Bayesian information criterion and Akaike information criterion) fail, one cannot easily decide what fit is the best. Therefore, we used the full parameter fits employing all parameters. In Table 3, we give the solution. The most correlated components of the fits are highlighted with italics.

Calculated versus observed parameters are shown in Fig. 9. We also show how observed and calculated coefficients correlate when only the particular amplitudes and phases used by Jurcsik & Kovacs (1996, given in their table 6) are used for the fit.

The compatibility parameter D_F is calculated according to equation (6) from Jurcsik & Kovacs (1996) as $D_F = |F_{\mathrm{obs}} - F_{\mathrm{calc}}|/\sigma_F$, where F_{obs} and F_{calc} rely on the observational and calculated values of a particular Fourier parameter F according to the fit in Table 3 (with the standard deviation σ_F). The maximum of $\{D_F\}$ is D_m, which actually serves for the decision about the applicability of the metallicity formula (if $D_m < 3$).

As was pointed out by Cacciari, Corwin & Carney (2005), the D_m parameter cannot be effectively used for distinguishing between non-modulated and BL stars as was originally suggested by Jurcsik & Kovacs (1996), because many BL stars have $D_m < 3$. However, almost all stars with $D_m > 3$ are modulated! This is clearly seen in Fig. 10. While unmodulated stars with all possible D_m and BL stars with $D_m < 3$ follow the same trend, BL stars with $D_m > 3$ are located in a completely different area in the R_{31} versus ϕ_{31} and ϕ_{21} versus R_{31} planes.

This led us to define a new limit for BL stars that is an alternative to the D_m criterion. The main streams in the R_{31} versus ϕ_{31} and ϕ_{21} versus R_{31} planes can be described by polynomials with the following forms:

$$\begin{aligned}\phi_{21} = 5.31 &- 6.53R_{31} + 32.4R_{31}^2 - 60.7R_{31}^3,\\ &\pm 0.04 \quad \pm 0.53 \quad \pm 2.1 \quad \pm 2.7,\end{aligned} \tag{2}$$

$$\begin{aligned}R_{31} = -0.66 &+ 1.1\phi_{31} - 0.36\phi_{31}^2 + 0.033\phi_{31}^3,\\ &\pm 0.03 \quad \pm 0.03 \quad \pm 0.01 \quad \pm 0.001.\end{aligned} \tag{3}$$

The dispersions of equations (2) and (3) are $\sigma = 0.083$ rad and $\sigma = 0.015$, respectively. As is seen from Fig. 10 and from Table 4, for the population of stars below 3σ from the fit, 94 per cent are BL stars. In other words, our equations could help to identify new BL stars in a large sample of stars with 94 per cent probability. We performed a detailed analysis of 360 randomly chosen non-modulated stars

[6] Fourier parameters were introduced by Simon & Lee (1981) for Cepheid light curves. The parameters are defined as: $R_{i1} = A_i/A_1$ and $\phi_{i1} = \phi_i - i\phi_1$, where A_i and ϕ_i are the amplitudes and phases of the pulsation harmonics of the Fourier decomposition.

[7] We note again that we used exclusively parameters derived and provided by Soszyński et al. (2014).

[8] Soszyński et al. (2014) do not provide amplitudes and phases of the Fourier decomposition.

Table 2. Comparison of the mean parameters of single-period RRL stars and stars with the BL effect. The uncertainties in the last digits (in parentheses) are the standard 1σ errors of the means. Fourier parameters are based on a cosine fit (Soszyński et al. 2014). Metallicity, intrinsic colour and absolute magnitude show differences only for stars with $D_m < 3$.

	$P_{\rm Puls}$ [days]	Amp$_I$ [mag]	R_{21}	R_{31}	ϕ_{21} [rad]	ϕ_{31} [rad]	RT	[Fe/H]	$(V-I)_0$ [mag]	M_I [mag]
nBL	0.564(1)	0.577(3)	0.491(1)	0.319(1)	4.450(4)	2.832(7)	0.169(3)	−0.962(5)	0.490(2)	0.198(2)
BL	0.533(1)	0.540(3)	0.458(1)	0.274(1)	4.367(4)	2.616(8)	0.219(8)	−0.969(5)	0.487(2)	0.202(2)

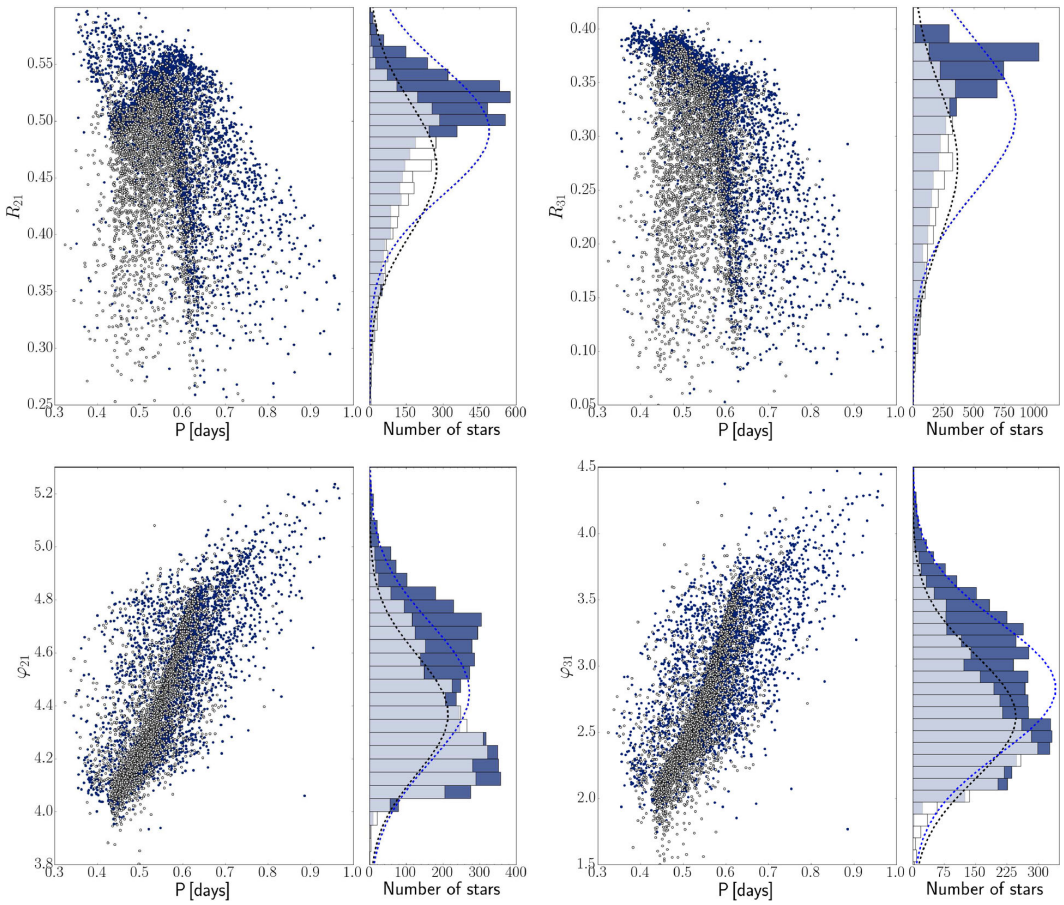

Figure 8. Low-order Fourier parameters. Normal distributions are shown with lines for comparison. The description of each plot is as in Fig. 5.

Table 3. Coefficients of the linear fit for the Fourier coefficients.

	Constant	A_1	A_2	A_3	A_4	A_5	A_6	ϕ_{21}	ϕ_{31}	ϕ_{41}	ϕ_{51}	ϕ_{61}	σ
A_1	−0.08(1)	–	*1.23(4)*	0.62(6)	−1.07(7)	1.5(1)	0.5(1)	0.045(6)	−0.003(4)	−0.008(2)	0.0027(6)	0.0014(4)	0.008
A_2	−0.082(5)	*0.243(8)*	–	0.58(3)	1.08(3)	−1.18(5)	0.14(5)	0.022(3)	0.005(2)	−0.0056(6)	0.0006(3)	−0.0009(2)	0.003
A_3	0.050(4)	0.36(2)	0.076(8)	–	*0.06(3)*	0.59(4)	−0.23(4)	0.009(2)	−0.011(2)	0.00005(50)	−0.0023(2)	0.0013(4)	0.003
A_4	0.059(3)	−0.075(6)	0.38(1)	*0.03(2)*	–	0.8(3)	−0.26(3)	−0.024(2)	−0.001(1)	0.0060(4)	0.0004(2)	−0.0006(1)	0.002
A_5	−0.035(2)	0.049(4)	−0.203(8)	0.16(1)	0.4(1)	–	*0.67(1)*	−0.016(1)	0.0150(6)	−0.0038(3)	0.0001(1)	−0.0005(8)	0.002
ϕ_{21}	0.22(4)	0.5(7)	1.3(2)	0.8(2)	−4.1(3)	−5.5(4)	5.0(4)	–	*0.426(9)*	0.038(5)	−0.007(2)	−0.005(2)	0.026
ϕ_{31}	1.94(6)	−0.1(1)	0.8(3)	−2.8(4)	−0.6(5)	14.3(6)	−14.7(5)	*1.16(3)*	–	0.022(8)	0.005(4)	0.013(3)	0.043
ϕ_{41}	−6.34(9)	−1.5(3)	−5.2(7)	0.1(1)	15(1)	−20(2)	25(1)	0.58(8)	*1.24(5)*	–	0.073(8)	−0.010(6)	0.102
ϕ_{51}	4.4(4)	3.7(8)	4(1)	−26(2)	8(3)	5(4)	−1(3)	−0.9(2)	0.2(1)	*0.56(6)*	–	*0.45(1)*	0.281

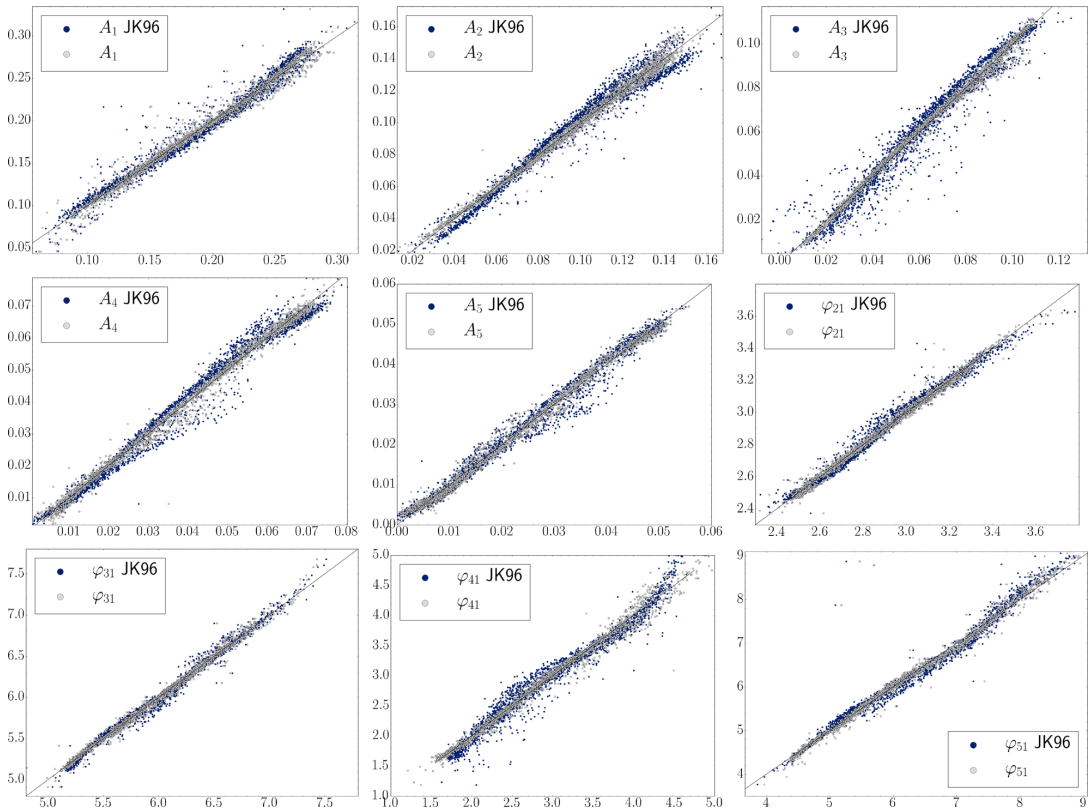

Figure 9. Calculated versus observed Fourier parameters. The straight line shows the 1:1 ratio.

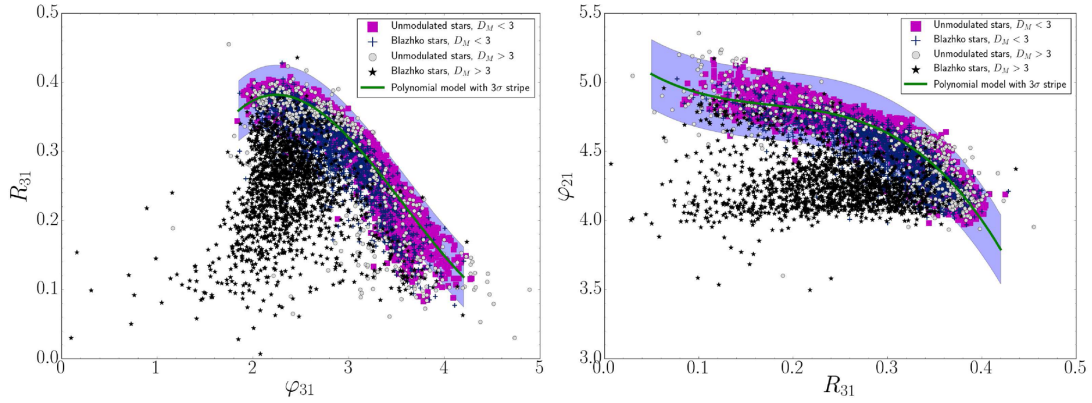

Figure 10. Relation of R_{31} with low-order phase parameters. The polynomial fits (equations 2 and 3 are shown with the solid line together with 3σ limits.)

Table 4. Occurrence rate of the BL stars and the total number of stars at different distances below the fits.

$n\sigma$	R_{31} versus ϕ_{21}	R_{31} versus ϕ_{31}
1	73.9 per cent (3231)	71.5 per cent (3695)
2	89.0 per cent (2111)	78.7 per cent (2855)
3	94.4 per cent (1602)	83.6 per cent (2281)

below the 1σ region and identified only eight additional stars that are in fact modulated, which is 2.2 per cent of all stars in this region.[9] This percentage could serve as the estimation of our failure in searching for the BL effect due to the human factor and the methods used. It is worth noting that these eight stars are somewhat

[9] These stars are marked with 'h' in Table 1.

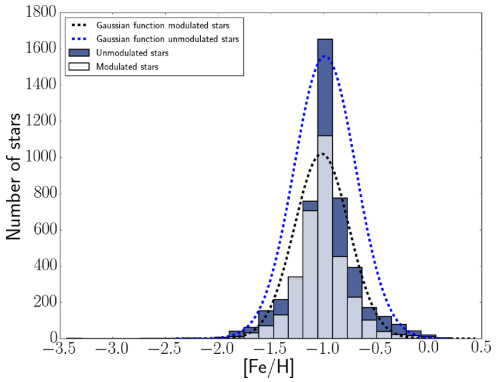

Figure 11. Distribution of metallicity for BL and single-period stars with $D_m < 3$. Gaussian distributions with the same parameters as those of the corresponding populations are shown with lines for comparison.

peculiar because the side peaks at higher harmonics have larger amplitudes than side peaks around f_0 and $2f_0$,[10] where we originally searched for the peaks.

4.6 Metallicity

For stars that meet the $D_m < 3$ criterion, we can apply the empirical relation from Jurcsik & Kovacs (1996) modified for the I filter by Smolec (2005, his equation 2) and investigate differences in metallicity for BL and non-modulated stars. The results, which are shown in Fig. 11 and in Table 2, suggest that there is no difference in metallicity between the two groups of stars at all. Thus, the (non)presence of modulation in a particular star more likely depends on other physical parameters (such as, for example, the size and density) than on the metal abundance. Similar results for the GB were reported by Smolec (2005), and by Skarka (2014a) for Galactic field stars.

4.7 Intrinsic colours and absolute magnitudes

Following Pietrukowicz et al. (2015), we computed the intrinsic colour $(V - I)_0$ using theoretical calibrations by Catelan, Pritzl & Smith (2004) based on calculations of synthetic horizontal branches. This approach simplifies the problem and allows us to compute the intrinsic colour without knowing the extinction. The formula used is:

$$(V - I)_0 = 1.817 + 1.132 \log P + 0.677 \log Z + 0.108(\log Z)^2, \quad (4)$$

where $\log Z$ is calculated as

$$\log Z = [\mathrm{Fe/H}] - 1.765. \quad (5)$$

BL and non-modulated stars with $D_m < 3$ have the same average $(V - I)_0$, suggesting that there is no correlation between the BL effect and colour in the GB (see Table 2 and Fig. 12).

The absolute magnitudes in various passbands could also be computed using the calibrations provided by Catelan et al. (2004). In

[10] For some of the stars, the side peaks around f_0 and $2f_0$ were even undetectable.

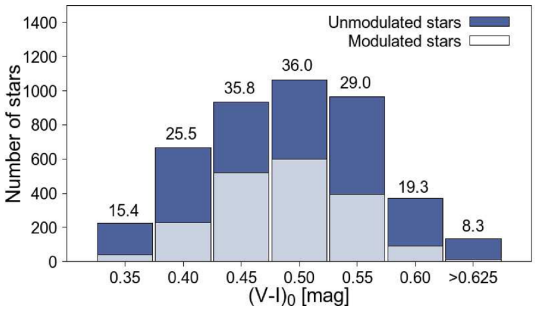

Figure 12. Distribution of $(V - I)_0$ for BL and single-period stars with $D_m < 3$. The percentage of BL stars is shown above each bin.

Table 2, we give the absolute magnitude in I for both groups, calculated as (equation 3 in Catelan et al. 2004)

$$M_I = 0.417 - 1.132 \log P + 0.205 \log Z. \quad (6)$$

The mean values in Table 2 show that modulated and nBL stars with $D_m < 3$ have the same average photometric absolute magnitude/luminosity.

4.8 Spatial distribution

The distribution of modulated stars seems to correlate with the spatial distribution of stars with nBL light curve with no preference towards any direction (Fig. 13). To our knowledge, this is the first time that an investigation of the spatial distribution of BL stars has been possible. In calculating the distance to the stars, we followed exactly the procedure described in Pietrukowicz et al. (2015). First, we calculated the extinction following Nataf et al. (2013):

$$A_I = 0.7465E(V - I) + 1.3700E(J - K) \quad (7)$$

where

$$E(V - I) = (V - I) - (V - I)_0. \quad (8)$$

The intrinsic colour index $(V - I)_0$ is calculated using equation (4). $(V - I)$ is the observed colour, which is the least certain value because V observations contain typically only between several tens and a few hundreds of data points. The reddening $E(J - K)$ comes from Gonzalez et al. (2012). Finally, the distance is calculated as

$$d = 10^{1-0.2(I-A_I-M_I)}. \quad (9)$$

Although the incidence rate of modulated stars slightly differs at different coordinates and distances, we did not detect any significant inhomogeneity, nor clustering of modulated stars (Fig. 13). The observed amplitudes and periods also do not show any apparent preference for any location or direction. Therefore, we see that BL and single-period stars are well mixed and that the spatial distribution has no influence on the BL effect.

5 SUMMARY AND CONCLUSIONS

We performed a detailed semi-automatic analysis of the frequency spectra of 8282 fundamental mode RRL stars located in the GB, aiming to identify the BL effect. To increase the chance of detecting modulation, we used only high-quality observations from the OGLE-IV project and carefully selected stars with suitable data.

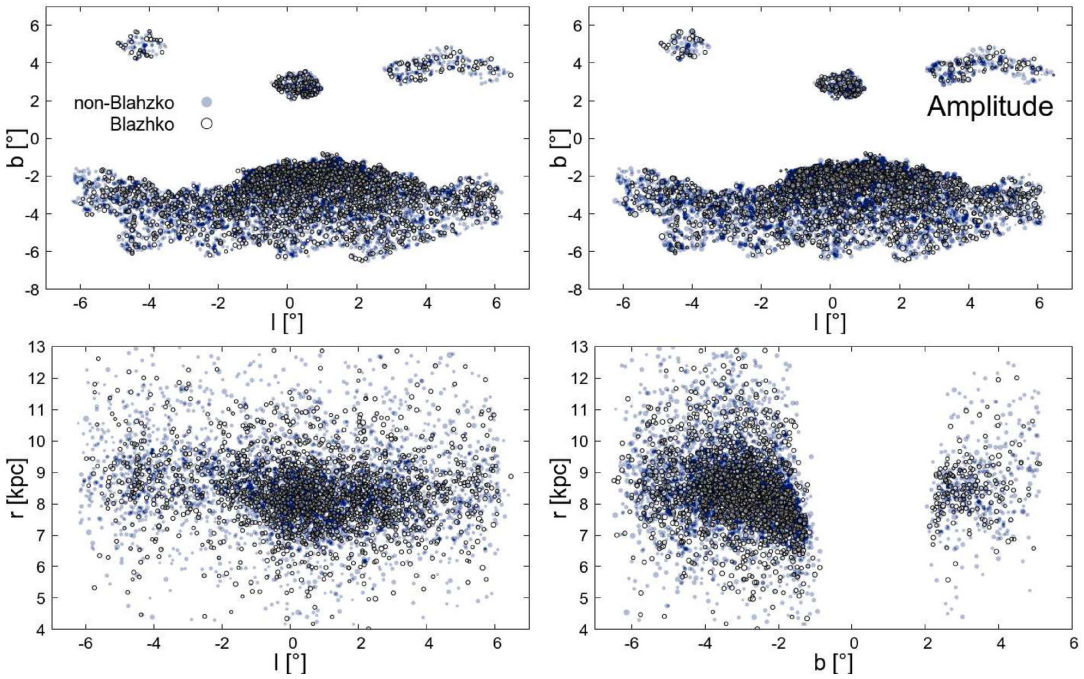

Figure 13. Spatial distribution of the sample of BL (white circles) and non-modulated stars (blue circles). The larger the points, the longer is the pulsation period. In the top right-hand panel, the sizes of the circles are proportional to the pulsation amplitude, for comparison.

After pre-whitening the spectra of all 8282 stars with 10 pulsation harmonics, we performed a thorough visual inspection of the vicinity of the main pulsation component f_0 and its harmonic $2f_0$ to identify possible side peaks. After identifying the BL stars, we were able to compare their basic pulsation properties, light curve characteristics and (computed) physical parameters with those of RRL stars without modulation. The main results of our work are summarized in the following points:

(i) We identified 3341 stars with modulation, which is almost twice as many as the number of all catalogued BL stars in all stellar systems so far. In addition, we identified 26 candidate stars and 53 stars showing secular/irregular period changes.

(ii) Half of the stars identified as PC in the OGLE-IV data set appeared to be BL stars in combined OGLE-III + OGLE-IV data sets, revealing the shortcomings of BL statistics based on a data set with a short time span.

(iii) The occurrence rate of BL stars is 40.3 per cent, which is about 10 per cent more than previous estimates in the GB, and a bit less than the current estimates for stars in the Galactic field. The true percentage is, however, surely higher than 40.3 per cent. There are a few reasons for that. For example, the incidence rate of identified stars is lower for stars with a low number of observations, the BL effect with the lowest amplitudes detected in space data cannot be detected in available ground-based observations, etc.

(iv) We provide clear and statistically significant evidence that BL stars occur rarely among stars with pulsation periods longer than 0.65 d. Due to the large analysed sample and good quality data, this could hardly be an observational bias (as it could be in some of the publications in the literature). Because other published studies of various stellar systems suggest a similar trend, the presence of BL stars only among short-pulsation-period RRL stars has very likely general plausibility.

(v) All the mean light-curve characteristics of modulated stars related to amplitudes and phases are smaller than for non-modulated stars. The average difference in the total mean amplitudes is linearly period-dependent with a mean value of 0.094(13) mag. The difference is significantly larger for stars with pulsation periods shorter than 0.425 d and smaller for stars with periods longer than 0.6 d.

(vi) We derived new interrelations between Fourier coefficients in the I passband, which allowed us to calculate the compatibility parameter D_m. We showed that BL stars with $D_m > 3$ significantly differ from other BL and non-modulated stars in the R_{31} versus ϕ_{31} and ϕ_{21} versus R_{31} planes. Regarding this finding, we propose a new approach for identifying BL stars using new empirical polynomial relations (equations 2 and 3). The portion of BL stars further than 3σ below the fitted polynomials is 94 per cent.

(vii) Using the empirical relations, we computed the metallicity, intrinsic colour and absolute magnitude for stars with $D_m < 3$. Modulated stars in the GB show the same metallicity, intrinsic $(V - I)_0$ colour index and absolute magnitude as stars with the nBL light curve, suggesting that in the GB there is no connection between the occurrence of the BL effect with these parameters.

It is not clear at the moment whether our percentage represents the general incidence rate of the BL stars in all stellar systems, or whether it is a unique, intrinsic characteristic of the GB RRL stars.

Our results show that searching for statistical differences between BL and non-BL stars based purely on single-filter photometry cannot help much in solving the BL enigma, even when using very good quality OGLE-IV observations and a large number of stars. The (non)presence of the BL effect in a particular RRL star is likely

influenced mainly by the mass and size of the RRL star because these parameters are directly connected with the pulsation period. Because the BL effect is very rare among RRL stars with long pulsation periods, it could be likely that modulation occurs only in stars that have precisely tuned mass and size, i.e. density. A certain mass–size limit could explain why modulation is common only in short-pulsation-period RRL stars and explain the sudden (dis)appearance of the modulation reported in the literature for several stars (e.g. RR Gem and V79 M3; Sódor et al. 2007; Goranskij, Clement & Thompson 2010). A detailed investigation of this idea would need extensive pulsation and evolution modelling complemented with a thorough analysis of the observational data, which is certainly out of the scope of this general paper.

Further details of BL stars in the GB will be elaborated in the forthcoming papers by Skarka et al. (modulation periods and amplitudes, in preparation) and Prudil, Skarka & et al. (the Oosterhoff phenomenon, in preparation).

ACKNOWLEDGEMENTS

We are very grateful to J. Jurcsik and G. Kovács for their very useful comments on the original version of the manuscript, and the anonymous referee for additional suggestions, which helped to improve the quality of the paper. We would also like to thank the OGLE team for their great job with the observations of the GB. MS acknowledges the support of the post-doctoral fellowship programme of the Hungarian Academy of Sciences at Konkoly Observatory as a host institution and the financial support of the Hungarian Nemzeti Kutatási, Fejlesztési és Innovációs Hivatal (NKFIH) grant K-115709.

REFERENCES

Alcock C. et al., 2003, ApJ, 598, 597
Arellano Ferro A., Bramich D. M., Figuera Jaimes R., Giridhar S., Kuppuswamy K., 2012, MNRAS, 420, 1333
Benkő J. M., Plachy E., Szabó R., Molnár L., Kolláth Z., 2014, ApJS, 213, 31
Benkő J. M., Szabó R., Derekas A., Sódor Á., 2016, MNRAS, 463, 1769
Blažko S., 1907, Astron. Nachr., 175, 325
Buchler J. R., Kolláth Z., 2011, ApJ, 731, 24
Cacciari C., Corwin T. M., Carney B. W., 2005, AJ, 129, 267
Catelan M., Cortés C., 2008, ApJ, 676, L135
Catelan M., Pritzl B. J., Smith H. A., 2004, ApJS, 154, 633
Collinge M. J., Sumi T., Fabrycky D., 2006, ApJ, 651, 197
Gonzalez O. A., Rejkuba M., Zoccali M., Valenti E., Minniti D., Schultheis M., Tobar R., Chen B., 2012, A&A, 543, A13
Goranskij V., Clement C. M., Thompson M., 2010, in Sterken C., Samus N., Szabados L., eds, Variable Stars, the Galactic Halo and Galaxy Formation. Sternberg Astronomical Institute of Moscow Univ., Moscow, p. 115
Hajdu G., Catelan M., Jurcsik J., Dékány I., Drake A. J., Marquette J.-B., 2015, MNRAS, 449, L113
Howell S. B. et al., 2014, PASP, 126, 398
Jurcsik J., Kovacs G., 1996, A&A, 312, 111
Jurcsik J., Smitola P., 2016, Commmunications Konkoly Obser. Hungary, 105, 167
Jurcsik J., Sodor A., Varadi M., 2005, Inf. Bull. Var. Stars, 5666
Jurcsik J. et al., 2009, MNRAS, 400, 1006
Jurcsik J., Szeidl B., Clement C., Hurta Z., Lovas M., 2011, MNRAS, 411, 1763
Jurcsik J. et al., 2012, MNRAS, 419, 2173
Kolláth Z., Molnár L., Szabó R., 2011, MNRAS, 414, 1111
Kovács G., 2016, Communications Konkoly Obser. Hungary, 105, 61
Lenz P., Breger M., 2004, in Zverko J., Ziznovsky J., Adelman S. J., Weiss W. W., eds, Proc. IAU Symp. 224, The A-Star Puzzle. Kluwer, Dordrecht, p. 786
Mizerski T., 2003, Acta Astron., 53, 307
Moskalik P., Poretti E., 2003, A&A, 398, 213
Nagy A., Kovács G., 2006, A&A, 454, 257
Nataf D. M. et al., 2013, ApJ, 769, 88
Nemec J. M., Cohen J. G., Ripepi V., Derekas A., Moskalik P., Sesar B., Chadid M., Bruntt H., 2013, ApJ, 773, 181
Pietrukowicz P. et al., 2015, ApJ, 811, 113
Prudil Z., Smolec R., Skarka M., Netzel H., 2017, MNRAS, 465, 4074
Simon N. R., Lee A. S., 1981, ApJ, 248, 291
Skarka M., 2014a, MNRAS, 445, 1584
Skarka M., 2014b, A&A, 562, A90
Skarka M., Liška J., Auer R. F., Prudil Z., Juráňová A., Sódor Á., 2016, A&A, 592, A144
Smolec R., 2005, Acta Astron., 55, 59
Smolec R., Prudil Z., Skarka M., Bakowska K., 2016, MNRAS, 461, 2934
Sódor Á., Szeidl B., Jurcsik J., 2007, A&A, 469, 1033
Sódor Á. et al., 2012, in Shibahashi H., Takata M., Lynas-Gray A. E., eds, ASP Conf. Ser. Vol. 462, Progress in Solar/Stellar Physics with Helio- and Asteroseismology. Astron. Soc. Pac., San Francisco, p. 228
Soszyński I. et al., 2011, Acta Astron., 61, 1
Soszyński I. et al., 2014, Acta Astron., 64, 177
Soszyński I. et al., 2016, Acta Astron., 66, 131
Szabó R. et al., 2010, MNRAS, 409, 1244
Szabó R. et al., 2014, A&A, 570, A100
Szczygieł D. M., Fabrycky D. C., 2007, MNRAS, 377, 1263
Szeidl B., 1988, in Kovacs G., Szabados L., Szeidl B., eds, Multimode Stellar Pulsations. Kultura, Quarter Observatory, Budapest, p. 45
Szeidl B., Jurcsik J., 2009, Communications Asteroseismology, 160, 17
Szeidl B., Hurta Z., Jurcsik J., Clement C., Lovas M., 2011, MNRAS, 411, 1744
Udalski A., 2003, Acta Astron., 53, 291
Udalski A., Szymanski M., Kaluzny J., Kubiak M., Mateo M., 1992, Acta Astron., 42, 253
Udalski A., Kubiak M., Szymanski M., 1997, Acta Astron., 47, 319
Udalski A., Szymański M. K., Szymański G., 2015, Acta Astron., 65, 1

SUPPORTING INFORMATION

Supplementary data are available at *MNRAS* online.

Table-BL-stars.txt

Please note: Oxford University Press is not responsible for the content or functionality of any supporting materials supplied by the authors. Any queries (other than missing material) should be directed to the corresponding author for the article.

This paper has been typeset from a TEX/LATEX file prepared by the author.

Paper 3

A cautionary tale of interpreting O-C diagrams: period instability in a classical RR Lyr Star Z CVn mimicking as a distant companion

Monthly Notices
of the
ROYAL ASTRONOMICAL SOCIETY

MNRAS **474,** 824–837 (2018) doi:10.1093/mnras/stx2737
Advance Access publication 2017 October 24

A cautionary tale of interpreting O−C diagrams: period instability in a classical RR Lyr Star Z CVn mimicking as a distant companion

M. Skarka,[1,2★] J. Liška,[2,3★] R. Dřevěný,[2,4] E. Guggenberger,[5,6] Á. Sódor,[1] T. G. Barnes[7] and K. Kolenberg[8,9]

[1]*Konkoly Observatory, Research Centre for Astronomy and Earth Sciences, Hungarian Academy of Sciences, Konkoly Thege Miklós út 15-17, H-1121 Budapest, Hungary*
[2]*Variable Star and Exoplanet Section of the Czech Astronomical Society, Vsetínská 78, CZ-757 01 Valašské Meziříčí, Czech Republic*
[3]*Central European Institute of Technology - Brno University of Technology (CEITEC BUT), Purkyňova 656/123, CZ-612 00 Brno, Czech Republic*
[4]*Znojmo Observatory, Vinohrady 57, CZ-669 02 Znojmo, Czech Republic*
[5]*Max-Planck-Institut für Sonnensystemforschung, Justus-von-Liebig-Weg 3, D-37077 Göttingen, Germany*
[6]*Stellar Astrophysics Centre, Department of Physics and Astronomy, Aarhus University, DK-8000 Aarhus C, Denmark*
[7]*The University of Texas at Austin, McDonald Observatory, 1 University Station, C1402, Austin, TX 78712, USA*
[8]*Institute of Astronomy, KU Leuven, Celestijnenlaan 200D, B-3001 Heverlee, Belgium*
[9]*Physics Department, University of Antwerp, Groenenborgerlaan 171, B-2020 Antwerpen, Belgium*

Accepted 2017 October 17. Received 2017 October 16; in original form 2017 August 18

ABSTRACT

We present a comprehensive study of Z CVn, an RR Lyrae star that shows long-term cyclic variations of its pulsation period. A possible explanation suggested from the shape of the O−C diagram is the light travel-time effect, which we thoroughly examine. We used original photometric and spectroscopic measurements and investigated the period evolution using available maximum times spanning more than one century. If the binary hypothesis is valid, Z CVn orbits around a black hole with minimal mass of 56.5 $\mathfrak{M}_{\odot}$ on a very wide ($P_{\rm orbit} = 78.3$ yr) and eccentric orbit ($e = 0.63$). We discuss the probability of the formation of a black hole–RR Lyrae pair, and, although we found it possible, there is no observational evidence of the black hole in the direction to Z CVn. However, the main objection against the binary hypothesis is the comparison of the systemic radial velocity curve model and spectroscopic observations that clearly show that Z CVn cannot be bound in such a binary. Therefore, the variations of pulsation period are likely intrinsic to the star. This finding represents a discovery/confirmation of a new type of cyclic period changes in RR Lyrae stars. By the analysis of our photometric data, we found that the Blazhko modulation with period of 22.931 d is strongly dominant in amplitude. The strength of the phase modulation varies and is currently almost undetectable. We also estimated photometric physical parameters of Z CVn and investigated their variations during the Blazhko cycle using the inverse Baade–Wesselink method.

Key words: methods: data analysis – techniques: photometric – techniques: spectroscopic – binaries: general – stars: individual: Z CVn – stars: variables: RR Lyrae.

1 INTRODUCTION

A significant portion of stars in the Universe are known to be bound in double or multiple systems (e.g. Abt 1983; Guinan & Engle 2006). Pulsating stars in such systems are of particular interest because their physical parameters can be determined independently both from pulsation characteristics and from investigation of their orbital motion (Prada Moroni et al. 2012; Lee et al. 2017). Moreover, eclipsing binaries offer the only chance to directly determine the mass of both components with very good accuracy without any additional assumptions (Hełminiak et al. 2009; Kiefer et al. 2016).

Many pulsating stars of various types have been identified in binary systems (see, for example, the lists by Szabados 2003; Soydugan et al. 2006; Zhou 2010). However, stars of RR Lyrae (RRL) type seem to be an exception. Apart from TU UMa, which is quite probably in binary with low-mass companion (Wade et al. 1999; Liška et al. 2016b),[1] not a single classical RRL has been

★ E-mail: maska@physics.muni.cz (MS); jiriliska@post.cz (JL)

[1] Unambiguous spectroscopic confirmation is still missing even in TU UMa.

unambiguously confirmed to reside in a binary system so far. There are only several tens known RRL binary candidates (see the online version of the list by Liška et al. 2016a; Liska & Skarka 2016)[2] out of more than one hundred thousands of catalogued RRL stars (field RRLs plus RRLs from the LMC, SMC and Galactic bulge, Watson, Henden & Price 2006; Soszyński et al. 2014, 2016). This is in clear contrast with stars of other types.

The vast majority of these candidates were detected indirectly by analysing cyclic variations of the pulsation period caused by hypothetical orbital motion around centre of mass together with an unseen companion – the well-known light travel-time effect (LTTE, Irwin 1952; Sterken 2005). In the case of RRLs, this method is the most promising because of their physical properties and evolutionary history. If the companion is of lower luminosity, mass or size, it would be hardly detectable via eclipses, radial-velocity (RV) measurements or colour peculiarity (see the discussion in Skarka et al. 2016). It could be naturally expected that only wide systems with very long orbital periods (typically more than hundreds of days) can be detected via LTTE because the changes in time delays are proportional to the size of the orbit. Tight systems with small orbital semi-major axis will cause only very small variations of the pulsation period of RRL that would be hardly detectable.

However, the wide systems identifiable using LTTE are the most important and interesting because the large separation secures that the RRL component is not affected by the mass transfer, which allows us to investigate a classical RRL that does not differ from an RRL star that evolved separately as an isolated single star. Evolution of stars in short-period semi-detached or contact systems can also produce stars that behave like a classical RRLs (the so called Binary Evolution Pulsators – BEPs, Pietrzyński et al. 2012; Smolec et al. 2013), but has different physical origin and characteristics. Karczmarek et al. (2017) showed that BEPs, which could contaminate about 0.8 per cent of genuine RRL stars, occur only among binaries with orbital periods shorter than about 2000 d. The vast majority of the recently discovered candidates (Hajdu et al. 2015; Liška et al. 2016a) have proposed orbital periods significantly longer than this limit (years to decades), suggesting that classical RRLs could be present in these candidate systems.

This is also the case of Z CVn (=GSC 03023-00942; J2000 $\alpha = 12^{\rm h}49^{\rm m}45^{\rm s}.4$, $\delta = +43^\circ46'25''.1$), which is the subject of this paper. Z CVn is an RRab type star discovered by Ceraski (1911). Besides the long-term cyclic period variations identified by Firmanyuk (1982) and Le Borgne et al. (2007), Z CVn shows significant short-period light curve modulation (the so-called Blazhko effect, Blažko 1907) with a period of about 22.75 d (Kanyó 1966). The phenomenon in this star is even more interesting, since the modulation period was reported to change with opposite sign to changes in the pulsation period (Le Borgne et al. 2012).

We performed extensive photometric (Section 2) and spectroscopic monitoring (Section 3) of Z CVn during four and two seasons, respectively. We utilized available maximum times from the literature and also collected available data from various sky surveys to get as many maximum times as possible for the investigation of cyclic long-term period changes during the past century (Section 4). In this section, we also model the possible binary orbit. In Section 5, we investigate the period variations on shorter timescales and investigate the Blazhko behaviour. The basic physical characteristics and their variations during the Blazhko cycle are investigated in Section 6. Thorough discussion about the binarity is given in Section 7. We summarize the results in Section 8.

[2] http://rrlyrbincan.physics.muni.cz/

2 PHOTOMETRIC OBSERVATIONS AND MAXIMUM TIMES

Z CVn was observed in the frame of *the Czech RR Lyrae stars observing project* (Skarka, Honkova & Jurysek 2013; Skarka et al. 2015a) during 2012–2015 at a private observatory in Znojmo, Czech Republic (see the data distribution in the top panel of Fig. 1). Multicolour $BVR_{\rm c}I_{\rm c}$ 120s exposures were gathered using an 8-inch Schmidt-Cassegrain telescope equipped with G2-0402 CCD camera (768×512 KAF-0402ME chip). Observations from Znojmo were complemented in 2015 with data gathered at the Observatory and Planetarium Brno (14-inch Schmidt-Cassegrain telescope equipped with G4-16000 CCD camera, KAF-16803 chip, five nights). In total, about 2400 points in each filter were collected during 53 nights spanning almost 1150 d[3] (for more details see Table 1 with the journal of observations).

Each observation was reduced in a classical way using dark and flat-field frames. We used C-MUNIPACK software[4] for the data reduction and for aperture photometry. USNO-B1.0 1339-0234455 and USNO-B1.0 1338-0234449 served as comparison and check stars (see Table 2). Relative accuracy of a photometric point was between 0.009 and 0.07 mag depending on used filter and observing conditions. The data were transformed to standard Johnson-Cousins system applying transformation coefficients determined on the basis of observation of Landolt (1992) fields in each season. Standard *BVri* magnitudes of the comparison stars were adopted from the UCAC4 catalogue (Zacharias et al. 2013). Johnson-Cousins $R_{\rm c}$ and $I_{\rm c}$ magnitudes were calculated from *r* and *i* Sloan magnitudes using equations from Jordi, Grebel & Ammon (2006).

Based on our photometric data, we estimated the light elements as

$$\mathrm{HJD}\ T_{\max} = 2456048.3301(7) + 0.6539498(3)\,\mathrm{d} \times \mathrm{E_p}. \quad (1)$$

These values were used for construction of the pulsation-phase curves shown in Fig. 1. The zero epoch from equation (1), which was chosen as the best defined among the maxima with the highest amplitude, was also used as the basic zero phase for blazhko-phased curves. For more details about the period investigation, methods and software used, see Sections 4 and 5.

From the well-covered maximum phases present in our *V* data set, we determined 18 maximum times using the polynomial-fitting method described in Skarka et al. (2015b). Moreover, we got three additional maximum times (in 2013 in Strömgren *y* and in 2016 in *V*) with different telescopes with unknown calibration coefficients.[5] New maximum times were complemented with maximum times from the GEOS RR Lyr data base[6] (version 2016 July 19, Boninsegna et al. 2002; Le Borgne et al. 2007). We also searched the literature for maximum times not listed in the GEOS data base, and determined new ones from various sky surveys. This gave us 19 values from Prager (1939), 1 value from Blažko (1926), 1 value from Strelkova (1964), 7 values from Lampe (1970), 6 determined from the SuperWASP survey (Pollacco et al. 2006; Butters et al. 2010),

[3] All the data are available online as a supporting material to this paper.
[4] http://c-munipack.sourceforge.net/
[5] This is the reason why these observations are not included in our photometric data set.
[6] http://rr-lyr.irap.omp.eu/dbrr/index.php

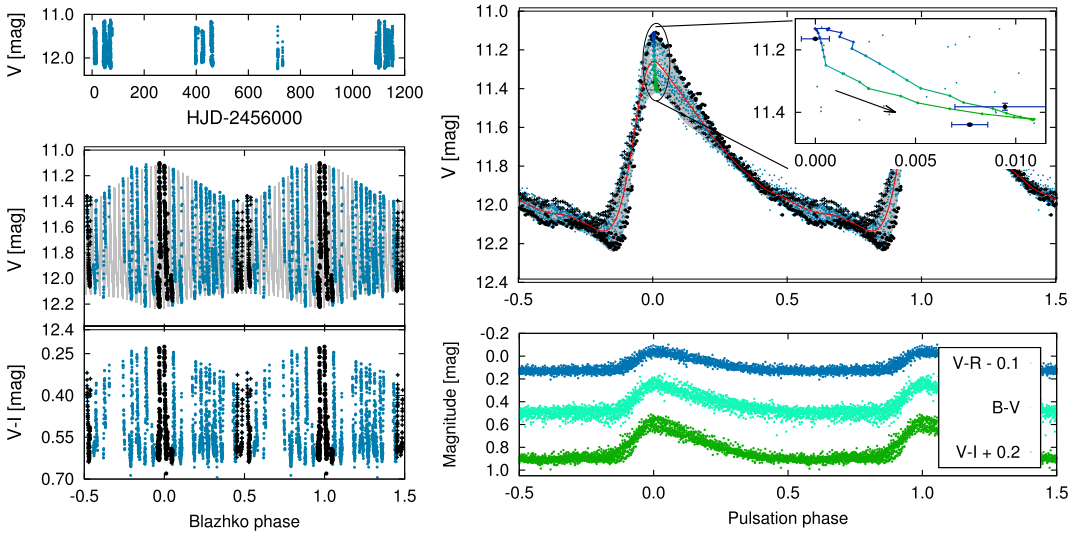

Figure 1. Distribution of the photometric data (top left-hand panel), data phased with Blazhko and pulsation period (bottom left- and top right-hand panels, respectively). The bottom right-hand panel shows the colour indices phased with the pulsation period. Blazhko phases around 0.0 and 0.5 are highlighted with black symbols. The grey dots show the synthetic light curve according to our model (see Section 5). The magnified part around the maximum light in the top right-hand panel shows synthetic maxima of the light curve during one modulation cycle (the direction of the movement is shown by the arrow). Three maxima from 2012 are shown with black circles. The full red line shows the mean light curve.

Table 1. Observation log. The last four rows show number of frames in particular filters.

Season	2012	2013	2014	2015	Total
Nights	21	12	3	17	53
Start	2456 008	2456 397	2456 712	2457 090	–
Span (d)	68	66	19	64	1146
B	968	428	82	961	2439
V	954	468	83	951	2456
R_c	957	443	82	935	2417
I_c	936	428	81	942	2387

Table 2. Stars used as comparison and check stars (USNO-B1.0 ID).

ID	1339-0234455	1338-0234449
RA (2000)	12 49 50.3	12 50 21.9
Dec. (2000)	+43 54 19.6	+43 54 19.6
B (mag)	12.770	13.457
V (mag)	12.037	12.743
R_c (mag)	11.721	12.387
I_c (mag)	11.326	11.897

6 from the NSVS (ROTSE) data (Woźniak et al. 2004) and 11 from the DASCH project (e.g. Grindlay et al. 2009).

Maximum times from sources with sparse data (NSVS, DASCH) were calculated as the mean maximum time from 30 points using template fitting method described in Liška et al. (2016b). We omitted data with high uncertainty and took into account various length of exposures of the photographic plates in case of the DASCH data (for details see Liška et al. 2016b). From the GEOS data base, we omitted maximum times marked as 'pr. com.', a few other values with unfindable source, and apparent outliers. All in all we used 227 maximum times (155 from GEOS data base), out from which 57 were photographic, 53 visual+unknown origin (51+2),[7] 14 photoelectric, 103 CCD+DSLR (101+2). Although our sample covers more than 120 yr[8] and contains a lot of maximum times, it cannot be considered as complete. For example, we did not succeed in finding original maximum times that Firmanyuk (1982) used to plot O−C in his fig. 4. All maximum times that we used are available online as a supporting material to this paper and at the CDS.

3 SPECTROSCOPY AND RADIAL VELOCITY

Z CVn was spectroscopically observed in 2015 and 2016 as one of the primary targets of the observing project focused on binarity among RR Lyrae stars announced by Guggenberger, Barnes & Kolenberg (2016). Observations were carried out at McDonald Observatory, Texas using *f*/13.5 Cassegrain focus of the 2.1-m Otto Struve telescope. Spectra were gathered with the Sandiford Echelle Spectrometer (McCarthy et al. 1993). We have continuous spectral coverage over the observed range of 4250–4750 Å with resolving power of $R \sim 55\,000$. Integration time was 1690 s for all observations (3 per cent of the pulsation period). Th- Ar spectra were taken for wavelength calibration after each stellar spectrum, and before the telescope was moved. The signal-to-noise ratios per resolution element are between 10 and 33, depending on the brightness of the star and the sky conditions.

[7] The two maximum times with unknown origin are probably based on visual observations as noted in the GEOS data base, but we did not succeed in finding the original papers by N. Florja cited in Prager (1939), where the maximum times come from.

[8] The first maximum time comes from Harvard plate collections and dates back to 1894 (Prager 1939).

Table 3. Newly determined and publicly available RV measurements for Z CVn.

T_{obs} [HJD −2400000]	RV [km s^{-1}]	Reference	T_{obs} (HJD −2400000)	RV (km s^{-1})	Reference
57087.7387	+6.3(1.9)	TS	57409.007	+15.0(4.7)	TS
57087.8201	+14.6(1.6)	TS	22884.743	+8.3(35)	A73
57087.9056	+18.2(1.4)	TS	24185.024	+34(35)	A73
57091.8589	+18.2(1.9)	TS	45460.721	+29(12)	HB85
57091.94	+10.2(0.9)	TS	45460.7345	+15(12)	HB85
57092.7161	−25.3(1.0)	TS	45462.6765	+7(12)	HB85
57176.6637	+1.4(1.1)	TS	45462.69	+14(12)	HB85
57177.6545	−7.1(2.4)	TS	47973.8224	−28(28)	L93, L94
57177.7476	−14.3(2.0)	TS	47974.879	+34(32)	L93, L94
57408.9802	+13.9(1.3)	TS			

Notes. A73 – (Abt 1973); HB85 – (Hawley & Barnes 1985); L93 – (Layden 1993); L94 – (Layden 1994); TS – This Study

We used standard IRAF[9] routines for data reduction. RV standard stars were observed several times during the course of each night from the Geneva list of CORAVEL standard stars (Udry et al. 1999).[10] The radial velocities were determined by cross-correlating the standard star spectra with the Z CVn spectra using the IRAF task fxcor. Only metal lines were used in the cross-correlation, as the hydrogen lines are known to have a phase offset and different velocity amplitudes compared to metal lines (Sanford 1949; Oke, Giver & Searle 1962; Sesar 2012). A total of 11 RVs estimated from our observations are given in Table 3.

Besides our measurements, we searched for the RVs in literature. The first RV measurement comes from Joy (1938). Unfortunately, his value was published without observing date. Other RV comes from Preston (1959, no time of observation given), who detected changes in spectral type during pulsation cycle as A8–F5 (Hγ-line) and A3–A7 (Ca II K-line). Furthermore, we found only three sources of RV measurements – two RVs from Abt (1973), four RVs from Hawley & Barnes (1985) and two RVs from Layden (1993, 1994).[11] All used RV values are listed in Table 3.

RV data setsfrom Abt (1973, observed in 1921 and 1925) were published without individual uncertainties, but Layden (1994) assign the measurements taken in the first half of the 20th century with common uncertainty of 35 km s^{-1}. Measurements by Hawley & Barnes (1985, also without individual uncertainties) have common uncertainties of 12 km s^{-1}, accuracy of Layden (1993, 1994) is within 30 km s^{-1}. Our measurements are of an order of magnitude better precision than these measurements (typically about 2 km s^{-1}).

The problem of using historical measurements is that the RVs were estimated on the basis of different spectral lines that form in different layers of the stellar atmosphere. Thus, the combination of historical measurements could be tricky. Abt (1973) does not provide information about used lines, Layden (1993, 1994) used Hβ and Hγ Balmer lines and the Ca II K line, whereas Hawley & Barnes (1985) like us used only metallic lines. To unify the heterogeneous RV estimations and determine the correct systemic RV, we used the RV templates from Sesar (2012), who provides normalized RV curves for Hα, Hβ, Hγ and metals.

[9] IRAF is distributed by the National Optical Astronomy Observatories, which are operated by the Association of Universities for Research in Astronomy, Inc., under cooperative agreement with the National Science Foundation.

[10] http://obswww.unige.ch/~udry/std/stdcor.dat

[11] He published only the mean RV. Therefore, we used measurements from his PhD thesis available at http://physics.bgsu.edu/layden/ASTRO/PUBL/THESIS/.

Table 4. Newly determined systemic RVs of Z CVn (third column), their errors (last column) and the mean date of the measurement (second column). The short cuts of the sources are the same as in Table 3.

Source	T_{mean}	γ (km s^{-1})	Err γ (km s^{-1})
A73	2423 535	8.1	13.0
HB85	2445 462	10.6	4.1
L94	2447 975	1.1	12.1
TS	2457 172	−0.9	2.2

We followed the approach described in Liška et al. (2016b). First, we modelled the template from metallic lines adopted from Sesar (2012) with high-order harmonic polynomial and compared them with the four observational data sets (Table 3) that were time-shifted according to cyclic period changes (subtraction of the model of the LTTE, Section 4.1). Individual systemic RV shifts (γ velocity) for each data set (Table 4) were estimated using non-linear least-squares method. Uncertainties were determined statistically using bootstrap-resampling method.

4 LONG-TERM PERIOD EVOLUTION

Already, Blažko (1922) noticed from his 25 maximum times determined between 1912 and 1917 that the pulsation period of Z CVn varies. Four years later, Blažko (1926) published the light elements that included quadratic term indicating slow lengthening of the pulsation period. Firmanyuk (1980a,b, 1982) was the first who showed that Z CVn undergoes strong cyclic period variations with period of about 60 yr and amplitude of the O−C of about 0.6 d. Similar cyclic pattern as the one shown in Firmanyuk (1982) also shows the O−C diagram in Le Borgne et al. (2007, Fig. 4).

The O−C diagram constructed from our set of maximum times also suggests that the pulsation period could be cyclically unstable with period of about 80 yr (main panel of Fig. 2). The amplitude of the period oscillations is huge and almost exceeds the length of the pulsation cycle. Such strong variations are not common among RR Lyrae type stars, but also not unique (see e.g. Firmanyuk 1982). However, our understanding of period changes in RRLs is still poor and such strong and possibly cyclic behaviour is difficult to explain.

The stellar evolution and pulsation theory suggest that RRLs should slowly change their pulsation periods during evolution through the instability strip simply because of slow change of their radius according to the period-mean density law $P\sqrt{\rho} \sim$ const (Ritter 1879). This smooth secular period changes, which can go in both directions (period shortens when the star evolves blueward, whereas it lengthens when the star evolves towards the red edge of the instability strip), are commonly observed in globular clusters (e.g. ω Cen, IC4499, M5, M3, Jurcsik et al. 2001; Kunder et al. 2011; Szeidl et al. 2011; Jurcsik et al. 2012a, just to mention some recent studies), but also in field stars (e.g. Le Borgne et al. 2007). However, significant portion of stars investigated in these studies show erratic abrupt changes (in the Galactic field it is, for example, XZ Cyg or RR Gem, LaCluyzé et al. 2004; Sódor, Szeidl & Jurcsik 2007) and/or rates of period changes that are an order of magnitude larger than evolutionary effects could explain (Iben & Rood 1970). This means that there must be some additional effects that act in RRL stars that could cause complex period

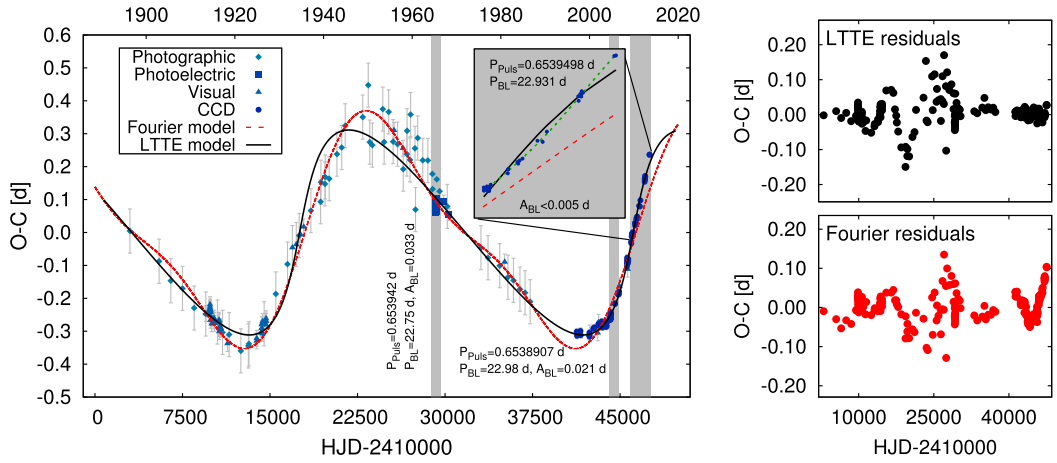

Figure 2. Left-hand panel: The overall period evolution over the time span of more than 100 years (main panel). Different symbols denote different types of observations (diamonds – photographic, squares – photoelectric, triangles – visual, circles – CCD). The full black line shows the model based on the LTTE assumption, whereas the red dashed line shows the Fourier fit with two sine components. The grey-shaded areas show the intervals when pulsation and modulation periods and modulation amplitude were determined (see the text for more details). Right-hand panel: Residuals after removing the models.

evolution on a significantly shorter than evolutionary time-scales. It was found that Blazhko stars show complex/irregular O−C s with large amplitudes more often than stars with stable light curve, thus, suggesting that Blazhko effect and rapid irregular period changes could have a common origin (Szeidl et al. 2011; Jurcsik et al. 2012a).

Sweigart & Renzini (1979) suggested that the discrete mixing events near the boundary of semiconvective zone of an RRL star could be responsible for the positive, negative, but also irregular period changes. Also Firmanyuk (1982) supposed that cyclic period variations could rise from changes of the internal structure of a star, but without any further details. However, Arellano Ferro et al. (2016) found that, at least for some stars in M5, the irregular O−C variations could be caused by improper counting of the cycles and that it must not be a real feature of a star.

An alternative explanation of the short-time-scale sudden variations of the pulsation period comes from Cox (1998), who suggests that the period changes could be caused by small changes in a helium composition gradient below the hydrogen and helium convection zones. He proposes that the time-scales of the variations could correspond to the time-scale of an occasional dredge up of helium caused by convective overshooting (∼days).

Another explanation, at this time relying to the origin of the cyclic period variations, counts with the hydromagnetic effects that take place periodically – analogue to the solar magnetic cycle (Stothers 1980). Change in the magnetic energy content during the cycle should result in a change of stars radius that will further affect the pulsation period. This effect was offered as a possible explanation of the cyclic O−C variations of BE Dor by Derekas et al. (2004). However, as they already noted, this explanation faces significant troubles since it seems that RRLs do not have strong surface magnetic fields (Chadid et al. 2004).

4.1 The LTTE

Because none of the proposed hypotheses were supported by observations, the most promising explanation of smooth, regular and possibly repetitive O−C variations of Z CVn is the binary scenario that could be modelled with LTTE. Among RRLs, the LTTE has been very rarely reported so far and is proposed only in a few dozens of candidates (Hajdu et al. 2015; Liška et al. 2016a; Liska & Skarka 2016).

We used the methods and codes thoroughly described in Liška et al. (2016b) to model the O−C variations and get parameters of suggested binary based on LTTE. During the fitting process, the best model is found using non-linear least squares method, and uncertainties of the final parameters are estimated statistically via bootstrap resampling (5 000 repetitions of the calculation with re-sampled data sets). The final model is shown with the full black line in the left-hand panel of Fig. 2 and pulsation and orbital parameters resulting from the fit are listed in Table 5. Note that the mean pulsation period during the assumed 80-yr cycle is significantly different (of about 10^{-4} d) from the actual period in equation (1). This demonstrates well how dramatic the variation is.

Because the uncertainties of the maximum times are often missing, unreliable or unrealistic, we assign photographic:visual+unknown:photoelectric:CCD+DSLR (shown with different symbols in the main panel of Fig. 2) with weights 1:7.7:14.2:50.4 that are based on the uncertainties of particular type of maxima that were estimated on the basis of scatter in the residual O−C (0.067:0.024:0.018:0.009 d). These errors are probably slightly larger than the real uncertainties because of additional scatter that could be present due to the Blazhko effect, which causes (small) variations in the O−C amplitude (Section 5).

The large amplitude of the O−C dependence, which provides information about the size of the orbit ($A_{\rm LTTE} = 0.3113$ d; $a_1 \sin i/c = 69.7$ au), in combination with a relatively short LTTE period ($P_{\rm orbit} = 28\,590$ d) suggests that the system must be very special with an exotic companion. If the binary hypothesis is correct, our model (Table 5) implies that Z CVn orbits around a massive black hole (BH) with a minimal mass of $\mathfrak{M}_{2,\rm min} \sim 57\,\mathfrak{M}_\odot$ at a very eccentric orbit with $e \sim 0.63$.

Alternatively, the O−C dependence could be comparatively well described with Fourier series (one frequency and its harmonics) with $P = 78$ yr. The dashed red line in the left-hand panel of

Table 5. Pulsation and orbital parameters for the binary hypothesis[a].

P_{puls} (*d*)	M_0 (HJD)	P_{orbit} (d)	T_0 (HJD)	e	ω (°)	A (light-day)	$a_1 \sin i$ (au)	$f(\mathfrak{M})$ ($\mathfrak{M}_\odot$)	$\mathfrak{M}_{2,min}$ ($\mathfrak{M}_\odot$)	K_1 (km s^{-1})	χ^2_R	N_{max}
0.65384853^{+11}_{-10}	2453531.6768^{+44}_{-52}	$28\,590^{+130}_{-110}$	2456149^{+74}_{-88}	0.6344^{+98}_{-85}	$0.7^{+1.6}_{-1.8}$	0.4027^{+55}_{-61}	$69.7^{+1.0}_{-1.1}$	$55.3^{+2.3}_{-2.6}$	$56.5^{+2.3}_{-2.6}$	34.33^{+52}_{-54}	1.074(95)	227

Notes. [a]Columns contain following parameters: P_{puls} – main pulsation period, M_0 – zero epoch of pulsations, P_{orbit} – orbital period, T_0 – time of periastron passage, e – numerical eccentricity, ω – argument of periastron, $A - a_1 \sin i$ in light days (semi-amplitude of LiTE A_{LTTE} can be calculated as $A_{LTTE} = A\sqrt{1-e^2\cos^2\omega}$), $a_1 \sin i$ – projection of semi-major axis of primary component (RRL) a_1 according to the inclination of the orbit i, $f(\mathfrak{M})$ – mass function, $\mathfrak{M}_{2,min}$ – the lowest mass of the second component, the value was calculated for inclination angle $i = 90°$ and adopted mass of primary $\mathfrak{M}_1 = 0.6\,\mathfrak{M}_\odot$, K_1 – semi-amplitude of RV changes primary component, χ^2_R – normalized value of χ^2, where $\chi^2_R = \chi^2/(N_{max} - g)$ for the number of used maxima times N_{max} and the number of free (fitted) parameters g (LTTE, $g = 7$), and N_{max} – number of used maximum times.

Fig. 2 shows the fit with two harmonics.)[12] Residuals after removing the main trend shown in the right-hand panels of Fig. 2 are still quite large and show similar dependence in both cases, suggesting some additional quasi-periodic long cycle. Naturally, the more harmonics are used, the lower the residuals. It is very difficult to decide whether the shape of residuals has real origin or is simply produced by the inappropriate models. In addition, residuals of the LTTE model after HJD 2453000 (populated mainly with high-quality CCD measurements) differ from the residuals before this date. This is also very suspicious and gives rise to doubts about the relevance of the O−C models. The binary hypothesis is thoroughly discussed in Section 7.

5 SHORT-TERM PERIOD EVOLUTION AND THE BLAZHKO EFFECT

The amplitude and phase/frequency modulation of the light curve of Z CVn is known since the study by Blažko (1922). From all panels of Fig. 1, it is apparent that the modulation is quite strong and dominates in amplitude, which exceeds almost 0.3 mag in *V*. Because our data are single-site and show strong seasonal pattern (top left-hand panel of Fig. 1), the frequency spectra are strongly dominated by daily and yearly aliases (see the spectral window shown in the top panel of Fig. 3).

PERIOD04 (Lenz & Breger 2005) was used for consecutive pre-whitening and proper identification of the significant peaks with S/N > 3.5.[13] We analysed the data in all passbands separately with permanent visual supervision at all steps, which was necessary to prevent confusion with aliases. As expected, we identified the basic pulsation frequency f_0 and its harmonics to the 10th order in *V* and R_c (see Table B1 with the full frequency solution in all four filters). In addition, close equidistant peaks near the pulsation harmonics $kf_0 \pm f_{BL}$, $kf_0 - f_M$ were identified (red arrows in the middle panels of Fig. 3). Such peaks are assumed to be the products of modulation with frequency that is equal to the spacing between pulsation harmonic and side-peak (Szeidl & Jurcsik 2009; Szeidl et al. 2011). No peak corresponding directly to the modulation frequency, which is usually present in the frequency spectra of high-quality data of Blazhko stars, was detected. Because this peak relates to the change of the mean magnitude (Szeidl et al. 2011), the mean magnitude varies by less than 0.006 mag, which is the significance limit in the region where the assumed peak should be situated.

[12] The error of this period is comparable with the value itself.

[13] The S/N is calculated as the ration between the amplitude of the peak and average amplitude of the frequency spectra in the ±1 c/d interval around the peak.

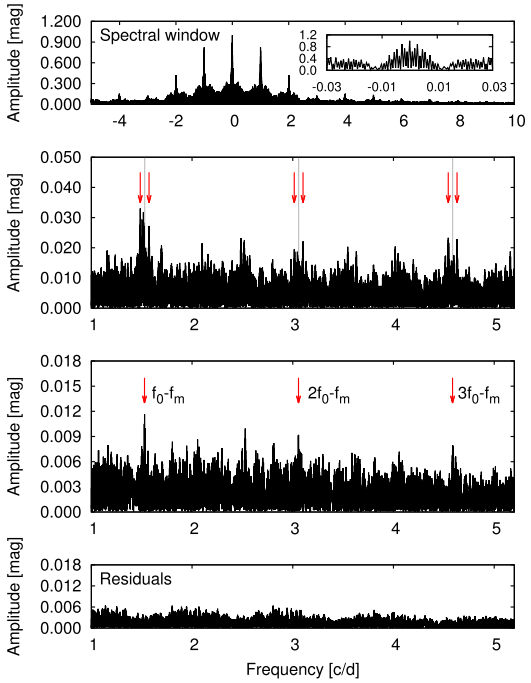

Figure 3. Frequency window (top panel) together with the frequency spectra during the pre-whitening process. The second panel from the top shows the frequency spectra after pre-whitening with the basic pulsation components. The positions of the side peaks are marked with arrows. The bottom middle panel shows the situation after the removal of the side peaks (arrows show the position of the side peaks related to additional long-term modulation). The bottom panel shows the residuals after pre-whitening with all frequencies listed in Table B1.

When the list with significant peaks was available, we used the LCFIT routine (Sódor 2012) and modelled the light changes using

$$A(t) = A_0 + \sum_{i=1}^{N} A_i \sin\left(2\pi f_i [t - T_0] + \varphi_i\right), \quad (2)$$

where A_i and φ_i is the amplitude and phase of the i-th component with frequency f_i, T_0 is the zero epoch from equation (1) and N is the number of the relevant detected peaks. Because the frequencies are not independent, we adjusted only f_0, $f_0 - f_{BL}$ and $f_0 - f_M$, the other frequencies were calculated from these three independent frequencies.

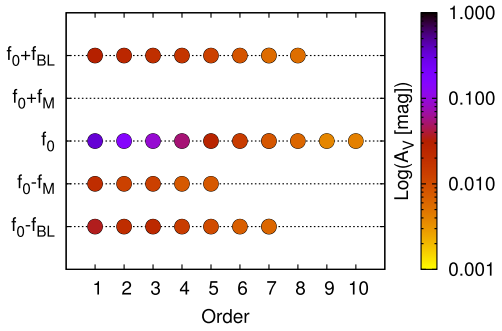

Figure 4. The diagram showing the structure and amplitude of the side peaks around ten detected harmonic orders of f_0. The spacing of the side peaks is not in scale.

The values of frequencies and corresponding pulsation and modulation frequencies slightly differ for each passband (within 2σ). Because there is no systematics from short- to long-wavelength filters and different period in different filters is also physically impossible, we assume that the differences result from different quality and point distribution in different filters. Thus, we calculated the periods as the average values from the BVR_cI_c data sets. The resulting pulsation, Blazhko and second modulation periods are $P_{puls} = 0.6539498(3)$ d, $P_{BL} = 22.931(4)$ d and $P_M = 1100(20)$ d. The long P_M could be an artefact of the secular period change because it is comparable with the time span of the data and corresponding side peaks always appear on the low-frequency side of the pulsation harmonics.

The structure of the side-peak multiplets is apparent from the echelle graph in Fig. 4. The highest side peak has amplitude ten times lower than f_0, and the lowest significant peak has amplitude of about 0.004 mag. It is apparent that the closer peak corresponding to the longer modulation/secular period change was detected only on the left-hand side of kf_0. The amplitudes of the Blazhko side peaks are almost equal at all orders,[14] but at some kf_0, the peak to the right-hand side has larger amplitude, whereas at other kf_0, the peak to the left-hand side is higher. Because the amplitude of the peaks can be influenced by the sampling and gaps in the data (Jurcsik et al. 2005), we assume that the effect of slightly different amplitude ration of the side peaks is caused by the data characteristics.

The modulation is well detectable also in the variation of the maximum brightness from our observations [$P_{BL} = 22.932(7)$ d, bottom right-hand panel of Fig. 5]. This P_{BL} agrees perfectly with the value that we got from the spacing of the side-peaks in the Fourier spectra of the time series. On the other hand, no significant periodicity close to P_{BL} with amplitude larger than about 0.005 d has been detectable in CCD O−Cs since 2012. It is directly apparent from the amplitude of the residuals after HJD 2450000 in the LTTE residuals in the left-hand panel of Fig. 2, and also from the top left-hand panel of Fig. 5, which shows O−C after removing the long-term trend (linear trend + sinusoid with period of about 2300 d) shown with the green dashed line in the insert in Fig. 2. The full amplitude of the phase changes during the Blazhko cycle corresponds to about 0.011 d (see the insert in Fig. 1), which is the full amplitude in the O−C shown in the top right-hand panel of Fig. 5. No wonder that

[14] This further indicates the dominance of the amplitude modulation (Benkő, Szabó & Paparó 2011).

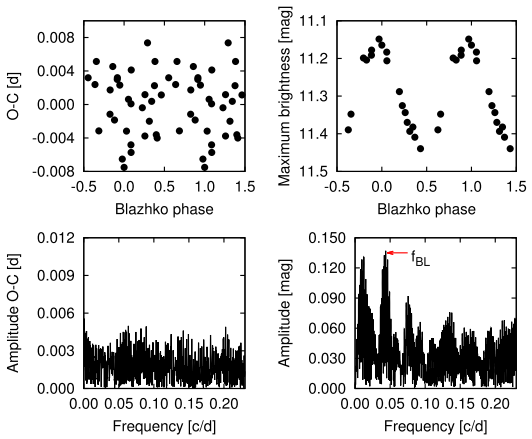

Figure 5. Brightnesses of the maximum light and O−C values phased with the detected Blazhko period $P_{BL} = 22.931$ d (top panels) and frequency spectra of the O−C and maximum magnitudes.

no periodicity is detected in the corresponding frequency spectra (bottom left panel of Fig. 5).

However, based on light-curve fitting in different Blazhko phases, we detected phase variations of the basic pulsation frequency peak that correspond to O−C variations with amplitude 0.01 d (see Section 6.1 and the second top plot in the left-hand panel of Fig. 7). Possible explanation is that maximum time takes into account only data points around light maximum, thus it has larger uncertainty than a Fourier phase that relies on the data from the full pulsation cycle.

A very weak period modulation during Blazhko cycle is in contrast to Le Borgne et al. (2012), who clearly detected also phase modulation with the peak-to-peak amplitude of 0.021 d and period $P_{BL} = 22.98$ d in their TAROT observations (see their fig. 7). They found that in Kanyó (1966) data around JD 2439000, the pulsation period was 0.653942 d, modulation period was 22.75 d and full amplitude of the O−C variations was 0.033 d. In TAROT data (JD 2454200), the pulsation period was shorter (0.653 8907 d), Blazhko period was longer (22.98 d) and the full O−C amplitude was 0.021 d (see the shaded areas and corresponding labels in the main panel of Fig. 2 to get a better picture).

At the time of our observations (after JD 2456000), the pulsation period roughly exceeds the period in the Kanyó's time, but the Blazhko period is longer than was around JD 2439000 and the amplitude of the O−C is so low that the modulation in period is undetectable. It is likely that the variation of the Blazhko period somehow follows the variation of the pulsation period, but since we have only three estimates (at Kanyós, Leborgne's and our times), we cannot say much about their correlation. If the O−C is periodic, it would be interesting to investigate the relation of the pulsation and modulation periods after the pulsation period starts to lengthen (after about 2462 000). It is also interesting to point out that the P_{BL}/P_{Puls} ratio oscillates around 35 and the actual value is very close to this value ($P_{BL}/P_{Puls} \sim 35.065$).

6 PHYSICAL CHARACTERISTICS

Unfortunately, our low S/N spectroscopy does not allow us to estimate the atmospheric parameters directly from comparison with theoretical spectrum. In addition, the spectra change during the

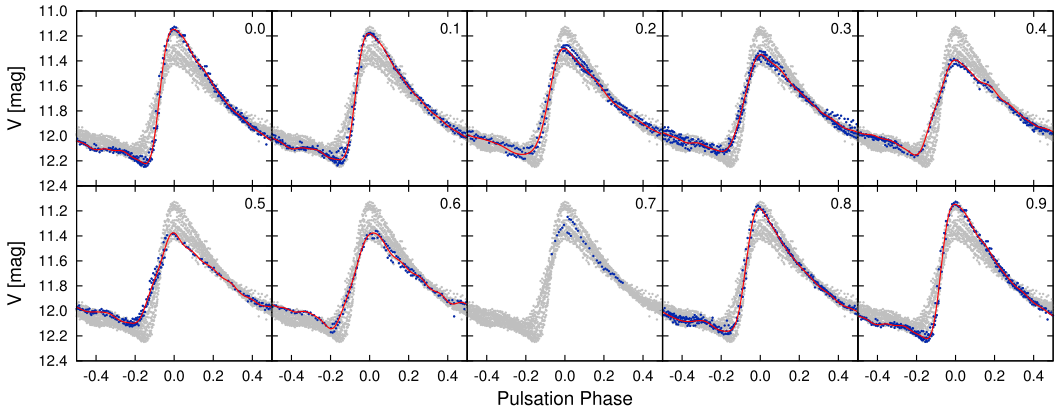

Figure 6. Data for particular Blazhko phases (blue points) folded with pulsation period. Grey dots show phase curves of all our *V*-observations. The model light curve is shown with the full red line for each Blazhko phase.

Blazhko cycle, and we have only very sparse observations. However, there is another simple way to get information about the basic physical parameters from photometry.

Because the light-curve characteristics necessarily reflect the physical conditions inside the star, it is possible to estimate them just by investigation of the shape of the light curve. This approach employing phase-independent Fourier parameters (Simon & Lee 1981) was applied many times and many calibrations were defined (e.g. Jurcsik & Kovács 1996; Jurcsik 1998; Kovács & Walker 2001; Nemec et al. 2013). We estimated the parameters in 10 different Blazhko phases (Fig. 6, Table A1), as the global value using the mean light curve shown in the top right-hand panel of Fig. 1, and using Blazhko-free light curve[15] after the modulation was subtracted. The averaged parameters over the Blazhko cycle are within the errors the same as the parameters coming from the global mean light curve (compare values for 'Average' and 'Mean LC' rows in Table A1), which confirms the already known finding by Jurcsik et al. (2009c). However, we prefer values based on modulation-free light curve because such light curve gives metallicity almost identical to the spectroscopic one (−1.92 in Zinn & West 1984 scale versus −1.98 estimated by Layden 1994). The details about the procedure and used empirical calibrations can be found in Appendix, Section A.

6.1 Inverse Photometric Baade–Wesselink Analysis

The inverse photometric Baade–Wesselink method (IPM – Sódor, Jurcsik & Szeidl 2009) was developed to derive global mean physical parameters of RRab stars from multicolour photometry, without spectroscopic RV measurements, as well as changes of these parameters during the pulsation and the modulation cycles. The method was successfully applied before to several Blazhko stars (Jurcsik et al. 2009b,a; Sódor 2009; Sódor et al. 2011; Jurcsik et al. 2012b; Sódor et al. 2012) to determine the variations in pulsation-phase-averaged mean radius, $\log g$, M_V, luminosity and effective temperature. During this study, we employed the IPM on Z CVn.

We followed the methodology detailed, for example, in Jurcsik et al. (2009a). As a first step, we attempted to determine the Blazhko-phase-independent constant parameters, mass ($\mathfrak{M}$), distance (d) and absolute visual magnitude (M_V). For this reason, we run the IPM on the Blazhko-free light curve of Z CVn with four different settings (see details in Sódor et al. 2009). We accepted metallicity of [Fe/H] $= -1.64$ (Table 6) for Z CVn. Unfortunately, when all unknown parameters were free during the fitting process, the method resulted in implausible high $\mathfrak{M}$, d and M_V values (about 1.1–1.4 $\mathfrak{M}_\odot$, 2300–2600 pc and from 0.0 to −0.25 mag, respectively). Therefore, we fixed the mass to the value from Table 6. We also fixed the distance at 1760 pc, $A_V = 0.05$ mag and $E(B-V) = 0.015$ mag were taken into account when running the IPM.

When the modulation-free values were determined, we proceeded with the analysis of the different Blazhko phases. To attain sufficient pulsation-light-curve coverage, we divided the data to 10 overlapping Blazhko-phase-bins, extending the bins by ±0.075 Blazhko phase towards both directions, that is, each bin had a width of 0.25 in modulation phase. Even though four equal-length non-overlapping bins would be completely independent and sufficient to resolve the variations with the Blazhko modulation, we chose to show the results for 10 overlapping bins to easily follow the character of the physical-parameter changes. The results, as the functions of Blazhko phase, are shown in Fig. 7 along with photometric variations derived directly from the light curve, without the need of the IPM (see details in Jurcsik et al. 2009a).

The left-hand column of Fig. 7 shows the parameters directly derived from the multicolour light curves, from the top to bottom: the V amplitude modulation in f_0; a rather weak but detectable phase modulation of f_0; variations in magnitude and intensity averaged mean V brightness; variations in different magnitude and intensity averaged $B-V$ colours; and the same in $V-I$ (all averages correspond to pulsation-phase). These diagrams reveal a very weak phase modulation corresponding to ≈0.01 d variations in O−C. The same result was obtained from the Fourier model of the light curve in Section 2. We also can observe from Fig. 7 that only the intensity-averaged magnitudes and their differences show variations with the modulation. Namely that Z CVn is the brightest in V and the warmest at high-amplitude Blazhko phase. This is a general property of all the Blazhko stars with similar detailed analyses (see the previous IPM results listed at the beginning of this section).

The right-hand panels of Fig. 7 show the results obtained by the IPM, from the top to bottom: mean radius, mean $\log g$, magnitude and intensity-averaged mean M_V, mean luminosity and

[15] The modulation was filtered out using the light-curve model with parameters in Table B1.

Table 6. The mean physical parameters of Z CVn. BL-free in the first column means light-curve fit after the modulation was subtracted, and IPM means inverse photometric method. The errors of IPM values come from four different settings (see details in Sódor et al. 2009) and are certainly underestimated.

	[Fe/H]$_{JK}$ (dex)	log L ($L_\odot$)	M_V (mag)	$(B-V)_0$ (mag)	log g (dex)	log $T_{\rm eff}$	$\mathfrak{M}$ ($\mathfrak{M}_\odot$)	d (pc)
BL-free	−1.64(12)	1.638(12)	0.54(3)	0.351(1)	2.699(1)	3.805(2)	0.59(16)	1760(120)
IPM	−1.64, fixed	1.753(8)	0.597(1)		2.6229(5)	3.8009(2)	0.59, fixed	1760, fixed

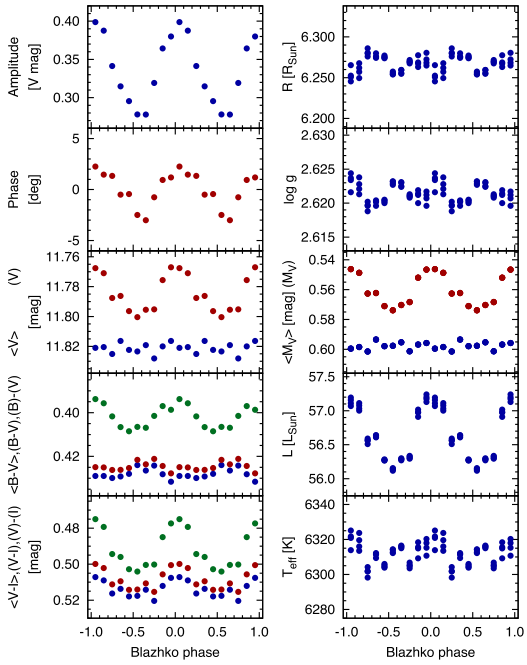

Figure 7. Variation of various parameters during the Blazhko cycle from the IPM method.

mean effective surface temperature (all averages correspond to pulsation-phase). Since the distance is obviously Blazhko-phase independent, M_V variations directly follow from V variations in the right-hand column. Apart from M_V, only the luminosity shows clear variations with Blazhko phase, and similarly to all previously investigated Blazhko stars, Z CVn is the most luminous at high-amplitude Blazhko phase. The other parameters do not show significant variations with modulation phase compared to their uncertainty, which is estimated from the spread of the data points obtained with four different IPM settings. Temperature variation is not evident, but the data hint a marginally higher temperature at high-amplitude Blazhko phase in accordance with the colour variations shown in the two bottom right-hand panels.

Comparing Fig. 7 with fig. 11 in Jurcsik et al. (2012b), we find remarkable agreement between the modulation behaviour of Z CVn and RZ Lyrae. Each parameter changes – or remains constant – very similarly. The only difference is that the changes of Z CVn are roughly half of those of RZ Lyr in each parameter. Z CVn is similarly metal poor as RZ Lyr, but its pulsation period is much longer than that of RZ Lyr (0.654 d versus 0.511 d).

The IPM results slightly differ from the results based on the empirical calibrations (see Table 6). For example, the difference in M_V is only 0.057 mag, which does not exceed 2 sigma. The most probable explanation of this discrepancy is that parameters calculated from empirical formulae with relatively large uncertainties were used as input parameters of the IPM. In addition, IPM works directly with the light curves in different passbands, thus any uncertainty in colours brings additional imprecision.

7 DISCUSSION OF THE BINARY HYPOTHESIS

Several RRL binary candidates are proposed to have companions with masses in a black hole range (Derekas et al. 2004; Liška et al. 2016a; Sódor et al. 2017), although all the respective authors considered this possibility with strong scepticism. However, the minimal mass of Z CVn companion calculated from our LTTE model (57 $\mathfrak{M}_\odot$) seems to be very unlike or unrealistic even in comparison with the other candidates. Before the detection of the gravitational waves produced by the coalescence of two black holes, the highest observed mass of a BH was about 15 $\mathfrak{M}_\odot$ (member of X-ray binary M33 X-7, Özel et al. 2010). Abbott et al. (2016) showed that the event GW150914 detected by the Laser Interferometric Gravitational-Wave Observatory (LIGO) was a product of merging of two BH with masses of 36 and 29 $\mathfrak{M}_\odot$. This is clear evidence that also 'heavy' stellar BHs must exist and that there must be a way to produce such massive BHs.

Theoretical studies by Spera, Mapelli & Bressan (2015) and Belczynski et al. (2016) showed that at low metallicity ($Z < 1/30\,Z_\odot$), the mass-loss in very massive stars with mass larger than 25 $\mathfrak{M}_\odot$ is strongly reduced giving enough space to form BHs with masses in the order of tens of solar masses. In addition, if strong magnetic field is present, the mass-loss driven by the strong stellar wind is even more effectively reduced, thus, further increasing the chance to form 'heavy' BHs (Petit et al. 2017). These studies show that progenitors with sufficient mass that could form a BH with 57 $\mathfrak{M}_\odot$ are theoretically possible. Because the metallicity of the companion is assumed the same as for Z CVn ($Z \sim 0.0003$, see Section 6), creation of heavy BH cannot be rejected.

The question now is whether we can detect the BH companion of Z CVn. If there were sufficient amount of material falling on to the BH, it would produce detectable high-energy radiation. There are three possible sources of matter in the hypothetical Z CVn-BH system. If the system were close enough, the RRL component could feed the BH via classical mass transfer through the inner Lagrangian point – a process well known in cataclysmic variables. But this is certainly not our case since the system is very wide. The remaining two sources of material, the stellar wind from RRL and the surrounding interstellar matter (ISM), can sum up and let the BH radiate via spherical, so called Bondi-Hoyle-Littleton (BHL) accretion (Hoyle & Lyttleton 1939; Bondi & Hoyle 1944; Bondi 1952).

It is generally assumed that RRLs loose mass during the evolution on the horizontal branch, but the rate of the mass-loss is unknown. Koopmann et al. (1994) estimated the maximal mass-loss rate that would not have significant effects on the horizontal branch morphology as $10^{-9}\,\mathfrak{M}_\odot\ \mathrm{yr}^{-1}$. If this was the case, the BH would be orders of magnitude brighter than the RRL itself. However, we do

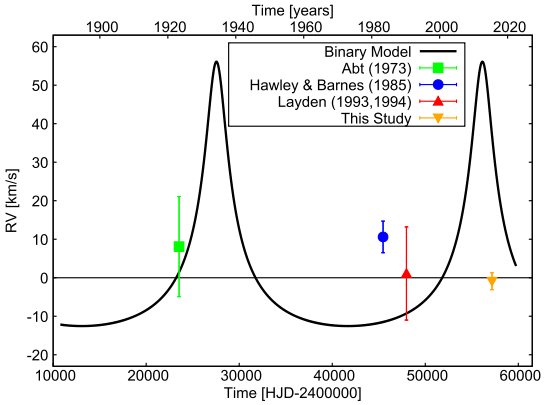

Figure 8. Synthetic γ-velocity curve (solid black line) with the systemic velocities from Table 4. No offset corresponding to the velocity of binary centre-of-mass is added.

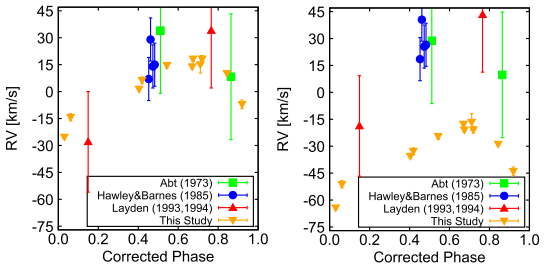

Figure 9. RV-observations folded with the pulsation period that was corrected from the LTTE using our O−C model. When also the model of the γ-velocity is removed, the points should stitch together. The opposite is observed (right-hand panel).

not know the true mass-loss rate, speed of the stellar wind particles, and we do not know the speed of sound in the out-flowing material, which is defined by the density and temperature of the material. Speed of sound (v_s) and relative speed of the BH and the ambient material v_r are the crucial quantities when calculating the rate of the accretion because $\dot{M} \sim (v_s^2 + v_r^2)^{-3/2}$. Thus, the luminosity of the BH could be several orders of magnitude larger, but also several orders of magnitude lower than the luminosity of Z CVn.

The problem is the same with pure ISM accretion. We do not know exactly what is the density of the ISM, its temperature and whether Z CVn moves through the ISM or corotates with it around the Galactic centre ($v_r = 0$). If we assume the density $n = 0.02\,\mathrm{cm}^{-3}$ (fig. 1 in Cox 2005, for $Z = 1.8$ kpc; Maintz & de Boer 2005), the resulting luminosity ranges from 10^{-5} to $10^4\,\mathrm{L}_\odot$ depending on the temperature (10^4–10^5 K) and $v_r = 0$ or $v_r = 178\,\mathrm{km\,s}^{-1}$ (calculated from the Galactocentric velocities, Maintz & de Boer 2005). Obviously, the accretion rate cannot be calculated properly. In any case, in the direction to Z CVn, no X-ray or gamma-ray source has been identified; thus, the confirmation of the presence of BH fails anyway.

If the star exploded as a supernovae, one can search for the envelope ejected during the explosion. This idea also faces serious problems. Very massive stars (>40 $\mathfrak{M}_\odot$) probably collapse directly to BH without exploding as supernovae (Fryer 1999). Even if the star exploded, it necessarily had to occur very shortly after formation of the system, i.e. billions of years ago. Since lifetime of the supernovae remnants is certainly less than this time, there is no chance to detect it at present days. Therefore, the chance to detect the supernova remnant is extremely low, even impossible.

We can also investigate the probability that an RRL star is bound with a 57-$\mathfrak{M}_\odot$ BH in wide system. Using the Salpeter (1955) IMF function

$$\xi(\mathfrak{M}) = \xi_0 \mathfrak{M}^{-2.35}, \quad (3)$$

we can estimate the ratio of the number of stars with >60 $\mathfrak{M}_\odot$ (BH progenitor) and number of RRL progenitors with ∼1 solar mass. This ratio is $\xi(\mathrm{BH})/\xi(\mathrm{RRL}) \sim 6.6 \times 10^{-5}$, thus one 60-$\mathfrak{M}_\odot$ star may exist for each ∼15 000 1-Solar mass stars. Not all stars are bound in binary systems. In case of RRLs, it is probably less than 4 per cent (Hajdu et al. 2015). With this estimate, the ratio is 1:375 000. At this point, the situation could look optimistic, because almost 100 000 RRL stars have been identified so far, which gives good chance to detect a system with 60-solar mass BH. However, independent and unambiguous confirmation of such system would be very difficult. We have to point out here that among 30 recently identified RRL binary candidates (see the online list by Liska & Skarka 2016) with orbital periods larger than 2 000 d, four systems are suspected to have a companion with mass in the BH range.

All the above discussion is only very uncertain, but we have strong evidence why to reject the RRL-BH hypothesis. From the model of the proposed orbit (parameters are in Table 5), we calculated the systemic RV curve and compared it with the RV values determined from the available measurements (Table 4). The result is shown in Fig. 8. Obviously, the observations do not match the theoretical RV curve at all. Our measurements from 2015 to 2016 should be shifted by about $50\,\mathrm{km\,s}^{-1}$ against the older measurements to fit the model. Also RV observations from Hawley & Barnes (1985) and Layden (1993, 1994) should have different values to fit the model.

We can safely declare that these shifts cannot be caused by the differences in usage of metallic/hydrogen lines in case when it was ambiguous (Abt 1973; Layden 1993, 1994) because this difference could be maximally about $5\,\mathrm{km\,s}^{-1}$ (estimated from different RV templates by Sesar 2012). The other source of systematic errors could be the presence of the Blazhko effect. According to our new observations that were obtained in different Blazhko phases, the scatter in RVs due to the Blazhko effect cannot be more than about $10\,\mathrm{km\,s}^{-1}$. Therefore, the proposed binary hypothesis can be safely rejected, because even if we assume the highest possible systematic errors, the observations cannot fulfil the model expectations.

The same is seen from Fig. 9, where the RV observations are plotted against time-corrected phase (LTTE subtracted). After the RV observations are corrected for the orbital motion (right-hand panel), the scatter should decrease. The opposite is seen from that figure. These two facts are strong evidence that the binary hypothesis is false and that the presumed cyclic long-term period variation is not caused by the LTTE, but by some different physical process that is intrinsic to the star. In fact, our results are consistent with a single star of $0\,\mathrm{km\,s}^{-1}$ centre-of-mass RV.

8 SUMMARY AND CONCLUSIONS

We present a comprehensive study of the period evolution of Z CVn and its light curve using original photometric and spectroscopic measurements, as well as observations from literature. The star was observed in 53 nights photometrically (four seasons) and in 6 nights spectroscopically (two seasons). We caught 18 maximum times and additional 209 were taken from the literature and from the GEOS

data base, creating a set of 227 maximum times (see the online list with maximum times) covering more than one century.

The shape of the general trend in the O−C diagram suggests that LTTE could be present. The detailed model of the period variations with the assumption of LTTE (Table 5) shows that the companion should be a BH with a mass of about $\mathfrak{M}_{2,\min} \sim 57\,\mathfrak{M}_{\odot}$. Although such RRL-BH configuration is theoretically possible, we do not have any clear evidence that this is the case of Z CVn. There is also no observational evidence of the BH (X-ray radiation) in the direction to Z CVn.

However, the rejection of the binary hypothesis was firmly confirmed by the spectroscopic measurements, which do not match the theoretical γ velocity at all. A further test with time-corrected phases and RV observations confirms this finding too. Thus, our analysis gives firm proofs that possibly cyclic variations of the pulsation period of Z CVn cannot be explained as LTTE caused by an unseen companion. This finding has large impact on the other known binary candidates with similar periods and period-variation-amplitudes, because it shows that there may be some unknown mechanism that causes large-amplitude period variations. Already, Firmanyuk (1982) pointed out that such variations are probably not a result of LTTE. Perhaps, some analogue to the Blazhko effect could be present, but with much longer modulation period. We do not have any physical explanation for such long period variations and formerly proposed scenarios for the long-term period variations are also unlikely (Section 4).

On the basis of our photometric observations, we estimated the basic pulsation period, but also detected the Blazhko effect with period of 22.391 d. This period was clearly detected in maximum brightness variation. Peaks suggesting additional modulation with period comparable with the length of the data set were also detected, but they could only be artefacts of the secular period change. We found that the modulation is almost exclusively in amplitude (with amplitude of about 0.3 mag) with period/phase modulation less than 0.01 d. This is in contrast with previous studies, when also period/phase modulation was detectable (Kanyó 1966; Le Borgne et al. 2012). Because the pulsation period is comparable with the one from Kanyó (1966), but the period/phase modulation is undetectable and the Blazhko period is longer than at Kanyó's time, our study contradicts the anticorrelation between the length of $P_{\rm Puls}$ and $P_{\rm BL}$ proposed by Le Borgne et al. (2012). However, the fact that $P_{\rm BL}$ continuously changes together with the major period variations means that these two effects might be somehow connected. This is another evidence against the LTTE assumption because possible companion at the orbit with 80 yr-long period certainly could not tidally influence the pulsation properties of the RRL component.

Although our spectroscopic measurements are of insufficient quality and coverage for reliable physical parameter determination, we estimated them from the shape of the light curve. The values based on modulation-free light curve are in excellent agreement with formerly determined values in literature (our [Fe/H = −1.64 versus −1.7,[16] our $r = 1760$ pc versus 1770 pc, Layden 1994). This experience suggests that parameters estimated from modulation-free light curve are of better reliability than those based on the mean-light-curve fitting or averaging parameters over the Blazhko cycle.

The star now lengthens its pulsation period and between HJD 2460000 and 2462500 is predicted to reach its maximum (if the period variation is really cyclic). After that it should shorten again. Monitoring of Z CVn is, therefore, desired and should prove the stability of the long-period cycle in Z CVn. If the long cycle is really intrinsic to the star, new theoretical explanation will be needed to explain not only behaviour of Z CVn, but also of other RRL stars (e.g. some candidates from Liška et al. 2016a; Sódor et al. 2017).

[16] After recalculating from Layden (1994) to Jurcsik & Kovács (1996), metallicity scale using the formula from (Sandage 2004).

ACKNOWLEDGEMENTS

We are pleased to express our gratitude to Ondřej Pejcha, Lenka Zychová and Norbert Werner for the discussion about black holes, BHL accretion and ISM. MS acknowledges the support of the postdoctoral fellowship programme of the Hungarian Academy of Sciences at the Konkoly Observatory as host institution. The financial support of the Hungarian Nemzeti Kutatási, Fejlesztési és Innovációs Hivatal (NKFIH) Grants K-115709, K-113117 and K-119517 is acknowledged. ÁS was supported by the János Bolyai Research Scholarship of the Hungarian Academy of Sciences. This research was carried out under the project CEITEC 2020 (LQ1601) with financial support from the Ministry of Education, Youth and Sports of the Czech Republic under the National Sustainability Programme II (JL). Travel support from McDonald Observatory to obtain the spectroscopy observations is gratefully acknowledged (TGB). The support of Brno Observatory and Planetarium is acknowledged. The research made use of the International Variable Star Index (VSX) data base, operated at AAVSO, Cambridge, Massachusetts, USA, NASA's Astrophysics Data System. We thank J.-F. LeBorgne and other people from GEOS for maintaining their RRL data base.

REFERENCES

Abbott B. P. et al., 2016, Phys. Rev. Lett., 116, 241102
Abt H. A., 1973, ApJS, 26, 365
Abt H. A., 1983, ARA&A, 21, 343
Arellano Ferro A., Ahumada J. A., Kains N., Luna A., 2016, MNRAS, 461, 1032
Belczynski K., Holz D. E., Bulik T., O'Shaughnessy R., 2016, Nature, 534, 512
Benkő J. M., Szabó R., Paparó M., 2011, MNRAS, 417, 974
Blažko S., 1907, Astron. Nachr., 175, 325
Blažko S., 1922, Astron. Nachr., 216, 103
Blažko S., 1926, Astron. Nachr., 228, 261
Bondi H., 1952, MNRAS, 112, 195
Bondi H., Hoyle F., 1944, MNRAS, 104, 273
Boninsegna R., Vandenbroere J., Le Borgne J. F., Geos Team, 2002, in Aerts C., Bedding T. R., Christensen-Dalsgaard J., eds, ASP Conf. Ser. Vol. 259, IAU Colloq. 185: Radial and Nonradial Pulsations as Probes of Stellar Physics. Astron. Soc. Pac., San Francisco, p. 166
Butters O. W. et al., 2010, A&A, 520, L10
Catelan M., Cortés C., 2008, ApJ, 676, L135
Ceraski W., 1911, Astron. Nachr., 190, 85
Chadid M., Wade G. A., Shorlin S. L. S., Landstreet J. D., 2004, A&A, 413, 1087
Cox A. N., 1998, ApJ, 496, 246
Cox D. P., 2005, ARA&A, 43, 337
Derekas A., Kiss L. L., Udalski A., Bedding T. R., Szatmáry K., 2004, MNRAS, 354, 821
Firmanyuk B. N., 1980a, Astronomicheskij Tsirkulyar, 1118, 1
Firmanyuk B. N., 1980b, Astronomicheskij Tsirkulyar, 1118, 3
Firmanyuk B. N., 1982, Inf. Bull. Var. Stars, 2247
Fryer C. L., 1999, ApJ, 522, 413
Grindlay J., Tang S., Simcoe R., Laycock S., Los E., Mink D., Doane A., Champine G., 2009, in Osborn W., Robbins L., eds, ASP Conf. Ser. Vol. 410, Preserving Astronomy's Photographic Legacy: Current State and

the Future of North American Astronomical Plates. Astron. Soc. Pac., San Francisco, p. 101
Guggenberger E., Barnes T. G., Kolenberg K., 2016, Commun. Konkoly Obs. Hungary, 105, 145
Guinan E. F., Engle S. G., 2006, Ap&SS, 304, 5
Hajdu G., Catelan M., Jurcsik J., Dékány I., Drake A. J., Marquette J.-B., 2015, MNRAS, 449, L113
Hawley S. L., Barnes III T. G., 1985, PASP, 97, 551
Hełminiak K. G., Konacki M., Ratajczak M., Muterspaugh M. W., 2009, MNRAS, 400, 969
Hoyle F., Lyttleton R. A., 1939, Proc. Camb. Phil. Soc., 34, 405
Iben Jr I., Rood R. T., 1970, ApJ, 161, 587
Irwin J. B., 1952, ApJ, 116, 211
Jordi K., Grebel E. K., Ammon K., 2006, A&A, 460, 339
Joy A. H., 1938, PASP, 50, 302
Jurcsik J., 1998, A&A, 333, 571
Jurcsik J., Kovács G., 1996, A&A, 312, 111
Jurcsik J., Clement C., Geyer E. H., Domsa I., 2001, AJ, 121, 951
Jurcsik J. et al., 2005, A&A, 430, 1049
Jurcsik J. et al., 2009a, MNRAS, 393, 1553
Jurcsik J. et al., 2009b, MNRAS, 397, 350
Jurcsik J. et al., 2009c, MNRAS, 400, 1006
Jurcsik J. et al., 2012a, MNRAS, 419, 2173
Jurcsik J. et al., 2012b, MNRAS, 423, 993
Kanyó S., 1966, Inf. Bull. Var. Stars, 146
Karczmarek P., Wiktorowicz G., Iłkiewicz K., Smolec R., Stłpień K., Pietrzyński G., Gieren W., Belczynski K., 2017, MNRAS, 466, 2842
Kiefer F. et al., 2016, MNRAS, 458, 3272
Koopmann R. A., Lee Y.-W., Demarque P., Howard J. M., 1994, ApJ, 423, 380
Kovács G., Walker A. R., 2001, A&A, 374, 264
Kunder A. et al., 2011, AJ, 141, 15
LaCluyzé A. et al., 2004, AJ, 127, 1653
Lampe G., 1970, Zentralinstitut Astrophys. Sternwarte Sonneberg Mitteilungen ueber Veraenderliche Sterne, 5, 137
Landolt A. U., 1992, AJ, 104, 340
Layden A. C., 1993, PhD thesis, Yale University
Layden A. C., 1994, AJ, 108, 1016
Le Borgne J. F. et al., 2007, A&A, 476, 307
Le Borgne J.-F. et al., 2012, AJ, 144, 39
Lee J. W., Hong K., Kim S.-L., Koo J.-R., 2017, ApJ, 835, 189
Lenz P., Breger M., 2005, Commun. Asteroseismology, 146, 53
Liska J., Skarka M., 2016, Commmun. Konkoly Obs. Hungary, 105, 209
Liška J., Skarka M., Zejda M., Mikulášek Z., de Villiers S. N., 2016a, MNRAS, 459, 4360
Liška J., Skarka M., Mikulášek Z., Zejda M., Chrastina M., 2016b, A&A, 589, A94
Maintz G., de Boer K. S., 2005, A&A, 442, 229
McCarthy J. K., Sandiford B. A., Boyd D., Booth J., 1993, PASP, 105, 881
Nemec J. M., Cohen J. G., Ripepi V., Derekas A., Moskalik P., Sesar B., Chadid M., Bruntt H., 2013, ApJ, 773, 181
Oke J. B., Giver L. P., Searle L., 1962, ApJ, 136, 393
Petit V. et al., 2017, MNRAS, 466, 1052
Pietrzyński G. et al., 2012, Nature, 484, 75
Pollacco D. L. et al., 2006, PASP, 118, 1407
Prada Moroni P. G., Gennaro M., Bono G., Pietrzyński G., Gieren W., Pilecki B., Graczyk D., Thompson I. B., 2012, ApJ, 749, 108
Prager R., 1939, Harvard Coll.Obs. Bull., 911, 1
Preston G. W., 1959, ApJ, 130, 507
Ritter A., 1879, Ann. Phys. Chem. Neue Folge, 8, 157
Salpeter E. E., 1955, ApJ, 121, 161
Sandage A., 2004, AJ, 128, 858
Sanford R. F., 1949, ApJ, 109, 208
Schlafly E. F., Finkbeiner D. P., 2011, ApJ, 737, 103
Schlegel D. J., Finkbeiner D. P., Davis M., 1998, ApJ, 500, 525
Sesar B., 2012, AJ, 144, 114
Simon N. R., Lee A. S., 1981, ApJ, 248, 291
Skarka M., Honkova K., Jurysek J., 2013, Inf. Bull. Var. Stars, 6051
Skarka M., Liska J., Dreveny R., Auer R. F., 2015a, Open Eur. J, Var. Stars, 169, 36
Skarka M. et al., 2015b, Open Eur. J. Var. Stars, 174, 1
Skarka M., Liska J., Zejda M., Mikulasek Z., 2016, Commun. Konkoly Obs. Hungary, 105, 141
Smolec R. et al., 2013, MNRAS, 428, 3034
Sódor Á., 2009, in Guzik J. A., Bradley P. A., eds, AIP Confer. Ser. Vol. 1170, Changes in Mean Global Physical Parameters of Blazhko RR Lyrae stars – Derived from Multicolor Photometry. Am. Inst. Phys., New York, p. 294
Sódor Á., Szeidl B., Jurcsik J., 2007, A&A, 469, 1033
Sódor Á., Jurcsik J., Szeidl B., 2009, MNRAS, 394, 261
Sódor Á. et al., 2011, MNRAS, 411, 1585
Sódor Á., Hajdu G., Jurcsik J., Szeidl B., Posztobányi K., Hurta Z., Belucz B., Kun E., 2012, MNRAS, 427, 1517
Sódor Á., Skarka M., Liška J., Bognár Z., 2017, MNRAS, 465, L1
Sódor A., 2012, Konkoly Obs. Occas. Tech. Notes, 15
Soszyński I. et al., 2014, Acta. Astron., 64, 177
Soszyński I. et al., 2016, Acta Astron., 66, 131
Soydugan E., Soydugan F., Demircan O., İbanoğlu C., 2006, MNRAS, 370, 2013
Spera M., Mapelli M., Bressan A., 2015, MNRAS, 451, 4086
Sterken C., 2005, in Sterken C., ed., ASP Conf. Ser. Vol. 335, The Light-Time Effect in Astrophysics: Causes and cures of the O-C diagram. Astron. Soc. Pac., San Francisco, p. 181
Stothers R., 1980, PASP, 92, 475
Strelkova E. P., 1964, Perem. Zvezdy, 15, 89
Sweigart A. V., Renzini A., 1979, A&A, 71, 66
Szabados L., 2003, Inf. Bull. Var. Stars, 5394
Szeidl B., Jurcsik J., 2009, Commun. Asteroseismology, 160, 17
Szeidl B., Hurta Z., Jurcsik J., Clement C., Lovas M., 2011, MNRAS, 411, 1744
Udry S. et al., 1999, in Hearnshaw J. B., Scarfe C. D., eds, ASP Conf. Ser. Vol. 185, IAU Colloquium 170. Astron. Soc. Pac., San Francisco, p. 383
Wade R. A., Donley J., Fried R., White R. E., Saha A., 1999, AJ, 118, 2442
Watson C. L., Henden A. A., Price A., 2006, The Society for Astronomical Sciences 25th Annual Symposium on Telescope Science, Society for Astronomical Sciences. p. 47
Woźniak P. R. et al., 2004, AJ, 127, 2436
Zacharias N., Finch C. T., Girard T. M., Henden A., Bartlett J. L., Monet D. G., Zacharias M. I., 2013, AJ, 145, 44
Zhou A.-Y., 2010, preprint (arXiv:1002.2729)
Zinn R., West M. J., 1984, ApJS, 55, 45
Özel F., Psaltis D., Narayan R., McClintock J. E., 2010, ApJ, 725, 1918

SUPPORTING INFORMATION

Supplementary data are available at *MNRAS* online.

Please note: Oxford University Press is not responsible for the content or functionality of any supporting materials supplied by the authors. Any queries (other than missing material) should be directed to the corresponding author for the article.

APPENDIX A: PHYSICAL PARAMETERS DETERMINATION BASED ON THE LIGHT-CURVE SHAPE

First, we divided the data according to their Blazhko phase into 10 segments (blue points in subplots in Fig. 6, using $P_{\rm BL} = 22.931$ d and the zero epoch from equation 1). Each subset was fitted using equation (2) with ten pulsation components (harmonics of

Table A1. The first two amplitude and phase Fourier parameters together with calculated physical characteristics. Obviously, metallicity and mass cannot change during Blazhko cycle, they are given only for completeness.

Blazhko phase	R_{21}	R_{31}	ϕ_{21} (rad)	ϕ_{31} (rad)	[Fe/H] (dex)	$\log L\,(L_\odot)$	M_V (mag)	$(B-V)_0$ (mag)	$\log g$ (dex)	$\log T_{\rm eff}$	$\mathfrak{M}\,(\mathfrak{M}_\odot)$
0.0	0.473	0.301	2.395	5.053	−1.769	1.651	0.511	0.339	2.699	3.808	0.605
0.1	0.474	0.299	2.452	5.102	−1.703	1.645	0.527	0.343	2.699	3.807	0.599
0.2	0.474	0.242	2.534	5.334	−1.391	1.611	0.602	0.353	2.699	3.806	0.573
0.3	0.444	0.224	2.509	5.278	−1.466	1.619	0.584	0.357	2.699	3.804	0.579
0.4	0.440	0.232	2.569	5.662	−0.950	1.565	0.709	0.361	2.699	3.806	0.538
0.5	0.421	0.238	2.470	5.406	−1.294	1.601	0.625	0.363	2.699	3.803	0.565
0.6	0.496	0.264	2.436	5.348	−1.373	1.610	0.606	0.364	2.699	3.803	0.572
0.7	–	–	–	–	–	–	–	–	–	–	–
0.8	0.483	0.309	2.410	5.039	−1.788	1.653	0.506	0.347	2.699	3.805	0.606
0.9	0.479	0.291	2.396	5.080	−1.732	1.648	0.520	0.340	2.699	3.808	0.602
Average	0.47(2)	0.27(3)	2.45(5)	5.21(12)	−1.56(20)	1.63(2)	0.56(5)	0.351(10)	2.699(1)	3.805(2)	0.59(2)
Mean LC	0.463(5)	0.255(5)	2.46(2)	5.21(2)	−1.56(6)	1.629(7)	0.56(2)	0.351(1)	2.699(1)	3.805(1)	0.59(8)
BL-free	0.447(2)	0.269(2)	2.42(7)	5.15(9)	−1.64(12)	1.638(12)	0.54(3)	0.351(1)	2.699(1)	3.805(1)	0.59(2)

the inverse mean period from equation 1) to get the mean light curve during each of the Blazhko phases shown with the full red line in Fig. 6. The used pulsation-phase-independent Fourier parameters follow the classical definition by Simon & Lee (1981) and are computed as

$$R_{i1} = A_i/A_1 \;\text{ and }\; \phi_{i1} = \phi_i - i\phi_1, \tag{A1}$$

where A_i and ϕ_i are amplitudes and phases of particular frequency harmonic. Resulting Fourier parameters for each Blazhko phase can be found in Table A1 together with physical parameters that were computed using empirical formulas taken from the following papers:

Metallicity (Jurcsik & Kovács 1996):

$$[\mathrm{Fe/H}]_{\rm JK} = -5.038 - 5.394\,P_{\rm Puls} + 1.345\phi. \tag{A2}$$

Luminosity (Jurcsik 1998):

$$\log L = 1.464 - 0.106[\mathrm{Fe/H}]_{\rm JK}. \tag{A3}$$

Absolute magnitude (Catelan & Cortés 2008):

$$M_V = 0.23[\mathrm{Fe/H}]_{\rm ZW} + 0.984. \tag{A4}$$

Extinction-free colour index (Jurcsik 1998):

$$(B-V)_0 = 0.308 + 0.163\,P_{\rm Puls} - 0.187A_1. \tag{A5}$$

Surface gravity (Jurcsik 1998):

$$\log g = 2.473 - 1.226\log P_{\rm Puls}. \tag{A6}$$

Effective temperature (Kovács & Walker 2001):

$$\log T_{\rm eff} = 3.884 - 0.3219(B-V)_0 + 0.0167\log g + 0.007[\mathrm{Fe/H}]_{\rm JK}. \tag{A7}$$

Mass (Jurcsik 1998):

$$\log \mathfrak{M} = -0.328 - 0.062[\mathrm{Fe/H}]_{\rm JK}. \tag{A8}$$

Metallicity scale $[\mathrm{Fe/H}]_{\rm JK}$ in these relations is from Jurcsik (1998), whereas $[\mathrm{Fe/H}]_{\rm ZW}$ is from Zinn & West (1984). The relation between these two scales is

$$[\mathrm{Fe/H}]_{\rm ZW} = 1.05[\mathrm{Fe/H}]_{\rm JK} - 0.2, \tag{A9}$$

(Sandage 2004).

We can also estimate the distance to Z CVn.

The parameters cannot be calculated in Blazhko phase 0.7 because of poor coverage. Also phase 0.4 is badly sampled and the parameters significantly differ from those in the other Blazhko phases (see Fig. 6 and Table A1). Therefore, values coming from these data were omitted when calculating the average values.

The distance was simply calculated using

$$\log d = \frac{V - M_V - A_V + 5}{5}, \tag{A10}$$

where M_V is the visual absolute magnitude, V is the observed mean magnitude and A_V is the interstellar extinction at the centre of V filter. Assuming $M_V = 0.54$ mag, $V = 11.82$ mag and $A_V = 0.05$ mag (Schlegel, Finkbeiner & Davis 1998; Schlafly & Finkbeiner 2011), the distance is 1760(120) pc.

APPENDIX B: FULL LIGHT-CURVE SOLUTION AND USED MAXIMUM TIMES

Table B1. The full solution of the light curves in different passbands. The values come from the best fit to the data.

ID	*B*			*V*			*R*			*I*		
	f(c/d)	A (mag)	ϕ (rad)	f(c/d)	A (mag)	ϕ (rad)	f(c/d)	A (mag)	ϕ (rad)	f(c/d)	A (mag)	ϕ (rad)
$f_0 - f_{BL}$	1.485 565	0.0452	3.7130	1.485 552	0.0359	3.7189	1.485 565	0.0291	3.7498	1.485 561	0.0205	3.8117
$f_0 - f_M$	1.528 252	0.0231	1.9522	1.528 267	0.0210	1.9723	1.528 252	0.0147	2.0658			
f_0	1.529 170	0.4448	4.0907	1.529 169	0.3407	4.0506	1.529 169	0.2688	3.9679	1.529 169	0.2128	3.8179
$f_0 + f_{BL}$	1.572 775	0.0370	3.9215	1.572 786	0.0312	3.9107	1.572 773	0.0246	3.9614	1.572 776	0.0186	3.9812
$2f_0 - f_{BL}$	3.014 735	0.0263	3.5113	3.014 721	0.0208	3.4969	3.014 735	0.0173	3.5151	3.014 730	0.0128	3.4917
$2f_0 - f_M$	3.057 422	0.0195	2.1554	3.057 436	0.0126	2.7507	3.057 421	0.0103	2.2792			
$2f_0$	3.058 340	0.2022	4.2486	3.058 338	0.1525	4.2404	3.058 339	0.1264	4.2352	3.058 338	0.1005	4.1627
$2f_0 + f_{BL}$	3.101 945	0.0286	3.9690	3.101 955	0.0247	3.9659	3.101 943	0.0183	3.9825	3.101 945	0.0136	4.0445
$3f_0 - f_{BL}$	4.543 905	0.0295	3.6360	4.543 891	0.0231	3.7130	4.543 904	0.0188	3.7161	4.543 899	0.0141	3.7504
$3f_0 - f_M$	4.586 592	0.0170	2.5104	4.586 605	0.0127	2.5669	4.586 591	0.0096	2.5709			
$3f_0$	4.587 510	0.1200	4.6937	4.587 507	0.0919	4.7330	4.587 508	0.0752	4.7169	4.587 506	0.0584	4.6486
$3f_0 + f_{BL}$	4.631 115	0.0259	4.2344	4.631 124	0.0197	4.2931	4.631 112	0.0171	4.3827	4.631 114	0.0139	4.4915
$4f_0 - f_{BL}$	6.073 075	0.0176	4.4841	6.073 060	0.0142	4.3331	6.073 073	0.0124	4.4282	6.073 067	0.0104	4.4810
$4f_0 - f_M$	6.115 762	0.0123	3.1709	6.115 774	0.0077	3.1279	6.115 760	0.0071	3.1759			
$4f_0$	6.116 680	0.0680	5.1909	6.116 676	0.0534	5.1848	6.116 677	0.0436	5.2208	6.116 675	0.0328	5.1517
$4f_0 + f_{BL}$	6.160 285	0.0229	5.0100	6.160 293	0.0166	5.0167	6.160 282	0.0143	5.0255	6.160 283	0.0116	5.1934
$5f_0 - f_{BL}$	7.602 245	0.0139	5.0402	7.602 229	0.0101	5.2303	7.602 243	0.0092	5.1281	7.602 236	0.0075	5.1680
$5f_0 - f_M$				7.644 943	0.0079	3.3327	7.644 929	0.0053	3.3548			
$5f_0$	7.645 850	0.0325	5.4723	7.645 845	0.0275	5.7006	7.645 847	0.0230	5.6589	7.645 844	0.0165	5.5656
$5f_0 + f_{BL}$	7.689 455	0.0145	5.4992	7.689 462	0.0124	5.3723	7.689 451	0.0100	5.4530	7.689 452	0.0085	5.6281
$6f_0 - f_{BL}$	9.131 415	0.0101	5.7017	9.131 398	0.0071	5.7274	9.131 412	0.0058	5.7233			
$6f_0$	9.175 020	0.0184	5.6101	9.175 014	0.0141	5.6243	9.175 016	0.0124	5.7004	9.175 013	0.0099	5.7340
$6f_0 + f_{BL}$	9.218 625	0.0106	5.9954	9.218 631	0.0085	5.9367	9.218 620	0.0074	6.0217	9.218 620	0.0066	6.2323
$7f_0 - f_{BL}$				10.660 567	0.0062	0.1001	10.660 581	0.0042	6.2283			
$7f_0$	10.704 190	0.0125	5.9270	10.704 183	0.0081	6.1613	10.704 185	0.0070	6.1231	10.704 181	0.0063	6.2027
$7f_0 + f_{BL}$	10.747 795	0.0084	0.2438	10.747 800	0.0057	0.2936	10.747 790	0.0046	0.3915	10.747 789	0.0046	0.5625
$8f_0 - f_{BL}$							12.189 751	0.0029	0.7305			
$8f_0$	12.233 360	0.0075	0.1595	12.233 352	0.0062	6.2551	12.233 355	0.0044	0.0253	12.233 350	0.0037	0.0415
$8f_0 + f_{BL}$				12.276 969	0.0054	0.9788	12.276 959	0.0040	0.9867			
$9f_0 - f_{BL}$							13.718 920	0.0028	1.0452			
$9f_0$				13.762 521	0.0038	0.5985	13.762 524	0.0026	0.4936			
$9f_0 + f_{BL}$							13.806 128	0.0020	1.3590	13.806 127	0.0029	1.7063
$10f_0 - f_{BL}$												
$10f_0$				15.291 690	0.0041	0.8719	15.291 693	0.0028	0.7726			
$10f_0 + f_{BL}$							15.335 298	0.0020	1.7188	15.335 295	0.0025	2.1285

This paper has been typeset from a TEX/LATEX file prepared by the author.

Paper 4

HD 99458: First time ever Ap-type star as a δ Scuti pulsator in a short period eclipsing binary?

Monthly Notices
of the
ROYAL ASTRONOMICAL SOCIETY

MNRAS **487,** 4230–4237 (2019) doi:10.1093/mnras/stz1478
Advance Access publication 2019 June 03

HD 99458: First time ever Ap-type star as a δ Scuti pulsator in a short period eclipsing binary?

M. Skarka [1,2★] P. Kabáth,[2★] E. Paunzen [1] M. Fedurco,[3] J. Budaj,[4] D. Dupkala,[2,5] J. Krtička,[1] A. Hatzes,[6] T. Pribulla,[4] Š. Parimucha,[3] Z. Mikulášek,[1] E. Guenther,[6] S. Sabotta,[6] M. Blažek [1,2] J. Dvořáková,[2,7] L. Hambálek [4] T. Klocová,[2] V. Kollár,[4] E. Kundra,[4] M. Šlechta[2] and M. Vaňko[4]

[1]*Department of Theoretical Physics and Astrophysics, Masaryk University, Kotlářská 2, CZ-61137 Brno, Czech Republic*
[2]*Astronomical Institute, Czech Academy of Sciences, Fričova 298, CZ-25165 Ondřejov, Czech Republic*
[3]*Faculty of Science, P. J. Šafárik University, Park Angelinum 9, Košice 04001, Slovak Republic*
[4]*Astronomical Institute, Slovak Academy of Sciences, 05960 Tatranská Lomnica, Slovak Republic*
[5]*Astronomical Institute, Charles University, Faculty of Mathematics and Physics, CZ-18000 Praha 8 V Holešovičkách 2, Czech Republic*
[6]*Thüringer Landessternwarte Tautenburg, Sternwarte 5, D-07778 Tautenburg, Germany*
[7]*Institute of Physics, Faculty of Philosophy and Science, Silesian University in Opava, Bezručovo nám. 13, 74601 Opava, Czech Republic*

Accepted 2019 May 24. Received 2019 May 13; in original form 2019 January 25

ABSTRACT

We present the discovery of a unique object, a chemically peculiar Ap-type star showing δ Scuti pulsations that is bound in an eclipsing binary system with an orbital period shorter than 3 d. HD 99458 is therefore a complex astrophysical laboratory opening doors for studying various, often contradictory, physical phenomena at the same time. It is the first Ap star ever discovered in an eclipsing binary. The orbital period of 2.722 d is the second shortest among all known chemically peculiar (CP2) binary stars. Pulsations of δ Scuti type are also extremely rare among CP2 stars and no unambiguously proven candidate has been reported. HD 99458 was formerly thought to be a star hosting an exoplanet, but we definitely reject this hypothesis using photometric observations from the *K2* mission and new radial velocity measurements. The companion is a low-mass red dwarf star ($M_2 = 0.45(2)\,M_\odot$) on an inclined orbit ($i = 73.2(6)$ deg) that shows only grazing eclipses. The rotation and orbital periods are synchronized, while the rotation and orbital axes are misaligned. HD 99458 is an interesting system deserving of more intense investigations.

Key words: techniques: photometric – techniques: spectroscopic – binaries: eclipsing – stars: chemically peculiar – stars: individual: HD 99458 – stars: oscillations.

1 INTRODUCTION

Chemically peculiar stars of the upper part of main sequence are usually slowly rotating stars where the processes of radiative diffusion and gravitational settling lead to abundance anomalies (Michaud et al. 1976). Because these diffusion processes are typically very slow, the atmospheres of chemically peculiar stars should be stable against mixing processes caused by, for example, rotation, binary interaction, stellar wind, and convection.

A class of chemically peculiar stars called CP2 is characterized by overabundance of heavy elements, frequent appearance of magnetic field, and slow rotation (Preston 1974). Heavy elements on the surface of CP2 stars concentrate in vast abundance spots that result in spectroscopic and light variability. Chemically peculiar stars show rotational modulation of the light curve that is due to the flux re-distribution in the abundance spots (e.g. Prvák et al. 2015).

Although the overall frequency of CP2 binaries is relatively high [Carrier et al. (2002) give 43 per cent, Mathys (2017) gives 51 per cent], this distribution is dominated by long-period systems. There appears to be a a significant deficiency of systems with period of the order days to tens of days and a complete lack of binaries with period below 2.9 d (Carrier et al. 2002; Landstreet et al. 2017; Mathys 2017). As a result, eclipsing binary systems are absent in the sample of known CP2 stars, which complicates the determination of stellar parameters and evolutionary stage of these stars. According to Ferrario et al. (2009) and Tutukov & Fedorova (2010), the presence of magnetic fields and lack of close binaries can be a result of the merger process. Consequently, a discovery of a CP2 in eclipsing

★ E-mail: marek.skarka@gmail.com (MS); petr.kabath@asu.cas.cz (PK)

binary would imply that the merger scenario cannot account for the origin of the magnetic field in all cases.

HD 99458 (EPIC 201534540, J2000 RA $= 11^{h}36^{m}36\overset{s}{.}28$, Dec. $= +01^{\circ}03'18\overset{''}{.}84$, $V = 8.163$ mag, $(B - V) = 0.241$ mag, see also Table A1) was identified as a transiting exoplanetary candidate with period of $P = 2.722$ d by Barros, Demangeon & Deleuil (2016). In this brief note, we show that the companion must be of stellar nature. We investigate the spectra and light curve and show that in terms of stellar physics this is an extremely interesting star. To our knowledge, this is the first discovery of its kind that can point us towards a better understanding of the A-type stars and their chemically peculiar subclass.

2 DATA

HD 99458 was observed in campaign 1 of the *K2* mission (Howell et al. 2014). We used the single-aperture light-curve (hereafter LC) data. The data set has a time span of 80 d and contains 3500 data points taken with an integration time of 29.4 min. For an easier handling we normalized the flux to 700 000 e- s^{-1}.

To validate the nature of the transits, we gathered 58 spectra in 2017 and 2018 with the Ondřejov echelle spectrograph (OES) mounted at the 2-m Perek telescope at the Ondřejov observatory, Czech Republic. This spectrograph has a resolving power $R = \lambda/\Delta\lambda = 50\,000$ (Koubský et al. 2004). Additional observations were taken with the fibre-fed echelle spectrograph mounted at the 60-cm telescope at Stará Lesná Observatory, Slovak Republic ($R =$ 11 000, Pribulla et al. 2015).

The typical S/N ratio was between 20 and 80 depending on the observing conditions and the air mass. The data were reduced with the standard IRAF 2.16 routines[1] (Tody 1993). For the estimation of radial velocities (RVs), we used IRAF FXCOR routine. To minimize the effects of data reduction and calibration, we cross-correlate the lines in 13 subsequent overlapping regions with the width of 100 Å between 4900 and 5500 Å. As a template, one of the best quality spectrum was selected. The instrumental shift was removed using telluric lines. The resulting RVs calculated as the weighted mean of the values assuming the weights based on the uncertainties provided by FXCOR were shifted with respect to their mean. Thus, we give only relative RVs in Table A2.

3 DATA ANALYSIS

To make all the performed procedures in binary modelling easier to follow, we summarize the steps here. First, we get the effective temperature, surface gravity, mass, and radius of the primary on the basis of astrometry, photometric, and spectroscopic observations, without considering it as a binary member. These parameters are then fixed and used as inputs for the next steps of the procedure. Other parameters of the primary are also derived at this stage, such as $\upsilon \sin i$ and $\upsilon_{\rm mic}$, but they are not relevant for the next steps of binary modelling.

The RV data are analysed to compute an orbital solution according to the standard procedure for spectroscopic binaries. Value of the orbital period was determined from our RV measurements, while the epoch of the phase origin was adopted from literature. Among the parameters derived at this stage, the RV semi-amplitude and the mass function are fixed and used as input for the next step.

The light curve is modelled to derive the following parameters of the secondary: effective temperature, mass and radius, as well as the inclination of the orbital plane.

3.1 Physical characteristics

First of all, we estimated the reddening, $T_{\rm eff}$, and $\log L/L_{\odot}$. The parallax from the Gaia DR2 is given as $\pi = 3.7774(699)$ mas that translates to a distance of 265 pc (Lindegren et al. 2018). The reddening was assumed to be zero (Green et al. 2018). Note that the Gaia DR2 lists a value of $E(B - V) = 0.1$ mag that seems to be too high. As the next step, we derived the $T_{\rm eff}$ using photometric colours. We have used the *BV* data published by Kharchenko (2001). The $JHK_{\rm s}$ magnitudes were taken from the 2MASS 6X Point Source Working Database (Skrutskie et al. 2006). The standard relations were taken from the updated list by Pecaut & Mamajek (2013). All colours give consistent values between 7 500 and 7 700 K, respectively. Again, the value in the Gaia DR2 of 8 199 K seems to be too high.[2] Assuming the bolometric correction taken from Flower (1996), we get a bolometric luminosity $\log L/L_{\odot} = 1.52(2)$. From the luminosity and the evolutionary tracks from Bressan et al. (2012), we estimated $\log g = 3.70(5)$.

For the investigation of the metallicity and the projected rotational velocity $\upsilon \sin i$ of the primary, synthesized spectra were computed using the program SPECTRUM[3] (Gray & Corbally 1994) and modified versions of the ATLAS9 code taken from the Vienna New Model Grid of Stellar Atmospheres, NEMO[4] (Heiter et al. 2002). We used a stellar atmosphere with $T_{\rm eff} = 7\,600$ K, $\log g = 3.6$, and $\upsilon_{\rm mic} = 2$ km s^{-1}.

The synthetic spectrum was first convolved with the instrumental profile and then with different rotational profiles yielding a best fit for a $\upsilon \sin i$ of 50 km s^{-1} with an uncertainty of about 2 km s^{-1}. To test the astrophysical parameters derived from photometry, a grid of atmospheres with effective temperatures and surface gravities around the input values were applied. The hydrogen lines are best fitted with the values mentioned above with the assumption that they are not sensitive to $\log g$. Also, the overall metallic line spectrum is well fitted. For spectra cooler than 7400 K, many lines appear that are not visible in the observed stellar spectrum. We have to emphasize that also a spectrum of 8000 K fits the metallic line spectrum, but this would mean that the abundances anomalies are even more pronounced because the overall metallic line spectrum gets weaker for hotter temperatures.

To estimate the [Z/H] values for the individual elements, we used different models with metallicities from +2 to −1 dex. Then, we compared all the individual lines of one element to the synthetic spectra resulting in a mean value for each traceable element with an heuristic error of about ±0.2 dex. We found that Fe, Si, and Ti are overabundant with >+1 dex compared to solar abundance, while Ca, Mn, Ni, and Y are slightly overabundant (from +0.2 to +0.8 dex). Such an abundance pattern is typical for magnetic Ap (CP2) stars (Bailey, Landstreet & Bagnulo 2014).

As the last step, we estimated the mass, radius, and age of the primary component using the isochrones by Bressan et al. (2012) and the values listed above. A 2D interpolation within this grid yields

[1] IRAF is distributed by the National Optical Astronomy Observatories, which are operated by the Association of Universities for Research in Astronomy, Inc., under cooperative agreement with the National Science Foundation.

[2] See Table A1 for comparison of the parameters available in the current literature.

[3] http://www.appstate.edu/~grayro/spectrum/spectrum.html

[4] http://www.univie.ac.at/nemo

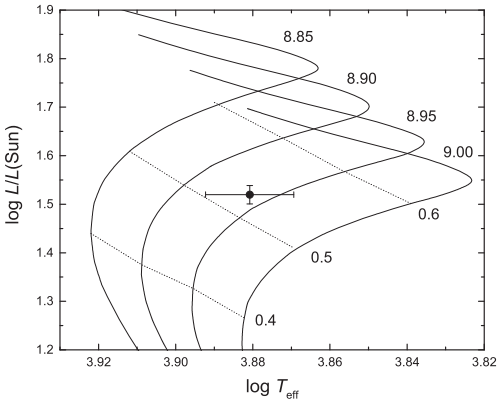

Figure 1. The location of the primary component within the log $L/L_\odot$ versus log $T_{\rm eff}$ diagram. The isochrones with log values from 8.85 to 9.0 were taken from Bressan et al. (2012). Lines of constant log $R/R_\odot$ values are also included.

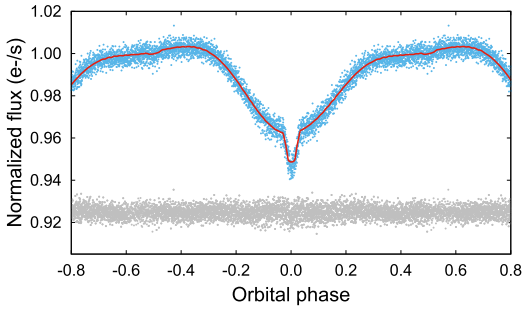

Figure 2. Photometric data phased according to equation (1). The solid line shows the PHOEBE fit asssuming two dark spots on the surface. The grey points in the bottom part of the figure show the residuals (RMS ∼0.003 e-s^{-1}).

$M_1 = 2.15(5)\,M_\odot$, log $R/R_\odot = 0.54(2)$, and log $t = 8.93(5)$ yr (see Fig. 1). The star is clearly a main-sequence star. Using the formula for rigid body rotation (assuming the period $P = 2.722$ d and radius $R = 3.467\,R_\odot$), applied for chemically peculiar stars (Paunzen & Maitzen 1998), we derived an equatorial rotational velocity $V_{\rm eq}$ of 64(2) km s^{-1} and an inclination i of 50(2) deg.

3.2 Binary model

Since the time base of our RV data is more than 10 times larger than photometric data from *K2*, we were able to improve the orbital period. For phasing the data (Figs 2 and 3), we used the ephemeris

$$T_{\rm min} = 2456814.4918 + 2.722045(9) \times E. \quad (1)$$

The zero epoch was taken from Barros et al. (2016).

The *K2* data shows smooth variations in brightness. There is a broad dip between phases −0.3 and 0.3 with an amplitude of about 4 per cent (normalized flux between approximately 0.96 and 1.01 in Fig. 2) and a sudden, 0.18-d long, 1.5 per cent drop at phase 0.0 that is caused by the transiting small companion (we will call it transit). At phase 0.5 the secondary eclipse is apparent.

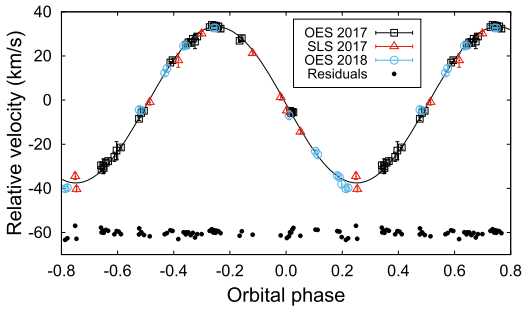

Figure 3. The radial velocity curve showing measurements from the two observing facilities in 2017 and 2018, the fit obtained with RADVEL (the solid line), and the residuals (the black dots around −60 km s^{-1}). SLS means Stará Lesná Spectrograph.

We assume that the changes out of the transit are due to photometric spot(s) on the surface of the primary star combined with the binary proximity effects (ellipticity of the components, possible reflection effect etc.). These phenomena cannot be easily distinguished from the broad-band long-cadence *K2* data itself, but multicolour photometry and high-resolution and high-SNR spectra that are currently unavailable would help in future. In Section 3.3, we investigate the residuals shown in the bottom part of Fig. 2 and identify short-period variations, probably arising from pulsations.

Analysis of the RV data (Fig. 3) including the use of RADVEL software (Pribulla et al. 2015) yielded a semi-amplitude of $K = 35.2(3)$ km s^{-1} and a mass function $f(M) = 0.0123(3)\,M_\odot$, which were together with the parameters from Section 3 (see Table A1) fixed and used as the input parameters for the light-curve model in PHOEBE (ver. 0.31, Prsa et al. 2011).

We fixed the eccentricity to zero because primary and secondary minima always occur at phases 0.0 and 0.5.[5] We also kept the effective temperature of the primary component fixed at 7600 K (derived from spectroscopy). Values of gravity darkening and albedo for the primary component were fixed to 1 because the effective temperature indicates the presence of radiative envelope (Claret 1999). Because we expected a smaller and colder companion, we fixed the albedo of the secondary component to 0.6 and the gravity darkening factor to 0.32 that are corresponding values for a convective envelope. A linear cosine law for limb darkening was used, with coefficients interpolated from van Hamme (1993) tables. During the whole procedure, we constrained the mass, surface gravity and radius of the primary component to the values obtained from spectroscopy.[6]

To get the starting values for the binary model, we first removed the main, out-of-transit photometric variations by modelling them with two-component harmonic polynomial.[7] Such photometric residuals were fitted simultaneously with the RV observations. However, due to the fact that the pre-whitening procedure discarded all the information about ellipsoidal variations caused by tidally deformed components, we decided to fit the eclipsing binary model

[5]RADVEL gives $e = 0.008 \pm 0.008$.
[6]The values stay within errors when they are left as free parameters during the fitting process.
[7]The same result can be achieved using 10th order algebraic polynomial.

Table 1. Ephemerides and results from the binary fitting.

P (d)	2.722045(9)	Fixed	$f(M)$ ($M_\odot$)	0.0123(3)	Fixed
T_0 (HJD)	2456814.4918	Fixed	R_1 ($R_\odot$)	3.47(16)	Fixed
a ($R_\odot$)	11.28(5)	–	R_2 ($R_\odot$)	$0.59^{+0.06}_{-0.14}$	–
$q = M_2/M_1$	0.21(1)	–	$\log g_1$ (cgs)	3.70(5)	Fixed
K_1 (km s^{-1})	35.2(3)	Fixed	$\log g_2$ (cgs)	4.55(5)	–
i (deg)	73.2(6)	–	Spot1		–
e	0	Fixed	Longitude (deg)	130	–
$T_{\rm eff1}$ (K)	7600(100)	Fixed	Colatitude (deg)	297	–
$T_{\rm eff2}$ (K)	3700	Fixed	Radius (deg)	90	–
$\Omega(L_1)$	2.26	–	$T_{\rm spot1}/T_{\rm eff1}$	0.9823	–
$\Omega(L_2)$	2.13	–	Spot2		–
Ω_1	3.52	Fixed	Longitude (deg)	18.5	–
Ω_2	$5.4^{+1.0}_{-0.5}$	–	Colatitude (deg)	65	–
M_1 ($M_\odot$)	2.15(5)	Fixed	Radius (deg)	46	–
M_2 ($M_\odot$)	0.45(2)	–	$T_{\rm spot2}/T_{\rm eff1}$	0.943	–

only with LC data in immediate vicinity of transit and secondary eclipse. This resulted in poor estimate of temperature of the secondary component, which we fix to 3700 K consistent with the radius and mass of the secondary (see next). After the first-order estimation of the input parameters of the secondary component, we modelled the original data by assuming two spots on the surface of the primary. The resulting model is shown with continuous line in Fig. 2. This is, of course, a huge simplification because spots on the surface of CP stars are not temperature spots but rather abundance spots having a different chemical composition than the surrounding photosphere (e.g. Prvák et al. 2015). Nevertheless, it demonstrates well that the variations can be parametrized using two spots on the surface.

The secondary is a small star on a circular orbit that makes a grazing eclipse (transit). Our model gives $M_2 = 0.45(2)\,M_\odot$, $R_2 = 0.59\,R_\odot$, $i = 73.2(6)$ deg. The full set of parameters is shown in Table 1. We conclude the secondary is an early M-type main-sequence star with an bolometric magnitude of about +8 mag (Pecaut & Mamajek 2013) that is about 6.5 mag fainter than the primary. The light contribution of the secondary component has no significant effect on the overall absolute magnitude and thus the luminosity.

If we assume that the rotational axis is aligned with the orbital axis ($i = 73.2(6)$ deg), we derive $V_{\rm eq} = 52\,{\rm km\,s^{-1}}$ and $\log R/R_\odot = 0.45$ for the primary star, respectively. The latter is clearly not compatible with the isochrones (Fig. 1). This implies that the rotational axis is misaligned by about 20 deg to the orbital axis. However, because the primary minimum and the out-of-transit variations have minimum always in phase 0, the orbital and rotational period of the primary star are equal.

3.3 Pulsations

In the previous section, we obtained good fit of the light curve assuming binary model with spots on the primary. In the next step, we subtracted this fit from the observations and performed a frequency analysis on photometric residuals using PERIOD04 (Lenz & Breger 2005). The power spectrum (Fig. 4) shows a series of peaks at low frequencies that are most likely artefacts due to instrumental effects and the orbital frequency and its harmonics. We attribute the cluster of peaks around 20 c/d to stellar variability. However, we cannot fully rule out that some of these peaks (but not all) are artefacts of removing the binary model.

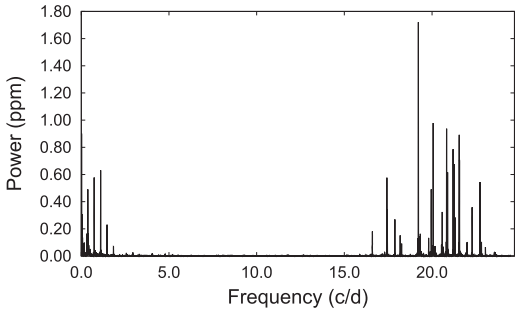

Figure 4. Power spectra of the residuals after the binary model was removed. The low-frequency peaks are relics of the orbital period, while the peaks around 20 c/d are real manifestations of pulsations of δ Scuti type.

Table 2. First six independent frequencies identified in the δ Scuti regime. The corresponding errors in the last digits are in parentheses.

Frequency (c/d)	Amplitude (ppt)	Phase (rad)
19.22089(31)	1.28(6)	3.252(45)
20.06710(40)	0.99(6)	0.072(57)
20.83067(40)	0.98(6)	0.696(58)
21.55110(43)	0.92(6)	0.906(62)
21.20216(43)	0.92(6)	0.729(62)
21.26344(47)	0.83(6)	1.472(69)

The highest peak at 19.2 c/d with amplitude of 1.28 ppt (in the power spectra ∼1.64 ppm) corresponds to the photometric variation with period of 1.25 h. We identified at least six independent frequencies that we give in Table 2. Photometric variations of amplitudes ∼mmag at frequencies higher than 5 c/d are typical for δ Scuti stars (Breger 2000). Therefore, the most natural explanation is that HD 99458 is a pulsating star of the δ Scuti type. However, other explanations are possible (see Sections 4.2 and 4.5). We do not explore further the pulsations because the long integration time of the data averages the short-time variations significantly.

4 DISCUSSION

4.1 Impact of fast rotation on the RV determination

The projected rotational velocity $\upsilon \sin i = 50\,\mathrm{km\,s^{-1}}$ is larger than the semi-amplitude of the RV curve (Fig. 3), which raises the question how the rotation influences the RV determination. First, RVs are measured using cross-correlation function method over a broad spectral region between 4900 and 5500 Å. The Si, Ti, and lines of other overabundant elements are fewer compared to other lines in the region (mainly Fe lines). These few lines cannot influence the final RV measurements.

Rotational modulation of $50\,\mathrm{km\,s^{-1}}$ would need that large chemical spots are both at the opposite edges of the disc; thus, their projected surfaces would be very small compared to the full disc area meaning no influence on the RV. Spots would need to be extremely large to have some impact on RV measurements.

The LC (Fig. 2) shows a maximum amplitude of 4 per cent. For Ap stars and their chemical spots, it is difficult to estimate the RV variations due to rotational modulation. For simplicity, let us assume that the photometric variations come from cool spots. We can then use the estimate of the RV amplitude of spots from Saar & Donahue (1997):

$$A_{\mathrm{spot}} \sim 6.5 f_{\mathrm{spot}}^{0.9} \upsilon \sin i, \quad (2)$$

where f_{spot} is the relative area of the spot in per cent and $\upsilon \sin i$ is in $\mathrm{km\,s^{-1}}$.

For a photometric amplitude of 2 per cent this corresponds to an RV amplitude of approximately $0.6\,\mathrm{km\,s^{-1}}$, or only about 2 per cent of the RV semi-amplitude. This translates into a change in stellar mass of the primary by the same amount. It is impossible that rotational modulation would account for a significant part of the RV variations as this would have resulted in much larger variations in the LC.

4.2 Contamination by nearby stars

Since HD 99458 is a unique object, all the observed features must be unambiguously confirmed to come from HD 99458. One possibility is that some of the features (e.g. δ Scuti variations) come from either of a few faint contaminants in the *K2* aperture. The brightest one is UCAC4 456-050614 that is 6 mag fainter than HD 99458 in V and is 1.5 arcmin apart from it.[8] We can safely exclude all the close stars as the source of the out-of-transit photometric variations because RVs correspond exactly to the photometric variations.

We can also exclude UCAC4 456-050614 as a source of oscillations because it has $B - V = 0.709$ (Zacharias et al. 2013), which is out of range for δ Scuti pulsations. However, in some circumstances, the (semi)periodic minutes-to-hours long variations could be due to granulation. If we consider the above-mentioned colour, $V = 14.081$ mag (Zacharias et al. 2013), $\pi = 1.453$ mas (Gaia Collaboration 2018), using standard relations from Pecaut & Mamajek (2013) we find that UCAC4 456-050614 is a solar analogue with temperature of about 5590 K.

Using the scaling relations from Samadi, Belkacem & Ludwig (2013a) and Samadi et al. (2013b) summarized in Cranmer et al. (2014), we get the maximal amplitude of the possible photometric variations as 0.05 ppt, which is orders of magnitude less than the amplitude of the observed variations (>1 ppt). Thus, granulation cannot explain the short-time variations either. A possible blend with a 14-mag star will also not impact the total amplitude of the photometric variations.

4.3 Origin of the out-of-transit photometric variations

Our analysis (Section 3.1) shows that the primary component of HD 99458 is a chemically peculiar star of CP2 type (Preston 1974).[9] This means that the surface is stratified due to different atomic diffusion rate of different elements (Michaud et al. 1976). Regions (spots) with different chemical abundances (typically iron-peak elements and Si, SrCrEu group of elements) can produce strictly periodic photometric variations due to rotation. To create and maintain chemical peculiarity in CP2 stars, a very stable atmosphere supported by the presence of strong large-scale globally organized magnetic fields is required (Niemczura, Smalley & Pych 2014). We suppose that the out-of-transit variation (see Fig. 2) is caused by chemical spots. We do not know the exact size and location of the spots because the models are ambiguous. One-spot model gives only a bit worse fit to the data then two-spot model. Without having multicolour photometry and high-resolution and high-SNR spectroscopy for line profile variation investigation we cannot say much more.

As an alternative explanation of the out-of-transit variations, we considered the presence of a cool accretion disc and cool companion filling its Roche lobe that feeds the accretion disc. The eclipse of the disc would then produce the out-of-transit variations. We modelled the LC with SHELLSPEC code (Budaj & Richards 2004). The geometry of the Roche lobe that intersects the orbital plane in the L1 point at an angle of about 115 ± 1 per cent deg (Plavec & Kratochvíl 1964) gives an upper limit for the duration of the eclipse as 0.32 in phase. Thus, we are unable to reproduce the very broad main drop in flux which lasts about 0.5 in phase. At the same time, it is very difficult to reproduce a relatively shallow major flux depression with the mass ratio of 0.21.

Additional structures or effects would have to be invoked. One possibility is that the two stars are surrounded by an optically thin cooler material located between the C1 and C2 Roche potential surfaces. We tried to model such an envelope as well but, unfortunately, we were not able to reproduce the observed light curve assuming the mass ratio of 0.21. Also, if such a disc were present in the system it might be seen in the form of a double peak emission in the strong lines such as Hα. However, there is no clear evidence for such emission. Thus, the spot model is far more likely than such a disc model.

4.4 Binarity

Binarity among CP stars is still not well understood. Among non-magnetic metallic-line enhanced (CP1) and non-magnetic mercury-manganese (CP3) stars, the binary fraction is about 70 and 90 per cent, respectively (Carquillat & Prieur 2007; Schöller et al. 2010). Among CP2 stars, the fraction of binary systems with long periods is similar to other A-type stars but only very few non-eclipsing SB binaries with periods less than 50 d have been discovered (Abt & Snowden 1973; Carrier et al. 2002; Landstreet et al. 2017; Mathys 2017). The only known binary with period below 3 d is HD 200405, which is non-eclipsing SB1 (Carrier et al. 2002). Concerning eclipsing binaries, there are two candidates

[8] The other stars are fainter than 19 mag in B.

[9] About 15–20 per cent of B–F stars are CP stars (Romanyuk 2007).

containing a Bp star: V772 Cas (Gandet 2008, period 5 d) and HD 66051 (Paunzen et al. 2018; Kochukhov et al. 2018, period 4.7 d), which both have ambiguous Bp classification. The lack of CP2 stars bound in close binary systems may be due to an interplay between binarity and magnetism that prevents Ap occurring in such binaries (Abt & Snowden 1973; Budaj 1999). HD 99458 represents an ideal laboratory for investigations of binary-magnetism relation, can shed some light on how the magnetic field influences formation of close binary pairs, and how the chemical anomalies are related to the presence of the companion.

HD 99458 can be used to test the hypothesis of forming CP2 stars in close binaries via merging (Ferrario et al. 2009; Tutukov & Fedorova 2010). It could hardly been formed via merging since it would require formation and existence of three stars on very close orbits. Such systems are dynamically unstable. Moreover, the third body (the current secondary component) would be probably kicked off further away by gaining the excess momentum from the merger process. HD 99458 is not the only known such star. Mathys (2017) listed several other short-period Ap binaries (HD 5550, HD 25267, HD 25823, HD 98088) and mentioned that the merging mechanism might not account for their formation. Tutukov & Fedorova (2010) also acknowledge the other process for the formation of Ap stars. Thus, HD 99458 is an additional example and argument for the existence of other channels of Ap star formation. However, this does not exclude the possibility that Ap stars that are not in close binaries have formed through merging.

4.5 Presence of pulsations

In the region of Hertzsprung–Russel diagram, where A–F main-sequence stars are located, pressure (p) and gravity (g) modes can be excited and produce rapid oscillations, δ Scuti and γ Doradus-type pulsations. In a few tens of CP2 stars, rapid oscillations with very short periods on the order of 5–20 min have been observed (roAp stars; Kurtz & Martinez 2000; Smalley et al. 2015). Recently, Bowman et al. (2018) analysed *K2* data of CP2 stars in order to investigate rotational and additional variability. In six of their sample stars, they found additional variations possibly caused by pressure and gravity modes but their results are not conclusive.

HD 99458 clearly shows fast photometric variations that can be hardly explained in other way than by δ Scuti-type oscillations (see Fig. 4 with the dominant frequency at 19.2 c/d). A simple test with granulation on the secondary component by considering values from Table A1 would yield maximal possible amplitude of 0.018 ppt, which is also orders of magnitude less than the observed amplitude. Because blends and granulation can be rejected as the origin of the fast variations, and artificial origin of all the peaks is unlike, we conclude that the observed δ Scuti variations are intrinsic to HD 99458 and are likely caused by the pulsations. The presence of δ Scuti oscillations makes HD 99458 unique object that can help investigate simultaneous presence of anomalous chemical composition in unstable atmospheric conditions.

5 SUMMARY AND FUTURE PROSPECTS

This short paper represents a brief investigation of a new class of objects represented by HD 99458. The aim is to bring the attention to this star and stimulate the observational follow-up efforts. We unambiguously proved that HD 99458 is a binary system consisting of A-type star and low-mass red dwarf, not a system hosting an exoplanet. The rotation and orbital periods are synchronous, however, the rotation and orbital axes are misaligned by about 20 deg. We clearly detected fast photometric variations that we attribute to pulsations of δ Scuti type that are intrinsic to the primary component.

HD 99458 shows spectacular out-of-transit variations, which we interpret as due to chemical spots on the surface of the primary star. Analysis of our spectra indicates that HD 99458 is a chemically peculiar star of CP2 type. As such, it would be the first Ap star in a short-period eclipsing binary system. We discovered a unique astrophysical laboratory where various physical phenomena co-exist and can be studied simultaneously. The available spectra and photometric data that were analysed allow only a very basic analysis. This study is just the beginning. Future high-SNR and high-resolution spectroscopy together with multicolour photometry will allow for better investigation of the chemical composition, distribution of the elements on the surface and the sizes of spots. Such observations will also help to disentangle the variations caused by spots and by proximity effects in the binary system, which are mixed and hard to distinguish because of synchronous rotation. High-cadence spectra and photometry will help to unambiguously confirm and better describe the pulsations. Spectropolarimetric series will allow for detection and orientation of the magnetic field and its variations. Such observations have already started and will be subject of a future paper.

ACKNOWLEDGEMENTS

We would like to thank all the technical staff that makes the observations possible. We are grateful to the anonymous referee who helped to improve the manuscript. We acknowledge SIMBAD and VizieR catalogue databases, operated at CDS, Strasbourg, France, and NASA's Astrophysics Data System Bibliographic Services. MS acknowledges the Postdoc@MUNI project CZ.02.2.69/0.0/0.0/16-027/0008360. PK would like to acknowledge the support from GACR international grant 17-01752J. JK and ZM were supported by grant GA ČR 18-05665S. JB and TP acknowledge VEGA 2/0031/18 and APVV 15-0458 grants, respectively. The research of MF was supported by the internal grant No. VVGS-PF-2018-758 of the Faculty of Science, P. J. Šafárik University in Košice. The data collection was partly funded by SAV-18-02 project.

This article is based on the data collected with Perek 2-m telescope.

REFERENCES

Abt H. A., Snowden M. S., 1973, ApJS, 25, 137
Bailey J. D., Landstreet J. D., Bagnulo S., 2014, A&A, 561, A147
Barros S. C. C., Demangeon O., Deleuil M., 2016, A&A, 594, A100
Bowman D. M., Buysschaert B., Neiner C., Pápics P. I., Oksala M. E., Aerts C., 2018, A&A, 616, A77
Breger M., 2000, in Breger M., Montgomery M., eds, ASP Conf. Ser. Vol. 210, Delta Scuti and Related Stars. Astron. Soc. Pac., San Fransisco, p. 3
Bressan A., Marigo P., Girardi L., Salasnich B., Dal Cero C., Rubele S., Nanni A., 2012, MNRAS, 427, 127
Budaj J., 1999, MNRAS, 310, 419
Budaj J., Richards M. T., 2004, Contrib. Astron. Obs. Skalnate Pleso, 34, 167
Carquillat J.-M., Prieur J.-L., 2007, MNRAS, 380, 1064
Carrier F., North P., Udry S., Babel J., 2002, A&A, 394, 151
Claret A., 1999, in Gimenez A., Guinan E. F., Montesinos B., eds, ASP Cof. Ser. Vol. 173, Stellar Structure: Theory and Test of Connective Energy Transport. Astron. Soc. Pac., San Fransisco, p. 277
Cranmer S. R., Bastien F. A., Stassun K. G., Saar S. H., 2014, ApJ, 781, 124

Ferrario L., Pringle J. E., Tout C. A., Wickramasinghe D. T., 2009, MNRAS, 400, L71
Flower P. J., 1996, ApJ, 469, 355
Gaia Collaboration, 2018, A&A, 616, A1
Gandet T. L., 2008, Information Bulletin on Variable Stars, 5848, 1
Gray R. O., Corbally C. J., 1994, AJ, 107, 742
Green G. M. et al., 2018, MNRAS, 478, 651
Heiter U. et al., 2002, A&A, 392, 619
Howell S. B. et al., 2014, PASP, 126, 398
Huber D. et al., 2016, ApJS, 224, 2
Kharchenko N. V., 2001, Kinematika Fiz. Nebesnykh Tel, 17, 409
Kochukhov O., Johnston C., Alecian E., Wade G. A., 2018, MNRAS, 478, 1749
Koubský P., Mayer P., Čáp J., Žďárský F., Zeman J., Pína L., Melich Z., 2004, Publ. Astron. Inst. Czech. Acad. Sci., 92, 37
Kurtz D. W., Martinez P., 2000, Balt. Astron., 9, 253
Landstreet J. D., Kochukhov O., Alecian E., Bailey J. D., Mathis S., Neiner C., Wade G. A., BINaMIcS Collaboration, 2017, A&A, 601, A129
Lenz P., Breger M., 2005, Commun. Asteroseismol., 146, 53
Lindegren L. et al., 2018, A&A, 616, A2
Mathys G., 2017, A&A, 601, A14
Michaud G., Charland Y., Vauclair S., Vauclair G., 1976, ApJ, 210, 447
Niemczura E., Smalley B., Pych W., 2014, Determination of Atmospheric Parameters of B-, A-, F- and G-Type Stars. Spriger, Berlin
Paunzen E., Maitzen H. M., 1998, A&AS, 133, 1
Paunzen E. et al., 2018, A&A, 615, A36
Pecaut M. J., Mamajek E. E., 2013, ApJS, 208, 9
Plavec M., Kratochvil P., 1964, Bull. Astron. Inst. Czech., 15, 165
Preston G. W., 1974, ARA&A, 12, 257
Pribulla T. et al., 2015, Astron. Nachr., 336, 682
Prsa A., Matijevic G., Latkovic O., Vilardell F., Wils P., 2011, Astrophysics Source Code Library, record ascl:1106.002
Prvák M., Liška J., Krtička J., Mikulášek Z., Lüftinger T., 2015, A&A, 584, A17
Romanyuk I. I., 2007, Astrophys. Bull., 62, 62
Saar S. H., Donahue R. A., 1997, ApJ, 485, 319
Samadi R., Belkacem K., Ludwig H.-G., 2013a, A&A, 559, A39
Samadi R. et al., 2013b, A&A, 559, A40
Schöller M., Correia S., Hubrig S., Ageorges N., 2010, A&A, 522, A85
Skrutskie M. F. et al., 2006, AJ, 131, 1163
Smalley B. et al., 2015, MNRAS, 452, 3334
Tody D., 1993, in Hanisch R. J., Brissenden R. J. V., Barnes J., eds, ASP Conf. Ser. Vol. 52, Astronomical Data Analysis Software and Systems II. Astron. Soc. Pac., San Fransisco, p. 173
Tutukov A. V., Fedorova A. V., 2010, Astron. Rep., 54, 156
van Hamme W., 1993, AJ, 106, 2096
Zacharias N., Finch C. T., Girard T. M., Henden A., Bartlett J. L., Monet D. G., Zacharias M. I., 2013, AJ, 145, 44

APPENDIX: TABLES

Table A1. Physical parameters of HD 99458 from literature and this study. The values refer to the primary component. The corresponding errors in the last digits are in parentheses. The references are (1) – Huber et al. (2016), (2) – Barros et al. (2016), (3) – Gaia Collaboration (2018).

$T_{\rm eff}$ (K)	log g (dex)	[Fe/H]	M ($M_\odot$)	R ($R_\odot$)	d (pc)	$V_{\rm eq}$(km s^{-1})	i (deg)	log t (year)	Ref.
6623	4.05	0.001	1.487	1.843	137				1
6815									2
8199					264.7				3
7600(100)	3.70(5)	0.0 +	2.15(5)	3.467(3)		64(1)	73.2(6)	8.90(5)	This study

Table A2. Relative radial velocities. In the columns Instr, OES means Ondřejov echelle spectrograph, while SLS means Stará Lesná spectrograph.

HJD	V (km s^{-1})	σ (km s^{-1})	Instr	HJD	V (km s^{-1})	σ (km s^{-1})	Instr
2457828.4466	− 8.5	0.8	OES	2457853.4894	26.5	3.2	OES
2457828.4679	− 5.8	1.8	OES	2457853.5107	28.8	1.4	OES
2457828.4937	− 4.9	0.8	OES	2457854.3795	− 4.8	1.7	SLS
2457829.4223	26.9	0.8	OES	2457874.3556	− 29.6	1.5	OES
2457829.4436	28.1	1.1	OES	2457874.3770	− 30.0	3.4	OES
2457839.4446	− 1.0	1.3	SLS	2457884.3490	− 4.8	1.3	OES
2457840.4426	21.2	0.8	SLS	2457884.3599	− 5.9	1.2	OES
2457841.4441	− 34.5	1.4	SLS	2457884.3708	− 5.4	0.8	OES
2457843.4364	1.3	1.3	SLS	2457884.3817	− 5.5	1.4	OES
2457844.4162	− 31.6	0.8	OES	2457891.3605	17.0	0.5	OES
2457844.4376	− 30.8	2.3	OES	2457891.3819	18.1	0.9	OES
2457844.4589	− 28.4	1.1	OES	2457901.3389	− 40.4	1.2	SLS
2457844.4802	− 27.6	1.5	OES	2457902.3264	17.9	3.1	SLS
2457844.5408	− 25.7	2.1	OES	2458203.3067	− 34.2	1.2	OES
2457844.5622	− 22.9	4.0	OES	2458203.3280	− 35.0	1.0	OES
2457844.5835	− 21.8	1.8	OES	2458203.3493	− 38.1	1.8	OES
2457844.6048	− 21.5	0.8	OES	2458203.3905	− 40.2	1.0	OES
2457845.3869	30.1	1.0	SLS	2458203.4118	− 39.7	1.5	OES
2457845.4646	33.1	0.8	OES	2458226.3160	24.6	1.7	OES
2457845.4859	34.1	0.6	OES	2458226.3373	24.7	1.4	OES
2457845.5072	33.7	1.5	OES	2458227.3385	− 6.9	2.0	OES
2457845.5286	33.6	1.7	OES	2458229.3268	32.7	0.2	OES
2457845.5499	33.4	1.5	OES	2458229.3481	32.7	0.4	OES
2457845.5712	32.4	1.2	OES	2458230.3165	− 23.2	0.9	OES
2457846.3440	− 14.4	1.0	SLS	2458230.3379	− 24.6	1.9	OES
2457853.4041	25.1	0.8	OES	2458231.3301	− 4.4	1.8	OES
2457853.4254	26.1	1.8	OES	2458231.3514	− 4.7	1.5	OES
2457853.4467	25.9	0.5	OES	2458253.3544	12.2	1.2	OES
2457853.4681	27.8	1.4	OES	2458253.3758	14.3	1.7	OES

This paper has been typeset from a TEX/LATEX file prepared by the author.

Paper 5

Blazhko effect in the Galactic bulge fundamental mode RR Lyrae stars
II. Modulation shapes, amplitudes, and periods

Monthly Notices of the ROYAL ASTRONOMICAL SOCIETY

MNRAS **494,** 1237–1249 (2020) doi:10.1093/mnras/staa673
Advance Access publication 2020 March 13

Blazhko effect in the Galactic bulge fundamental mode RR Lyrae stars – II. Modulation shapes, amplitudes, and periods

M. Skarka [1,2]★ Z. Prudil[3]★ and J. Jurcsik[4]

[1]*Department of Theoretical Physics and Astrophycis, Masaryk University, Kotlářská 2, 611 37 Brno, Czech Republic*
[2]*Astronomical Institue of the Czech Academy of Sciences, Fričova 298, 251 65 Ondřejov, Czech Republic*
[3]*Astronomisches Rechen-Institut, Zentrum für Astronomie der Universität at Heidelberg, Mönchhofstr. 12-14, D-69120 Heidelberg, Germany*
[4]*Konkoly Observatory, Konkoly Thege Miklós út 15-17, H-1121 Budapest, Hungary*

Accepted 2020 March 6. Received 2020 March 6; in original form 2019 December 21

ABSTRACT

The number of stars observed by the Optical Gravitational Lensing Experiment (OGLE) project in the Galactic bulge offers an invaluable chance to study RR Lyrae stars in a statistical manner. We used data of 3141 fundamental-mode RR Lyrae stars showing the Blazhko effect observed in OGLE-IV to investigate a possible connection between modulation amplitudes and periods, light curve, and pulsation characteristics. We found that there is no simple monotonic correlation between any combination of two parameters concerning the Blazhko and pulsation amplitudes, periods, and the shape of the light curves. There are only systematic limits. There is a bottom limit of the modulation period with respect to the pulsation period. We also found that the possible range of modulation amplitudes decreases with increasing pulsation period, which could point towards that the Blazhko effect is suppressed in cooler, larger, more luminous, and less metal abundant bulge RR Lyrae stars. Our investigation revealed that the distribution of the modulation periods can be described with two populations of stars with the mean modulation periods of 48 and 186 d. There is a certain region with a low density of the modulated stars, which we call the Blazhko valley, in the pulsation period–modulation period plane. Based on the similarity of the modulation envelopes, basically every star can be assigned to one of six morphological classes. The double modulation was found in 25 per cent of the studied stars. Only 6.3 per cent of modulated stars belong to the Oosterhoff group II.

Key words: methods: data analysis – methods: statistical – techniques: photometric – stars: horizontal branch – stars: variables: RR Lyrae.

1 INTRODUCTION

Various studies show that about 40–50 per cent of classical RR Lyrae stars (RRLs) pulsating in the fundamental mode show the quasi-periodic variations in amplitude and phase of light curves (see Kovacs 2016). Kovacs (2018) even proposes based on *K2* data (Howell et al. 2014) that up to 100 per cent of RRLs has the Blazhko effect, which is, however, in contrast to results by Plachy et al. (2019), who used the method of extended aperture photometry and detected only 45 per cent of stars to be modulated. This light curve modulation, which is usually called the Blazhko effect (Blažko 1907), lacks the explanation even a century after its discovery.

Most of the proposed models face problems to explain one or more observed characteristics (see the discussion in Kolláth 2018). Currently, it seems that the most likely explanation of the modulation is in the resonance 9:2 between the fundamental and the ninth overtone modes (Kolláth, Molnár & Szabó 2011; Kolláth 2018). The same resonance can explain the period doubling observed in Blazhko stars (Buchler & Kolláth 2011). This model is in accordance with the current findings by Jurcsik & Hajdu (2017), Jurcsik et al. (2018), and Jurcsik (2018), who revealed that radius changes connected to the modulation occur only in the outermost layers of the atmosphere, and the change of the radius at the photospheric layers is constant during the modulation cycle. Consequently, the modulation is caused primarily by changes in the temperature variation.

Large sample(s) of stars are needed to fully cover the stunning diversity of the modulation properties (see e.g. Benkő et al. 2010). A successful model must comply with describing the large variety in amplitudes, periods, and shape of the modulation. Even with a good model of the modulation, there still remains lots of questions to be answered. Why some stars show modulation and others not when there is no difference in the mean characteristics of the modulated and non-Blazhko stars (Smolec 2005; Skarka 2014; Prudil & Skarka 2017)? Is the occurrence of the modulation driven

★ E-mail: maska@physics.muni.cz (MS); prudilz@ari.uni-heidelberg.de (ZP)

by some particular physical property (e.g. temperature, chemical composition, Jurcsik et al. 2011; Arellano Ferro et al. 2016)? Why is the occurrence of modulated RRLs lower among stars with longer pulsation periods (Jurcsik et al. 2011; Skarka 2014)? Is there any relation between the modulation period and light curve characteristics (Jurcsik, Sodor & Varadi 2005c; Jurcsik et al. 2005a; Benkő et al. 2014)?

The aim of our study is to describe the modulation and investigate the possible relations between modulation and pulsation light-curve characteristics. Thus, we investigate the relations between modulation periods, amplitudes, shapes of the light curves, and frequency spectra. We also describe the modulation envelopes and define six basic morphological types of the modulation shapes. At last, we investigate the possible connection between the Blazhko effect and the Oosterhoff dichotomy (Oosterhoff 1939). We do not deal with a detailed investigation of the frequency spectra of particular stars and period variations at all.

The whole study is based on the paper by Prudil & Skarka (2017), where we carefully analysed OGLE-IV data (Soszyński et al. 2014; Udalski, Szymański & Szymański 2015) of more than 8000 fundamental-mode RRLs located in the Galactic bulge. We identified more than 3000 Blazhko stars, which creates the most extensive sample of modulated RRLs ever studied. Because the data were gathered with one telescope with the same detector, with similar cadence and time-span, this gives a unique chance to get a reliable overall picture of the modulation periods and amplitudes among the Blazhko stars.

The paper is structured as follows: In Section 2, we briefly describe the sample of the stars, give details about methods and definition of the parameters we use, and define the six modulation classes. Results on modulation properties can be found in Section 3. We discuss our results in Section 4 and sum up the content of the paper in Section 5.

2 THE SAMPLE AND METHODS

In Prudil & Skarka (2017), we found 3341 stars to show the Blazhko effect based on the look of the frequency spectra and the presence of the equidistant side peaks with amplitudes above SNR[1] > 3.5. This sample was studied again employing automatic procedures and applying subsequent visual inspection of all the frequency spectra of the studied stars to discard the stars with ambiguous modulation. Since we are now interested in the characteristics of the Blazhko effect, we performed additional data examination and analysis.

2.1 Frequency spectra

The modulation period $P_{\rm BL}$ can be defined as the reciprocal value of the difference between the side peaks and the basic pulsation frequency in the frequency spectrum. As the value of the modulation frequency $f_{\rm m}$, we chose the one defined by the side peak with higher SNR:

$$P_{\rm BL} = 1/|f_{0\pm}^{\rm SNR} - f_0| = 1/f_{\rm m}, \quad (1)$$

where $f_{0\pm}^{\rm SNR}$ stands for the side peak with the highest SNR close to f_0. From our previous analysis performed in Prudil & Skarka (2017), we roughly knew the length of the modulation period, which allowed us to automatically identify the position of the side peaks in all sample stars.

First we fit the data with 10 harmonics using the `lcfit` routine (Sódor 2012) to refine the pulsation frequency f_0 and its uncertainty[2] (columns 2 and 3 in Table 1) to estimate and the mean magnitude $I_{\rm mean}$ and the mean amplitude $A_{\rm mean}$ (columns 13 and 16 in Table 1).The mean magnitude $I_{\rm mean}$ is the zero-point of the fit. The mean amplitude $A_{\rm mean}$ is simply defined as the difference between two points with maximum and minimum brightness of the 10-harmonic model with 1000 points over the pulsation cycle. Subsequently, we pre-whitened the frequency spectra with 10 pulsation harmonics keeping the basic pulsation frequency fixed and searched for the highest peaks within ±0.0005 c/d around the expected positions $f_0 \pm f_{\rm m}$. This interval was found as optimal for the automatic proper identification of the peaks. The value 0.0005 c/d roughly corresponds to the inverse of the time-span of the data for most of the stars.

In case of positive identification including visual check, we extracted the exact position of the peaks ($f_+ = f_0 + f_{\rm m}$ and $f_- = f_0 - f_{\rm m}$ for the right-hand and left-hand peak, respectively). Then we re-fit the full data set with 10 harmonics of f_0 (fixed), including f_+ and f_-, which were left as free parameters. We did not include any other frequency since this would need careful and deep frequency analysis of every data set which is out of scope of this paper. After this fitting procedure, we got f_- and f_+ (columns 7 and 10 in Table 1), including their amplitudes A_+, A_- (columns 9 and 12 in Table 1), and we were able to calculate the Blazhko period $P_{\rm BL}$ (equation 1 and its error using the Gauss law of error propagation, columns 5 and 6 in Table 1). We also got information about the amplitude of the residuals of the frequency spectra in the ±0.3 c/d vicinity of f_0 after removing 10 pulsation frequency harmonics defining the noise level ($\rm ARES_{f_0 \pm 0.3}$, column 4 in Table 1).

The knowledge of the position of the side peaks and their amplitudes allowed us to compute the amplitude asymmetry parameter Q defined by Alcock et al. (2003) as

$$Q = \frac{A_+ - A_-}{A_+ + A_-}, \quad (2)$$

and the frequency asymmetry parameter is

$$\Delta f = f_+ + f_- - 2f_0. \quad (3)$$

For each of the sample stars, we plotted the data, the frequency spectra for a fixed ±0.3 c/d vicinity of the basic pulsation frequency and a plot showing more details for a smaller range defined by the the modulation frequency (Fig. 1).

For the stars that have longer modulation period than the half of the time-span of the OGLE-IV data (till the end of 2014)[3], we stitched the data with OGLE-III data (Soszynski et al. 2011) to get longer time base (for details see section 3 in Prudil & Skarka 2017). Then, the frequency spectra and phase light curves of all stars were visually inspected. We discard stars that have too scattered data, showed bunch of peaks next to the basic pulsation frequency or modulation frequencies signalizing some long-term variations. We also removed stars that appeared to show side peaks with SNR below 3.5 and stars with modulation period longer than two-thirds of the longest possible time base (OGLE-III + OGLE-IV).

[1] Signal-to-Noise Ratio

[2] The uncertainty of f_0 is the formal error resulting from the least-square method.

[3] In 2018, the new data up to 2017 were released. We did not use these data.

Table 1. The example of the full table with all the important pulsation, modulation, frequency spectra, and light-curve parameters. All other parameters can be calculated from these parameters. The full table has 30 columns and 3141 rows and is available as a supporting material to the paper and at the CDS portal. The columns have the following meaning: ID # – five-digit number of the star complementing the full designation OGLE-BLG-RRLYR-XXXXX; f_0 – the pulsation frequency; Err_{f_0} – the error of the pulsation frequency; $\mathrm{ARES}_{f_0\pm0.3}$ – the amplitude of the residuals around the ±0.3 c/d vicinity of f_0 after removing 10 pulsation components; P_{BL} – the modulation period; $\mathrm{Err}_{P_{\mathrm{BL}}}$ – the error of the modulation period; f_- – the frequency of the left-hand-side peak; Err_{f_-} – the error of the frequency of the left-hand-side peak; A_- – amplitude of the left side peak in the frequency spectrum; f_+ – the frequency of the right-hand-side peak; Err_{f_-} – the error of the frequency of the right-hand-side peak; A_+ – amplitude of the right-hand-side peak; I_{mean} – the mean brightness of the star; $I^{\mathrm{MAX}}_{\mathrm{mean}}$ – the mean brightness during the Blazhko maximum amplitude; $I^{\mathrm{MIN}}_{\mathrm{mean}}$ – the mean brightness during the Blazhko minimum amplitude; A_{mean} – the mean amplitude of the light curve; $A^{\mathrm{MIN}}_{\mathrm{mean}}$ – the amplitude of the light curve during the minimal-amplitude; $A^{\mathrm{MAX}}_{\mathrm{mean}}$ – the amplitude of the light curve during the maximal-amplitude; $A^{\mathrm{TOP}}_{\mathrm{env}}$ – the amplitude of the top envelope; $A^{\mathrm{BOT}}_{\mathrm{env}}$ – the amplitude of the bottom envelope; $RT^{\mathrm{TOP}}_{\mathrm{env}}$ – the rise time of the top envelope; $RT^{\mathrm{BOT}}_{\mathrm{env}}$ – the rise time of the bottom envelope; R_{21}, φ_{21}, R_{31}, and φ_{31} – amplitude and phase Fourier coefficients; RT_{LC} – rise time of the mean light curve; Oo group – Oosterhoff group; Morph type – morphological type; Comments – information about additional peaks (AdP), and period variation (UP).

ID #	f_0 (c/d)	Err_{f_0} (c/d)	$ARES_{f_0\pm0.3}$(mag)	P_{BL} (d)	$\mathrm{Err}_{P_{\mathrm{BL}}}$ (d)	f_- (c/d)	Err_{f_-} (c/d)	A_- (mag)	→
00162	1.8304213	0.0000022	0.00142	171.23	1.02	1.82458	0.00003	0.0106	→
00172	2.0945254	0.0000021	0.00155	119.05	0.62	2.08610	0.00005	0.0094	→
00184	1.8750512	0.0000016	0.00136	47.24	0.08	1.85392	0.00008	0.0062	→
...	...	...	...	...	...	...	...	...	→
→	f_+	Err_{f_+} (c/d)	A_+ (mag)	I_{mean} (mag)	$I^{\mathrm{MAX}}_{\mathrm{mean}}$ (mag)	$I^{\mathrm{MIN}}_{\mathrm{mean}}$ (mag)	A_{mean} (mag)	$A^{\mathrm{MIN}}_{\mathrm{mean}}$ (mag)	→
→	1.83613	0.00008	0.0049	15.941	15.943	15.948	0.656	0.528	→
→	2.10293	0.00004	0.0096	15.797	15.799	15.801	0.713	0.544	→
→	1.89622	0.00004	0.0111	15.769	15.781	15.757	0.730	0.668	→
→	...	...	...	...	...	...	...	...	→
→	$A^{\mathrm{Max}}_{\mathrm{mean}}$ (mag)	$A^{\mathrm{TOP}}_{\mathrm{env}}$ (mag)	$A^{\mathrm{BOT}}_{\mathrm{env}}$ (mag)	$RT^{\mathrm{TOP}}_{\mathrm{env}}$	$RT^{\mathrm{BOT}}_{\mathrm{env}}$	R_{21}	φ_{21} (rad)	R_{31}	→
→	0.7132	0.119	0.066	0.74	0.58	0.531	4.330	0.334	→
→	0.865	0.235	0.114	0.50	0.52	0.474	4.165	0.341	→
→	0.8304	0.073	0.037	0.44	0.50	0.485	4.162	0.367	→
→	...	...	...	...	...	...	...	...	→
→	φ_{31} (rad)	RT_{LC}	Oo group	Morph type	Comments				
→	2.619	0.17	1	a	–				
→	2.295	0.15	1	a	–				
→	2.296	0.14	1	–	–				
→	...	...	...	...	...				

After this procedure, we were left with 3141 stars. We include information about additional peaks in the vicinity of the basic pulsation frequency that could signalize additional modulation (Additional Peaks – AdP) or long-term period change (Unresolved peaks – UP). The full table is available only electronically as supplementary material to this paper and the example of a few first rows is shown in Table 1.

2.2 Amplitudes, rise time, and envelope parameters

To get the amplitude of the modulation and variation of the mean magnitude, we first phased the data with the modulation frequency with the zero epoch t_0 corresponding to the brightest point in the data set. In a vast majority of the stars, the brightest point corresponds to the maximal amplitude during the Blazhko effect. Then we separated the data into 10 or 20 bins centered to t_0 taking into account the number of points[4] and modelled the light curve in each bin j with the Fourier series

$$m_j(t) = m_{0,j} + \sum_{i=1}^{N_j} a_{i,j} \sin\left(2\pi i \frac{t - t_0}{P_{\mathrm{puls}}} + \varphi_{i,j}\right), \quad (4)$$

where t_0 is the zero epoch, $a_{i\,\mathrm{and}\,j}$ and $\varphi_{i\,\mathrm{and}\,j}$ are the amplitudes and phases of the ith component in jth bin, respectively. The degree of the fit in the jth bin N_j was selected in such a way that the amplitude of the N_jth component was four times higher than the noise level. Typically, N_j was between 4 and 10.

The total amplitude A_j in a particular Blazhko phase (in the jth bin) was defined simply as the difference between the brightest and faintest point of the fit in the same way as the value of the mean amplitude A_{mean} – as the difference between two model points with maximum and minimum brightness. The amplitude of the modulation is defined in two comparable ways. First, as the difference between the maximal $A^{\mathrm{MAX}}_{\mathrm{mean}}$ and minimal $A^{\mathrm{MIN}}_{\mathrm{mean}}$ photometric pulsation amplitudes (columns 18 and 17 in Table 1)

$$A^{\mathrm{BL}}_{\mathrm{Puls}} = A^{\mathrm{MAX}}_{\mathrm{mean}} - A^{\mathrm{MIN}}_{\mathrm{mean}}. \quad (5)$$

The second definition of the modulation amplitude, we adopted is the sum of the top and bottom amplitude of the envelopes ($A^{\mathrm{TOP}}_{\mathrm{env}}$ and $A^{\mathrm{BOT}}_{\mathrm{env}}$; columns 19 and 20 in Table 1):

$$A^{\mathrm{BL}}_{\mathrm{env}} = A^{\mathrm{TOP}}_{\mathrm{env}} + A^{\mathrm{BOT}}_{\mathrm{env}}. \quad (6)$$

To get this information, we divided the Blazhko-phased data into 20 bins and got the highest and lowest points of the envelopes in each bin. With such definitions, the zero epoch of the modulation plays no role, because the maximal and minimal amplitudes are chosen regardless of the original Blazhko phasing described above.

The amplitude of the variation of the mean magnitude during the Blazhko cycle is defined as

$$\Delta I = I^{\mathrm{MAX}}_{\mathrm{mean}} - I^{\mathrm{MIN}}_{\mathrm{mean}}, \quad (7)$$

where $I^{\mathrm{MAX}}_{\mathrm{mean}}$ and $I^{\mathrm{MIN}}_{\mathrm{mean}}$ are the mean magnitudes during maximal and minimal amplitudes of the Blazhko cycle, respectively (columns 14

[4]Ten bins for stars with less than 1000 points, 20 bins for stars with more data points.

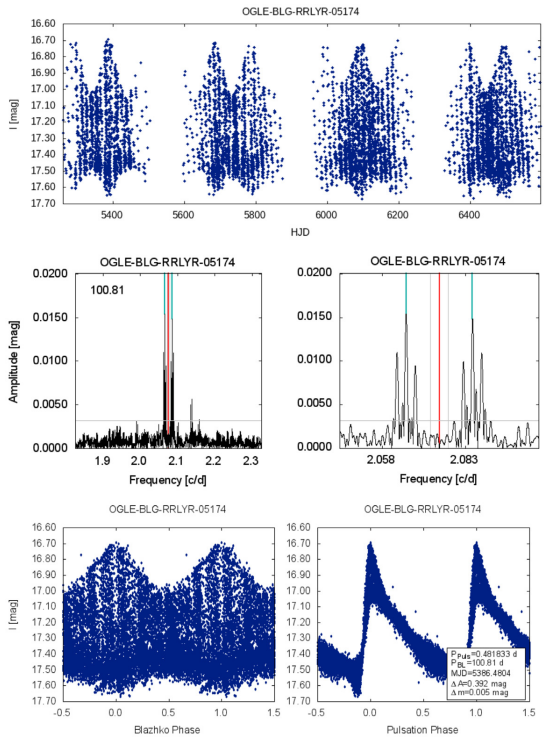

Figure 1. Examples of plots that we used for visualization while studying the sample stars: the data (top panel), frequency spectra (the two middle panels), and Blazhko- and pulsation-phased light curves (the two bottom panels). The vicinity of the basic pulsation frequency (red continuous line) is zoomed for better readability in the middle right-hand panel. The vertical cyan lines show the exact positions of the side peaks, the vertical grey lines show the positions of yearly aliases of f_0, and finally, the horizontal grey line shows the SNR $\sim$ 3.5 limit. The bottom right-hand panel shows the data phased with the modulation period, while the bottom left-hand panel shows the folded light curve with the basic pulsation frequency. Additional information about the modulation characteristics is given in the bottom right-hand corner of the bottom right-hand panel.

and 15 in Table 1). As such, they do not necessarily correspond to the maximal mean-magnitude difference during the cycle.

From the binning of the Blazhko-phased light curve, we also have information about the rise times ($RT_{\rm env}$) of the envelopes, which correspond to the phase differences between maximum and minimum brightness of the envelopes:

$$RT_{\rm env} = \phi_{\rm env}^{\rm MAX} - \phi_{\rm env}^{\rm MIN}. \quad (8)$$

The exact minimal and maximal phases $\phi_{\rm env}^{\rm MIN}$ and $\phi_{\rm env}^{\rm MAX}$ of the envelopes were determined as the minimal and maximal values of the fit of the 20 points from the 20 bins. The low-degree Fourier series employing the Blazhko period was the model function of the fit. Through the text, we mention exclusively the $RT_{\rm env}^{\rm TOP}$ (column 21 in Table 1) of the top envelope since it is better defined and is very similar to the bottom envelope in most stars.

2.3 Morphological types

Based on the visual inspection of the Blazhko-phased light curves, we divided the star into six basic morphological types:

(i) *Class a* – The top and bottom envelopes are nearly symmetric and sinusoidal and are close to antiphase (the top left-hand panel of Fig. 2). Sometimes the top envelope has a sharp maximum.
(ii) *Class b* – The Blazhko phase curve is flat during minimal modulation amplitude and the phase modulation well apparent (the top middle panel of Fig. 2).
(iii) *Class c* – The bottom envelope is flat (the top right-hand panel of Fig. 2).
(iv) *Class d* – The bottom envelope has a double minimum (the bottom left panel of Fig. 2).
(v) *Class e* – The bottom envelope has a larger amplitude than the top envelope (the bottom middle panel of Fig. 2).
(vi) *Class f* – The top and/or bottom envelope has a bump (the bottom right-hand panel of Fig. 2).

It is possible that some morphological types are contaminated with RRLs from other classes because the sorting is based on a pure visual inspection. In addition, it is also possible that some of the types actually constitute only one class (see Section 4). We did not assign stars with a low number of points and/or with a small amplitude and/or bad phase coverage with any of the thypological classes. Only 2449 stars (78 per cent) were assigned to one of the types. The basic statistical properties of the various classes can be found in Table 2.

According to Benkő, Szabó & Paparó (2011), Benkő (2018), and Szeidl et al. (2012), the variation of the light curve shape can be well approximated using the notation of the data transfer signal as the amplitude and phase/frequency modulation of the carrier wave. We aim at investigating purely amplitude modulation and the shape of the modulation envelopes not taking into account the period modulation. This would need the full frequency analysis of every particular star, which is clearly out of scope of this paper. Following Benkő (2018), pure amplitude-modulated signal can be expressed as

$$m^{\rm A}(t) = \left[a_0^{\rm A} + f_{\rm m}^{\rm A}(\Omega, t)\right] m(t), \quad (9)$$

where $f_{\rm m}^{\rm A}(\Omega, t)$ is the function that describes amplitude modulation with the angular frequency $\Omega = 2\pi f_{\rm m}$, $a_0^{\rm A}$ and a_0 are the zero-point constants and $m(t)$ is the non-modulated light curve (equation 4). The amplitude modulation can generally be complex and non-sinusoidal. In such case, $f_{\rm m}^{\rm A}(\Omega, t)$ can be expanded into a sine series and the shape of the envelope will depend on the amplitudes but also on the phases of the modulation components $\varphi_{i{\rm m}}^{\rm A}$.

3 RESULTS

3.1 Modulation periods

The distribution of the modulation periods is shown in Fig. 3. The shortest found Blazhko period is 4.84 d (OGLE-BLG-RRLYR-04885), which is the shortest known modulation period among fundamental-mode RRLs.[5] Among the first-overtone RRLs, the shortest ever detected modulation period is 2.23 d (Netzel et al. 2018). On the other hand, the longest detected modulation period among our sample stars is 2857 d, which is far not the longest known

[5]The former record holder was SS Cnc with the modulation period of 5.3 d (Jurcsik et al. 2006). We note that OGLE-BLG-RRLYR-04885 has the side peak near the SNR limit for identifying it as Blazhko star.

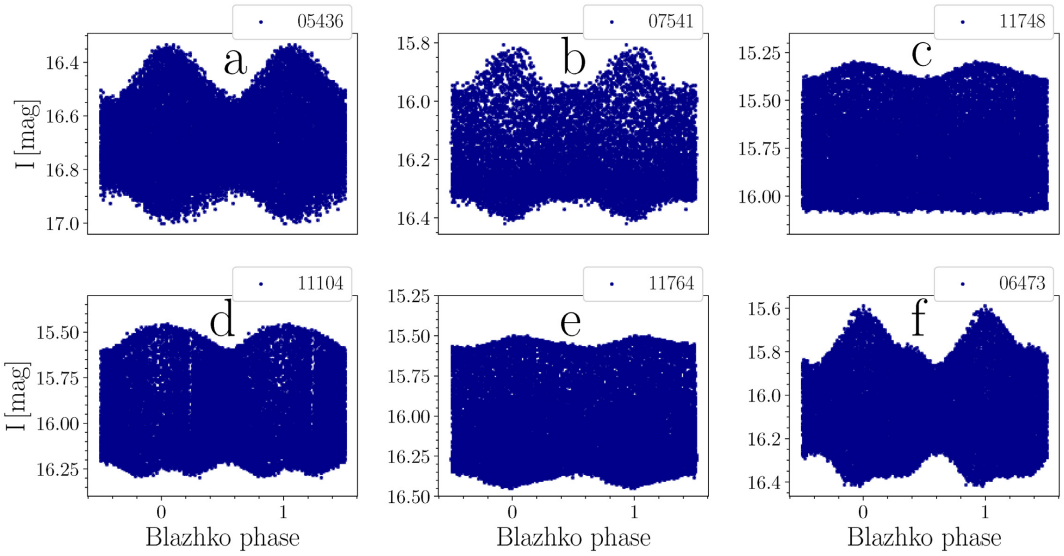

Figure 2. The prototypes of the basic morphological types showing different shapes of the modulation envelopes. The data are phased with the Blazhko period, the legend of each panel denotes the ID of a given star in the form OGLE-BLG-RRLYR-ID. See the text for more details.

Table 2. The basic statistical data of the stars, which were assigned to one of the six classes. N in the second column is the number of stars in a given sample, Rate shows the percentage of the stars according to the full sample, $\langle P_{\rm Puls}\rangle$ is the mean pulsation period, $\langle A_{\rm Puls}\rangle$ is the mean pulsation amplitude, $\langle P_{\rm BL}\rangle$ is the mean Blazhko period, while $\langle A_{\rm BL}\rangle$ shows the mean modulation amplitude. The tilde over variables stands for median value. The last column shows the percentage of the Oosterhoff II stars in a given sample.

ID	N	Rate (per cent)	$\langle P_{\rm Puls}\rangle$ (d)	$\widetilde{P}_{\rm Puls}$ (d)	$\langle A_{\rm Puls}\rangle$ (mag)	$\widetilde{A}_{\rm Puls}$ (mag)	$\langle P_{\rm BL}\rangle$ (d)	$\widetilde{P}_{\rm BL}$ (d)	$\langle A_{\rm Puls}\rangle$ (mag)	$\widetilde{A}_{\rm BL}$ (mag)	OoII (per cent)
All	2449	100	0.532	0.532	0.531	0.633	116	111	0.26	0.351	6.3
a	2205	90	0.534	0.532	0.529	0.538	116	60.3	0.259	0.248	5.9
b	95	3.9	0.492	0.49	0.545	0.541	107	69.44	0.399	0.4	0.0
c	53	2.1	0.545	0.546	0.565	0.555	103	56.18	0.109	0.103	7.5
d	41	1.7	0.517	0.52	0.563	0.559	93	65.66	0.165	0.161	0.0
e	29	1.2	0.522	0.509	0.528	0.59	152	63.98	0.155	0.156	0.0
f	26	1.1	0.506	0.499	0.523	0.519	170	134.34	0.4	0.377	0.0

value.[6] Median and average values of the modulation periods are 59.6 and 126 d, respectively. The median value is basically the same as what was found by Skarka et al. (2016).

The distribution of the logarithm of the Blazhko periods is not Gaussian as it is best apparent from the bottom panels of Fig. 3. We tested the non-normality of the distribution using statistical tests from the Python `Scipy` library (Virtanen et al. 2020). Both, the Kolmogorov–Smirnov and Shapiro–Wilk tests give the p-values orders of magnitude less than the critical value set to 1 per cent (0.01). The Anderson–Darling normality test also rejects the normality – the statistical value 46.5 is much higher than the significance level for 1 per cent which is 1.091.

Although tests using the mean, median, standard error, skewness, and kurtosis show that the distribution in Fig. 3 is unimodal (Rohatgi & Székely 1989; Basu & DasGupta 2006), the cumulative distribution function and the probability plot shown in the bottom panels of Fig. 3 suggest either multimodality or possibly also log-normal distribution. If we take the logarithm of the logarithm of the modulation period and perform the above mentioned normality tests, we come to the conclusion that such distribution is also unimodal and non-Gaussian but shows peculiarities. Thus, the log-normality cannot explain the features seen in the bottom panels of Fig. 3.

In order to verify the existence of the two populations, we used the `Gaussian mixture model` from the `scikit-learn` library (Pedregosa et al. 2011). First, we generated 1000 random realization of the Blazhko modulation periods assuming its error follows the Gaussian distribution. For each randomly generated distribution, we calculated the `Gaussian mixture model` with a varying number of Gaussians (from 1 to 10). Based on the Bayesian information criterion (BIC) and Akaike information criterion (AIC), we estimated the suitable number of Gaussian components in each distribution. Both criteria suggested using at least 2–3 Gaussians to describe the distribution of modulation periods. We note that the errors in modulation periods (in Table 1) are estimated based on the Gaussian error propagation and are most likely underestimated. To reduce this effect in this analysis,

[6] Jurcsik & Smitola (2016) found that V144 in the M3 globular cluster has a modulation period longer than 25 yr.

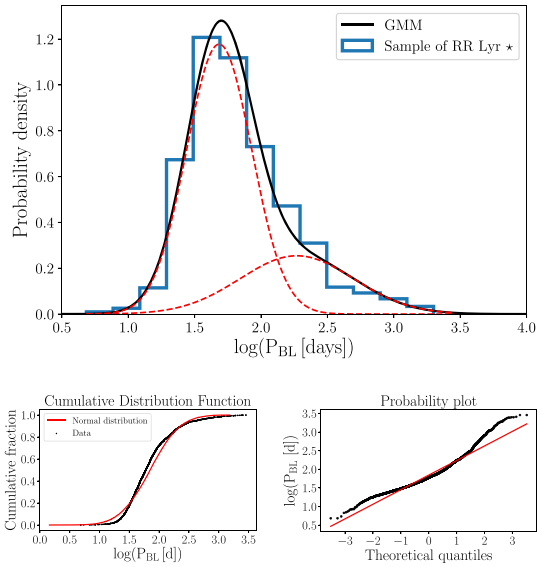

Figure 3. The distribution of the modulation periods of the sample stars modeled by the two Gaussian distributions (two-dashed lines) and their sum (black solid line, top panel). The bottom panels show the cumulative distribution function (bottom left-hand panel) and the probability plot (bottom right-hand panel).

we artificially increased the errors by a factor of ten and run the `Gaussian mixture model` analysis again.

Even with artificially increased errors, the two-population model with the mean modulation periods of 48 and 186 d (shown by the different Gaussian fits represented by the red-dashed lines in the top panel of Fig. 3) is the best result of the Gaussian mixture model analysis. The mean modulation periods are roughly in 1:4 ratio but this could be a coincidence.

The two populations suggested from the Gaussian mixture model analysis are also apparent from the plots in Fig. 4. There is a valley separating the two populations in the density plot, which we call the Blazhko valley (the top panel of Fig. 4). The center of the Blazhko valley is schematically shown by the upper dashed line in the bottom panel of the same figure. If the valley were horizontal, the two populations would be more distinct in the distribution of $\log(P_{\rm BL})$.

The stars of the long-modulation period population (above the upper dashed line in the bottom panel of Fig. 4) have the spread of pulsation periods similar to the population below the Blazhko valley. Thus, the reason for their longer Blazhko periods can hardly account for the mean density, which mainly defines the pulsation period. It seems that the stars of all morphological types populate the whole distribution of the $P_{\rm Puls}$versus $P_{\rm BL}$, but the number of a-type stars decreases with longer modulation periods (the bottom panel of Fig. 4), while the distribution of other classes is more or less uniform. This results in more frequent occurrence of the non-sinusoidal modulation among stars with long modulation periods. We did not find any difference in the mean parameters between the long- and short-modulation period populations when the stars were separated based on the upper dashed line in the bottom panel of Fig. 4.

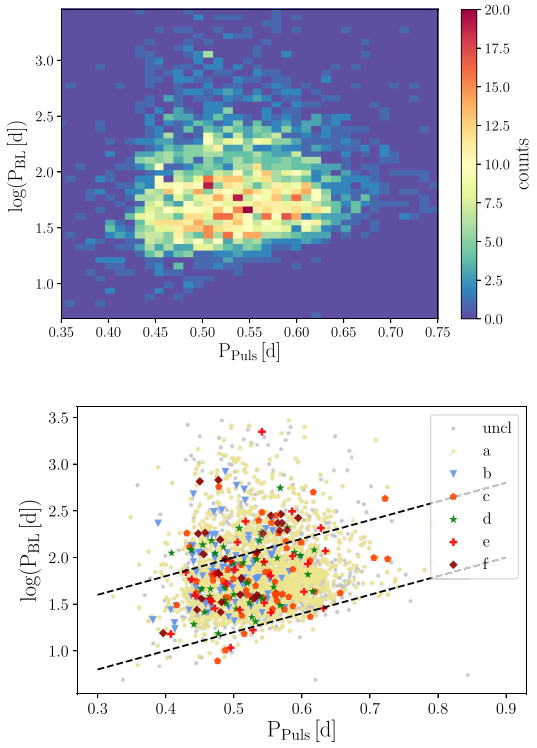

Figure 4. Top panel: density plot of the modulation periods. The bottom panel shows the modulation periods against pulsation period. Different modulation types are plotted with different symbols, the light-grey dots show unclassified stars. The bottom dashed line shows the limit of the modulation period with respect to the pulsation period ($\log P_{\rm BL} \approx 2P_{\rm Puls} + 0.2$), the upper dashed line shows the position of the Blazhko valley (the bottom line shifted $+0.8$ in $\log P_{\rm BL}$).

There are certain limits for the modulation periods. The bottom dashed line in the bottom panel of Fig. 4 says that stars with short pulsation periods can have modulation periods of all lengths, while stars with long pulsation periods can have periods from a certain limit. For example, stars with $P_{\rm Puls} > 0.6$ d can have $P_{\rm BL} > \sim 20$ d. This is exactly what Jurcsik et al. (2005c) found. In the $P_{\rm BL}$versus $P_{\rm Puls}$ plane, the liming line can be expressed as $\log P_{\rm BL} \approx 2P_{\rm Puls} + 0.2$. When this boundary line is shifted by 0.8 in $\log P_{\rm BL}$, it falls exactly in the center of the Blazhko valley. The same slope of the line hints that there can really be some physical background for the valley.

3.2 Modulation and mean brightness amplitudes

The modulation amplitude, which we determined using equation (5) and alternatively as a sum of the amplitudes of the top and bottom modulation envelopes (equation (6)), corresponds to the strength of the amplitude modulation. The two approaches of determining the modulation amplitude are in great agreement and are, therefore, equally usable (Fig. 5). The determination of the modulation

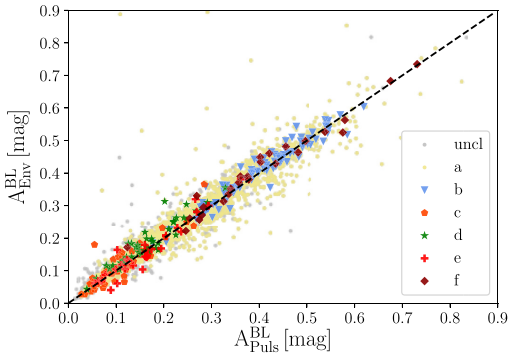

Figure 5. The comparison of the modulation amplitude determined on the basis of different approaches. The sum of amplitudes of the bottom and top envelopes is on the vertical axis, while the modulation amplitude based on the difference between total pulsation amplitude in Blazhko maximum and minimum phase is on the horizontal axis. The dashed black line shows the 1:1 correlation.

amplitudes failed in a few tens of stars because of the data sparseness and/or inadequate time distribution. The values for these stars are not reliable but are easily distinguishable, as the outliers in Fig. 5.

The largest modulation amplitude is observed in OGLE-BLG-RRLYR-09437 ($A^{BL}_{Puls} = 0.85$ mag). This star shows two modulations that are in resonance. Thus, the maximal amplitude is very large, while the minimal amplitude is low. The smallest detected modulation amplitude is 0.0145 mag in OGLE-BLG-RRLYR-05757. The cumulative distribution function (Fig. 6) shows that 99.2 per cent of all the modulation amplitudes are below 0.6 mag. Only very exceptionally, the amplitudes are higher.

The overall distribution of amplitudes (Fig. 6) is defined mainly by stars from class a, which is the most populated (90 per cent of all stars). The stars from other types have very different modulation amplitudes that can be naturally expected because of the definition of the classes (Section 2.3). Stars of b and f types have the largest amplitudes, while type-c stars have the smallest amplitudes (see both panels of Figs 6 and 9). Note that types b and f and types d and e have very similar distributions.

Definition of the modulation amplitude based on the amplitudes of the frequency side peaks, as used and discussed by Jurcsik et al. (2005c) and Benkő & Szabó (2015), can be difficult because the amplitudes of the side peaks (or their sum) are not exactly proportional, nor equal to the modulation amplitude. The quality and distribution of the data, as well as the presence of the additional amplitude and/or phase modulation influence the amplitudes of the frequency peaks (Jurcsik et al. 2005b; Benkő et al. 2011). We demonstrate this issue in Fig. 7. The figure shows how the sum of the amplitudes of the $f_0 \pm f_m$ peaks depends on the modulation amplitude determined from equation (5). The sum of the amplitudes of the $f_0 \pm f_m$ peaks is 5 to 20 times smaller than the modulation amplitude.

Variation of the mean magnitude produces peak with frequency equivalent to the modulation frequency in the mmag regime. Benkő et al. (2014) found in the *Kepler* data that the amplitude of this peak is proportional to the modulation period. We can test it by plotting the amplitude of the mean-magnitude variation ΔI (equation 7). We did not find any dependence even among stars with the largest number of points with the most reliable determination of ΔI (Fig. 8).

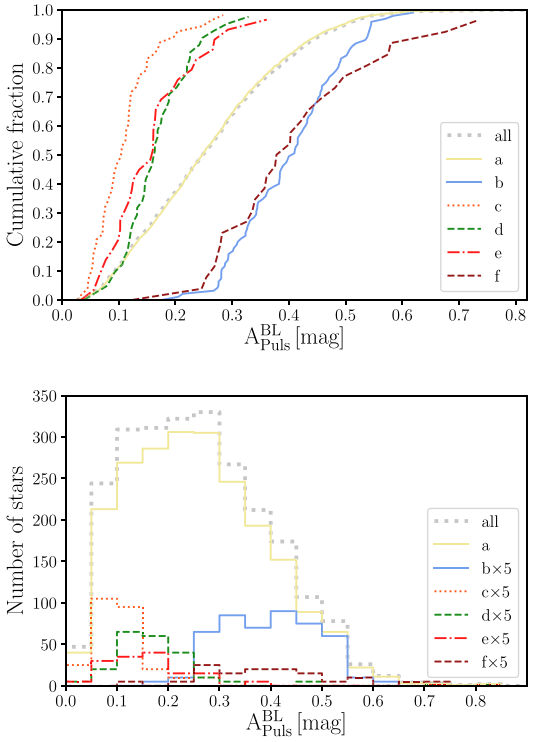

Figure 6. Cumulative distribution functions (top panel) and the distribution of the modulation amplitudes of the sample stars (bottom panel). The light-grey dotted curves show the full sample including non-classified stars.

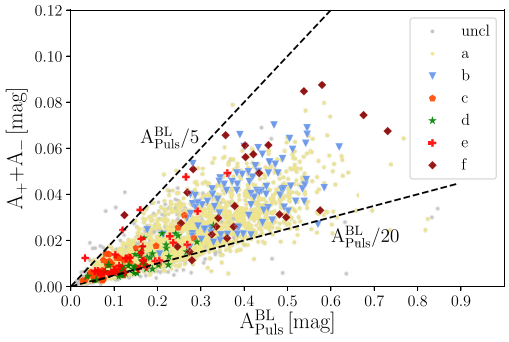

Figure 7. Dependence of the sum of the side peak amplitudes versus modulation amplitude. The dashed lines show the total Blazhko amplitude A^{BL}_{Puls} divided by 5 and 20, respectively.

Because the impact of the modulation is the most apparent in the variation of the upper modulation envelope in most of the stars, it can be naturally expected that most of the stars will be brighter during the maximum Blazhko amplitude ($\Delta I < 0$). The opposite is true (the top panels of Fig. 8). Thus, test with fluxes was performed. First, we transformed magnitudes into fluxes, calculated the difference in mean fluxes and transformed the difference back

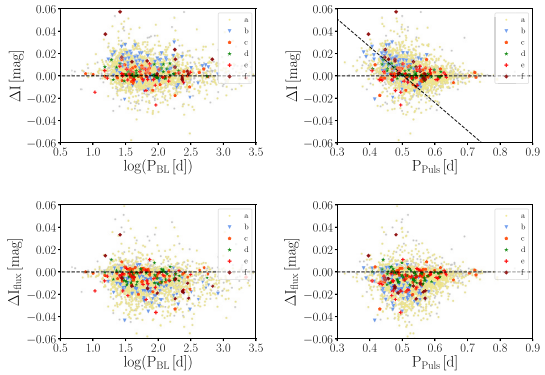

Figure 8. Dependence of the amplitude of the mean magnitude variation ΔI versus modulation (left-hand panels) and pulsation period (right-hand panels). The negative values mean that the mean brightness during minimal Blazhko phase is larger than during maximal Blazhko phase (see the definition of ΔI in equation (7)). The top panels show the ΔI variation based simply on the OGLE-IV magnitudes, the bottom panels show $\Delta I_{\rm flux}$ when the magnitudes are transformed into fluxes, the difference is calculated and transformed back to magnitudes.

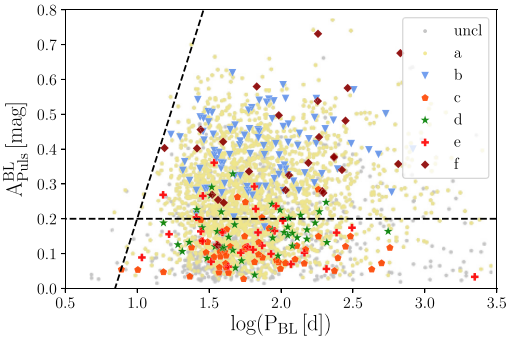

Figure 9. Dependence of the amplitude of the modulation versus modulation period. The tilted black-dashed line shows the upper limit for the amplitude in the range of modulation periods of 0–30 d. The slope is 1.3. The horizontal line shows the 0.2-mag limit separating b- and f-type stars from the others.

to magnitudes. The result is shown in the bottom panels of Fig. 8. Now the situation is as can be logically expected. This test reveals that using magnitudes can be misleading and can can give strange results. The difference in ΔI looks completely different when it is determined on the basis of OGLE magnitudes and when it is calculated from the flux-transformed values.

The study by Benkő & Szabó (2015) suggests that the amplitude of the modulation envelope is monotonically proportional to the modulation period. In other words, the longer the Blazhko period, the larger the amplitude of the modulation envelope.[7] They note that large data sample is desired for confirmation of what they found, which is exactly our case. In Fig. 9, we show that there is no monotonic dependence between the modulation amplitude and

[7]Similarly as for the amplitude of the low-frequency peak raised by the variation of the mean brightness.

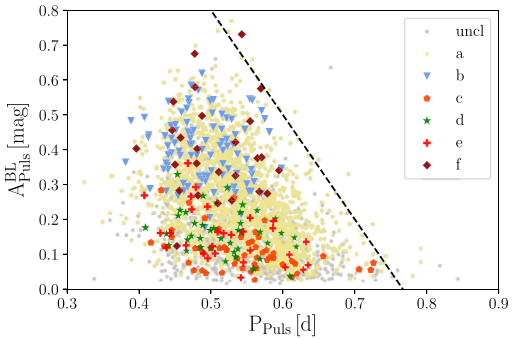

Figure 10. Dependence of the amplitude of the modulation versus pulsation period. The black-dashed line shows the upper limit for the amplitude in the range of modulation periods of 0.5–0.9 d. The slope is -3.

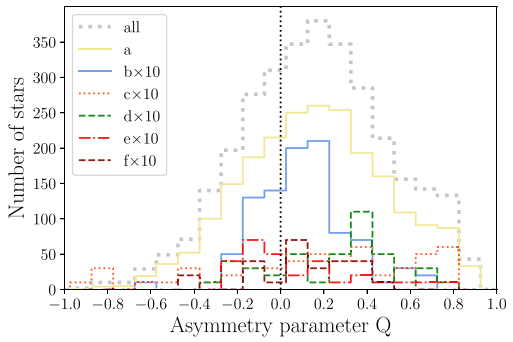

Figure 11. The distribution of the asymmetry parameter Q. Almost 70 per cent have $Q > 0$ (the vertical-dashed line).

the modulation period. We can only find a hint of some limit (the tilted dashed line in Fig. 9) saying that stars with Blazhko periods shorter than about 30 d (∼1.5 in logarithmic scale) can only have certain modulation amplitudes. It is interesting to point out that b- and f-type stars have predominantly amplitudes larger than 0.2 mag, while those of c–e types below 0.2 mag.

Fig. 10 shows that there is also top limit for modulation amplitudes for stars with pulsation periods above 0.5 d (shown schematically with the dashed line). The modulation amplitude clearly decreases with increasing pulsation period, which was already observed in stars from globular clusters, Galactic field, and LMC by Jurcsik et al. (2005c). This hints towards that in RRLs with long pulsation periods, which are generally cooler, larger, and more luminous than the short-period RRLs, some effect exists that suppresses the amplitude of the Blazhko effect.

Because RRLs with large modulation amplitudes have short pulsation periods, we can naturally expect that the stars with short pulsation periods will have larger variation in the mean brightness, which is really observed (see the bottom panel of Fig. 8).

3.3 Frequency spectra and multiple modulation

We investigated only the vicinity of the basic pulsation frequency f_0. The difference between the f_+ and f_- components (equation 3) is for 99.7 per cent of the stars (3σ) smaller than 0.00016 c/d. The

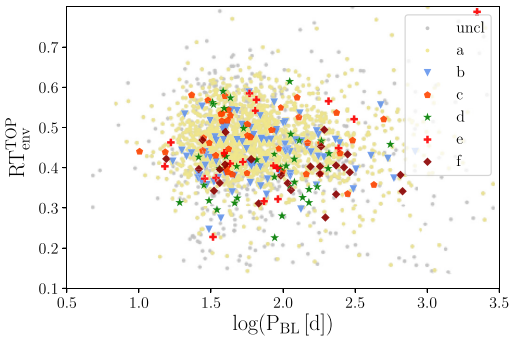

Figure 12. The rise time of the top modulation envelope. In totol, 60 per cent of stars have RT_{env}^{TOP} <0.5.

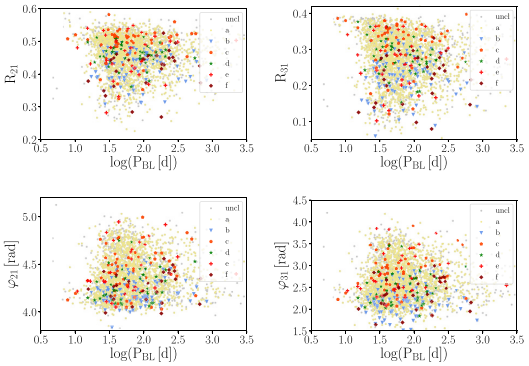

Figure 13. Low-degree Fourier coefficients of the sample stars. Amplitude coefficients R_{21}, R_{31} (top panels) and phase coefficients φ_{21} and φ_{31} (bottom panels), as a function of the Blazhko period are shown.

distribution of the asymmetry parameter Q (equation 2) shows that 70 per cent of the stars has larger peak on the right-hand side of f_0 (f_+) than on the left-hand side f_-. All morphological classes have similar statistics, but type d, where only 14.6 per cent of the stars show a larger peak at a higher frequency. Probably it could reflect the double minimum envelope of the modulation.

According to the mathematical description of the modulation presented by Benkő et al. (2011), peak with larger amplitude at the higher frequency side means that the phase difference ϕ_m between amplitude and phase modulation is $\pi < \phi_m < 2\pi$. Such stars show counterclockwise movement in the maximum brightness versus maximum phase diagrams. Our analysis shows that 70 per cent of all Blazhko stars in GB comply with this. Alcock et al. (2003) found a similar value (74 per cent) based on the study of 731 stars in the Large Magellanic Cloud.

About 25 per cent of the studied stars (799 stars marked with AdP in Table 1) show additional modulation, which we deduce from the additional peaks present in the vicinity of f_0. All morphological classes show similar percentages of stars with additional peaks, but type b. Stars with additional peaks in this group constitute only 11.6 per cent of all the b-type stars. Some stars (at least 25) show also unresolved peaks that could mean period instability.

3.4 Asymmetry of the envelopes

The asymmetry of the modulation envelopes can be deduced from the RT_{env}^{TOP} parameter of the envelope (equation 8, Fig. 12). For 60 per cent of all studied stars, it is less than 0.5, which means that 60 per cent of the Blazhko stars has asymmetric envelopes with steep rise to maximum. In case of class-b stars, it is 87 per cent and all the members of f-class show the steeper envelope rise to the maximum.

3.5 Fourier coefficients of the pulsation light curve

We also investigated the connection between light-curve shape and the modulation properties. From the fit of the data with 10 pulsation harmonics, we obtained amplitudes and phases of the particular components and calculated the Fourier amplitude and phase coefficients[8] describing the shape of the pulsation light curve (columns 23–26 in Table 1). As seen from Fig. 13, there is no apparent correlation between the low-degree Fourier coefficients and the length of the modulation period. In addition, no correlation between modulation amplitude or the RT_{env}^{TOP} was observed.

3.6 Photometric metallicity

The usability of the photometric metallicity among Blazhko stars has been discussed many times. We estimated the photometric metallicity using two- and three-parameter empirical relations from Smolec (2005). Our results show that the difference of the metalicity determined at maximal and minimal Blazhko amplitude can be larger than 2–3 dex (Fig. 14). The scatter is 0.5 and 0.7 dex, respectively. Thus, the distance of a Blazhko star in the Galactic bulge (≈8.3 kpc) determined in minimal and maximal Blazhko phases[9] differs by 400–800 pc in average. Furthermore, the median metallicity of the whole sample based on the mean light curve slightly differs for two- and three-parameter relations (−1.00 dex versus −1.11 dex). This difference is due to the A_2 parameter in equation 3 from Smolec (2005). For comparison, Prudil et al. (2019) found that non-modulated fundamental mode RR Lyrae stars in the Galactic bulge have median photometric metalicity −1.05 dex using the three-parameter equation from Smolec (2005). Therefore, since the majority of Blazhko stars in our sample lies at the short pulsation period end, one would expect that they would be more metal-rich using the equation 3 in Smolec (2005), but we find the opposite. The generally large difference shows that the full phase coverage over the whole Blazhko cycle is absolutely crucial (Jurcsik et al. 2009; Nemec et al. 2013) and the estimation of metallicity (and all other parameters calculated from metallicity) is generally not trustworthy in particular Blazhko stars and can be unreliable although in average the mean light curves give results similar to non-modulated stars (Jurcsik 2019).

3.7 The Blazhko stars with respect to Bailey's diagram

The open question of bimodality among the Milky Way globular clusters, based on the properties of RR Lyrae stars they contain, also

[8]The parameters introduced by Simon & Lee (1981) are defined as $R_{ij} = A_i/A_j$ and $\varphi_{ij} = \varphi_i - i\varphi_j$, where $A_{i,j}$ are amplitudes and $\varphi_{i,j}$ are phases of the particular harmonics.

[9]Depending on the used formula from Smolec (2005) and the slope of M-[Fe/H] formula between 0.2 and 0.3 (Clementini et al. 2003; Smolec 2005).

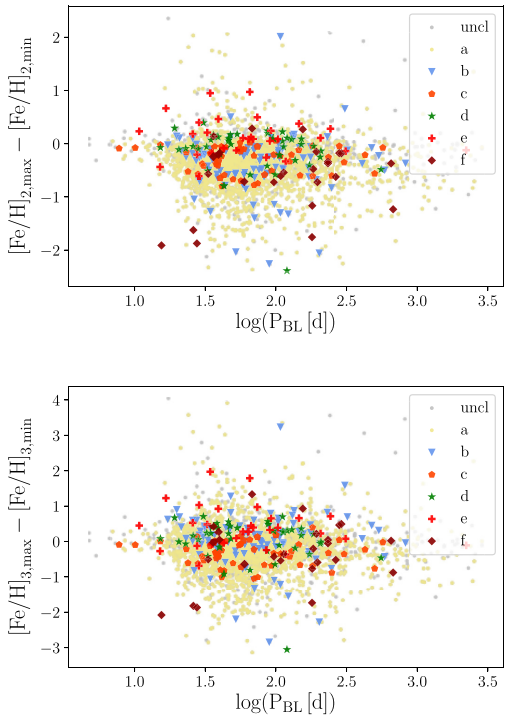

Figure 14. Difference between photometric metallicity in maximum and minimum amplitude based on the two- and the three-parameter formula (top and bottom panels, respectively).

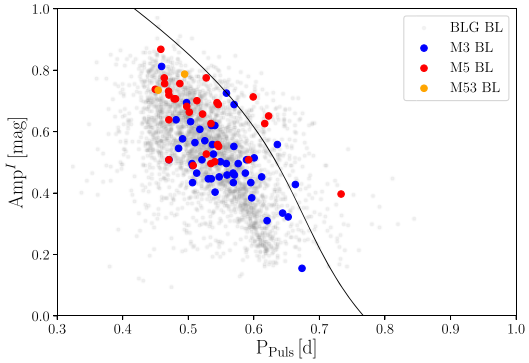

Figure 15. The period–amplitude diagram for studied modulated stars. The light black dots represent RR Lyrae stars with the Blazhko effect from our sample, the blue, red, and orange points stand for modulated RRLs from globular clusters M3, M5, and M53, respectively. The black line separates variables into OoI and II.

known as the Oosterhoff dichotomy (Oosterhoff 1939), is almost as old as the Blazhko effect itself. In this section, we investigate the relation between the Blazhko effect and Oosterhoff dichotomy. To complement this investigation, we utilized photometric data (mean magnitudes) and pulsation properties (amplitudes and pulsation periods) for RR Lyrae stars in globular clusters M3 (Benkó, Bakos & Nuspl 2006; Jurcsik et al. 2012), M5 (Arellano Ferro et al. 2016), and M53 (Dékány & Kovács 2009; Arellano Ferro et al. 2012). We also used the identification of modulated stars from the aforementioned papers. In the case of M53, we used Blazhko stars identified by Dékány & Kovács (2009), which is based on period analysis of observed variables. We selected these globular clusters based on a high number of RR Lyrae stars and information about their modulation.

To divide stars into the Oosterhoff groups, we used the period–amplitude diagram in Fig. 15. For the transformation of *V*-band amplitudes into *I*-band for RRLs in globular clusters with missing *I* observations, we used equation 16 from Prudil et al. (2019). The black line in Fig. 15 outlines the boundary between Oosterhoff type I (hereafter OoI) and Oosterhoff type II (hereafter OoII) variables. This line is based on third-degree polynomial relation from table 1 in Prudil et al. (2019) and a shift in the pulsation period by 0.045 d from Miceli et al. (2008). We note, that the boundary between OoI and II globular clusters shifts with metallicity and the transformation of *V* amplitudes into *I* band can affect the association of individual modulated stars in the Oosterhoff groups. Neither of these effects can substantially change the overall distribution of modulated stars in the Oosterhoff groups, but in a handful of cases, it can change the association of a few RR Lyrae stars.

From Fig. 15, we clearly see that the vast majority of studied pulsators belong to the OoI group and that OoII group is deficient in modulated stars. In our sample, OoII stars constitute only 6.3 per cent of all stars. Similar percentage of Blazhko RRLs is in globular clusters: M5 – 13.3 per cent, and M53 – 0 per cent of modulated stars belong to the OoII population. However, the data of M5 and M53 are not sufficient enough to define reliable BL percentage. The percentage of OoII BL stars in M3 is 40 per cent (Jurcsik et al. 2017). The small percentage of OoII BL stars, when selected according to the their mean amplitudes, is most likely caused by the depreciation of the amplitudes among Blazhko stars in comparison with non-modulated variables. Using the amplitudes in the maximum of the Blazhko modulation phase (see Section 2.2) for sample variables and applying the aforementioned separation, we get 22.6 per cent representation of the Blazhko stars in the OoII group. This new ratio between OoI and OoII population of modulated stars corresponds better with the non-modulated sample used in Prudil et al. (2019) where they found 25 per cent of the Galactic bulge RR Lyrae stars to be associated with the OoII group. The only morphological types that contain OoII stars are groups a and c. Other types do not contain OoII stars (see Table 2).

The average length of the modulation period is similar for both Oosterhoff groups. However, the amplitude of the modulation is of about factor of 2 smaller for OoII RRLs than for the OoI stars. Similarly as for the OoI stars, the modulation amplitude of OoII BL stars gets smaller with increasing pulsation period.

4 DISCUSSION

The variety of modulation-envelope shapes and amplitudes, modulation periods and the look of the frequency spectra is stunning. What drives the modulation? What rules which type of modulation is raised? Lots of the modulation properties can be easily deduced from the mathematical expressions. Modulation of a-type stars seems to be modulated with a simple sinusoid.

The modulation shapes in b- and f-type stars (see Fig. 2) can be explained with the non-sinusoidal modulation (see the examples in fig. 6 in Benkő et al. 2011). The modulation function f_m^A in equation (9) can then be expanded in a sine series. The specific set

of amplitudes and phases of the components of $f_{\rm m}^{\rm A}$ can produce very wide set of modulation envelopes. From that point of view, b- and f-type stars can actually be members of one single group. This idea is supported by the mixture and similar distribution of the modulation amplitudes, which is most apparent from Figs 6, 9 and 10 and Table 2. Also similar $RT_{\rm env}$ of the upper envelopes supports the idea that groups b and f can actually constitute only one typological group. However, there must be some reason that these stars choose more often set of parameters that produce b-type stars rather than f-type stars.

Types c–e are not so easy to explain. It is very difficult to reproduce the flat bottom envelope (type c), double bottom envelope while the top envelope is single (type d) and larger bottom amplitude (type e) by simply employing amplitude modulation. The frequency modulation and/or other effects (double/multiple modulation, additional pulsation modes) must be present to obtain these features.

In total, 25 per cent of the stars show additional modulation. It means that the modulation function $f_{\rm m}^{\rm A}$ (equation 9) has at least two components with different modulation frequencies and amplitudes. In presence of the double modulation, it is relatively commonly observed that the modulation frequencies are in resonance with small integer numbers (e.g. Sódor et al. 2011; Benkő et al. 2014). A nice example from our sample is OGLE-BLG-RRLYR-09745 showing 5:1 resonance between the two modulation components. By fine-tuning the parameters of the multiple-modulation components, it could be possible to explain the variation in the modulation cycles as well as the secular decrease/increase of the amplitude of the modulation (see fig. 8 in Benkő et al. 2014).

The full description of the modulation in the large sample of stars, including all the mentioned effects would require a detailed investigation of every particular star or at least of several representatives, which are typical for every of the six morphological types. The first results regarding the phase modulation of the Bulge RR Lyrae stars have been published recently by Jurcsik et al. (2020). They found that the amplitude of the phase modulation decreases with increasing pulsation period similarly as the amplitude modulation studied in this paper. The full solution of the modulation in thousands of Galactic bulge RRLs would be the natural next step giving a better picture of the Blazhko effect.

However, the description of the modulation is only the first step to understand the physics behind the modulation. The successful model has to explain all the variety of the observed features and what rules the choice of the modulation properties. Geometrical (e.g. Shibahashi 2000) and resonant models (van Hoolst 2000) alone surely fail in explaining the variety of amplitudes, shapes, and periods. The currently most promising 9:2 resonance model (Kolláth et al. 2011) will have to comply in explaining this behaviour if it wants to succeed. However, what if we observe more effects simultaneously which are mixed in different ratios? Then the presence of non-radial pulsations as well as radial modes, aspect ratio and, alternatively, also some other physical effect, such as variable turbulent convection (Stothers 2006), could be the important parameters. This is, however, pure guessing far out of our capabilities.

Out of the speculations, there must be a physical reason why stars that pulsate with longer periods may not have modulation periods under a certain limit (Fig. 3) and why the modulation amplitude decreases with increasing pulsation period (Fig. 10). This seems to be a common feature regardless of the Oosterhoff groups. Stars that have longer periods are less dense (period of the fundamental mode is inversely proportional to the square root of the mean density). These stars are generally larger, cooler and more luminous than their short-period counterparts. Thus, the modulation amplitude and percentage of BL stars decreases towards the red edge of the instability strip and larger luminosities. The physical conditions apparently do not allow the modulation to rise in stars pulsating with long periods.

The fact that the majority of modulated stars are located in the OoI group also tells a little bit about their physical properties in comparison with OoII stars. For example, the difference in masses between both Oosterhoff groups has been suggested in the past (Catelan 1992; Cacciari & Bruzzi 1993; Sandage 2006; Prudil et al. 2019), where the masses of OoII stars should be equal or larger in comparison with the OoI group. More importantly, the OoI variables lie close to the blue-edge of the instability strip and on are, on average, intrinsically hotter by several hundred Kelvins (Prudil et al. 2019). This would mean that modulated stars are, on average, hotter and possibly less massive than non-modulated stars, under the assumption that they are located on a zero-age horizontal giant branch.

The reason for the existence of the two populations of modulation periods is a complete mystery (Fig. 3 and 4).

5 SUMMARY AND CONCLUSIONS

We investigated 3141 RRL stars from the Galactic bulge using the OGLE-IV and OGLE-III photometry. For all the studied stars, the Blazhko period could be reliably determined. The high-quality data and the large sample of modulated stars allowed us to investigate the modulation in a statistical matter. We determined the modulation periods, pulsation, and modulation amplitudes, described the shape of the light curves and modulation envelopes. The visual inspection allowed us to identify six basic morphological shapes of the modulation and assign 2449 stars with good-enough data and large-enough amplitudes to one of these six modulation types (Fig. 2 and Table 2).

We also got information about the look of the frequency spectra – the position, amplitudes, and asymmetry of the peaks. We also investigated the Oosterhoff phenomenon regarding the Blazhko effect. The full Table 1 containing 30 columns is available online. We also provide plots showing the time distribution of the data, frequency spectra, and phase light curves online (Fig. 1).

Our main results and findings can be summarized in the following points:

(i) The distribution of the modulation periods (Fig. 3) and results from the Gaussian mixture modelling show that there could be two populations with different mean modulation periods of 48 and 186 d (see Fig. 4). The pulsation periods of the stars from the two populations are similar and also the numbers of stars of different morphological types are similar in both populations. The only difference is that the incidence rate of the a-type stars is lower in the long-modulation period population. This result is in line with the asymmetric modulation envelopes, which are more common among stars with long Blazhko periods. The Blazhko valley, as we defined the area between the two populations in the $P_{\rm BL}$ versus $P_{\rm Puls}$ plane, seems to be real.

(ii) The only observed systematics in the length of the modulation period is that there is a bottom limit defining the shortest possible modulation period which increases with the pulsation period (bottom panel of Fig. 4). This is in accordance with Jurcsik et al. (2005a). We also observed a limit saying that in stars with longer modulation period the modulation amplitude can be larger (Fig. 9).

(iii) There is no simple dependence, nor a correlation between modulation period and amplitude of the modulation envelope, as suggested by Benkő & Szabó (2015) observed in the OGLE RRLs we studied.

(iv) The modulation amplitude decreases with increasing pulsation period (Fig. 10).

(v) In total, 70 per cent of the stars have larger frequency peak at the right-hand side from the basic pulsation frequency suggesting that the phase difference ϕ_m between amplitude and phase modulation is $\pi < \phi_m < 2\pi$.

(vi) In total, 25 per cent of stars we, observed additional peaks suggesting additional modulation.

(vii) About 60 per cent of stars show asymmetric upper modulation envelope with steeper rise to maximum than the decrease to minimum. All stars of f-type behave like this.

(viii) We warn in using photometric metallicity of the Blazhko stars because it can introduce uncertainty in the order of hundreds of parsecs in the distance of the Galactic bulge RR Lyrae Blazhko stars. Good sampling over the whole Blazhko cycle is undoubtely needed for a reliable metallicity estimation.

Especially point (iv) suggests that there is some physical limit that prevents star to show the Blazhko effect. It seems that stars close to the red edge of the instability strip rarely show the Blazhko effect. This was already observed in a sample of 83 BL stars in M3 (Jurcsik 2019). The lack of correlations between various parameters and the modulation period and amplitudes could mean that there is actually no simple general rule how and why some stars are modulated.

The next natural step of the investigation of the Blazhko effect will be thorough description of the modulation of the representatives of the different morphological types. Additional photometric and spectroscopic observations of the selected representatives will also help to set up the input parameters for the theoretical modelling.

ACKNOWLEDGEMENTS

MS acknowledges the financial support of the Operational Program Research, Development and Education – Project Postdoc@MUNI (No. CZ.02.2.69/0.0/0.0/16_027/0008360). ZP acknowledges the support of the Hector Fellow Academy. JJ acknowledges the OTKA NN-129075 grant. We would like to thank the OGLE team for their great job with the observations of the GB.

REFERENCES

Alcock C. et al., 2003, ApJ, 598, 597
Arellano Ferro A., Bramich D. M., Figuera Jaimes R., Giridhar S., Kuppuswamy K., 2012, MNRAS, 420, 1333
Arellano Ferro A., Luna A., Bramich D. M., Giridhar S., Ahumada J. A., Muneer S., 2016, Ap&SS, 361, 175
Basu S., DasGupta A., 2006, Theory Probab. Appl., 41, 210
Benkó J. M., Bakos G. Á., Nuspl J., 2006, MNRAS, 372, 1657
Benkő J. M., 2018, MNRAS, 473, 412
Benkő J. M., Plachy E., Szabó R., Molnár L., Kolláth Z., 2014, ApJS, 213, 31
Benkő J. M., Szabó R., 2015, Eur. Phys. J. Web Conf., 101, 06008
Benkő J. M., Szabó R., Paparó M., 2011, MNRAS, 417, 974
Benkő J. M. et al., 2010, MNRAS, 409, 1585
Blažko S., 1907, Astronomische Nachrichten, 175, 325
Buchler J. R., Kolláth Z., 2011, ApJ, 731, 24
Cacciari C., Bruzzi A., 1993, A&A, 276, 87
Catelan M., 1992, A&A, 261, 457
Clementini G., Gratton R., Bragaglia A., Carretta E., Di Fabrizio L., Maio M., 2003, AJ, 125, 1309
Dékány I., Kovács G., 2009, A&A, 507, 803
Howell S. B. et al., 2014, PASP, 126, 398
Jurcsik J., 2018, in Smolec R. K., Kinemuchi K., Anderso R. I., eds, Proc. Polish Astron. Soc., Vol. 6, The RR Lyrae 2017 Conference. Revival of the Classical Pulsators: from Galactic Structure to Stellar Interior Diagnostics, Poland, p. 181
Jurcsik J., 2019, MNRAS, 490, 80
Jurcsik J., Hajdu G., 2017, MNRAS, 470, 617
Jurcsik J., Hajdu G., Dékány I., Nuspl J., Catelan M., Grebel E. K., 2018, MNRAS, 475, 4208
Jurcsik J., Smitola P., 2016, Commmun. Konkoly Obs. Hungary, 105, 167
Jurcsik J., Sodor A., Varadi M., 2005c, Inf. Bull. Var. Stars, 5666, 1
Jurcsik J., Szabó P., Prudil Z., Skarka M., Hajdu G., 2020, in Kinemuchi K., Lovekin C., Neilson H., Vivas K., eds, The RR Lyrae and Cepheid Conf. 2019: Frontiers of Classical Pulsators - Theory and Observations
Jurcsik J., Szeidl B., Clement C., Hurta Z., Lovas M., 2011, MNRAS, 411, 1763
Jurcsik J., Szeidl B., Nagy A., Sodor A., 2005a, AcA, 55, 303
Jurcsik J. et al., 2005b, A&A, 430, 1049
Jurcsik J. et al., 2006, AJ, 132, 61
Jurcsik J. et al., 2009, MNRAS, 400, 1006
Jurcsik J. et al., 2012, MNRAS, 419, 2173
Jurcsik J. et al., 2017, MNRAS, 468, 1317
Kolláth Z., 2018, in Smolec R., Kinemuchi K., Anderson R. I., eds, Proc. Polish Astron. Soc. Vol. 6, The RR Lyrae 2017 Conference. Revival of the Classical Pulsators: from Galactic Structure to Stellar Interior Diagnostics, Poland. p. 137
Kolláth Z., Molnár L., Szabó R., 2011, MNRAS, 414, 1111
Kovacs G., 2016, Commmun. Konkoly Obs. Hungary, 105, 61
Kovacs G., 2018, A&A, 614, L4
Miceli A. et al., 2008, ApJ, 678, 865
Nemec J. M., Cohen J. G., Ripepi V., Derekas A., Moskalik P., Sesar B., Chadid M., Bruntt H., 2013, ApJ, 773, 181
Netzel H., Smolec R., Soszyński I., Udalski A., 2018, MNRAS, 480, 1229
Oosterhoff P. T., 1939, The Observatory, 62, 104
Pedregosa F. et al., 2011, J. Mach. Learn. Res, 12, 2825
Plachy E. et al., 2019, Astrophys. J. Suppl. Ser. , 244, 16,
Prudil Z., Dékány I., Catelan M., Smolec R., Grebel E. K., Skarka M., 2019, MNRAS, 484, 4833
Prudil Z., Skarka M., 2017, MNRAS, 466, 2602
Rohatgi G. K., Székely G. J., 1989, Stat. Probab. Lett., 8, 297
Sandage A., 2006, AJ, 131, 1750
Shibahashi H., 2000, in Szabados L., Kurtz D., eds, ASP Conf. Ser. Vol. 203, IAU Colloq. 176. The Impact of Large-Scale Surveys on Pulsating Star Research, Astron. Soc. Pac., San Franciscop. 299
Simon N. R., Lee A. S., 1981, ApJ, 248, 291
Skarka M., 2014, MNRAS, 445, 1584
Skarka M., Liška J., Auer R. F., Prudil Z., Juráňová A., Sódor Á., 2016, A&A, 592, A144
Smolec R., 2005, AcA, 55, 59
Soszynski I. et al., 2011, AcA, 63, 1
Soszyński I. et al., 2014, AcA, 64, 177
Stothers R. B., 2006, ApJ, 652, 643
Szeidl B., Jurcsik J., Sódor Á., Hajdu G., Smitola P., 2012, MNRAS, 424, 3094
Sódor A., 2012, Konkoly Observatory Occasional Technical Notes15
Sódor Á. et al., 2011, MNRAS, 411, 1585
Udalski A., Szymański M. K. , Szymański G., 2015, AcA, 65, 1
van Hoolst T., 2000, in Szabados L., Kurtz D., eds, ASP Conf. Ser. Vol. 203, IAU Colloq. 176. The Impact of Large-Scale Surveys on Pulsating Star Research, Astron. Soc. Pac., San Francisco, p. 307
Virtanen P. et al., 2020, Nat. Methods, 17, 261

SUPPORTING INFORMATION

Supplementary data are available at *MNRAS* online.

Please note: Oxford University Press is not responsible for the content or functionality of any supporting materials supplied by the authors. Any queries (other than missing material) should be directed to the corresponding author for the article.

This paper has been typeset from a TEX/LATEX file prepared by the author.

Paper 6

Periodic variable A-F spectral type stars in the northern TESS continuous viewing zone
I. Identification and classification

A&A 666, A142 (2022)
https://doi.org/10.1051/0004-6361/202244037

Astronomy & Astrophysics

Periodic variable A-F spectral type stars in the northern TESS continuous viewing zone

I. Identification and classification*

M. Skarka[1,2,3], J. Žák[4], M. Fedurco[5], E. Paunzen[2], Z. Henzl[3,10], M. Mašek[3,7], R. Karjalainen[1], J. P. Sanchez Arias[1], Á. Sódor[6,9], R. F. Auer[3], P. Kabáth[1], M. Karjalainen[1], J. Liška[3,8], and D. Štegner[3]

[1] Astronomical Institute of the Czech Academy of Sciences, Fričova 298, 25165 Ondřejov, Czech Republic
e-mail: skarka@asu.cas.cz
[2] Department of Theoretical Physics and Astrophysics, Masaryk University, Kotlářská 2, 61137 Brno, Czech Republic
[3] Variable Star and Exoplanet Section of the Czech Astronomical Society, Vsetínská 941/78, 757 01 Valašské, Meziříčí, Czech Republic
[4] European Southern Observatory, Karl-Schwarzschild-str. 2, 85748 Garching, Germany
[5] Department of Theoretical Physics and Astrophysics, Institute of Physics, Faculty of Science, University of Pavol Jozef Šafárik, Park Angelinum 9, 04154 Košice, Slovakia
[6] Konkoly Observatory, Research Centre for Astronomy and Earth Sciences, Konkoly Thege Miklós út 15–17, 1121 Budapest, Hungary
[7] FZU – Institute of Physics of the Czech Academy of Sciences, Na Slovance 1999/2, 18221, Praha, Czech Republic
[8] Central European Institute of Technology, Brno University of Technology, Purkňova 123, 61200 Brno, Czech Republic
[9] MTA CSFK Lendület Near-Field Cosmology Research Group, Konkoly Thege Miklós út 15–17, 1121 Budapest, Hungary
[10] Hvězdárna Jaroslava Trnky ve Slaném, Nosačická 1713, Slaný 1, 27401 Slaný, Czech Republic

Received 16 May 2022 / Accepted 21 July 2022

ABSTRACT

Context. In the time of large space surveys that provide tremendous amounts of precise data, it is highly desirable to have a commonly accepted methodology and system for the classification of variable stars. This is especially important for A-F stars, which can show intrinsic brightness variations due to both rotation and pulsations.
Aims. The goal of our study is to provide a reliable classification of the variability of A-F stars brighter than 11 mag located in the northern TESS continuous viewing zone. We also aim to provide a thorough discussion about issues in the classification related to data characteristics and the issues arising from the similar light-curve shape generated by different physical mechanisms.
Methods. We used TESS long- and short-cadence photometric data and corresponding Fourier transform to classify the variability type of the stars. We also used spectroscopic observations to determine the projected rotational velocity of a few stars.
Results. We present a clear and concise classification system that is demonstrated on many examples. We find clear signs of variability in 3025 of 5923 studied stars (51%). For 1813 of these 3025 stars, we provide a classification; the rest cannot be unambiguously classified. Of the classified stars, 64.5% are pulsating stars of g-mode γ Doradus (GDOR) and p-mode δ Scuti types and their hybrids. We realised that the long- and short-cadence pre-search data conditioning simple aperture photometry data can differ significantly not only in amplitude but also in the content of instrumental and data-reduction artefacts, making the long-cadence data less reliable. We identified a new group of stars that show stable light curves and characteristic frequency spectrum patterns (8.5% of the classified stars). According to the position in the Hertzsprung–Russell diagram, these stars are likely GDOR stars but are on average about 200 K cooler than GDORs and have smaller amplitudes and longer periods. With the help of spectroscopic measurements of $v \sin i$, we show that the variability of stars with unresolved groups of peaks located close to the positions of the harmonics in their frequency spectra (16% of the classified stars) can be caused by rotation rather than by pulsations. We show that without spectroscopic observations it can be impossible to unambiguously distinguish between ellipsoidal variability and rotational variability. We also applied our methodology to three previous studies and find significant discrepancies in the classification.
Conclusions. We demonstrate how difficult the classification of variable A-F stars can be when using only photometric data, how the residual artefacts can produce false positives, and that some types cannot actually be distinguished without spectroscopic observations. Our analysis provides collections that can be used as training samples for automatic classification.

Key words. stars: variables: general – stars: oscillations – stars: rotation – methods: data analysis – catalogs

1. Introduction

The photometric space missions have provided us with invaluable insight into the mechanisms that produce variations in brightness. The ultra-precise data are especially important in the region of the Hertzsprung–Russell diagram where A-F stars are located ($6000 < T_{\rm eff} < 10\,000$ K). This is the location where we can observe the transition between slow and fast rotation of stars, energy transfer via radiation and convection, and the transition between complex local magnetic fields and stable fossil fields. Stars in this region can also pulsate, both in acoustic (p) and gravity (g) modes.

* Full Table 5 is only available at the CDS via anonymous ftp to cdsarc.u-strasbg.fr (130.79.128.5) or via http://cdsarc.u-strasbg.fr/viz-bin/cat/J/A+A/666/A142

We can thus observe several types of variability, often present at the same time. Among A-F pulsating stars, we can find: high-order g-mode γ Doradus (GDOR) type pulsations with periods of the order of hours to days (Balona et al. 1994; Kaye et al. 1999) generated by the convective-flux blocking mechanism (Guzik et al. 2000; Dupret et al. 2005); and δ Scuti (DSCT) low-radial-order p-mode pulsators (Breger 2000) with pulsations excited by the opacity mechanism in the He II layer (Cox 1963; Breger 2000) and by turbulent pressure (Houdek 2000; Antoci et al. 2014) with periods of hours. There are also hybrid stars that show both DSCT and GDOR pulsations (Henry & Fekel 2005; Handler 2009; Grigahcène et al. 2010; Sánchez Arias et al. 2017). SX Phe stars, which are Population II stars, have similar pulsational characteristics as DSCTs, which are Population I stars (Balona & Nemec 2012). Another type of pulsation appearing among chemically peculiar A-F stars with strong magnetic fields are p-mode oscillations with periods of the order of minutes observed in rapidly oscillating (roAp) stars (Kurtz 1982). GDOR, DSCT, and roAp stars observed by the Transiting Exoplanet Survey Satellite (TESS, Ricker et al. 2015) in sectors 1 and 2 were thoroughly studied by Antoci et al. (2019) and Cunha et al. (2019).

Rotation can also cause photometric variations. In stars with stable atmospheres, light elements (e.g. He) can diffuse downwards, and others (usually Si and rare-earth elements, such as Sr, Cr, and Eu) can be levitated to the surface and create chemical spots (Michaud 1970; Preston 1974). In the presence of a magnetic field, these spots can be sustained and cause rotational modulation (Stibbs 1950; Kochukhov 2011). In some of the A-F type stars, variability similar to solar activity and spots was observed (Balona 2013). Rapidly oscillating Ap stars also often show rotational modulation. Those observed in the first two TESS sectors were studied by Cunha et al. (2019).

Among rotationally variable stars, we can also find ellipsoidal variables, that is, stars in non-eclipsing binary systems that are tidally deformed and, due to gravitational darkening, can also show brightness variations as the stars orbit around the common centre of mass (Morris 1985; Beech 1985). For completeness, we should not forget to mention classical variable stars such as RR Lyrae stars (Catelan & Smith 2015) and systems containing the intrinsic variable stars mentioned above, such as eclipsing binaries and exoplanetary candidates. Flare-like events have also been observed in A-type stars (Balona 2012). However, Pedersen et al. (2017) find that the flares can come from nearby stars and companions in binary systems, raising doubts about flares among A-type stars.

The classification of variable stars observed by space missions is usually based on common light-curve characteristics and on characteristics of the frequency spectra (e.g. Debosscher et al. 2011; Uytterhoeven et al. 2011b; Balona et al. 2011; Balona 2011; Bradley et al. 2015). Most of the classifications have been performed semi-automatically employing visual inspection. Nowadays, with the tremendous increase in data quantity, automatic procedures using (supervised) machine learning and neural networks are being developed (e.g. Debosscher et al. 2011; Audenaert et al. 2021). Although there are some basic common criteria, the classification methodology is not unified and the classifications can differ. In addition, due to the data quality, data characteristics, and/or similar manifestations of different physical mechanisms, ambiguities in classification can emerge. Therefore, it is important to properly identify the physical mechanism causing the light variations and classify the stars accordingly.

In this paper, we investigate A-F stars observed by the TESS space mission (Ricker et al. 2015) near the northern ecliptic pole (Sects. 2 and 2.1). The time base of the TESS observations of the stars in this region is the longest available, providing a great opportunity for the most reliable classification of periodically variable stars and studying changes with periods of the order of days to tens of days. We perform a careful case-by-case visual classification of the variability type of every particular star using 30- and 2-min cadence data and provide a large catalogue of variable stars. The motivation for this work was to identify interesting targets for detailed study. However, a deeper investigation of particularly interesting targets is a topic for separate paper(s).

A significant portion of the paper is dedicated to the discussion of effects that influence the identification of variability, false variability connected with the instrumental and data-reduction artefacts, and how the data themselves affect the results (Sects. 3–5). We describe the precise criteria adopted for the classification and discuss ambiguities across different variability types (Sect. 5). The results of our analysis are given in Sect. 6. The summary of the paper and future prospects are in Sect. 7.

2. Observations and data products

The heart of the TESS satellite consists of four cameras with four $2\mathrm{K} \times 2\mathrm{K}$ CCDs each that produce combined field of view (FOV) of $24^\circ \times 96^\circ$ (Ricker et al. 2015). Due to the large FOV, the angular resolution per pixel is only 21" px^{-1}. The part of the sky that is observed for two consecutive TESS orbits ($\sim 2 \times 13.7$ days) around the Earth is called a "sector". After the observation of a sector is finished, the FOV moves 27° along the ecliptic for the next sector. The whole hemisphere is scanned in a "cycle". TESS avoids regions closer than 6° to the ecliptic plane to eliminate the disruptive light of the Solar System bodies and the Moon. This observing strategy means that the sectors overlap around the ecliptic poles, the TESS continuous viewing zone (CVZ) providing almost uninterrupted observations with the time base of about 350 days. Such data are the most suitable for investigations of stellar variability.

The full frame images (FFIs) are downloaded every 30 min and serve as an input for a so-called long-cadence (LC) photometry that is provided for all observed objects down to 16–17 mag. Dedicated postage-stamp images, target pixel files (TPFs), of selected targets are downloaded every 2 min. These data serve as an input for a so-called short-cadence (SC) photometry. The TPFs and the light curves processed by the TESS Science Processing Operations Center (SPOC; Jenkins et al. 2016) are available at the Mikulski Archive for Space Telescopes (MAST)[1]. SPOC provides two kinds of photometric data – simple aperture photometry (SAP) and pre-search data conditioning (PDC) SAP flux with long-term trends removed (Twicken et al. 2010). At MAST, also products from the quick-look pipeline (QLP; Huang et al. 2020a,b) with the 30-min sampling are available.

2.1. Sample selection and data retrieval

To select stars that are close to the TESS CVZ, we first cross-matched the TESS Input Catalogue (TIC) v8.0 (Stassun et al. 2019) with the SIMBAD database (Wenger et al. 2000) around the northern ecliptic pole (RA = $18^\mathrm{h}00^\mathrm{m}00^\mathrm{s}$, Dec = +66°30′00″) with the radius of 15 deg using the CDS X-Match service (Boch et al. 2012; Pineau et al. 2020). The cross-match with the

[1] https://archive.stsci.edu/

Table 1. Distribution of the number of stars in particular temperature (top part) and brightness (bottom part) ranges of the sample stars (from the TIC; Stassun et al. 2019).

$T_{\rm eff}$ (K)	N
6000–7000	4305
7000–8000	1110
8000–9000	353
9000–10 000	155
V (mag)	N
<6	31
6–8	229
8–10	2017
>10	3646

SIMBAD database gives a good chance that there is some available information about the stars in the literature if needed. The initial sample for our work consists of 67 093 stars in and close to the TESS CVZ.

In the next step, we limited our sample to stars with $6000 < T_{\rm eff} < 10\,000$ K to get only stars with A-F spectral types[2]. We also limited our sample to stars with brighter than 11 mag in Johnson V filter to select only stars with good quality data that are bright enough to be suitable for spectroscopic observations with 1-metre class telescopes and for further studies. After omitting duplicates, 5923 stars were accepted for the analysis. The basic distribution of the temperatures is shown in the upper part of Table 1, while the brightness distribution of the sample stars is shown in the bottom part of Table 1.

Since our work started in February of 2021, we only downloaded data observed in Cycle 2, and thus we only analysed data from sectors 14–26 (July 2019–June 2020). SPOC SC and LC data (3403 and 5787 stars, respectively) and QLP LC data (5923 stars) were obtained from the MAST archive using the LIGHTKURVE v2.0 software (Lightkurve Collaboration 2018; Barentsen & Lightkurve Collaboration 2020). LIGHTKURVE v2.0 was also used for merging the data from different sectors. The median time span of the datasets is 352 days for both LC and SC SPOC data, respectively. This means that the vast majority of the studied stars were observed in sectors spread out over the whole of cycle 2. The median number of points per dataset is 12 000 and 170 000 for LC and SC data, respectively.

The spatial distribution and number of sectors in which the particular stars were observed are shown in Fig. 1. We note here that the SPOC products were not always available for all the sectors in which the star was observed. For example, there should be data for TIC 229412873 available from 12 sectors from Cycle 2, but there are SPOC data products only for three sectors (all 12 sectors in the QLP routine).

For the forthcoming analysis, we transformed the immediate flux F_i to relative magnitudes Δm_i by using Pogson's equation:

$$\Delta m_i = -2.5 \log\left(\frac{F_i}{F_{\rm mean}}\right), \quad (1)$$

where $F_{\rm mean}$ is the mean flux of the observations.

We have not applied any additional cleaning or detrending procedures, filtering of the data or outlier removal. We simply used the PDCSAP data as they are provided, because careful examination of selected data, show they are almost free of strong outlier points or glitches. The additional modification of the datasets would need individual approaches for each of the stars in the sample, which is beyond the scope of this paper.

[2] We used $T_{\rm eff}$ from the TIC catalogue (Stassun et al. 2019).

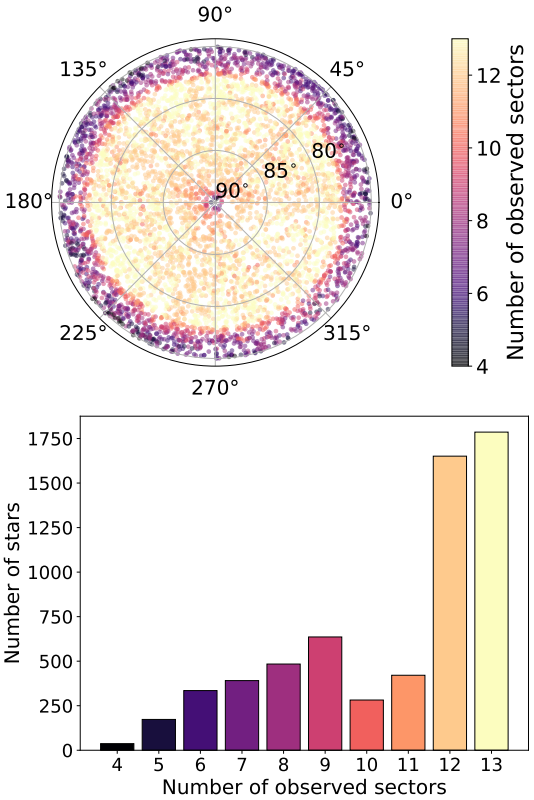

Fig. 1. Position of the investigated stars around the northern ecliptic pole in the ecliptic coordinates (*top panel*). The colour coding shows the number of sectors in which the data were available in the SPOC routine. The *bottom panel* shows in how many sectors the data were available for how many stars.

2.2. Spectroscopic supporting data

To help to better classify the stars, we gathered available low-resolution spectra of 126 of our targets from the Large Sky Area Multi-Object Fiber Spectroscopic Telescope (LAMOST; $R = \lambda/\Delta\lambda \approx 1800$, spectral range 3700–9000 Å) of the Chinese Academy of Science (Cui et al. 2012; Zhao et al. 2012) and determined their spectral type by using the MKCLASS code (Gray & Corbally 2014). This software is able to recover the spectral type with results that are comparable to the manual classification (e.g. Gray & Corbally 2014).

We also gathered new high-resolution spectra ($R = \lambda/\Delta\lambda \approx 40\,000$ at Hα, spectral range 3800–9100 Å) to prove the rotational variability via projected rotational velocity of six stars that may be classified as pulsating stars. The stars were observed with the Ondřejov Echelle Spectrograph (OES) mounted on the 2 m Perek Telescope, Academy of Sciences, Czech Republic (Kabáth et al. 2020). All the spectra had signal-to-noise ratio (S/N) above 100 near Hα.

The spectra were modelled with the iSpec software (Blanco-Cuaresma et al. 2014; Blanco-Cuaresma 2019). As the input parameters for the fitting with radial transfer code SPECTRUM (Gray & Corbally 1994) and MARCS model atmosphere (Gustafsson et al. 2008), we used the values of $T_{\rm eff}$ and $\log g$ from the TIC catalogue (Stassun et al. 2019) and adjusted them to better fit the spectra if necessary. Subsequently, we fixed these values and left $v \sin i$ as a free parameter and determined the projected rotational velocity.

3. Identification of variability and data shortcomings

Stellar variability in the space data is usually investigated in the time (light curve) and frequency domains via Fourier transform (FT) of the data (e.g. Balona 2011; Bradley et al. 2015). We created the FT of the LC and SC SPOC and QLP data[3] by using a Python implementation of the non-uniform fast FT[4] that is significantly faster than a classical Lomb-Scargle periodogram (Lomb 1976; Scargle 1982) but gives basically the same results for TESS data.

The periodic signal with frequency f in the data is usually considered as real if the S/N of the corresponding peak in the frequency spectrum is larger than four (Breger et al. 1993). However, higher S/N might be needed in case of stars with dense Fourier peaks (Bognár et al. 2020). We define the S/N as the ratio of the amplitude of the peak at a given frequency f and the mean amplitude of the peaks in the vicinity of the peak $f \pm 1$ c/d. This is a more conservative approach than using power-amplitude spectra or defining the S/N as the ratio of the amplitude of the peak and the standard deviation of the peaks in the immediate vicinity, as is often done (e.g. Balona 2011; De Medeiros et al. 2013). We did not apply any amplitude threshold (as was done e.g. by Uytterhoeven et al. 2011b; Bradley et al. 2015) because each target has a different noise level.

The basic problem in the identification (and classification of the variability in general) arises from the natural characteristics of the data (noise, sampling, time span of the data, data reduction and detrending) in combination with the variability timescales and amplitudes. We illustrate these issues in Figs. 2–3. The data reduced with different routines and with different sampling must naturally be different. As is apparent from the top panel of Fig. 2, the amplitude of the light variations in the LC data have smaller amplitudes averaging out the fast variations.

The QLP routine removes the large-amplitude variations by applying a high-pass filter (the bottom panel of Fig. 2, orange points, Huang et al. 2020a). From the bottom panel of Fig. 2, it is also apparent that residual instrumental and reduction artefacts due to imperfect background subtraction and/or poorly defined aperture might be present in the data (magenta diamonds, SPOC LC data). These artefacts appear more often in the SPOC LC data than in the SPOC SC or QLP data and can cause serious issues when classifying variability types. In the worst case, the artefacts can lead to a completely wrong classification. The QLP routine can even fully remove the variations (Fig. 2, bottom panel). A nice comparison of the available data products and their suitability for the large-amplitude variables investigation, particularly for Cepheids and RR Lyrae stars, observed by the *Kepler* (Borucki et al. 2010) and TESS missions, can be found in Plachy et al. (2019) and Molnár et al. (2022), respectively.

[3] In the range of 0–300 and 0–24 c/d for the SC and LC data, respectively.
[4] https://github.com/dfm/python-nufft

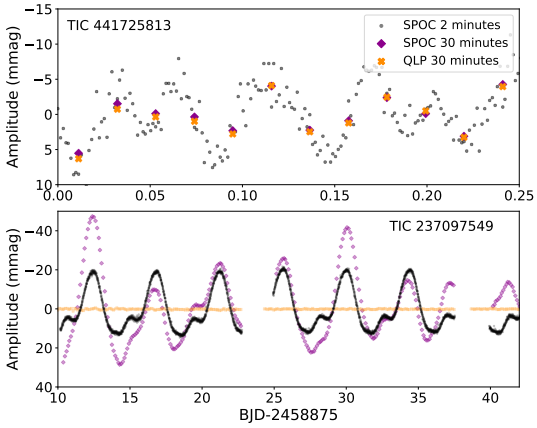

Fig. 2. Comparison of the data with different samplings obtained using different routines. In low-amplitude short-period variable stars, the LC data from QLP and SPOC data products give similar results but with smaller amplitudes (the *upper panel*). The *bottom panel* shows that in stars with amplitudes of the order of tens of millimagnitudes, the LC data can already suffer from some instrumental variations (magenta points), but the QLP routine (orange points) fully removes the variability. In both stars, the LC data are less reliable than the SC data in determining the amplitudes of brightness variations and in determining the variability type.

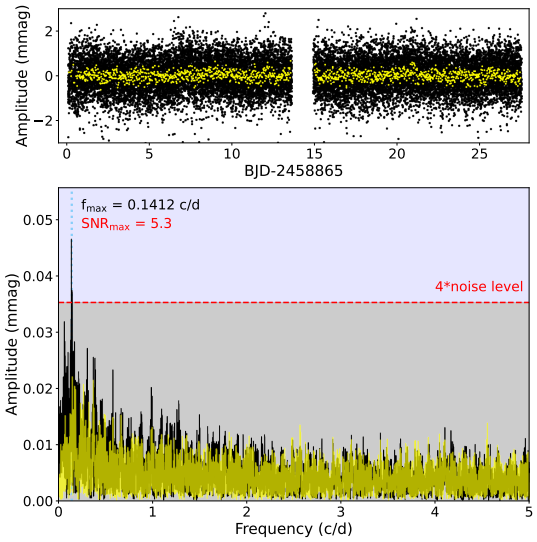

Fig. 3. SPOC data of TIC 2116199 from sector 14 (*top panel*) and frequency spectra based on four available sectors with a time span of 352 days (*bottom panel*). The LC data and the corresponding frequency spectrum are shown with yellow, and the SC data and the corresponding frequency spectrum with black. The horizontal dashed red line shows four times the noise level limit, while the vertical dotted blue line shows the most significant frequency.

Figure 3 shows an example of how the frequency spectra for the SPOC data with different sampling can differ. There is a significant peak with $S/N > 4$ in the SC data (black line and points), while there is no significant peak in the FT of the LC data (yellow line and points). According to the SC data and the peak, TIC 2116199 should be considered as a variable star.

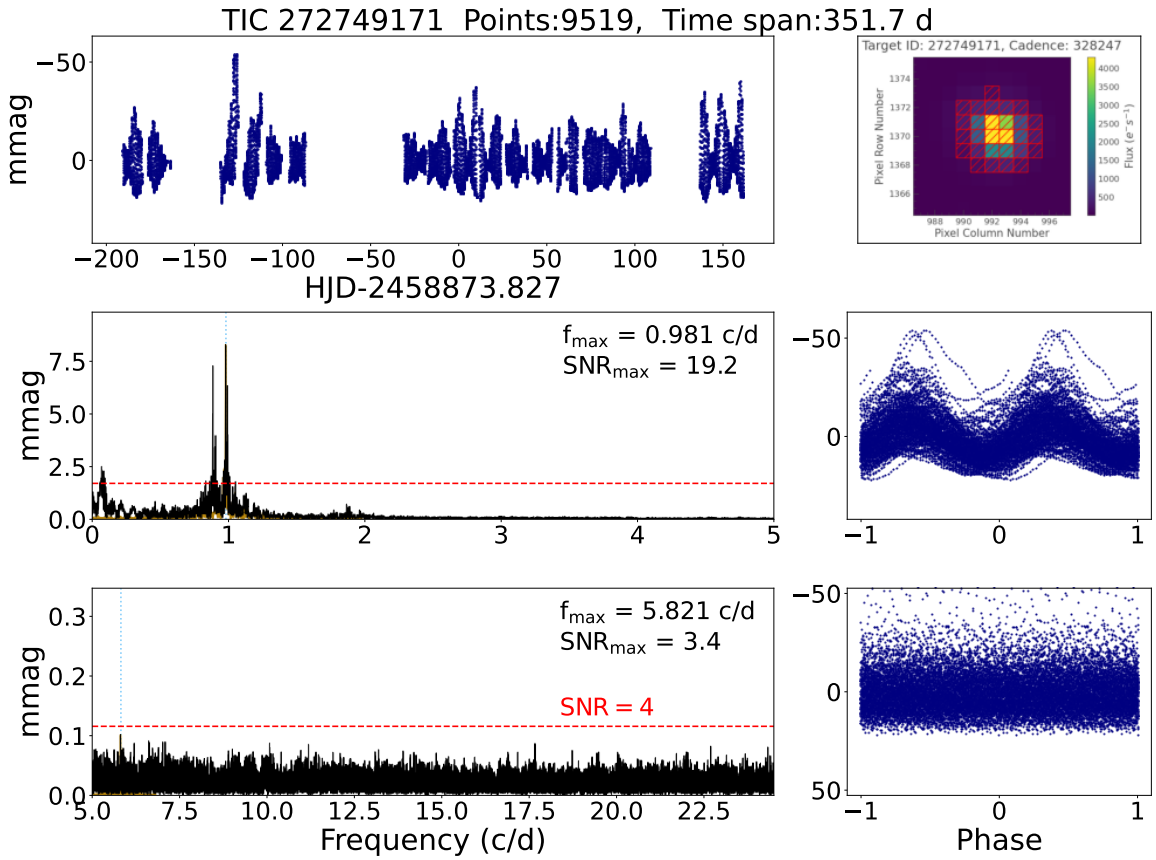

Fig. 4. Example of the figures that have been produced and used for the basic classification of each of the stars in the sample. The *upper left panel* shows the data, the *top right panel* shows the TPF with the aperture, and the *middle and bottom panels* show the frequency spectra (*left*) and the data phase-folded with the most prominent peaks in the frequency spectra (*right*).

However, because the FT of LC data shows no significant peak and there is actually no apparent variability in the light curve, we assume that the possible variation is of artificial nature and classify TIC 2116199 as a non-variable star.

From all the above mentioned reasons, we performed careful individual investigation of all available datasets for each star giving the preference to the SPOC SC data (where available) that seem to be the most reliable. The identification of variability and subsequent classification was performed on an individual basis. In addition, in case of LC data, the cadence is a significant fraction of the DSCT period and longer than that of a roAp star. Further shortcomings of the classification are discussed in Sect. 5.

4. Classification scheme and notation

Similar to the identification of real variations (see Figs. 2–3), classification based solely on the photometric data can be a difficult task, leading to an ambiguous solutions. Usually, multi-parametric classification employing periods, light curves, and frequency spectra characteristics are used (e.g. Uytterhoeven et al. 2011b; Balona et al. 2011; Bradley et al. 2015). Some types of variable stars are recognizable upon a first look (typically the high-amplitude variables, for instance, eclipsing binaries of Algol type), but in some variability types the classification may even be impossible. For example, the light curve of an ellipsoidal variable can look the same (including periods and amplitudes) as an over-contact eclipsing variable of W UMa type, pulsating RRC star, or spotted chemically peculiar star; pulsations can mimic rotation, eclipses, and so on. (see Sect. 5).

For each star, we produced a figure showing the time series data, data phase-folded with the dominant frequencies below and above 5 c/d, a TPF with the aperture, and frequency spectra divided into parts below and above 5 c/d (Fig. 4). This frequency limit is a usually accepted value dividing the GDOR and DSCT pulsations (Grigahcène et al. 2010) that has been applied in many studies dealing with the data obtained from space (e.g. Uytterhoeven et al. 2011b; Balona et al. 2011; Bradley et al. 2015). Plots shown in Fig. 4 served as the main decision factors for the classification. If needed, particular stars were investigated more closely.

The basic variability types were adopted from the Variable Stars Index (VSX) catalogue[5] (Watson et al. 2006). The notation is based on the classification system by the General Catalogue of Variable Stars (GCVS; Samus et al. 2009). For the stars that

[5] https://www.aavso.org/vsx/index.php?view=about.vartypes

are certainly variable but we were not able to determine the variability type, we used "VAR". If there is ambiguity between two or more variability types, we use the pipe symbol "|" meaning "or". If a star shows a combination of variability types, we give plus sign with the variability type of larger amplitude listed first.

Because the temperature of the stars in our sample covers a wide range, the expected mixture of physical mechanisms of variability are also very broad. Thus, we examined the general characteristics of the light variations and put an emphasis on explaining the physical mechanism of the variability.

We considered finer divisions to more specific types only in high-amplitude stars (for example, EA versus EB, RRAB versus RRC, etc.). There were attempts to perform a more delicate classification also in low-amplitude classes of variables. For example, Balona et al. (2011) introduced three subclasses of GDOR stars according to their light-curve shape: symmetric (SYM), asymmetric (ASYM), and multiple modes (MULT). Similarly, Balona (2011) introduced three classes of rotationally variable stars: SPOT (multi-periodic with dominant frequency), SPOTM (clear travelling wave), and SPOTV (clear dominant period). Similar notation as for GDOR stars created by Balona et al. (2011) was introduced also for DSCT stars by Bradley et al. (2015). However, we did not perform such a detailed classification. The reasons are that there can be ambiguity in the variability types. Instead, we decided to build a classification on the assumed physical mechanisms rather than on the look of the light curve (see Sects. 4–5). We also did not distinguish between DSCT and SX Phe stars and do not divide DSCT into LADS and HADS classes (Frolov & Irkaev 1984; Petersen & Christensen-Dalsgaard 1996). Similarly, we do not distinguish between low- and high-amplitude GDOR stars (Paunzen et al. 2020).

The variability types and criteria for classification are listed in Tables 2–4 including light curves and corresponding frequency spectra of the typical examples. The types and results are explored in details in Sects. 5–6. In Sect. 5, we discuss details and problems in classification. In Tables 2–4, we do not show the minor variability types identified in our sample. We identified two RRAB/BL stars (RR Lyrae of AB type showing the Blazhko effect)[6] and one RRC star[7] accompanied with one RRAB and two RRC candidates that have amplitudes only in the mmag range, which is very suspicious. These two RRC candidates may belong to a new class of horizontal-branch variables (Wallace et al. 2019). We also found five candidates of roAp stars that show frequencies above 100 c/d.

In Table 5, we provide the identification, classification, frequency of the dominant peak in the FT and the amplitude of the brightness variation. We also give a cross-match of our sample with the VSX catalogue with the distance limit of 20". There are 172 variable stars from our sample in the VSX (version 2022-02-21), while in 10 of the VSX stars we did not find any variation. For eclipsing binaries, we also give the zero epoch M_0 of the primary eclipse in Table 5.

The amplitude given in Table 5 is a rough visual estimate of the maximum amplitude (from minimum to maximum light) seen in the data. For example, the amplitude of TIC 272749171 shown in Fig. 4 is 70 mmag. This value is only indicative and can be different from the real amplitude of the variations. For example, the data might not contain the extrema of the variations, the light of the object can be contaminated by the light of nearby stars, the amplitude may be decreased by the LC in case of fast variations.

5. Ambiguity in classification and other related shortcomings

5.1. Blending

One of the reasons why we give only a rough estimate of the amplitude in Table 5 is that the value can be significantly affected by stars contaminating the light in the apertures (TESS has a spatial resolution of only 21″ px^{-1}, Ricker et al. 2015). In an extreme case, the star in the sample itself can be stable and the variation can come from a nearby variable star. We did not investigate this issue in detail but we performed a quick analysis concerning stars within our sample. We checked stars that were closer than 10 pixels from each other. Based on the amplitude of the peaks in the frequency spectrum, we decided which star is variable and which is not.

Figure 5 shows two examples of blended stars. In the top panel, we can see that the variability comes from the fainter star, TIC 232681382, which has peaks in the FT with higher amplitudes. In the bottom panel, the situation is the opposite: the brighter star (TIC 233545407) is the variable. In our sample, we identified 29 such couples among stars classified as variable from which 21 pairs show the same FT with different amplitudes. For these cases, we comment in the last column of Table 5 that the variability is caused by a close companion.

There might be more blends with fainter stars, but a detailed inspection of the stars around each object in our sample is beyond the scope of this paper. Nevertheless, we cross-matched our sample with the *Gaia* DR2 catalogue (Gaia Collaboration 2018) and identified all stars that are less than 5 mag fainter (in *Gaia g* filter) than our variable star and are closer than 105″ (5 px) to it. We give the number of such stars in the last column of Table 5. This value gives at least a warning about possible blends that can also cause false positive identifications of variable stars.

5.2. Instrumental, data reduction artefacts, and semi-regular and long-period variations

The data we used is the SAP processed with the PDC pipeline (Smith et al. 2012; Stumpe et al. 2014). This pipeline uses co-trending basis vectors to remove systematics such as those resulting from the focus changes, spacecraft pointing jitter, and other stochastic errors, as well as the crowding problems (see e.g. Jenkins et al. 2016; Jenkins & et al. 2020; Kinemuchi et al. 2012). Mostly because of scattered light and due to improper aperture definition, there might be additional light variations present in the data (as already pointed out in Sect. 3) that is not intrinsic to the star. It is not always possible to distinguish between stellar variation and instrumental and reduction artefacts.

Generally, we expect that the instrumental/reduction artefacts will cause irregular or semi-regular variations with periods longer than 1 day producing groups of low-amplitude peaks with frequencies below 1 c/d in the FT. Typically, artefacts can be confused with stellar activity, rotational modulation due to spots, or GDOR type pulsations. From the high risk of instrumental artefacts or misclassification, we conservatively assigned spurious cases with a "VAR" label although some of the stars could be assigned with a particular variability class. Actually, stars showing similar light curves and FTs as TIC 334678134 and TIC 417734885 (shown in the top row of Table 3) have been

[6] Saw-tooth light-curve shape, harmonics of the basic frequency in FT.
[7] More sinusoidal shape, harmonics of the basic frequency in FT.

Table 2. Typical examples of the variability types caused by the binarity of the stars.

Type	Light curve	Frequency spectrum	Physical origin
EA; EP	constant light in maximum, sharp minima (with the same depth in the event of EP)	many well-defined harmonics of the basic frequency	eclipses in binary system with detached components; transits of an exoplanet
	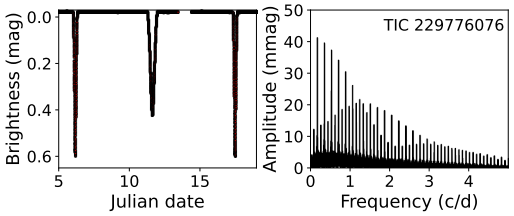		
EB	variation in maximum light, well-defined minima with (generally) different depths	many well-defined harmonics of the basic frequency with decreasing amplitude	eclipses in binary system with deformed component(s)
	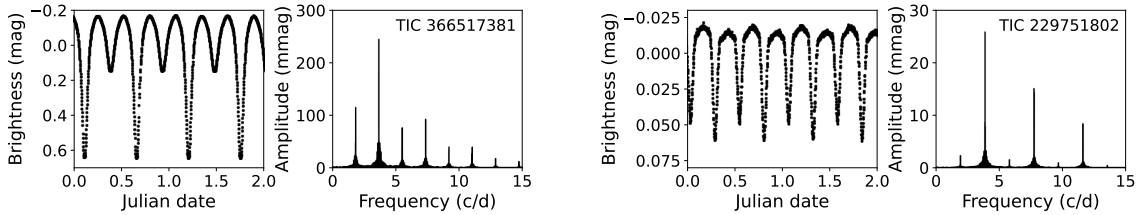		
EW	smooth brightness variation, flat bottom of eclipse(s) may be present, amplitudes >100 mmag	well-defined harmonics of the basic frequency with quickly decreasing amplitudes towards higher frequencies	eclipses in binary system with components filling their Roche lobes, common envelope binaries
	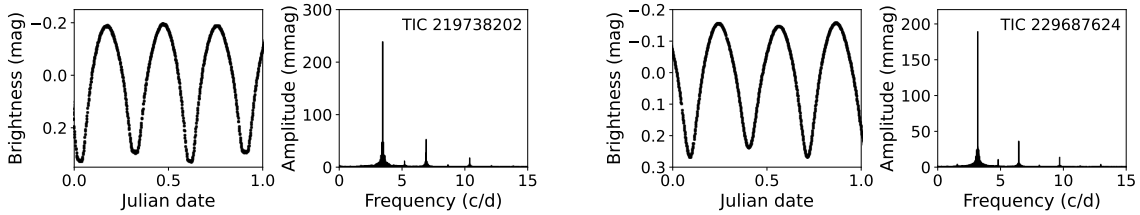		
ELL	smooth brightness variation, strictly symmetric and repeating light curve without sharp features, maxima have the same brightness	one or two dominant peaks at harmonics ($f_1 = 2f_2$), additional low-amplitude harmonics may be present, amplitudes <100 mmag	non-eclipsing binary system with tidally deformed components
	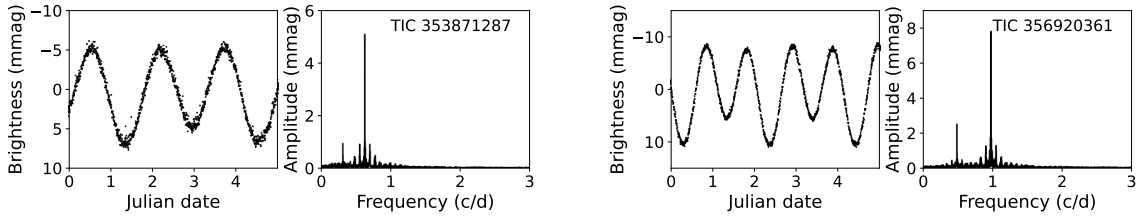		

Notes. The notation is in the first column, 'Type', a description of the characteristic features present in the light curve is in the second column, and characteristic features in the FT are described in the third column. The assumed physical origin of the brightness variations is in the fourth column. For each variability type we show the parts of the light curves that reflect the basic variability for two example stars, including the FTs of the full available datasets. The Julian date is arbitrarily shifted. Note the different scales of the vertical axes.

Table 3. Typical examples of the variability types assumed to be caused by stellar pulsations.

Type	Light curve	Frequency spectrum	Physical origin
VAR	weak or no signs of variability (low amplitude) and/or ambiguity in classification	single peak (with frequency usually below 1 c/d) and/or peaks with unclear nature, peaks with S/N slightly above 4	unknown origin, possible stellar activity or instrumental artefacts
	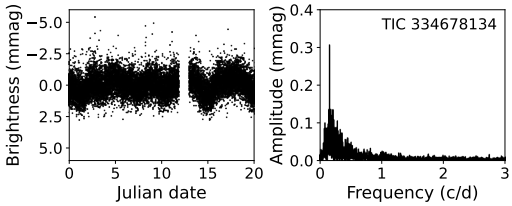		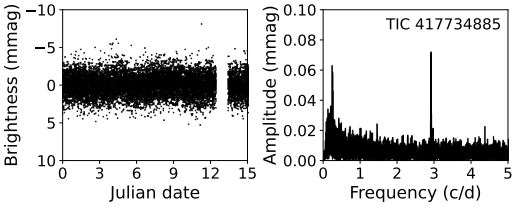
DSCT	(ir)regular fast variations, beating, bumps, interference	two or more independent peaks above 5 c/d	*p*-mode pulsations
	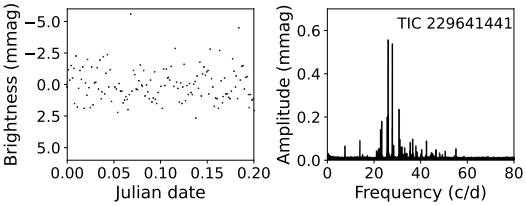		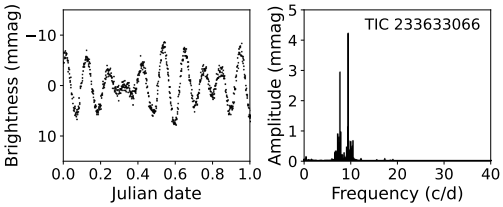
GDOR	(ir)regular variations, beating, bumps, interference, sharp variations	two or more independent peaks below 5 c/d, peaks are usually in groups, well-defined single peaks are not harmonics, groups of peaks can be close to the positions of their harmonics	*g*-mode pulsations
	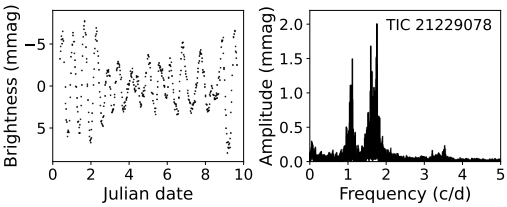		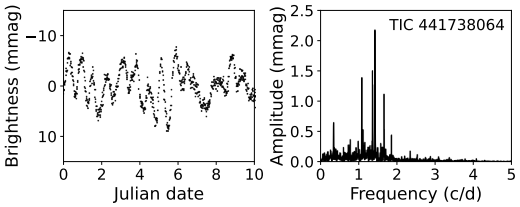
GDOR+DSCT; DSCT+GDOR	(ir)regular variations, beating, bumps, interference, sharp variations	two or more independent peaks below and above 5 c/d	simultaneous *p*- and *g*-mode pulsations
	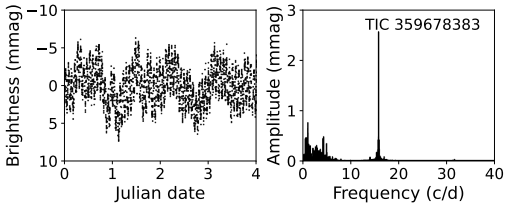		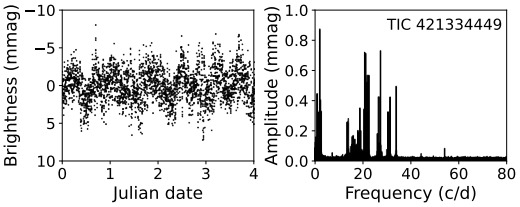

Notes. The columns are the same as in Table 2.

often considered as stars showing rotational modulation or stellar activity (e.g. Balona 2011, 2013; Bradley et al. 2015).

5.3. Pulsating variable stars

There are three types of pulsators in the region of A-F stars near the main sequence. First of them are DSCT stars ($p-$mode pulsators) that are easily recognizable and the class is well defined because basically any variability with frequencies above 5 c/d is caused by pulsations of DSCT type (for examples see the figures in Table 3). There are also Population II stars that show similar behaviour as DSCT stars (SX Phe stars). However, we do not distinguish between these two types.

Regarding the FT, the upper limit of 100 c/d differentiates DSCTs from the second pulsating type, roAp stars (Kurtz 1982).

Table 4. Typical examples of the variability types caused by the rotation of a single star.

Type	Light curve	Frequency spectrum	Physical origin
ROTM	strictly repeating pattern, smooth variation without sharp features, maxima and minima generally different, superposition of two waves	one or two dominant peaks that are harmonics of the basic rotational frequency ($f_2 = 2f_1$), low-amplitude harmonics of f_1 may be present	rotation of a star with abundance anomaly spots
	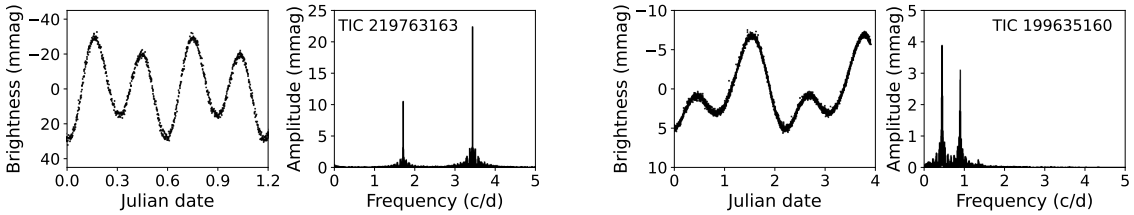		
ROTS	semi-regular variations superimposed on a basic periodic pattern	groups of (unresolved) peaks at positions close to harmonics of the strongest peak	rotation of a star with migrating (and forming or disappearing) spots, activity similar to our Sun, possible instrumental or data reduction artefacts
	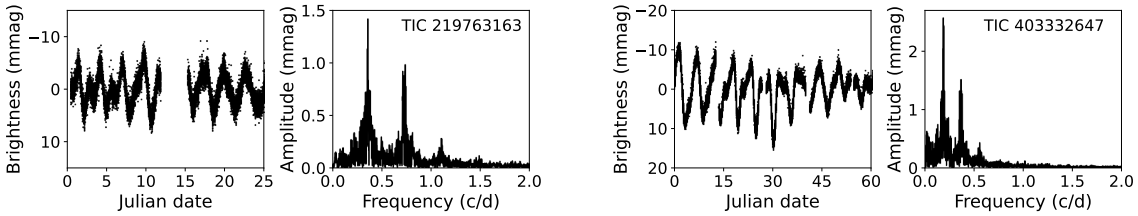		
ROT	repeating stable features	harmonics of the strongest frequency	likely some phenomena related to the rotation of the star
	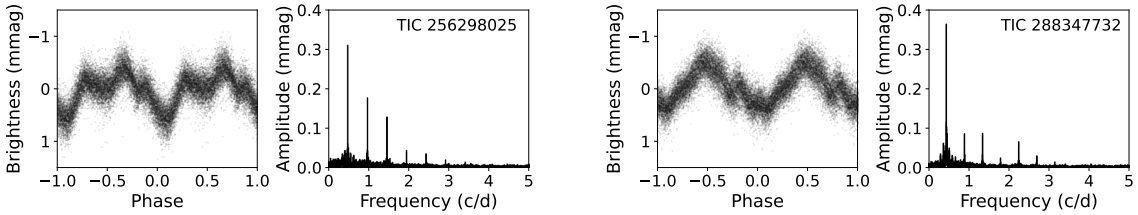		

Notes. The columns are the same as in Table 2. For the type 'ROT' we show the phase curves because the variations are more visible.

Table 5. Sample of our classification table.

TIC	RA (deg)	Dec (deg)	TYPE	Sp. type	f (c/d)	M_0	ΔT (mmag)	VSX	VSX type	Blend	$N_{\rm stars}$
21002602	272.7745522	53.4938379	ROTS		0.376		4.0				0
21018571	273.0771419	52.66231947	ELL		0.993		2.0				0
21031802	273.3209365	52.41759483	DSCT		9.391		10.0				3
...	...	...	...	...	...	...	...	...	...	...	...

Notes. Shown are the designation in the TIC catalogue (column 1), positions (columns 'RA' and 'Dec'), classification of the stars ('TYPE'), spectral type based on the LAMOST spectra, dominant frequency ('f'), zero epoch 'M_0' (for eclipsing binaries), amplitude of the brightness variation ('ΔT'), and the designation and classification in the VSX catalogue (VSX and VSX type) of the sample stars. The column 'Blend' gives a TIC number of the blending star that is variable, while the last column '$N_{\rm Stars}$' gives the number of stars that are closer than 5 pixels from the object and the difference between object and the blending star is less than 5 mag. The full table is only available in electronic form at the CDS.

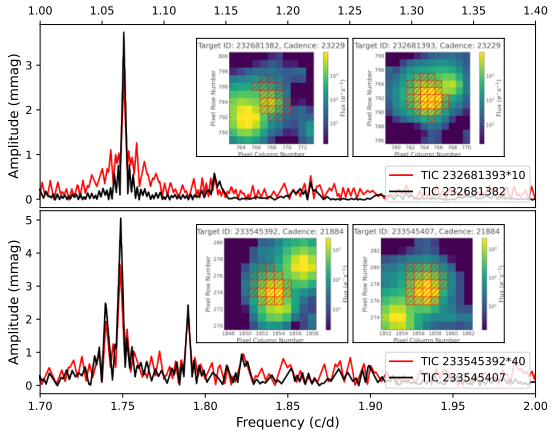

Fig. 5. Frequency spectra of two couples of blending stars. The apertures are shown in the insets. The red spectra correspond to non-variable stars contaminated by the nearby variables. The amplitudes of the peaks of non-variable blends are multiplied for a better visibility, by 10 and 40.

However, the upper limit is not firmly set and depends on the particular author. The mechanism responsible for the rapid oscillations is not yet known. Currently the most accepted is the opacity mechanism in the hydrogen ionisation layer where the convection is suppressed by the magnetic field (Balmforth et al. 2001). Recently, Balona (2022) found that high frequencies appear also in non-magnetic stars, while DSCT frequencies were found in magnetic stars where they should be damped (Saio 2005; Murphy et al. 2020). Balona (2022) also found that there is no frequency limit differentiating DSCT from roAp frequencies and argues that there is no need for the roAp class.

The last type of pulsations occurring among A-F type main sequence stars are pulsations of GDOR type. The g-mode pulsations are believed to be excited by the convective flux blocking mechanism (Guzik et al. 2000; Dupret et al. 2005). Frequencies observed in GDOR pulsators are usually between 0.3 and 3 c/d (Kaye et al. 1999; Henry et al. 2011), but can also be above 5 c/d, although with small amplitudes (Grigahcène et al. 2010). Similarly, the DSCT pulsations can have frequencies below 5 c/d but with small amplitudes (Grigahcène et al. 2010). This can lead to a misclassification between GDOR and DSCT stars in a small fraction of stars. We classified a star as a GDOR if it shows two or more peaks with frequencies below 5 c/d that are not harmonics of each other. Peaks in the FT of GDOR stars often appear in groups (Balona et al. 2011; Saio et al. 2018). Such a pattern is characteristic for a significant portion of GDOR stars (see the examples in Table 3 and Fig. A.1). We cannot exclude the possibility that in clear GDOR stars some of the peaks can be caused by spots and rotation.

A significant fraction of the A-F pulsators show both GDOR and DSCT pulsations (see the examples in Table 3 and in Fig. A.2). Some of them were known prior to space missions (e.g. Henry & Fekel 2005; Handler 2009). These stars are called hybrids. Balona (2014) found that basically all DSCT stars show low-frequency peaks and are, therefore, hybrids, although some exceptions do exist (Bowman 2017). We marked a star as a hybrid when at least two significant peaks ($S/N > 4$) with frequencies below and above 5 c/d are present. This is a somewhat weaker criterion than has been used, for example, by Uytterhoeven et al. (2011b) and Bradley et al. (2015) who used an amplitude threshold and required that the amplitudes of the peaks in GDOR and DSCT regimes are similar (factor of 5–7). There is a risk that some of the frequencies can actually be a combination of other frequencies (Balona 2014; Bowman & Kurtz 2018). This could lead to a wrong hybrid classification. Further, in rapidly rotating GDOR stars, some of the peaks above 5 c/d can actually be g modes shifted to higher frequencies due to rotation (Bouabid et al. 2013). However, we assume that these issues would be present only in a small fraction of the stars. Because a detailed individual frequency analysis of the data is beyond the scope of this paper, we have not considered these effects in our classification.

A more serious problem for the classification and identification of the real highest peak in the FT is the presence of sub-Nyquist artefacts. In case of perfectly sampled data with a 30-min cadence, the value of the Nyquist frequency would be $f_{\rm Nyquist} = 24$ c/d. Frequencies of some of the pulsation modes of DSCT stars can lie above this limit. A frequency $f_{\rm Real}$ in range of $24 < f_{\rm Real} < 48$ c/d will be reflected to a position $f_{\rm Reflected} = 2f_{\rm nyquist} - f_{\rm Real} = 48 - f_{\rm Real}$. DSCT frequencies close to $2f_{\rm Nyquist}$ will be reflected to a low-frequency region, where they possibly could mimic GDOR and ROTS frequencies. However, such frequencies will be heavily damped in amplitude, since the corresponding period of the pulsation cycle is comparable to the exposure time of the LC data (Balona 2014). We performed a simple test and compared the FT of LC and SC data and found out that about half of the GDOR candidates show a peak with higher amplitude close to $2f_{\rm Nyquist}$ than close to 0 c/d in the LC data. However, the SC data showed in all cases that the frequencies below 5 c/d are the real ones and that there is no considerable risk that the GDOR stars are confused with DSCT stars due to Nyquist reflections.

Concerning the DSCT stars, the SC data ensure that the DSCT frequencies are identified properly and the classification is correct. In the LC data, the perfect sampling is disrupted by the downlink of the data, which causes the observations to not restart after exactly $n\times30$ min (where n is an integer). This de-phasing is boosted in the TESS CVZ by multiple gaps (downlinks) and should allow for a reliable identification of the real pulsation frequencies of DSCT stars even if they are higher than $f_{\rm Nyquist}$ (Murphy 2015). However, the identification is not always perfect.

For stars classified as DSCT based on the LC data, we performed the FT analysis again in the range 0–60 c/d to retrieve possible frequencies above 24 c/d. To check how reliable these frequencies are in the LC data, we compared the results of 16% of all DSCT that have both LC and SC data (examples are shown in Fig. 6). The frequency with the highest amplitude identified in the SC data was successfully retrieved in only 50% of the test cases in the LC data (see panel D in Fig. 6). Thus, the DSCT frequencies above 24 c/d in Table 5 may be wrong in 50% of stars that do not have SC data. However, the classification as DSCT remains correct. Furthermore, we noticed that the frequency with the highest amplitude in the FT of SC data (that we expect to be the real dominant frequency) might not necessarily be the dominant frequency in the FT of LC data (panels A–C in Fig. 6). This is probably the result of the different sampling behaviour and smaller amplitude of the fast light variations in LC data.

5.4. Rotationally variable stars

Rotation is a stable phenomenon. Thus, in rotating stars, we expect regular pattern in form of harmonics (kf_0) of the basic rotation frequency (f_0). The rotational variability can be induced

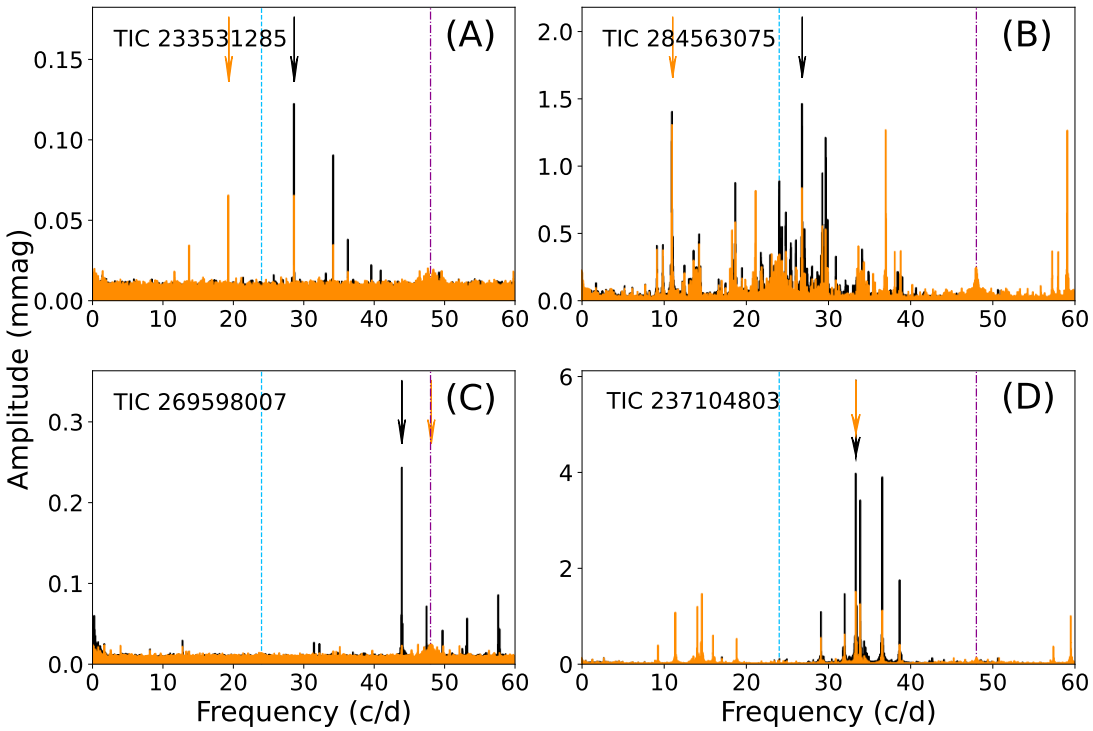

Fig. 6. Comparison of the FT based on the LC (orange) and SC (black) data for four DSCT stars. Frequencies with the highest amplitudes in the LC and SC data are marked with arrows of corresponding colour. The Nyquist frequency and its harmonic at $2f_{\rm Nyquist}$ are shown with the vertical light blue and magenta lines, respectively. *Panel A* shows the example when the Nyquist reflection of the highest peak would be detected in LC data, *panel B* shows the situation when the peak with the second highest amplitude would be the highest in the LC data, and *panel C* illustrates a situation when almost no variation is seen in the LC data and the identification completely failed in LC data. *Panel D* shows an example of when the proper peak would also be identified in LC data.

by orbital motion of tidally deformed components of a non-eclipsing stars (ELL type, the last row in Table 2) or by spots on the surface of a single rotating star (Table 4). Among A-F type stars, these spots are believed to form via gravitational settling of light elements (He) and radiative levitation of heavy and earth-rare elements (e.g. Si, Sr, Cr, and Eu) forming a class of chemically peculiar stars (Michaud 1970; Preston 1974). If a strong dipole magnetic field (inclined with respect to the rotational axis) is present, the spots formed usually around the magnetic poles can produce a rotational variability (Stibbs 1950; Kochukhov 2011).

The rotation periods of spotted stars are long – mostly of the order of days (Sikora et al. 2019) to hundreds of days or even years (Mathys 2017; Mathys et al. 2020). With 1-yr-long time base (at best), we are confined maximally to tens-of-days-long periods. The light curves of magnetic chemically peculiar stars have mostly sinusoidal or doubly sinusoidal light curves (Jagelka et al. 2019). We assign stars with stable light curves showing two (or more) harmonics in the FT as "ROTM" (meaning magnetic rotators, figures in the top row of Table 4) since we assume that the variation is caused by stable chemical spots that require strong magnetic fields[8]. Possible additional long-term variations are interpreted as instrumental/reduction artefacts (see Fig. 2). We do not assign sinusoidal variation (one significant peak in FT) as ROTM since it cannot be unambiguously distinguished from ELL type, and we classify these stars as ROTM|ELL (see Sect. 5.5).

As shown by many authors (e.g. Balona 2011, 2013; Hümmerich et al. 2018; Sikora et al. 2019), A-F stars can also show more complex light curves including amplitude variations. The variation can be highly irregular and can cause variations from cycle to cycle (see figures in the second row of Table 4 and also figures in e.g. Balona 2013; De Medeiros et al. 2013; Sikora et al. 2019; Trust et al. 2020). These variations are usually attributed to rotation and activity of a star with spots that can form and disappear and migrate due to differential rotation (solar-like activity; e.g. Balona 2011; Debosscher et al. 2011). However, one should be aware that mixing artefacts with real variations (see Fig. 2) can mimic time-varying spots.

Sikora et al. (2020) studied projected rotational velocities of 44 A- and late B-type stars showing rotational modulation in their light curves and found out that more than 10%, but likely fewer than 30% of main sequence A-type stars show this type of variability. This is surprising, since stellar activity of this type is not expected in hot stars without large convective envelopes. We assign stars showing semi-regular variations producing groups of (un)resolved peaks at positions of harmonics in the FT as ROTS – rotators of solar type (figures in the second row of Table 4 and

[8] Jagelka et al. (2019) show that the role of the magnetic field in forming the chemical spots may not be as important as is formerly supposed.

Fig. A.3). The groups of peaks are assumed to be the result of differential rotation.

Usually, authors assume that also semi-regular variations with small amplitude and variations producing one group of peaks (or a single peak) are signs of rotation or activity (e.g. Balona 2011; Uytterhoeven et al. 2011b; Bradley et al. 2015). We are more conservative and define such stars as VAR (see also Sect. 5.2).

Because there are many stars that show regular periodic patterns in the light curve that transforms into harmonics in the FT, we define the last type of rotational variability that is labelled as ROT (the last row in Table 4, Fig. A.3). The nature of these variations is, however, unclear. The origin can be explained by stable spots or some co-rotating structures governed by high-order magnetic multipoles, as suggested by Mikulášek et al. (2020) and Krtička et al. (2022) for the hot, chemically peculiar stars. However, more likely, these stars are a subgroup of GDOR stars (see Sect. 6).

5.5. Spotted stars or non-eclipsing binaries?

Without spectroscopic observations, based purely on single-passband photometry, there might be ambiguity between ROTM and ELL classes. In principle, the light variation of a spotted star (the top right-hand panel and red crosses in the middle panel of Fig. 7) can be equally described assuming gravity darkening caused by the tidal deformation of the components of a non-eclipsing system (the top left-hand panel and continuous line in the middle panel of Fig. 7). In addition, the amplitudes of the variations can be similar, as well as the periods and the FT.

Due to geometric reasons, ELL stars must reach the same brightness in maximum light twice a period. However, the same variation can be reproduced assuming two spots with different sizes on the opposite sides of a star (middle panel of Fig. 7). Thus, this is not a decisive criterion for ELLs. On the other hand, different maximum light typical to ROTM stars can be easily modelled assuming one spot on one of the components of a non-eclipsing binary system. Thus, again, different height of maxima should not be taken as the decisive criterion between ROTM and ELL types but only as a hint. In addition, there can be artefacts that cause a deformation in the light curve, making the correct classification more difficult (Fig. 2).

The ambiguity between ELL and ROTM can be demonstrated with a known ELL star IP Dra (the bottom panel of Fig. 7) that was spectroscopically confirmed to be a binary system (Kjurkchieva & Marchev 2014). The case of IP Dra shows the need of spectroscopic observations for reliable classification.

It was shown by Morris (1985) and Beech (1985) that if the light curve of ELL variables is described by the sum of sine and cosine functions ($m = A_0 + \sum_{i=1}^{N} A_i \cos(i\Theta) + \sum_{i=1}^{N} B_i \sin(i\Theta)$, Θ being phase, A_i and B_i amplitudes, A_0 zero term), the term with the highest amplitude is $\cos(2\Theta)$. This criterion is sometimes used as a support for the assumption of the ellipsoidal variability (e.g. Dal & Sipahi 2013; Li & Liu 2021). The light curve shown in Fig. 7 also shows dominant $\cos(2\Theta)$. Since the dependence can be explained also with spots, the criterion with dominant $\cos(2\Theta)$ is not sufficient for classifying the star as ELL.

Stable chemical spots and rotational modulation are usually observed in hot stars and only exceptionally occur among stars with $T_{\rm eff} < 7000$ K (Renson & Manfroid 2009; Hümmerich et al. 2018). In addition, the amplitude of the brightness variations usually decreases towards longer wavelengths (e.g. Krtička et al. 2007, 2015; Prvák et al. 2015). Therefore, we expect only negligible incidence rate of ROTM type among stars with temperatures below 7000 K and assign variations similar to those shown in Table 2 and Fig. 7 as ELL. Stars hotter than 7000 K showing rotational modulation with constant maximum brightness we assign as ROTM|ELL because of the ambiguity between these two types.

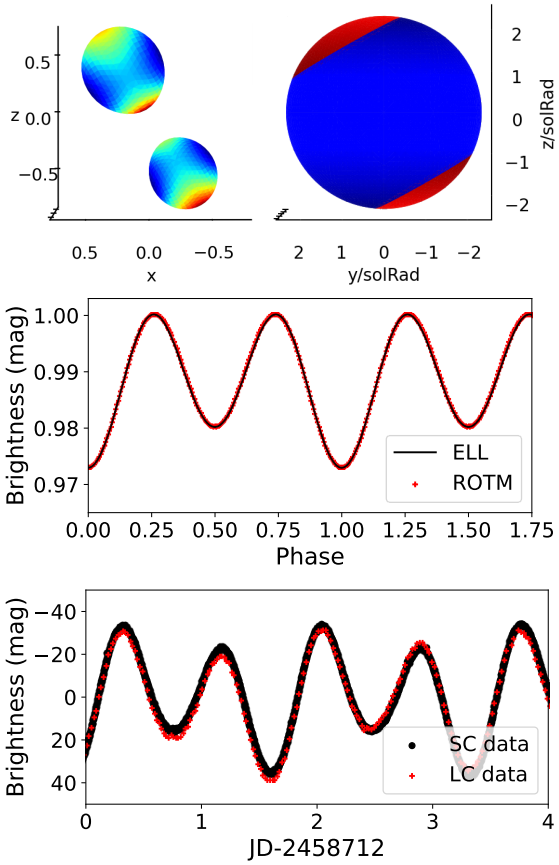

Fig. 7. Generated light curve (*middle panel*) assuming a non-eclipsing binary star with tidally deformed components (ELL, *top left panel*, black line in the *middle panel*) and a spotted star (ROTM, *top right-hand panel*, red crosses in the *middle panel*). An example of the light curve of a spectroscopically confirmed ELL star, IP Dra, that would rather be classified as ROTM is shown in the *bottom panel*. The models were generated using ELISa (Čokina et al. 2021).

Faigler et al. (2012) found seven binary stars that show light curves typical to ROTM stars and confirmed them spectroscopically. They explain the shape of the light curves as a combination of reflection effects, ellipticity and Doppler boosting (Faigler & Mazeh 2011). Thus, it can easily happen that some of the stars classified as ROTM can actually be ELL. This example shows the unavoidable necessity of the spectroscopic observations in all ELL and ROTM stars to be properly classified.

5.6. Pulsations or rotation?

To our best knowledge, there are no definitive criteria how to distinguish between rotation and pulsations based purely on photometric data. The issue with discriminating between pulsations and rotation was already pointed out by many studies, such as

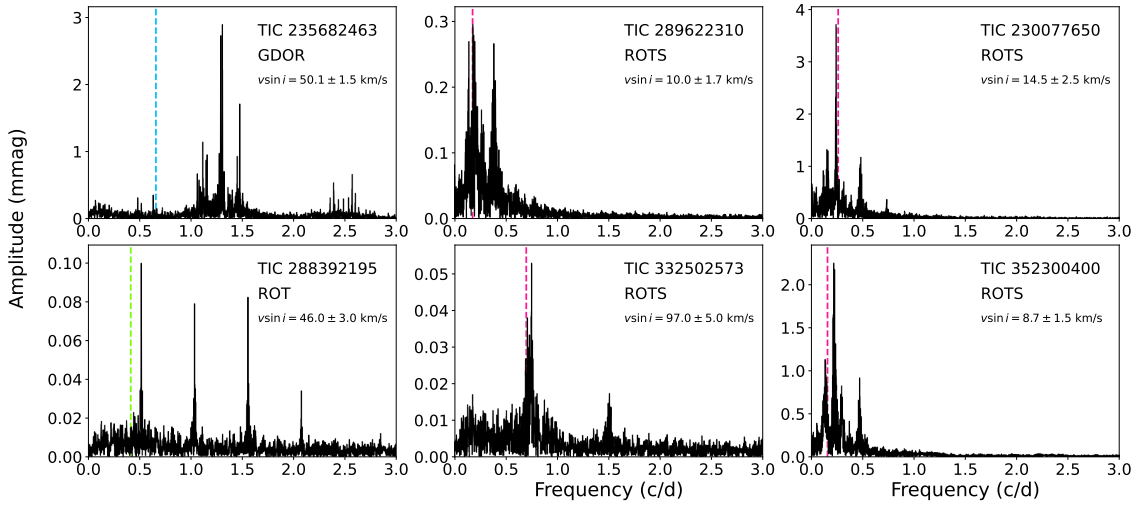

Fig. 8. Examples of FTs of GDOR (*top left panel*), ROT (*bottom left panel*), and ROTS stars (*middle and right panels*), showing also the position of frequencies calculated from observed $v \sin i$ and catalogue radii of the stars (vertical colour lines). It is apparent that the calculated frequency corresponds well with the observed peaks in the FT of ROTS stars.

De Medeiros et al. (2013), who claimed that a better selection of rotating variables can only be made using spectroscopic observations. Balona et al. (2011) pointed out that irregular light curves can be attributed to slowly rotating stars and that the frequencies of the GDOR stars showing symmetric light curves or obvious beating are comparable to rotation frequencies. Actually, most of the studies dealing with the stellar classification based on the space data warn about the possible misclassification between pulsating stars and stars showing rotational variability (e.g. Uytterhoeven et al. 2011b; Balona 2011).

The typical rotational frequencies calculated from the median projected rotational velocity $v \sin i$ and median radius R for A-F stars are between 0.5 and 0.75 c/d (Royer et al. 2007). However, the rotation frequencies can be as high as the critical rotational velocity, which corresponds to about 3–3.7 c/d in the fastest main sequence A-type stars (Sikora et al. 2019). Thus, there is a strong overlap of rotational variability and pulsations in the FT.

We performed a very simple test inspired by Sikora et al. (2020). We selected six bright examples of ROT, ROTS and GDOR stars and gathered spectra with the OES echelle spectrograph mounted at the Perek 2m telescope in Ondřejov, Czech Republic (see Sect. 2.2). We modelled the spectra using ıSpec and measured the $v \sin i$ (see Sect. 2.2). We calculated the bottom limit of the rotational frequency ($v \sin i \leq v_{\rm equatorial}$) by employing radii of the stars from the TIC catalogue (Stassun et al. 2019). The results are shown in Fig. 8.

Apparently, the measured frequencies agree well with the frequencies detected in the FT of the photometric data of the ROTS stars, while for GDOR and ROT stars the frequencies do not match well. However, the calculated frequencies shown with vertical dashed lines in Fig. 8 are only lower limits. It is possible that some of the peaks shown in the left panels of Fig. 8 can be addressed with inclined rotation axis and rotation. Thus, this test alone is not a proof that the variation in stars producing (un)resolved peaks at their harmonic positions in the FT are caused by rotation rather than pulsations. It is only strong support for this explanation. In addition, rotation of a star can shift

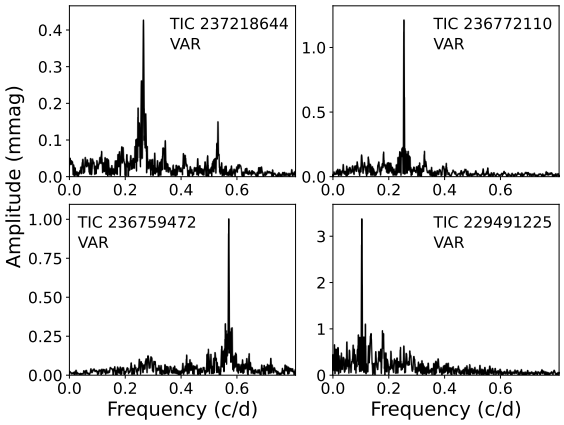

Fig. 9. Examples of frequency spectra of stars with ambiguous classification and, therefore, conservatively classified as VAR. See the text for details.

the pulsation frequencies. An example how difficult the correct classification of such stars can be was published by Uytterhoeven et al. (2011a). They found that variations in HD 171834, which produce unresolved peaks at the harmonic positions in the FT, are caused by rotation rather than pulsations.

It is likely that there remain spurious cases in our sample that would need detailed investigation including spectroscopic observations. TIC 237218644 (top left panel of Fig. 9) would be classified as ROTS according to our methodology, but the temperature of 9087 ± 204 K (Stassun et al. 2019) suggests that the origin of the variations is probably pulsations rather than rotation, since at such high temperatures, stellar activity linked with convection is not expected. There might also be uncertainty in temperature. Due to all these issues, we classify TIC 237218644 as VAR. The remaining panels of Fig. 9 contain stars that show

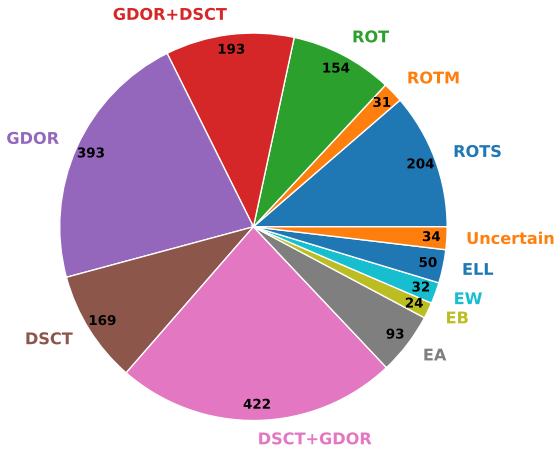

Fig. 10. Numbers of stars in particular variability classes.

only one significant peak in the FT. These stars could possibly be classified as ROTS but also as GDOR, ELL or ROTM types. We conservatively classify such stars as VAR.

6. Results and discussion

We identified 3025 stars (out of 5923 in our sample, 51%) that show brightness variations. This is 12% less than reported on the basis of preliminary results (Skarka et al. 2021). From the 3025 stars, we were able to assign 1813 stars (60%) to a specific variability type. The number of stars in particular classes are shown in Fig. 10. The most numerous are GDOR and DSCT classes and their hybrids (together 64.9% of the variable stars). This is in excellent agreement with Uytterhoeven et al. (2011b) who found 63% of stars to show oscillations. Regarding eclipsing binaries (EA, EP, EA|EP, EB and EW classes), we found only 56% of our binary candidates in the TESS eclipsing binary catalogue[9] (Prša et al. 2022). This discrepancy, however, comes from the fact that they used only 2-min cadence. If we use only the SC data, then the agreement of our identification with the TESS EB catalogue is 95%.

In the 'Uncertain' class, there are 34 stars with ambiguous classification with two equally probable types, for example ELL|ROTM and EA|EP. It was not possible to reliably classify the rest of the variable stars, marked as VAR (1212 stars; see Sect. 5). These are not shown in Fig. 10. In addition to the numbers given in Fig. 10, we identified 6 RR Lyrae stars (1 RRAB, 2 RRAB/BL, 3 RRC) and 7 heartbeat (HB) stars. In five stars we detected frequencies in the roAp range. However, it is not clear whether these are not combination frequencies. Not counting GDOR and DSCT hybrids, 50 stars show a combination of variability types, for example, EA+DSCT and GDOR+HB.

Plotting all the stars in the Hertzsprung–Russell diagram[10] (HRD; Fig. 11) show some (expected) clumping. The vast majority of GDOR stars is located in a narrow part of the HRD well within the theoretical instability strip (IS) by (Dupret et al. 2005), as shown in the left panel of Fig. 11. The distribution of GDOR stars has maximum at around 7000 K and mean luminosity at about $\log L/L_\odot = 0.8$ (Fig. 12). GDOR stars located outside the IS above approximately 7500 K are uniformly spread over the whole temperature range. Different behaviour of stars in and out of the IS suggests that the hot stars marked as GDOR outside of IS are not of the same type although the nature of the variability is likely to be g-mode pulsations.

The temperature distribution of DSCT and DSCT+GDOR hybrids is similar, although DSCT+GDOR hybrids are about 200 K hotter on average. GDOR+DSCT hybrids have preferentially lower temperatures than their DSCT-dominant counterparts but have the same average temperature as DSCT stars (see Fig. 12). There are a few GDOR, DSCT, and hybrid stars with unexpectedly low temperature. We checked them and would all of them classify as they are (see Fig. A.4). The unexpected behaviour at low temperatures might indicate contamination of the light by nearby stars or less reliable temperatures, although the error bars are similar to other stars in our sample. The groups of the rotating variables are well separated in the HRD. In addition, they have different temperature distributions. The ROTS stars (11.3%) dominate the low-temperature part of the HRD, which can be naturally expected as the variations are supposed to be caused by the spots of solar type. The ROTM stars (1.7%) are well spread out over the whole temperature range above 7000 K.

ROT stars (8.5%) are almost exclusively located near and within the cool edge of the GDOR instability strip. This suggests that the observed brightness variations are likely connected with pulsations rather than with rotation. Alternatively, rotation and pulsation can be present simultaneously and ROT stars could be a subclass of GDOR stars. The GDOR stars have an average temperature of 7043 K and a frequency of 1.358 c/d, while ROT stars have a mean temperature of 6777 K and a mean frequency of 0.578 c/d. The mean amplitude is significantly lower for ROT stars (1.5 mmag) than for GDOR stars (9.8 mmag).

Our classification is in a very good agreement with the VSX classification. There are, of course, small differences but the variability types we provide are more specific or the same as in the VSX (with only a few exceptions). We applied our classification scheme to three of the previous studies dealing with the classification of variable stars based on the space data (Uytterhoeven et al. 2011b; Balona 2013; Bradley et al. 2015) to see the differences in the classification paying special attention to stars with frequencies below 5 c/d where the ambiguity between pulsation and rotation can emerge (see Sect 5.6). We downloaded the *Kepler* data of the stars with LIGHTKURVE and performed the analysis exactly in the same way as for the stars in our sample.

Among 87 stars classified by Uytterhoeven et al. (2011b) as GDOR we found only 4 stars that we classified as ROTS and two stars that we classified as VAR. Thus, the agreement is excellent. However, in one third of stars classified by them as rotation or activity, we found that they are actually GDOR stars or hybrids (see examples in the four upper left-hand panels of Fig. 13). This is a significant discrepancy. In 25% of the stars classified as rotational variables by Balona (2013)[11] we found GDOR variability (examples are shown in the four upper right-hand panels of Fig. 13) but we found perfect agreement for all 9 stars classified by Balona (2013) as GDOR.

The worst agreement with our classification is the classification by Bradley et al. (2015). From their sample of 195 GDOR stars we classified 9 as non-variable stars, 39 as VAR, 29 as ROTS, 6 as ROT, 2 as ROTM/ELL and one clear RR Lyrae (four bottom left panels of Fig. 13). This means that we classified 44% of stars marked by Bradley et al. (2015) as GDOR into a

[9] http://tessebs.villanova.edu/

[10] Temperatures are taken from Stassun et al. (2019), luminosity of the stars calculated from temperatures and radii from Stassun et al. (2019).

[11] We checked only the first 200 stars from the list of Balona (2013).

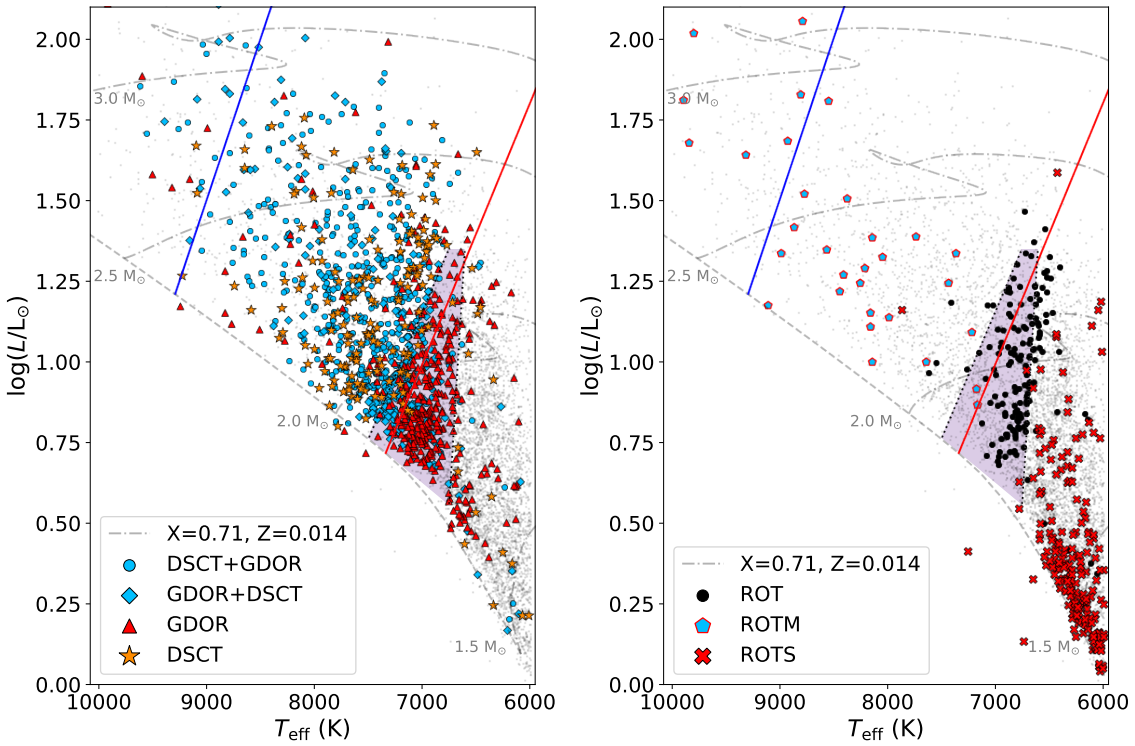

Fig. 11. Hertzsprung–Russell diagram showing pulsating stars (*left panel*) and rotationally modulated stars (*right-hand panel*). The dashed line shows the zero-age main sequence, dash-dotted lines show the evolutionary tracks for stars with different masses, all taken from Murphy et al. (2019). The blue and red continuous lines show the empirical boundaries of the instability strip determined by Murphy et al. (2019). The shaded area enclosed by the dotted lines shows the GDOR instability region, following Dupret et al. (2005). The grey dots show all stars including non-variable stars in our sample.

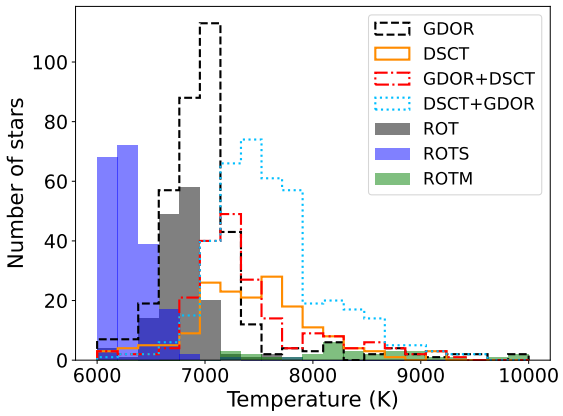

Fig. 12. Distribution of the stars with respect to their temperature.

different variability class. We also checked 551 stars classified by Bradley et al. (2015) as rotating variables. We classified 403 of them (73%) as VAR or non-variables although the variability of the majority of these stars can be caused by the stellar activity (see the examples in four bottom right panels of Fig. 13). The rest of the stars in their sample we classified as ROTM, ROTS and ROT stars with only insignificant contamination of GDOR. In general, variability of a significant part of stars in the VAR class can be actually caused by stellar activity, but these variations usually have small amplitudes and the classification is not trustworthy. If we assume that all the stars from the sample of Bradley et al. (2015) classified by us as VAR are rotational variables, then the agreement with their study would be very good.

Misclassification can be a serious issue in statistical studies and in training procedures based on machine learning and neural network methods. All the issues and discrepancies described above show that a commonly accepted methodology and classification system is desirable but difficult to be built. The border cases with ambiguous classification will always be present. It is the reason why our classification is rather conservative. Theoretical limits for the frequencies of GDOR pulsations, would be very helpful to distinguish between rotation and pulsations in a significant part of stars. It is worth to mention that we have not noticed any flare in the light curves of the sample stars.

7. Conclusions and future prospects

We have performed a careful individual classification of 5923 A-F stars (temperatures between 6000 and 10 000 K) brighter than 11 mag located close by and in the northern TESS CVZ. The classification is based on the TESS photometric

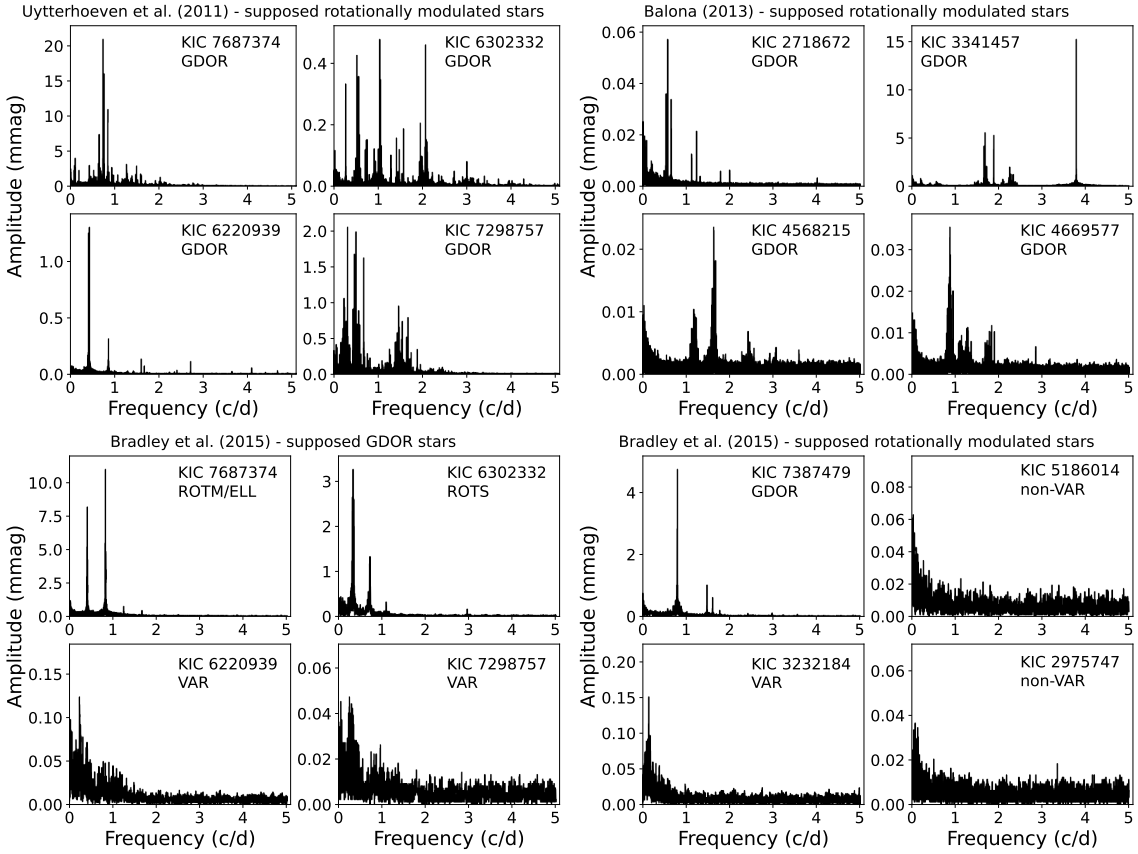

Fig. 13. Frequency spectra of stars observed by the *Kepler* mission and classified in previous studies (shown on the top of every four plots). The labels give how the stars would be classified using our methodology.

data and the properties of the frequency spectra. We discussed the data, crowding, the effects of residual variations caused by improper data reduction, aperture definition, and the influence of these effects on the classification of the variable stars. We have also discussed differences and similarities between the classes and paid special attention to a proper classification. We did not aim to study variability classes in detail, nor did we highlight any particular star. We also did not show any of the interesting cases. These remain for future dedicated studies.

We adopted the VSX classification scheme. We did not deal with the morphological classification of the variable stars within the variability classes, as was done by previous authors (e.g. Balona et al. 2011; Bradley et al. 2015). Our classification of the intrinsic variability is based on the assumption of the basic physical phenomena, that is, rotation and pulsations. We introduced three classes of rotationally modulated stars: stars with stable chemical spots (ROTM), stars with regular brightness variations (ROT), and stars showing semi-regular variations assumed to be caused by the forming or ceasing of the spots in combination with differential rotation (ROTS).

Our main results and findings can be summarised as follows:

– The PDCSAP data with different cadences are generally different in both amplitude and cadence. Mainly the 30-min data suffer from lots of residual variability that is not coming from the stars. This can lead to false positives and wrong classifications;
– We provide a well-defined classification scheme and methodology for the proper classification of A-F variable stars based on the light-curve shape and the corresponding FT (Tables 2–4);
– We find that the identification of the real pulsation frequencies above the Nyquist limit based purely on the amplitudes of the corresponding peaks in the FT can be wrong in up to 50% of cases;
– We identify a new (sub)class of variables that show regular periodic light-curve shapes and harmonics of the basic frequency in the FT. First we assumed that these variations must be connected with rotation, but the position of these stars close to and within the GDOR instability strip suggests that the variations are likely caused by pulsations. ROT stars have longer periods (1.7 versus 0.74 days), smaller amplitudes (1.5 versus 9.8 mmag), and are cooler on average (6777 versus 7043 K) than GDOR stars. The position of the stars in the HRD also suggests that the idea of co-rotating structures governed by high-order magnetic multipoles (Mikulášek et al. 2020; Krtička et al. 2022) likely cannot explain the variations in these relatively cool stars that are not expected to have strong stellar winds;

– Measurements of $v \sin i$ of four stars that show semi-regular brightness variations and unresolved groups of peaks near the harmonics of the basic frequency give a hint that the observed light variations may be linked with rotation rather than with pulsations. Stars in this group, called ROTS, can be mostly easily recognised from the GDOR stars;
– If the model of the light curve provides physically plausible results, there is no way to unambiguously distinguish between ellipsoidal variables and ROTM types purely on the basis of single-channel photometry. We have demonstrated this issue on IP Dra and generated models (Fig. 7).

On the comparison with previous studies, we have demonstrated that a commonly accepted classification scheme should be agreed upon. Our approach offers a well-defined system of classification with many examples. There still might be spurious cases, mainly regarding the GDOR, ROTS, and ROT classes; however, our sample should be clear of such ambiguous stars since we classified the spurious cases as VAR. The theoretical study of the limits of g-mode pulsations and all the possible patterns that can be expected in the FT would be very helpful in the future to better distinguish between rotation and pulsations. The only way to reliably classify the variable stars is via a detailed case-by-case investigation that includes spectroscopic data. We warn about any blind usage of the (mainly LC) TESS data.

The approach presented in the paper is rather conservative. Our groups of stars provide good and reliable samples of stars without significant contamination suitable for statistical studies and the training of neural networks. We are planning spectroscopic observations and detailed investigations of particularly interesting stars identified during the analysis of the data. We will perform the same analysis for the southern TESS CVZ.

Acknowledgements. M. S., P. K., and R. K. acknowledge the support by Inter-transfer grant no LTT-20015. M. M. acknowledges the support by MEYS (Czech Republic) under the project MEYS LTT17006. This paper includes data collected with the TESS mission. Funding for the TESS mission is provided by the NASA Explorer Program. Funding for the TESS Asteroseismic Science Operations Centre is provided by the Danish National Research Foundation (Grant agreement no.: DNRF106), ESA PRODEX (PEA 4000119301) and Stellar Astrophysics Centre (SAC) at Aarhus University. We thank the TESS team and staff and TASC/TASOC for their support of the present work. We also thank the TASC WG4 team for their contribution to the selection of targets for 2-min observations. The TESS data were obtained from the MAST data archive at the Space Telescope Science Institute (STScI). We acknowledge the usage of the data taken with the Perek telescope at the Astronomical Institute of the Czech Academy of Sciences in Ondřejov and would like to thank the observers for their work. We thank the referee for useful comments that improved the manuscript.

References

Antoci, V., Cunha, M., Houdek, G., et al. 2014, ApJ, 796, 118
Antoci, V., Cunha, M. S., Bowman, D. M., et al. 2019, MNRAS, 490, 4040
Audenaert, J., Kuszlewicz, J. S., Handberg, R., et al. 2021, AJ, 162, 209
Balmforth, N. J., Cunha, M. S., Dolez, N., Gough, D. O., & Vauclair, S. 2001, MNRAS, 323, 362
Balona, L. A. 2011, MNRAS, 415, 1691
Balona, L. A. 2012, MNRAS, 423, 3420
Balona, L. A. 2013, MNRAS, 431, 2240
Balona, L. A. 2014, MNRAS, 437, 1476
Balona, L. A. 2022, MNRAS, 510, 5743
Balona, L. A., & Nemec, J. M. 2012, MNRAS, 426, 2413
Balona, L. A., Krisciunas, K., & Cousins, A. W. J. 1994, MNRAS, 270, 905
Balona, L. A., Guzik, J. A., Uytterhoeven, K., et al. 2011, MNRAS, 415, 3531
Barentsen, G., & Lightkurve Collaboration. 2020, in American Astronomical Society Meeting Abstracts, 235, 409.04
Beech, M. 1985, Ap&SS, 117, 69
Blanco-Cuaresma, S. 2019, MNRAS, 486, 2075
Blanco-Cuaresma, S., Soubiran, C., Heiter, U., & Jofré, P. 2014, A&A, 569, A111
Boch, T., Pineau, F., & Derriere, S. 2012, in Astronomical Society of the Pacific Conference Series, Astronomical Data Analysis Software and Systems XXI, eds. P. Ballester, D. Egret, & N. P. F. Lorente, 461, 291
Bognár, Z., Kawaler, S. D., Bell, K. J., et al. 2020, A&A, 638, A82
Borucki, W. J., Koch, D., Basri, G., et al. 2010, Science, 327, 977
Bouabid, M. P., Dupret, M. A., Salmon, S., et al. 2013, MNRAS, 429, 2500
Bowman, D. M. 2017, Amplitude Modulation of Pulsation Modes in Delta Scuti Stars (Springer International Publishing)
Bowman, D. M., & Kurtz, D. W. 2018, MNRAS, 476, 3169
Bradley, P. A., Guzik, J. A., Miles, L. F., et al. 2015, AJ, 149, 68
Breger, M. 2000, in Astronomical Society of the Pacific Conference Series, Delta Scuti and Related Stars, eds. M. Breger, & M. Montgomery, 210, 3
Breger, M., Stich, J., Garrido, R., et al. 1993, A&A, 271, 482
Catelan, M., & Smith, H. A. 2015, Pulsating Stars (Wiley-VCH)
Čokina, M., Fedurco, M., & Parimucha, Š. 2021, A&A, 652, A156
Cox, J. P. 1963, ApJ, 138, 487
Cui, X.-Q., Zhao, Y.-H., Chu, Y.-Q., et al. 2012, Res. Astron. Astrophys., 12, 1197
Cunha, M. S., Antoci, V., Holdsworth, D. L., et al. 2019, MNRAS, 487, 3523
Dal, H. A., & Sipahi, E. 2013, PASA, 30, e016
De Medeiros, J. R., Ferreira Lopes, C. E., Leão, I. C., et al. 2013, A&A, 555, A63
Debosscher, J., Blomme, J., Aerts, C., & De Ridder, J. 2011, A&A, 529, A89
Dupret, M. A., Grigahcène, A., Garrido, R., Gabriel, M., & Scuflaire, R. 2005, A&A, 435, 927
Faigler, S., & Mazeh, T. 2011, MNRAS, 415, 3921
Faigler, S., Mazeh, T., Quinn, S. N., Latham, D. W., & Tal-Or, L. 2012, ApJ, 746, 185
Frolov, M. S., & Irkaev, B. N. 1984, Inform. Bull. Variable Stars, 2462, 1
Gaia Collaboration (Brown, A. G. A., et al.) 2018, A&A, 616, A1
Gray, R. O., & Corbally, C. J. 1994, AJ, 107, 742
Gray, R. O., & Corbally, C. J. 2014, AJ, 147, 80
Grigahcène, A., Antoci, V., Balona, L., et al. 2010, ApJ, 713, L192
Gustafsson, B., Edvardsson, B., Eriksson, K., et al. 2008, A&A, 486, 951
Guzik, J. A., Kaye, A. B., Bradley, P. A., Cox, A. N., & Neuforge, C. 2000, ApJ, 542, L57
Handler, G. 2009, MNRAS, 398, 1339
Henry, G. W., & Fekel, F. C. 2005, AJ, 129, 2026
Henry, G. W., Fekel, F. C., & Henry, S. M. 2011, AJ, 142, 39
Houdek, G. 2000, in Astronomical Society of the Pacific Conference Series, Delta Scuti and Related Stars, eds. M. Breger & M. Montgomery, 210, 454
Huang, C. X., Vanderburg, A., Pál, A., et al. 2020a, RNAAS, 4, 204
Huang, C. X., Vanderburg, A., Pál, A., et al. 2020b, RNAAS, 4, 206
Hümmerich, S., Mikulášek, Z., Paunzen, E., et al. 2018, A&A, 619, A98
Jagelka, M., Mikulášek, Z., Hümmerich, S., & Paunzen, E. 2019, A&A, 622, A199
Jenkins, J. M., Twicken, J. D., McCauliff, S., et al. 2016, SPIE Conf. Ser., 9913, 99133E
Jenkins, J. M., et al. 2020, Kepler Science Document KSCI-19081-003
Kabáth, P., Skarka, M., Sabotta, S., et al. 2020, PASP, 132, 035002
Kaye, A. B., Handler, G., Krisciunas, K., Poretti, E., & Zerbi, F. M. 1999, PASP, 111, 840
Kinemuchi, K., Barclay, T., Fanelli, M., et al. 2012, PASP, 124, 963
Kjurkchieva, D., & Marchev, D. 2014, Inform. Bull. Variable Stars, 6096, 1
Kochukhov, O. 2011, in Physics of Sun and Star Spots, eds. D. Prasad Choudhary, & K. G. Strassmeier, 273, 249
Krtička, J., Mikulášek, Z., Zverko, J., & Žižňovský, J. 2007, A&A, 470, 1089
Krtička, J., Mikulášek, Z., Lüftinger, T., & Jagelka, M. 2015, A&A, 576, A82
Krtička, J., Mikulášek, Z., Kurfürst, P., & Oksala, M. E. 2022, A&A, 659, A37
Kurtz, D. W. 1982, MNRAS, 200, 807
Li, X.-Z., & Liu, L. 2021, New Astron., 84, 101539
Lightkurve Collaboration, (Cardoso, J. V. d. M., et al.) 2018, Lightkurve: Kepler and TESS time series analysis in Python, Astrophysics Source Code Library [record ascl:1812.013]
Lomb, N. R. 1976, Ap&SS, 39, 447
Mathys, G. 2017, A&A, 601, A14
Mathys, G., Kurtz, D. W., & Holdsworth, D. L. 2020, A&A, 639, A31
Michaud, G. 1970, ApJ, 160, 641
Mikulášek, Z., Krtička, J., Shultz, M. E., et al. 2020, in Stellar Magnetism: A Workshop in Honour of the Career and Contributions of John D. Landstreet, eds. G. Wade, E. Alecian, D. Bohlender, & A. Sigut, 11, 46
Molnár, L., Bódi, A., Pál, A., et al. 2022, ApJS, 258, 8
Morris, S. L. 1985, ApJ, 295, 143
Murphy, S. J. 2015, MNRAS, 453, 2569

Murphy, S. J., Hey, D., Van Reeth, T., & Bedding, T. R. 2019, MNRAS, 485, 2380
Murphy, S. J., Saio, H., Takada-Hidai, M., et al. 2020, MNRAS, 498, 4272
Paunzen, E., Bernhard, K., Hümmerich, S., et al. 2020, MNRAS, 499, 3976
Petersen, J. O., & Christensen-Dalsgaard, J. 1996, A&A, 312, 463
Pedersen, M. G., Antoci, V., Korhonen, H., et al. 2017, MNRAS, 466, 3060
Pineau, F.-X., Boch, T., Derrière, S., & Schaaff, A. 2020, in Astronomical Society of the Pacific Conference Series, Astronomical Data Analysis Software and Systems XXVII, eds. P. Ballester, J. Ibsen, M. Solar, & K. Shortridge, 522, 125
Plachy, E., Molnár, L., Bódi, A., et al. 2019, ApJS, 244, 32
Preston, G. W. 1974, ARA&A, 12, 257
Prvák, M., Liška, J., Krtička, J., Mikulášek, Z., & Lüftinger, T. 2015, A&A, 584, A17
Prša, A., Kochoska, A., Conroy, K. E., et al. 2022, ApJS, 258, 16
Renson, P., & Manfroid, J. 2009, A&A, 498, 961
Ricker, G. R., Winn, J. N., Vanderspek, R., et al. 2015, J. Astron. Telesc. Instrum. Syst., 1, 014003
Royer, F., Zorec, J., & Gómez, A. E. 2007, A&A, 463, 671
Saio, H. 2005, MNRAS, 360, 1022
Saio, H., Bedding, T. R., Kurtz, D. W., et al. 2018, MNRAS, 477, 2183
Samus, N. N., Kazarovets, E. V., Durlevich, O. V., Kireeva, N. N., & Pastukhova, E. N. 2009, VizieR Online Data Catalog: B/gcvs
Sánchez Arias, J. P., Córsico, A. H., & Althaus, L. G. 2017, A&A, 597, A29
Scargle, J. D. 1982, ApJ, 263, 835
Sikora, J., David-Uraz, A., Chowdhury, S., et al. 2019, MNRAS, 487, 4695
Sikora, J., Wade, G. A., & Rowe, J. 2020, MNRAS, 498, 2456
Skarka, M., Auer, R. F., Henzl, Z., et al. 2021, in Posters from the TESS Science Conference II (TSC2), 31
Smith, J. C., Stumpe, M. C., Van Cleve, J. E., et al. 2012, PASP, 124, 1000
Stassun, K. G., Oelkers, R. J., Paegert, M., et al. 2019, AJ, 158, 138
Stibbs, D. W. N. 1950, MNRAS, 110, 395
Stumpe, M. C., Smith, J. C., Catanzarite, J. H., et al. 2014, PASP, 126, 100
Trust, O., Jurua, E., De Cat, P., & Joshi, S. 2020, MNRAS, 492, 3143
Twicken, J. D., Chandrasekaran, H., Jenkins, J. M., et al. 2010, SPIE Conf. Ser., 7740, 77401U
Uytterhoeven, K., Mathias, P., Baglin, A., et al. 2011a, ArXiv e-prints [arXiv:1111.1840]
Uytterhoeven, K., Moya, A., Grigahcène, A., et al. 2011b, A&A, 534, A125
Wallace, J. J., Hartman, J. D., Bakos, G. Á., & Bhatti, W. 2019, ApJ, 870, L7
Watson, C. L., Henden, A. A., & Price, A. 2006, 25th Annual Symposium, The Society for Astronomical Sciences, 47
Wenger, M., Ochsenbein, F., Egret, D., et al. 2000, A&As, 143, 9
Zhao, G., Zhao, Y.-H., Chu, Y.-Q., Jing, Y.-P., & Deng, L.-C. 2012, Res. Astron. Astrophys., 12, 723

Appendix A: Examples of typical light curves and frequency spectra

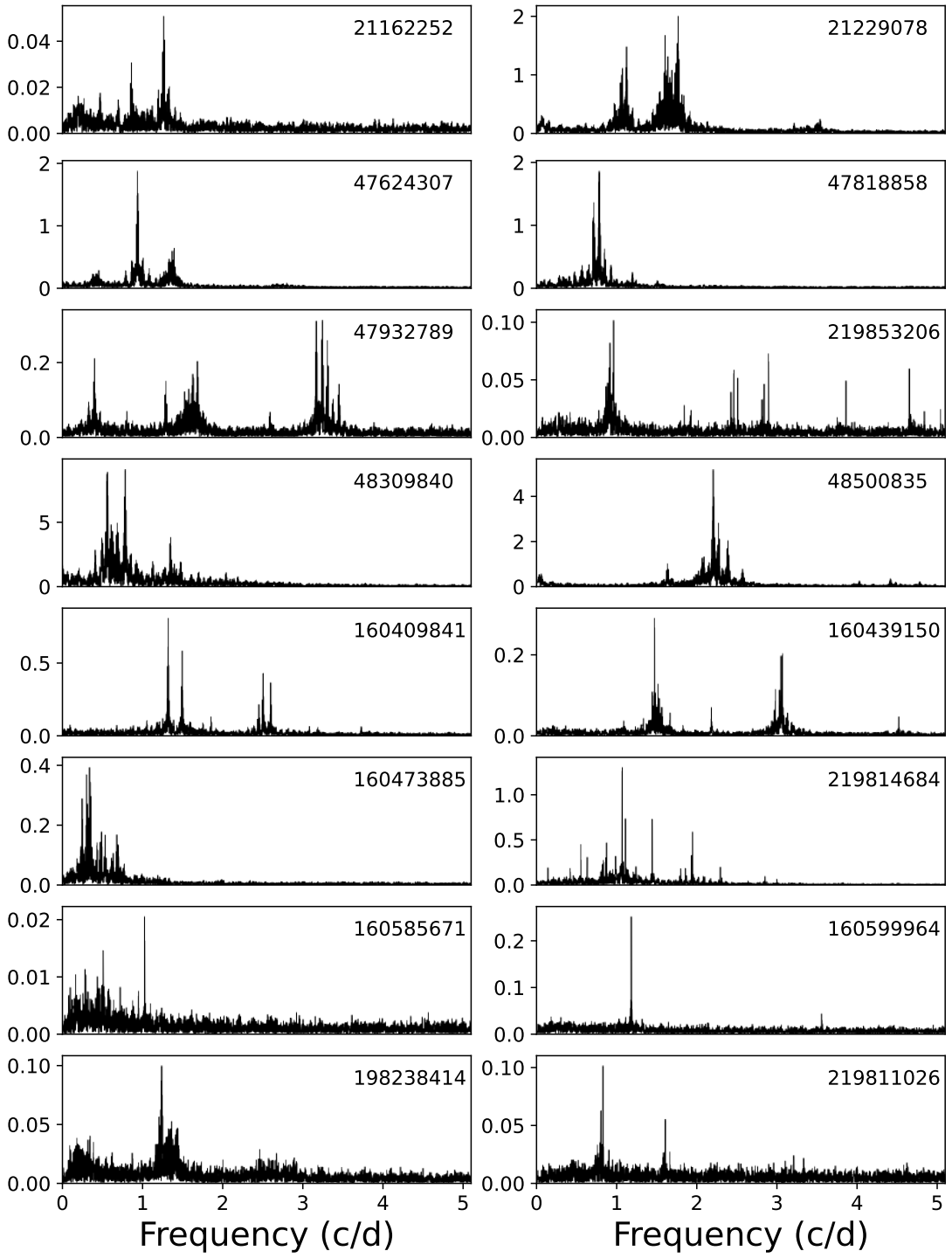

Fig. A.1. Typical frequency spectra of GDOR stars. The four bottom-most plots show less certain cases. The scale on the vertical axis is in mmag. The labels show the TIC numbers.

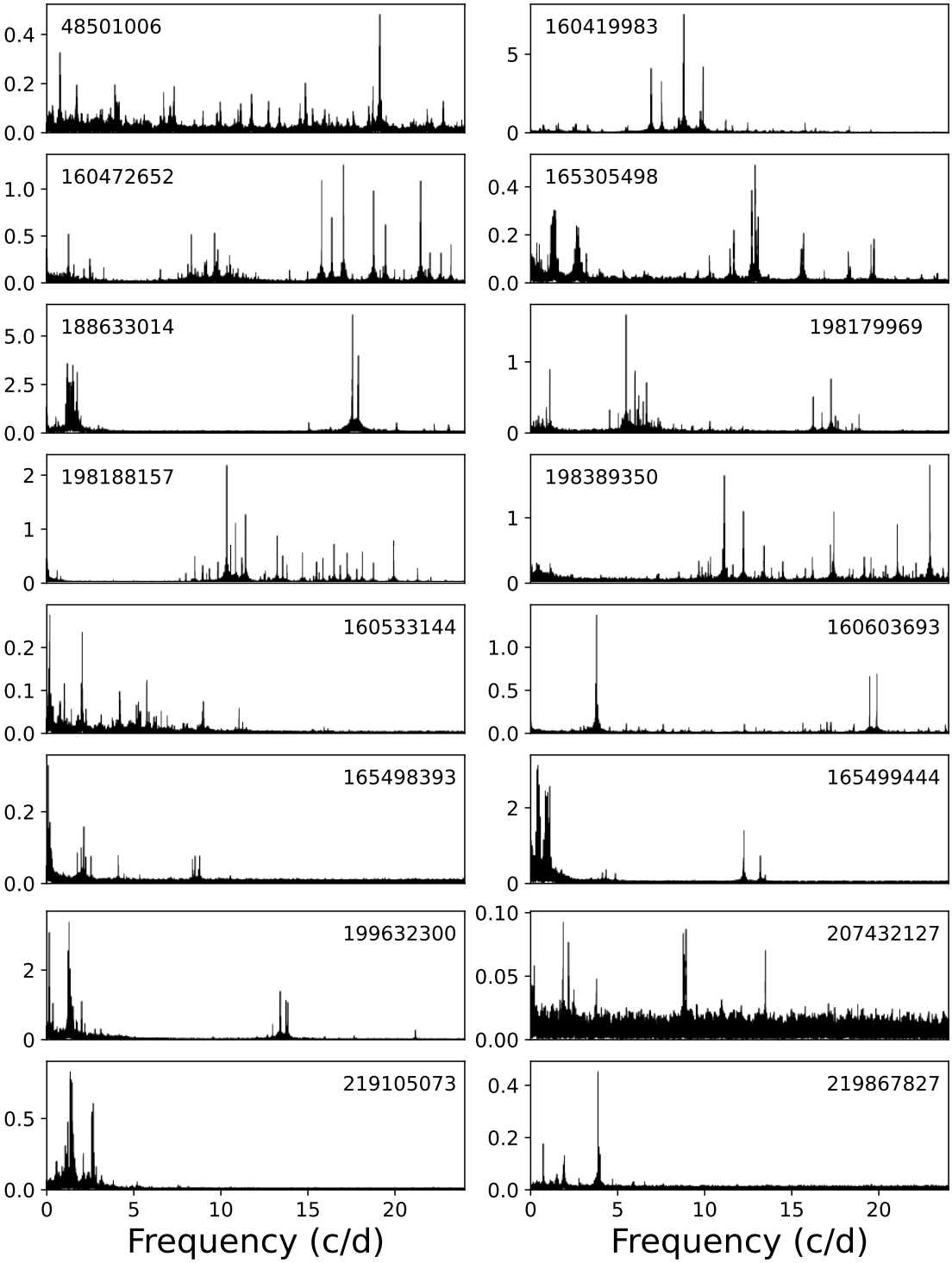

Fig. A.2. Typical frequency spectra of GDOR and DSCT Hybrid stars. The eight upper panels show DSCT dominant, while the eight bottom panels show the GDOR dominant hybrids. TIC 198188157 and 198389350 show weak peaks in the GDOR regime and, thus, are less certain hybrids. TIC 219105073 and 219867827 show only low-amplitude peaks in the DSCT regime and, thus, are less certain hybrids. The less certain hybrids can possibly be classified as pure GDOR or DSCT stars. The scale on the vertical axis is in mmag.

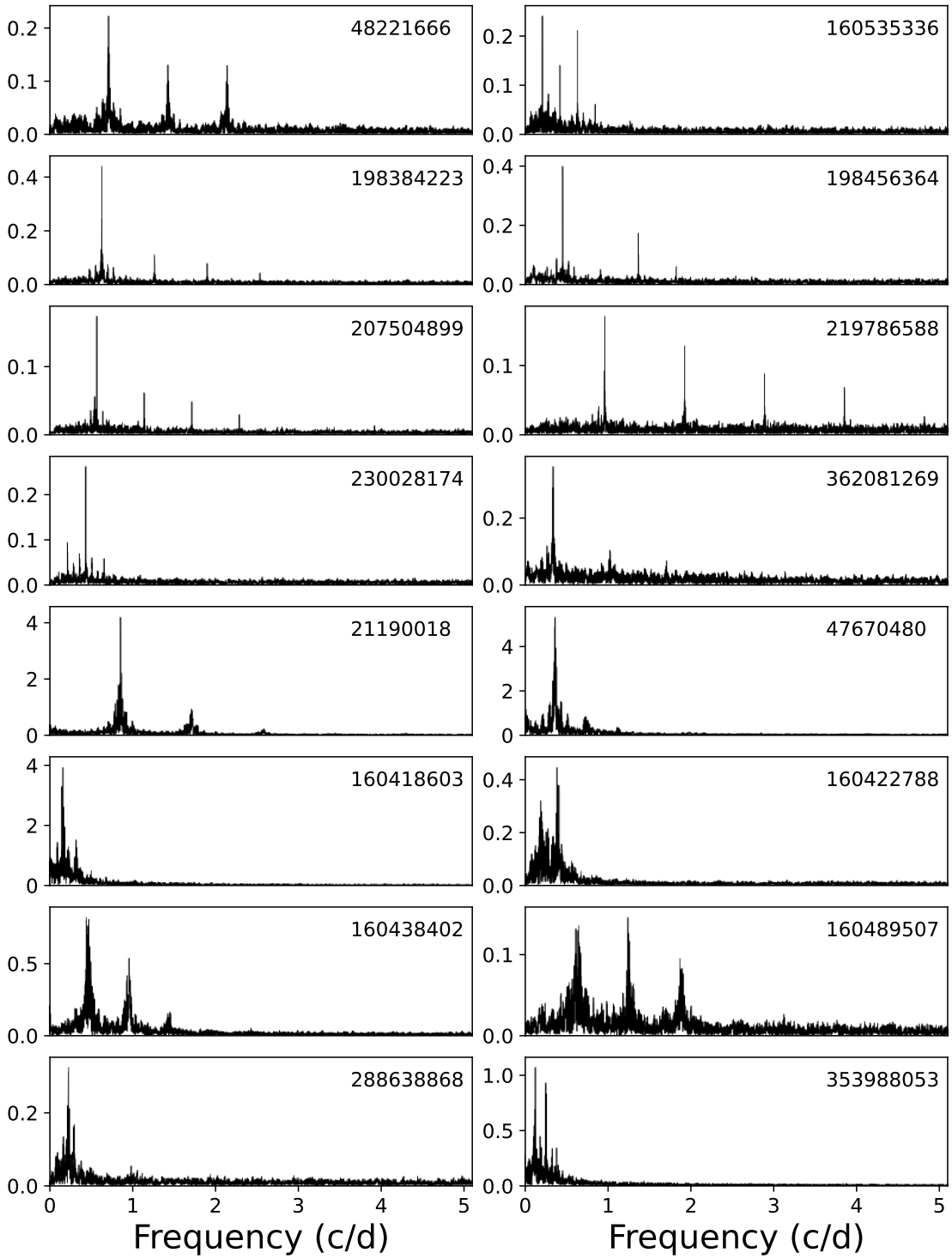

Fig. A.3. Typical frequency spectra of ROT (eight upper panels) and ROTS stars (eight bottom panels). The scale on the vertical axis is in mmag.

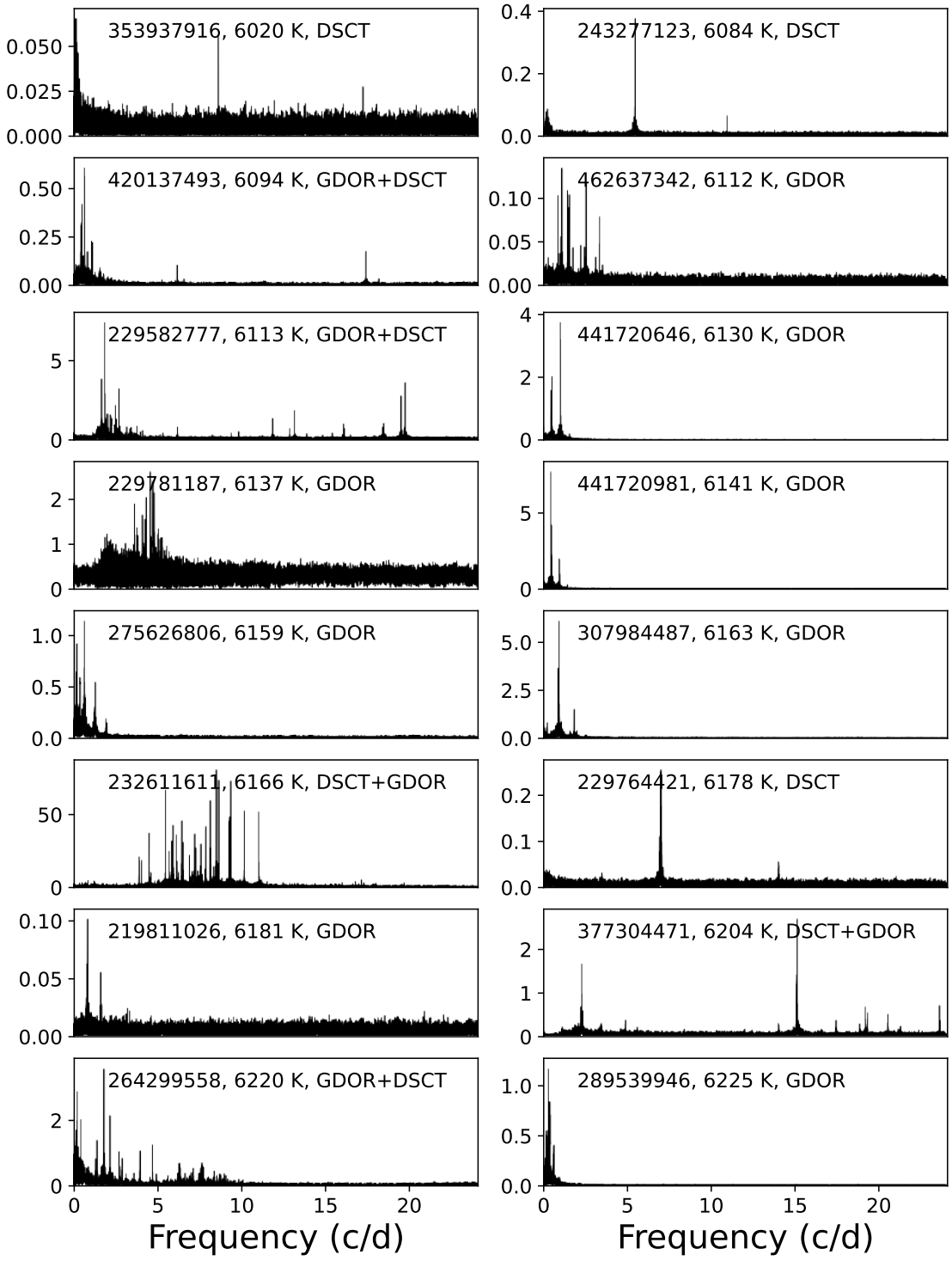

Fig. A.4. Frequency spectra of the coolest pulsating stars in our sample. The first number is the TIC number, the second number gives the temperature from TIC catalogue. The scale on the vertical axis is in mmag.

Paper 7

Periodic variable A-F spectral type stars in the southern TESS continuous viewing zone
I. Identification and classification

A&A, 688, A25 (2024)
https://doi.org/10.1051/0004-6361/202450711

Astronomy & Astrophysics

Periodic variable A-F spectral type stars in the southern TESS continuous viewing zone

I. Identification and classification⋆

M. Skarka[1,2,3] and Z. Henzl[3,4]

[1] Astronomical Institute of the Czech Academy of Sciences, Fričova 298, 25165 Ondřejov, Czech Republic
e-mail: skarka@asu.cas.cz
[2] Department of Theoretical Physics and Astrophysics, Masaryk University, Kotlářská 2, 61137 Brno, Czech Republic
[3] Variable Star and Exoplanet Section of the Czech Astronomical Society, Fričova 298, 251 65 Ondřejov, Czech Republic
[4] Hvězdárna Jaroslava Trnky ve Slaném, Nosačická 1713, Slaný 1, 27401 Slaný, Czech Republic

Received 14 May 2024 / Accepted 15 June 2024

ABSTRACT

Aims. Our primary objective is to accurately identify and classify the variability of A-F stars in the southern continuous viewing zone of the TESS satellite. The brightness limit was set to 10 mag to ensure the utmost reliability of our results and allow for spectroscopic follow-up observations using small telescopes. We aim to compare our findings with existing catalogues of variable stars.
Methods. The light curves from TESS and their Fourier transform were used to manually classify stars in our sample. Cross-matching with other catalogues was performed to identify contaminants and false positives.
Results. We have identified 1171 variable stars (51% of the sample). Among these variable stars, 67% have clear classifications, which includes δ Sct and γ Dor pulsating stars and their hybrids, rotationally variables, and eclipsing binaries. We have provided examples of the typical representatives of variable stars and discussed the ambiguous cases. We found 20 pairs of stars with the same frequencies and identified the correct source of the variations. Additionally, we found that the variations in 12 other stars are caused by contamination from the light of faint nearby large-amplitude variable stars. To compare our sample with other variable star catalogues, we have defined two parameters reflecting the agreement in identification of variable stars and their classification. This comparison reveals intriguing disagreements in classification ranging from 52 to 100%. However, if we assume that stars without specific types are only marked as variable, then the agreement is relatively good, ranging from 57 to 85% (disagreement 15–43%). We have demonstrated that the TESS classification is superior to the classification based on other photometric surveys.
Conclusions. The classification of stellar variability is complex and requires careful consideration. Caution should be exercised when using catalogue classifications.

Key words. methods: data analysis – catalogs – stars: oscillations – stars: rotation – stars: variables: general

1. Introduction

In order to study the physical origin of stellar variability, it is necessary to investigate groups of stars that have similar observational characteristics. This means that we need clear observational criteria to accurately classify the type of variability being observed. Since stellar variability is most prominent in brightness variations, the usual and natural way of classification is based on the shape and amplitude of the light curves and typical timescales of the variations (Samus et al. 2009; Watson et al. 2006). However, even for stars with well-defined classification parameter spaces, such as those with large amplitudes of brightness variations and typical light-curve shapes like eclipsing binaries or RR Lyrae stars, classification can be a challenging task. This calls for visual inspection and the utilisation of additional information and various analytical methods (e.g. Soszyński et al. 2016, 2019; Prša et al. 2022; Iwanek et al. 2022).

The classification of stars that exhibit low-amplitude variations caused by high-order radial and non-radial pulsations, spots of various types, deformation of the spherical shape of stars, and stellar activity is a challenging task. This is because these effects have similar amplitudes and timescales, thereby making it difficult to distinguish between them. The situation is further complicated by a combination of different mechanisms that can be present simultaneously, especially for stars with intermediate masses of 1−3 $M_\odot$ (F-A spectral-type stars).

Moreover, the classification of stars becomes more complicated with the availability of ultra-precise space observations from the *Kepler* (Borucki et al. 2010) and TESS satellites (Ricker et al. 2015). These observations have revealed new phenomena with similar amplitudes to the intrinsic stellar variations, which are related to the contamination from nearby stars, instrumental effects, and trends induced into the observations by the data reduction procedures. Especially in the mmag and sub-mmag regimes, human supervision can be biased and subjective, making even manual classification at least partially questionable.

In some cases, the frequency limits that are commonly accepted for classifying stars by their variability are not firmly established or cannot be generally applied. For instance, Balona (2022) argues that there is no need for the roAp class (rapidly oscillating Ap stars, Kurtz 1982) because there is no frequency

⋆ Table 4 is available at the CDS via anonymous ftp to cdsarc.cds.unistra.fr (130.79.128.5) or via https://cdsarc.cds.unistra.fr/viz-bin/cat/J/A+A/688/A25

Table 1. Number of stars in particular temperature ranges (based on temperatures from TIC, Stassun et al. 2019).

$T_{\rm eff}$ (K)	N
6000–7000	1308
7000–8000	603
8000–9000	222
9000–10 000	169

limit that differentiates roAp and δ Sct (DSCT) stars. Similarly, the commonly accepted limit of 5 c/d (Grigahcène et al. 2010) that differentiates γ Dor (GDOR) and DSCT stars can be questionable, since DSCT frequencies can appear below this limit and GDOR frequencies can be above 5 c/d (Grigahcène et al. 2010).

Lastly, our limited understanding of the physics behind stellar variability does not allow for precise constraints on the physical limits of different physical mechanisms. These limits, in addition, cannot be generalised and are different for every particular star. For example, the position of the empirical DSCT instability strip (IS) borders is different from the theoretical limits, and there are non-pulsating stars inside the IS and pulsating stars outside this region (see figures in e.g. Murphy et al. 2019; Antoci et al. 2019).

The identification and classification of variable stars is a complex task, as there are many factors that can affect the accuracy of automatic classification using modern computational methods (e.g. Audenaert et al. 2021; Audenaert & Tkachenko 2022). Additional information, such as multi-colour photometric, spectroscopic, and astrometric observations, are often needed to ensure reliable classification. In a recent study by Skarka et al. (2022, hereafter S22), they discussed the challenges of identifying and classifying bright A-F stars in the northern TESS continuous viewing zone (CVZ) based on TESS photometric data. We proposed a conservative classification scheme and compared the results with previous studies.

This paper presents a similar analysis for A-F stars in the southern TESS CVZ, using the same criteria and methods as the previous study. We provide conservative samples of variable stars that are suitable for follow-up spectroscopic observations with small telescopes and that can serve as a starting point for further detailed studies.

2. Sample selection and data retrieval

We used the same methodology as in S22. Initially, we selected a sample of 337798 point sources located within a 15-degree circle around the southern ecliptic pole (RA = $6^{\rm h}00^{\rm m}00^{\rm s}$, Dec = $-66°33'00''$) from the TESS Input Catalogue (TIC) v8.0 (Stassun et al. 2019). From this sample, we filtered out duplicate stars and selected only 2302 stars with a record in the SIMBAD database (Wenger et al. 2000) that have a temperature range of $6000 < T_{\rm eff} < 10\,000$ K and a brighter than 10 mag in Johnson V. The temperature distribution of the stars is shown in Table 1. Most of the stars are fainter than 8 mag (2043 stars), with only 17 stars being brighter than 6 mag.

We obtained all available data, which was processed by the TESS Science Processing Operations Center (SPOC; Jenkins et al. 2016) and the quick-look pipeline (QLP; Huang et al. 2020a,b), using the LIGHTKURVE software (Lightkurve Collaboration 2018; Barentsen & Lightkurve Collaboration 2020). We extracted the pre-search data conditioning simple aperture photometry (PDCSAP) flux with long-term trends removed (Twicken et al. 2010) and transformed the normalised flux to magnitudes. We did not apply any additional de-trending or data filtering to preserve possible variability.

Table 2. Statistics of the analysed datasets.

	SC SPOC	LC SPOC	QLP
Stars	1978	2249	2302
med Pts	202441	48078	53095
Sect	1–26	1–26	4–26
med Sect	13	23	23
TS (d)	22–1064	24–1064	296–1064
med TS (d)	901	1064	1064

Notes. The 'Stars' column gives the number of stars, 'med Pts' gives the median of points, 'Sect' gives the range of available sectors, 'med Sect' gives the median of available sectors, and 'TS' and 'med TS' are the time span of the data and its median, respectively.

However, it was not possible to download data from all observed sectors for some stars using LIGHTKURVE. Therefore, for some stars, only one sector was available, despite them being observed in multiple sectors. We analyzed data from cycles 1 (sectors 1–13) and 3 (sectors 27–39) in this paper. The SPOC routine provided 2-minute and 20-second cadence data (SC) for cycles 1 and 3, respectively, and 30- and 10-minute cadence data (LC) for cycles 1 and 3, respectively. The QLP routine only provided LC data.

Table 2 presents an overview of the available datasets in different routines and their statistics. It is clear from the table that data for all the sample stars are available in QLP, while SC SPOC data are missing for more than 300 stars. The data from more than 20 sectors are available for most of the stars in SPOC LC and QLP routines, whereas about half of the stars have SC data in only 13 sectors. Additionally, the LC routines generally provide a larger time span than is available for the SC data.

3. Classification of the variable stars

We followed the same approach discussed in S22, mainly in their sects. 3 and 4. The QLP data products have improved since the publication of S22 and are of comparable quality to the SPOC LC data. However, we used QLP data only when no SPOC data were available. The LC SPOC and QLP data contain various artificial signals and they provide only integrated brightness over a longer period, significantly reducing the amplitude of fast variations. Therefore, we used SPOC SC data whenever possible for the analysis. We used SPOC LC and QLP data only when there was a lack of SC data or when we needed to complement SC data with data having a longer time base.

We carefully examined each light curve, analyzing the most prominent frequency in the frequency spectrum, and the overall characteristics of the frequency peaks, including their position, content, and morphology. Our classification system is based on the criteria described in detail in tables 2–4 in S22. For a better orientation among the variability types used in this work, we give their basic description in Table 3.

In cases where it was difficult to determine the variability type, but the star was clearly variable, we designated it as 'VAR'. These stars typically exhibit probable harmonics (which can include eclipsing binaries, ROT, ROTS, ELL, ROTM, RRL, etc.) and additional peaks with unclear nature (panels d-h in

Skarka, M., and Henzl, Z.: A&A, 688, A25 (2024)

Table 3. Description of variability types used in this work together with the basic light-curve and frequency spectra characteristics.

	Binarity	
ECL (eclipsing binary of unclear type)	Apparent minima	Harmonics of the basic frequency
EA, EP (Algol type, exoplanet)	Constant light in maximum, clearly defined minima	Many well defined harmonics of the basic frequency
EB (β Lyr type)	Variation in maximum light, well defined minima	Many well defined harmonics of the basic frequency
EW (W UMa type)	Smooth brightness variations	Well defined harmonics of the basic frequency
ELL (ellipsoidal variables)	Regular, smooth brightness variations	One or two harmonics of the basic frequency
	Rotation	
ROTM (magnetic rotators)	Regular, smooth brightness variations	A few harmonics of the basic frequency
ROTS (Solar-like rotator)	Semi-regular variations	Unresolved peaks close to harmonics of the basic frequency
ROT (non-specified rotator)	Repeating stable features	A few harmonics of the basic frequency
	Pulsations	
RRL, DCEP (RR Lyr, Cepheids)	Fast rise to maximum, large amplitude	A few harmonics of the basic frequency
GDOR (γ Dor, g-mode pulsators)	(ir)regular variations, beating, bumps	two and more independent peaks below 5 c/d
DSCT (δ Sct, p-mode pulsators)	(ir)regular variations, beating, bumps	two and more independent peaks above 5 c/d

Table 4. Classification of stars in our sample.

TIC	RAJ2000	DEJ2000	CR	Blends	Type	V (mag)	$T_{\rm eff}$ (K)	L ($L_\odot$)
25078674	60.18200711	–71.16679809	0.0002	0	VAR	6.60	9150	26.3
25117240	61.65684312	–69.26155744	0.3208	2	GDOR	9.40	6743	15.4
25117273	61.38801709	–69.40047833	0.0005	0	DSCT+LF	9.52	7175	10.4
25117406	61.51260808	–69.87130832	0.0006	0	DSCT+GDOR	7.45	7231	36.7
25117492	61.58357233	–70.24478618	0.0015	1		9.80	8197	17.3
25118797	61.93961418	–69.05238972	0.5487	1		9.86	6122	3.4
25132222	62.00132424	–68.36099381	0.0105	0		9.73	6064	3.3
25132314	62.12780124	–68.70223768	0.0006	0	GDOR	8.38	6867	7.1
25133052	62.13967593	–71.63984666	0.0016	2		8.64	6315	2.7
25153007	62.8648749	–70.73842226	0.0024	0	ROT	9.22	7109	5.3
...	...	...	...	...	...	...	...	...

Notes. The full table that is available at CDS. The 'CR' column gives the contamination ratio (Paegert et al. 2021). 'Blends' gives the number of stars with a magnitude difference less than 5 mag from the target stars. Values of V, $T_{\rm eff}$, and L are taken from Stassun et al. (2019).

Fig. 1). Some VAR stars display a single peak or low-frequency (0-0.5 c/d) and low-amplitude (<0.1 mmag) peaks that may be of instrumental origin. Some of the stars classified as STABLE (panels a–c in Fig. 1) can be VAR in fact, but the decision about the variability and/or the true source of variability was impossible either due to the small amplitude of the variations (mostly apparent only in the Fourier transform) or due to the number of contaminants. The complete classification is provided in Table 4.

3.1. Stars with well-defined equidistant peaks

Periodic variations associated with rotation (ROT, ROTM, and ROTS classes), orbital motion (EA, EB, EW, ELL), or non-sinusoidal pulsations (e.g., DCEP, RRL) produce peaks at the fundamental frequency and its harmonics, resulting in an equidistant pattern in the frequency spectrum. This pattern is easy to recognize. However, the classification of these variations is not straightforward.

Identifying and classifying eclipsing binaries is usually an easy task due to prominent eclipses. However, binary stars can be confused with other possible classes if the eclipses are shallow and/or deformed, and not distinct. Distinguishing non-eclipsing

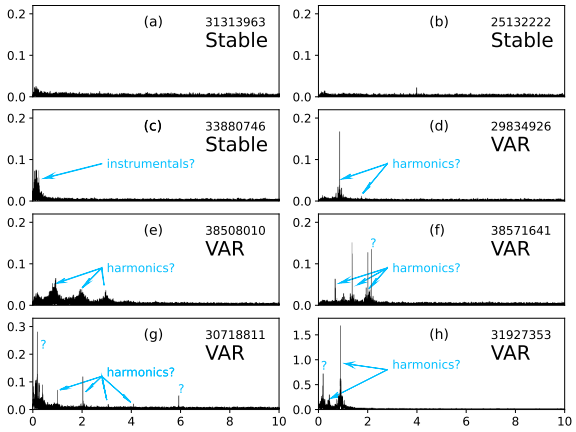

Fig. 1. Examples of frequency spectra of stable stars and stars marked as VAR with unclear classification. The horizontal axis shows frequency in c/d, while the vertical axis shows brightness in mmag. The numbers given in the labels are the TIC numbers.

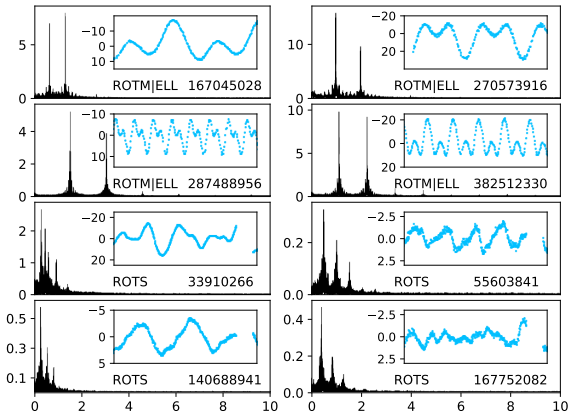

Fig. 2. Examples of rotationally variable stars. The horizontal axis shows frequency in c/d, while the vertical axis shows brightness in mmag. The insets show the data in 5 days (four upper panels) and 10 days, respectively. The numbers given in the labels are the TIC numbers.

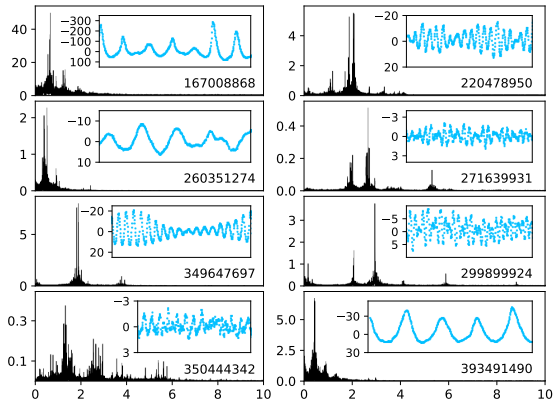

Fig. 3. Examples of GDOR stars. The horizontal axis shows frequency in c/d, while the vertical axis shows brightness in mmag. The insets show the data in 10 days. The numbers given in the labels are the TIC numbers.

binary stars with tidally deformed components (ellipsoidal variables and contact binaries) from spotted chemically peculiar stars ('ROTM' class) based on single-channel TESS photometry can be an extremely difficult task, as is discussed in S22. Both classes show a dominant frequency and usually one well-defined harmonic in the frequency spectrum (see the four upper panels of Fig. 2). The contamination of ellipsoidal (ELL) stars from ROTM stars is likely not too high because the incidence rate of spotted chemically peculiar stars of Ap type is small, only about 10% among the A-spectral type stars (Sikora et al. 2019b).

The light curves of ELL stars can be distorted by various effects like Doppler beaming, reflection effects, and spots (Faigler & Mazeh 2011). Therefore, we decided to use a more conservative approach and classify such stars as 'ROTM|ELL', instead of distinguishing between ROTM (rotational modulation) and ELL. In the example shown in Fig. 2, only TIC 270573916 is an ELL star with high probability. To make a final decision between ROTM and ELL classes, spectroscopic observations are necessary. In a study by Green et al. (2023), only 50% of 97 suspected ellipsoidal variables showed clear radial velocity variations upon spectroscopic observation, indicating possible contamination with spotted stars. We have also included stars that exhibit apparent simple variability with a single peak in the frequency spectrum to the ROTM|ELL class.

It is important to note that there can be confusion between rotation and pulsations in stars that exhibit temperature spots similar to our Sun. These stars belong to a category called 'ROTS' and their frequency spectra can be similar to GDOR pulsators. Active stars of the solar type show groups of peaks around harmonics with rotational frequency due to differential rotation. In Fig. 2, the four bottom panels show typical examples of such stars with TIC 33910266 being a bit questionable, showing five harmonics with gaps at $4f_{\rm rot}$ and $6f_{\rm rot}$.

Stars that exhibit sharp, isolated peaks and their harmonics in the frequency spectra, which cannot be classified accurately, are categorised as 'ROT'. These stars can be of various types such as ELL, ROTM, ROTS, RRL, DCEP, eclipsing binaries, and others that display equidistant frequency peaks. Therefore, the classification of 'ROT' stars should be considered only as preliminary and rough, similarly to stars in the VAR class. The frequency spectra of VAR stars shown in panels f–h in Fig. 1 can be considered as belonging to the ROT class.

Rotationally variable stars can be false positives because their light can be contaminated by the light of far-away large-amplitude pulsating stars (for example, RR Lyr and Cepheids) or eclipsing binaries. Such stars and systems can have periods of variations similar to rotational periods of A-F stars and show harmonics in their frequency spectra. In cases of contamination, the amplitude and number of detectable harmonics are strongly reduced. Examples of the contaminants are discussed in Sect. 3.3.

3.2. Pulsating stars

Assigning a star with GDOR (gravity-mode, g-mode pulsators), DSCT (pressure-mode, p-mode pulsators), GDOR+DSCT, and DSCT+GDOR (hybrid pulsators) classes can also be challenging task. The first difficulty arises with the definition of the GDOR class, specifically concerning the frequency content and pattern in the frequency spectra. The gravity-mode pulsations of GDOR stars are excited by the convective flux blocking mechanism (Guzik et al. 2000; Dupret et al. 2005). This type of pulsation does not produce equally spaced structures in the frequency domain (harmonics are possible). The GDOR frequencies are usually between 0.3 and 3 c/d (Kaye et al. 1999; Henry et al. 2011), with the most likely position being approximately 1.2–1.3 c/d (see Fig. 1 in Tkachenko et al. 2013). However, when shifted by the rotation, the frequencies can reach up to five cycles per day or even more (Grigahcène et al. 2010). The usually accepted limit to distinguish between g-mode and p-mode pulsators is 5 c/d (Uytterhoeven et al. 2011), but other limits, such as 4 c/d (Antoci et al. 2019), are also being utilised.

The frequency pattern that is characteristic for the GDOR stars is a comb of close, sometimes unresolved, peaks (for example, Balona et al. 2011; Uytterhoeven et al. 2011; Tkachenko et al. 2013, our Fig. 3) that can also be found around harmonics (see Fig. 3 in Saio et al. 2018, and our Fig. 3). This can cause confusion with spotted solar-type stars, which is best apparent in TIC 393491490 in the bottom right panel of Fig. 3. On the other hand, the peaks can also be randomly distributed (e.g., Uytterhoeven et al. 2011; Balona et al. 2011, and TIC 350444342 in the bottom left panel of Fig. 3). We classified stars as GDOR

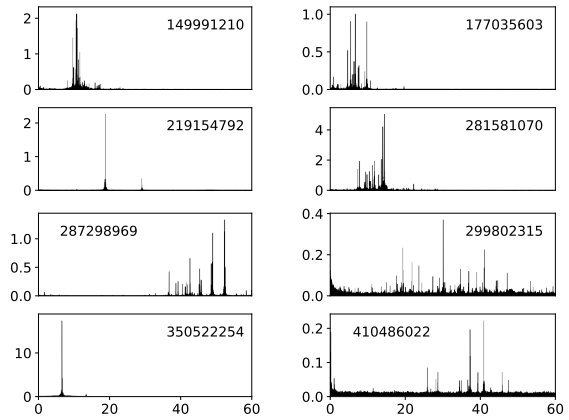

Fig. 4. Examples of frequency spectra of DSCT stars. The horizontal axis shows frequency in c/d, while the vertical axis shows brightness in mmag. The numbers given in the labels are the TIC numbers.

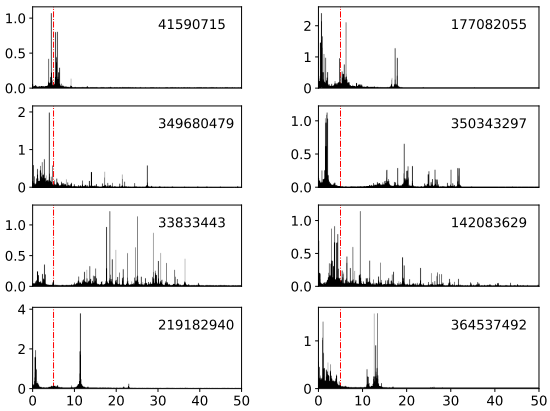

Fig. 5. Examples of frequency spectra of hybrid GDOR+DSCT stars. Frequency on the horizontal axis is in c/d, while brightness on the vertical axis is in mmag. The numbers given in the labels are the TIC numbers. The upper four panels show GDOR-dominating hybrids, while the bottom four panels show DSCT-dominating hybrids. The vertical dash-dotted red lines indicate 5 c/d.

when several peaks were present in the range of approximately 0.3–5 c/d. At the same time, the frequency pattern did not comply with the requirements for rotationally variable stars (see Sect. 3.1). In addition, the amplitude of the frequency peaks has to be larger than 0.1 mmag.

It is important to note that we do not differentiate between slowly pulsating B stars (SPB stars Waelkens et al. 1998; De Cat & Aerts 2002) and GDOR stars as SPB stars are hotter and may contaminate our sample at high temperatures. Additionally, we do not distinguish between low- and high-amplitude GDOR stars (HAGDOR, Paunzen et al. 2020) because the boundary between the two is not well defined, and amplitudes in TESS data may not be reliable due to contamination and data processing. TIC 167008868 is an excellent candidate for HAGDOR (top left panel of Fig. 3) with one of the largest peak-to-peak amplitudes ever observed in HAGDOR (about 0.4 mag in TESS pass band, SPOC routine).

The second important class of pulsating stars among A-F spectral type stars are DSCT pulsators. The pulsations in these low-radial-order p-mode pulsators are excited by the κ mechanism operating in the HeII ionisation zone and by turbulent pressure (Breger 2000; Antoci et al. 2014). As was already mentioned, five cycles per day are usually taken as the border between GDOR and DSCT pulsations (Uytterhoeven et al. 2011). However, some authors use 4 c/d (Antoci et al. 2019). The upper limit is also not firmly defined. Balona (2022) state that there is no sharp transition between roAp (Kurtz 1982) and DSCT stars and that the roAp class should be dropped. In fact, DSCT and roAp stars are different objects and such a comparison concerns only the frequency content (Holdsworth et al. 2024). Nevertheless, we mark a star as a DSCT pulsator if it shows at least one strong peak above 5 c/d. Due to the faster cadence in cycle 3, the Nyquist reflections are not a significant problem, since the Nyquist frequency is 72 c/d, which is well above the dominant frequency for most of the DSCT stars.

The variety of DSCT frequency spectra has been shown many times (e.g. Grigahcène et al. 2010; Uytterhoeven et al. 2011). Examples of frequency spectra of DSCT stars in our sample are in Fig. 4. We can see stars with a single dominant pulsation mode (e.g. TIC 350522254) and stars with a comb of peaks (e.g. TIC 149991210), but also stars with peaks across the whole frequency range (e.g. TIC 299802315).

Ultra-precise space observations revealed that basically all DSCT and GDOR stars show peaks in both regimes (Grigahcène et al. 2010; Uytterhoeven et al. 2011; Balona 2014). Balona (2014) also showed that most of the low frequencies observed in DSCT stars cannot be explained by the non-linear combination of the DSCT modes and by rotation. Thus, the vast majority of stars showing peaks in both DSCT and GDOR regimes are likely hybrids.

The only situation in which it is difficult to identify hybrid pulsators is in stars in which the amplitudes of the frequency peaks are different or the frequency content is poor and the frequency peaks cannot be properly interpreted. There is no commonly accepted amplitude threshold specifying that a particular star is a pure GDOR or DSCT pulsator or a hybrid. The ratio of the amplitudes in both regimes used by Uytterhoeven et al. (2011) and Bradley et al. (2015) are only empirical thresholds (a factor of 5–7 in the amplitude ratio) not saying anything about the hybrid nature. In addition, each author uses a different amplitude limit to consider the frequencies for the classification. All of the mentioned problems add ambiguity to the classification.

As each dataset is unique, we did not adopt any amplitude threshold because even peaks in the sub-mmag regime can be significant. We cannot avoid mixing hybrids with pure DSCT or GDOR stars showing combination peaks without detailed frequency analysis, which is out of the scope of this paper. However, this will be the case in only a minority of stars. For instance, TIC 177035603 (top right-hand panel of Fig. 4) can be classified as a hybrid pulsator with a similar probability as pure DSCT. Similarly, TIC 350444342 in the bottom left panel of Fig. 3 can be also considered as a hybrid pulsator, not a pure GDOR star. Examples of frequency spectra of hybrid pulsators are shown in Fig. 5. The least reliable classification among the shown stars is in TIC 41590715 because the peaks are grouped around 5 c/d and the classification can be all of pure GDOR, pure DSCT, or hybrid pulsator. We give 'DSCT+LF' classification to more than 60% of the DSCT stars showing low-amplitude peaks below 5 c/d meaning DSCT stars with low-frequency (LF) peaks with unclear interpretation. Some of these stars can be hybrid stars, but some can also be rotationally variable.

3.3. Contamination and identification issues

The southern TESS CVZ includes the Large Magellanic Cloud (LMC), where many stars are strongly affected by contamination. This is especially problematic due to the low angular resolution of TESS, which is 21 $''$ px^{-1} (Ricker et al. 2015). Contamination can cause several issues such as distortion of the light curve, mixing of variability, and a decrease in the brightness amplitude. The new data releases of *Gaia* catalogues (Gaia Collaboration 2018, 2023) led to the identification of redundant entries in the TICv8.0 catalogue (Stassun et al. 2019). In TICv8.2, Paegert et al. (2021) identified 'phantom' stars, which arise from diffraction spikes around bright stars, mismatches between different catalogues, and from a combination of two or more fainter stars mimicking one target.

We have found 13 such duplicate entries in our sample by comparing TIC8.0 and TIC8.2 catalogs. The numbers of the duplicates are followed with a 'p21' suffix in the 'Type' column of Table 4. We also adopted the contamination ratio from Paegert et al. (2021) in column CR, which gives the ratio of contaminating flux and flux of the target star. Furthermore, we have cross-matched the positions from TIC8.0 with the *Gaia* DR3 catalogue (Gaia Collaboration 2023) within a distance of 105$''$ (5 px). The number of blending stars with a magnitude difference less than 5 mag from the target star is given in the 'Blend' column of Table 4. This information can at least help to identify problematic targets. The most contaminated target is TIC 372913472, which has 13 contaminants. Automatic procedures for identifying the true source of the variation signal (e.g., Higgins & Bell 2023) are not effective in our case, as they do not work well with a single frequency. Therefore, each target would require a detailed investigation of the frequency spectrum to get reliable and unambiguous results, which is beyond the scope of this paper.

We also compared the strongest identified frequencies of categorised stars and visually examined the frequency content to identify any obvious contaminants. We considered a star with a larger amplitude peak as the real variable, while the other star with the same frequency but lower amplitude was deemed a duplicate contaminated by the variable star. In Table 4, we provide the TIC number of the real variable (the contaminant) in the 'Type' column. There are 20 such cases.

It is important to note that there may be nearby large-amplitude variables, such as eclipsing binaries or Cepheids, located just a few pixels away from the target star. Even when the brightness difference is quite large (more than 5 mag), these variables can contaminate the light of the target and cause false identification of variability. Two examples of this are TIC 358460464 and TIC 277293156, as is shown in Fig. 6. The contaminants are approximately 3 and 2 pixels away from TIC 358460464 and TIC 277293156, respectively. Additionally, the contaminants are 6.2 and 7.3 mag fainter than their respective target stars.

The contaminant of TIC 358460464 is an EW ASAS-SN J075559.67-644238.3, which is a 15.2-mag star. Only the second and third harmonics of the orbital frequency are apparent in the frequency spectrum of TIC 358460464; thus, we classified it as DSCT (top panel of Fig. 6). On the other hand, three harmonics of the pulsation frequency of ASAS-SN J053737.66-702553.4 (DCEP star, 15.62 mag) are apparent in the frequency spectrum of TIC 277293156 (bottom panel of Fig. 6), which makes it belong to the ROT category.

In both cases, the classification is wrong, although the contamination ratio is as low as 0.34% in TIC 358460464 (in TIC 277293156 it is 10%). Such wrongly identified stars add noise to the statistics when investigating common characteristics of the stars in particular variability classes. After this finding, we cross-matched our sample with the *Gaia* DR3 variable star catalogue (Rimoldini et al. 2023) and ASAS-SN variable star catalogue (Jayasinghe et al. 2018) within a 100 arcsecond (5 px) radius and compared the frequencies (and their harmonics) from the catalogues with frequencies identified by us. This helped us to identify 12 contaminants (Table 5), which are typically eclipsing binaries and pulsating stars. We have therefore classified our contaminated stars mostly as eclipsing binaries, DSCT and VAR. Such stars are marked with an additional '-C' in the column type in Table 4.

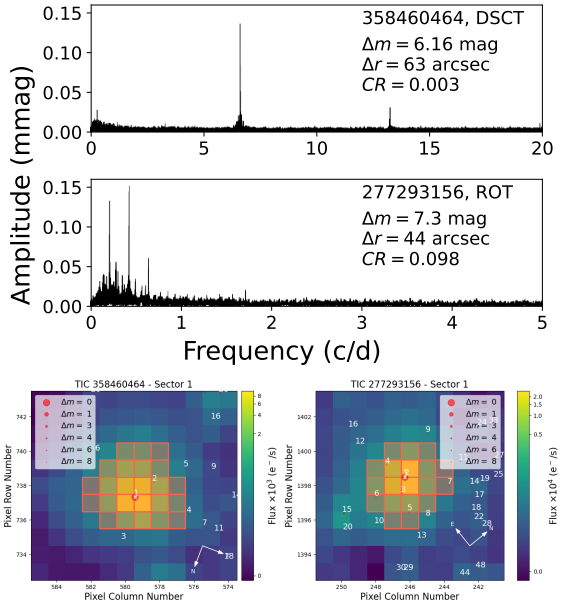

Fig. 6. Two identified variable stars that are actually not variable, the light of which is contaminated by nearby stars. The numbers show the TIC identification, variability type, magnitude difference (Δm) between the contaminant and target star, distance of the target from the contaminant (Δr), and the contamination ratio (CR). In the charts generated with TPFPLOTTER (Aller et al. 2020) in the bottom part of the figure, the contaminating stars are numbers 4 and 6 in the left- and right-hand panels, respectively.

This exercise underscores the risks of misidentifying and misclassifying variable stars, which is far more common than we previously realised. In the *Gaia* DR3 variable star catalogue, only 20% of stars in the vicinity of our target stars have had their frequencies determined. Identifying the true variable star is further complicated by the fact that there may be multiple stars within 100 arcseconds of the target (we only considered the brightest one). Additionally, bright stars can contaminate the light from even larger distances than 5 pixels. As a result, we can expect the number of contaminants to be much larger than the 12 cases we list in Table 5.

Finally, there is high probability that many of the sample stars are bound in physical binary or multiple systems. In such cases, the observed variability is a combination of variability of system components. This can also lead to misclassification of the variability type.

Table 5. Identification of the contaminating stars.

TIC	Type	G (mag)	Type-Cont	ID ASAS-SN	ID *Gaia* DR3	Δr (arcsec)	Δm (mag)	$f_{\rm TESS}$ (c/d)	$f_{\rm Literature}$ (c/d)
30469454	VAR	9.7	EW	J045847.67-661118.7		85.0	4.1	0.7569	1.5138
141484981	DSCT|EW	9.3	EW	J054857.15-733629.1	4650219988274730000	62.4	5.0	2.9631	5.9262
177022232	DSCT|EW	8.8	EW	J064932.91-674043.5	5281603511044130000	64.7	7.0	3.6288	7.2574
260127863	DSCT+LF	9.9	EW	J060839.75-582809.0	5494885264769510000	75.8	4.5	3.5486	7.0970
260160453	VAR	7.9	ECL		5482506511890750000	67.7	5.4	1.6843	3.3685
308538268	VAR	9.0	EW	J080338.45-603047.4	5290787834752610000	77.4	4.7	2.2401	4.4810
340312485	VAR	8.9	EW	J073934.70-595741.0		50.2	5.8	4.4852	8.9682
349647697	GDOR	8.8	RRC	J072849.42-643817.6		78.5	7.5	3.6138	1.8951
358460464	DSCT+LF	9.0	EW	J075559.67-644238.3	5275843994260360000	62.8	6.2	3.3086	6.6174
358465355	EB	9.6	EB	J075605.94-601606.3	5290937849368120000	48.9	4.5	1.7528	3.5050
372911993	DSCT+GDOR	9.0	ECL		5289793459627240000	51.3	5.6	2.8177	5.6355
410452496	VAR	9.6	EW	J075944.49-612807.4	5289891938931840000	85.9	4.5	2.3923	4.7846

Notes. The 'Type-Cont' column gives the type of the contaminant from literature. If both ASAS-SN and *Gaia* DR3 designations are given, the contaminant was known to both ASAS-SN and *Gaia* DR3 variable stars catalogues (Jayasinghe et al. 2018; Rimoldini et al. 2023).

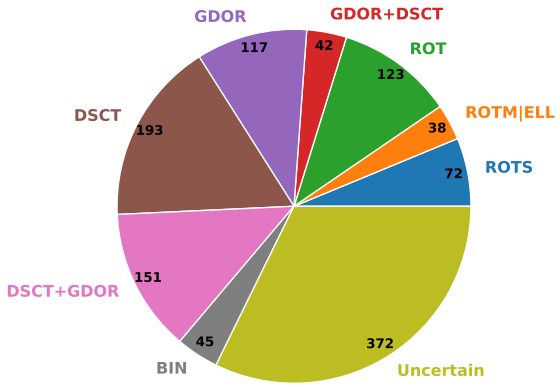

Fig. 7. Types of stars identified in our sample.

4. Results and discussion

We have found that 50.9% of the 1171 stars in our sample (excluding 33 duplicates) show clear variability. This is in agreement with the percentage of variable stars in the northern TESS CVZ (51%, S22). We were able to determine the type of variability in 67.2% of the stars, which is a better performance than in S22, in which only 60% of stars were unambiguously classified. Remaining 372 variable stars were unclassified[1]. The higher number of data points, longer time span, and increase in the number of sectors observed may have contributed to our better performance in classifying the stars.

The numbers of the classified variable stars are shown in Fig. 7. We have identified a total of 503 pulsating stars, which includes DSCT, GDOR, and their hybrids plus one RRAB star (43% of the variable stars). This count is about 22% less than that of the northern TESS CVZ (S22). We can only speculate about the reasons for the discrepancy.

The diagram in Fig. 8 shows that DSCT and hybrid stars are evenly distributed throughout the empirical IS from Murphy et al. (2019). Pure GDOR stars, on the other hand, are clustered within the theoretical GDOR IS from Dupret et al. (2005), although they can also be found across the entire temperature range. At the hotter end of the scale, GDOR and DSCT stars are likely to mix with SPB and β Cep stars.

As was expected, the ROTS stars are found at the lowest temperatures between 6000–7000 K, while ROTM|ELL stars

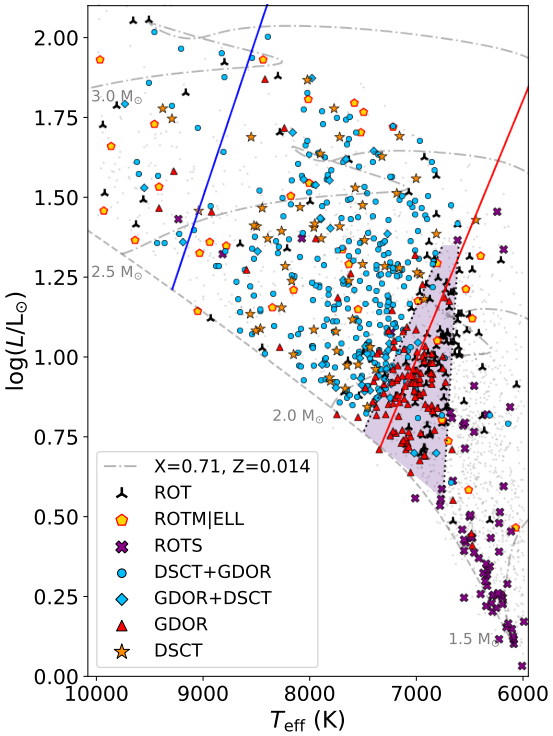

Fig. 8. Hertzsprung-Russell diagram showing our categorised stars. The dashed line shows the zero-age main sequence, while the evolutionary tracks are shown with the dash-dotted lines. The empirical boundaries of the DSCT IS are shown with continuous blue and red lines. The ZAMS, evolutionary tracks, and IS boundaries are taken from Murphy et al. (2019). The GDOR instability region (Dupret et al. 2005) is shown with the shaded area limited by the dotted lines. All the stars in our sample including non-variable stars are shown with grey dots.

[1] Considering ROTM|ELL stars as categorised stars.

are spread out across the entire temperature range. This indicates that the population of ROTM|ELL is a mix of ELL and ROTM stars. The ROT stars tend to prefer temperatures around the cooler GDOR edge but can also be found spread out up to 10000 K, similar to the distribution found in S22.

We cross-matched our sample with other catalogues within a distance of 21″ (1 px) from our targets to compare the classifications. We used TOPCAT (Taylor 2005) and CDS X-Match service (Boch et al. 2012; Pineau et al. 2020) to cross-match the catalogues. We can use two parameters describing the agreement of the two catalogues. The first parameter is the classification agreement percentage (CAP), which gives the percentage of stars with the same classification in both catalogues. The second parameter is the detection agreement percentage (DAP), which gives the fraction of stars identified and classified as VAR and other variability types in our sample while being assigned with the same variability type or as VAR in the other catalogue.

For instance, if we classify a star as DSCT and the catalogue identifies it as VAR (and vice versa), it will count towards DAP. However, if we classify a star as DSCT and the catalogue identifies it as EW, it will not count. Similarly, if the catalogue gives a variability type, and we do not detect any variability, it will not count. The DAP is useful in reflecting the uncertainty in the classification, as it gives the chance of the classification being correct in at least one of the compared catalogues.

There are 97 sample stars present in the VSX catalogue (Watson et al. 2006). This catalogue is a compilation of variable stars identified in various sky surveys and projects but also by individual observers (for example, NSVS (Woźniak et al. 2004), ZTF (Chen et al. 2020), and the CzeV catalogue (Skarka et al. 2017)). However, only 85 of these 97 stars have been categorised. In 15 of the VSX-declared variables, we did not notice any variation. Of the remaining 82 stars that have been classified in the VSX catalogue, we agree with the classification of only 26 stars (32%). The CAP for our classification and VSX is, therefore, 26 out of 97 (27%).

We show examples of where our classification differs from that of the VSX catalogue in Fig. 9. Specifically, we have classified TIC 31925242 (CR Hyi) as a GDOR variable, whereas it is classified as ELL in the VSX catalogue (see the top panel of Fig. 9). Similarly, TIC 350522254 (XY Pic) is classified as DSCT by us[2], while it is classified as EW in the VSX catalogue. The data of TIC 350522254 show a beating caused by the presence of two close frequencies at about 6.7 c/d (Fig. 9). For the VSX catalogue, the DAP is 77%.

Of the 84 stars in our sample, 80 are classified as VAR in the ASAS-SN catalogue (Jayasinghe et al. 2018, 2019), while only four are categorised. Among the four categorised stars, one star is classified as GCAS (our ROTM|ELL, TIC 348898673, see Fig. 9), and another star is listed as ROT (our EA, TIC 349480507). However, we did not detect any variation in the remaining two stars that should be classified as GCAS according to Jayasinghe et al. (2018, 2019). Furthermore, we did not detect variation in nine of the declared variable stars. It is worth noting that there is no agreement between our classification and the ASAS-SN catalogue (CAP = 0%). The DAP for our classification and the ASAS-SN catalogue is 85%, but this is only because most of the stars are labelled as VAR in the ASAS-SN catalogue.

We crossmatched our sample of stars also with the *Gaia* DR3 variables (Rimoldini et al. 2023) within a 21″ radius, and found 219 entries for our stars[3]. The CAP parameter is 48%, while the DAP is 57%. The high value of CAP is because most stars in our sample have a broad variability type classification in Rimoldini et al. (2023). For example, *Gaia* DR3 classification ACV|CP|MCP|ROAM|ROAP|SXARI complies with our ROT, ROTS, ROTM|ELL stars, SOLAR LIKE complies with our ROTS, ROT and ROTM|ELL classes, DSCT|GDOR|SXPHE complies with our GDOR, DSCT and their hybrid classes. We found no variability in 35 stars declared as variables in Rimoldini et al. (2023).

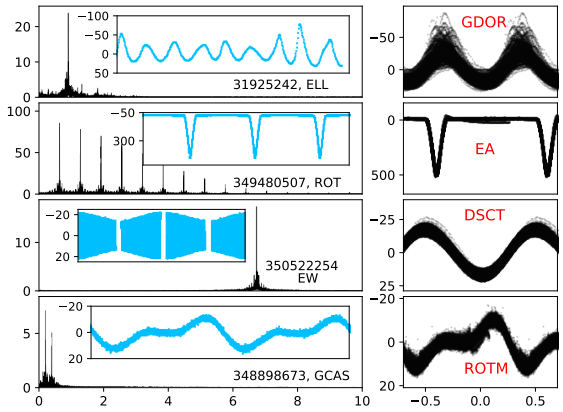

Fig. 9. Stars with incorrect classification in the catalogues. The left panels show the frequency spectra with the part of the time series (the catalogue classification is given together with the TIC number), while the right-hand panels show the data phase-folded with the dominant frequency together with the correct variability type.

In their study, Fetherolf et al. (2023) created a comprehensive list of variable stars from the TESS prime mission by searching for periodicity and variability using the Lomb-Scargle periodogram (Lomb 1976; Scargle 1982). Since we used the same data and analysis method, we expected to obtain similar results. Our sample overlapped with 1141 stars from Fetherolf et al. (2023) catalogue, including 16 duplicates and nine false positives (stars that were blends with faint large-amplitude variables). Unfortunately, Fetherolf et al. (2023) did not provide a classification of the variable stars, so we could only calculate the DAP, which was only 63%. Most of the stars that we disagreed on did not exhibit apparent variability and displayed low-frequency peaks similar to those shown in panel c of Fig. 1. The frequencies of variable stars found by Fetherolf et al. (2023) perfectly matched with frequencies found by us (including our VAR stars). However, in stars that we marked as stable, the frequencies identified by (Fetherolf et al. 2023) differed from the frequencies identified by us. This is an additional argument against assigning these stars as variable.

Forty-four stars from our sample are listed in the binary-star catalogue by Prša et al. (2022). However, we classified three of them not as eclipsing binaries but as ROTM|ELL (TIC 382512330, 306578324, and 141127435) and TIC 142148228 and 150187916 as VAR stars. The CAP and DAP with Prša et al. (2022) are both 89%. This result is no surprise, since variations of eclipsing binaries are characteristic and usually have large amplitudes.

[2] The variability type DSCT of XY Pic was already discussed by Dall (2005).

[3] By omitting three stars that are apparent blends with other stars in our sample.

Table 6. Agreement (1st column) in per cent of our classification with the large catalogues and dedicated studies.

CAP/DAP (%)	Type	Catalogue
27/77	General	VSX (Watson et al. 2006)
0/85	General	ASAS-SN (Jayasinghe et al. 2018)
48/57	General	*Gaia* DR3 (Rimoldini et al. 2023)
–/63	General	TESS PM (Fetherolf et al. 2023)
89/89	Binaries	(Prša et al. 2022)
55/55	ROT	(Sikora et al. 2019b)
83/83	DSCT	(Antoci et al. 2019)

Regarding rotational variable stars, 29 stars from our sample appear in Sikora et al. (2019a). The variations are connected with rotation or orbital motion in only 16 of them. The rotational nature of the other 13 stars is ambiguous. The CAP and DAP are both 55%.

Twelve of our sample stars are listed in Antoci et al. (2019), which deals with DSCT stars. Nine of them were also identified as DSCT (or hybrids) by us, and one of the stars was found to be constant in agreement with Antoci et al. (2019). In TIC 260416268, which was identified as a rot/binary Am star by Antoci et al. (2019), we detected no variability. The same applies to the roAp candidate TIC 238185398. The CAP and DAP are both 83%.

The discrepancies between our results and results from literature arise from the superior characteristics of the TESS data compared to other catalogues meaning better precision, cadence, and often also time span. The agreement in classification with previous studies and catalogues is summarised in Table 6.

5. Conclusions

We carefully classified variable stars using data from TESS from cycles 1 and 3. This data is useful for detecting fast variations, such as DSCT pulsations, as well as variations that occur over several days. We discussed the limitations of our classifications, including the general shortcomings in variable stars classification. Furthermore, we compared our results with existing databases and variable star catalogues.

We confirm the previous issues with the classification of rotationally variable stars and hours- to days-long pulsations of GDOR type. It is also often difficult to distinguish between ellipsoidal and/or contact binary variables and spotted stars without additional information. Additionally, the classification can be influenced by nearby stars, and the level of contamination depends on the distance of the contaminating star, the amplitude of variations, and the difference in brightness. This mainly affects the classification of rotationally variable stars and stars that show a combination of different types of variation.

We found intriguing discrepancies in the classification in variable stars catalogues that can be up to 100%. To address this issue, we have introduced two parameters - CAP and DAP. The CAP reflects the classification, while the DAP concerns the detection of variability without a specific variability type. Our results show that we have a relatively good agreement with the *Gaia* catalogue (CAP = 48% Rimoldini et al. 2023). The best agreement is with the studies dedicated to particular variability types. For instance, the agreement of our classification is almost 90% with the database of eclipsing binaries (Prša et al. 2022) and 83% in the case of DSCT variables (Antoci et al. 2019). Surprisingly, the agreement of our results with a study by Fetherolf et al. (2023), which is also based on the TESS data, is only 63%. We have also demonstrated that large-amplitude variables can contaminate the light of the target stars up to 100 arcseconds from the star, which can lead to incorrect identification and classification.

It has been shown that classifying variable stars is a complex task and may produce ambiguous or incorrect results. It is not advisable to blindly use samples of variable stars without individually checking each star. This is especially important in the usage of samples based on automatic classifiers. To create reliable catalogues of variable stars, it is necessary to analyze not only single-channel photometric observations but also multi-colour and spectroscopic observations, and to estimate reddening and distance. Additionally, one must be very careful in handling contamination. Only then can we be confident that the variations of specific objects are caused by the proposed effect(s).

The first *PLATO* mission field (LOPS2, Nascimbeni et al. 2022) will include the southern TESS CVZ. Our classification represents a good starting point for studies of stellar variability in the *PLATO* field.

Acknowledgements. M.S. acknowledges the support by Inter-transfer grant no LTT-20015. This paper includes data collected with the TESS mission. Funding for the TESS mission is provided by the NASA Explorer Program. Funding for the TESS Asteroseismic Science Operations Centre is provided by the Danish National Research Foundation (Grant agreement no.: DNRF106), ESA PRODEX (PEA 4000119301) and Stellar Astrophysics Centre (SAC) at Aarhus University. We thank the TESS team and staff and TASC/TASOC for their support of the present work. We also thank the TASC WG4 team for their contribution to the selection of targets for 2-min observations. The TESS data were obtained from the MAST data archive at the Space Telescope Science Institute (STScI).

References

Aller, A., Lillo-Box, J., Jones, D., Miranda, L. F., & Barceló Forteza, S. 2020, A&A, 635, A128
Antoci, V., Cunha, M., Houdek, G., et al. 2014, ApJ, 796, 118
Antoci, V., Cunha, M. S., Bowman, D. M., et al. 2019, MNRAS, 490, 4040
Audenaert, J., Kuszlewicz, J. S., Handberg, R., et al. 2021, AJ, 162, 209
Audenaert, J., & Tkachenko, A. 2022, A&A, 666, A76
Balona, L. A. 2014, MNRAS, 437, 1476
Balona, L. A. 2022, MNRAS, 510, 5743
Balona, L. A., Guzik, J. A., Uytterhoeven, K., et al. 2011, MNRAS, 415, 3531
Barentsen, G., & Lightkurve Collaboration. 2020, AAS Meeting Abstracts, 235, 409.04
Boch, T., Pineau, F., & Derriere, S. 2012, ASP Conf. Ser., 461, 291
Borucki, W. J., Koch, D., Basri, G., et al. 2010, Science, 327, 977
Bradley, P. A., Guzik, J. A., Miles, L. F., et al. 2015, AJ, 149, 68
Breger, M. 2000, ASP Conf. Ser., 210, 3
Chen, X., Wang, S., Deng, L., et al. 2020, ApJS, 249, 18
Dall, T. H. 2005, Information Bull. Variable Stars, 5617, 1
De Cat, P., & Aerts, C. 2002, A&A, 393, 965
Dupret, M. A., Grigahcène, A., Garrido, R., Gabriel, M., & Scuflaire, R. 2005, A&A, 435, 927
Faigler, S., & Mazeh, T. 2011, MNRAS, 415, 3921
Fetherolf, T., Pepper, J., Simpson, E., et al. 2023, ApJS, 268, 4
Gaia Collaboration (Brown, A. G. A., et al.) 2018, A&A, 616, A1
Gaia Collaboration (Vallenari, A., et al.) 2023, A&A, 674, A1
Green, M. J., Maoz, D., Mazeh, T., et al. 2023, MNRAS, 522, 29
Grigahcène, A., Antoci, V., Balona, L., et al. 2010, ApJ, 713, L192
Guzik, J. A., Kaye, A. B., Bradley, P. A., Cox, A. N., & Neuforge, C. 2000, ApJ, 542, L57
Henry, G. W., Fekel, F. C., & Henry, S. M. 2011, AJ, 142, 39
Higgins, M. E., & Bell, K. J. 2023, AJ, 165, 141
Holdsworth, D. L., Cunha, M. S., Lares-Martiz, M., et al. 2024, MNRAS, 527, 9548
Huang, C. X., Vanderburg, A., Pál, A., et al. 2020a, Res. Notes Am. Astron. Soc., 4, 204
Huang, C. X., Vanderburg, A., Pál, A., et al. 2020b, Res. Notes Am. Astron. Soc., 4, 206
Iwanek, P., Soszyński, I., Kozłowski, S., et al. 2022, ApJS, 260, 46

Jayasinghe, T., Kochanek, C. S., Stanek, K. Z., et al. 2018, MNRAS, 477, 3145
Jayasinghe, T., Stanek, K. Z., Kochanek, C. S., et al. 2019, MNRAS, 485, 961
Jenkins, J. M., Twicken, J. D., McCauliff, S., et al. 2016, SPIE Conf. Ser., 9913, 99133E
Kaye, A. B., Handler, G., Krisciunas, K., Poretti, E., & Zerbi, F. M. 1999, PASP, 111, 840
Kurtz, D. W. 1982, MNRAS, 200, 807
Lightkurve Collaboration (Cardoso, J. V. d. M., et al.) 2018, Astrophysics Source Code Library [record ascl:1812.013]
Lomb, N. R. 1976, Ap&SS, 39, 447
Murphy, S. J., Hey, D., Van Reeth, T., & Bedding, T. R. 2019, MNRAS, 485, 2380
Nascimbeni, V., Piotto, G., Börner, A., et al. 2022, A&A, 658, A31
Paegert, M., Stassun, K. G., Collins, K. A., et al. 2021, arXiv e-prints [arXiv:2108.04778]
Paunzen, E., Bernhard, K., Hümmerich, S., et al. 2020, MNRAS, 499, 3976
Pineau, F.-X., Boch, T., Derrière, S., & Schaaff, A. 2020, ASP Conf. Ser., 522, 125
Prša, A., Kochoska, A., Conroy, K. E., et al. 2022, ApJS, 258, 16
Ricker, G. R., Winn, J. N., Vanderspek, R., et al. 2015, J. Astron. Telesc. Instrum. Syst., 1, 014003
Rimoldini, L., Holl, B., Gavras, P., et al. 2023, A&A, 674, A14
Saio, H., Bedding, T. R., Kurtz, D. W., et al. 2018, MNRAS, 477, 2183
Samus, N. N., Kazarovets, E. V., Durlevich, O. V., Kireeva, N. N., & Pastukhova, E. N. 2009, VizieR Online Data Catalog: B/gcvs
Scargle, J. D. 1982, ApJ, 263, 835
Sikora, J., David-Uraz, A., Chowdhury, S., et al. 2019a, MNRAS, 487, 4695
Sikora, J., Wade, G. A., Power, J., & Neiner, C. 2019b, MNRAS, 483, 3127
Skarka, M., Mašek, M., Brát, L., et al. 2017, Open European J. Variab. Stars, 185, 1
Skarka, M., Žák, J., Fedurco, M., et al. 2022, A&A, 666, A142
Soszyński, I., Pawlak, M., Pietrukowicz, P., et al. 2016, Acta Astron., 66, 405
Soszyński, I., Udalski, A., Wrona, M., et al. 2019, Acta Astron., 69, 321
Stassun, K. G., Oelkers, R. J., Paegert, M., et al. 2019, AJ, 158, 138
Taylor, M. B. 2005, ASP Conf. Ser., 347, 29
Tkachenko, A., Aerts, C., Yakushechkin, A., et al. 2013, A&A, 556, A52
Twicken, J. D., Chandrasekaran, H., Jenkins, J. M., et al. 2010, SPIE Conf. Ser., 7740, 77401U
Uytterhoeven, K., Moya, A., Grigahcène, A., et al. 2011, A&A, 534, A125
Waelkens, C., Aerts, C., Kestens, E., Grenon, M., & Eyer, L. 1998, A&A, 330, 215
Watson, C. L., Henden, A. A., & Price, A. 2006, Soc. Astron. Sci., 25, 47
Wenger, M., Ochsenbein, F., Egret, D., et al. 2000, A&AS, 143, 9
Woźniak, P. R., Vestrand, W. T., Akerlof, C. W., et al. 2004, AJ, 127, 2436

Paper 8

50 Dra: Am-type twins with additional variability in a non-eclipsing system

A&A, 698, A48 (2025)
https://doi.org/10.1051/0004-6361/202452341

Astronomy & Astrophysics

50 Dra: Am-type twins with additional variability in a non-eclipsing system

M. Skarka[1,⋆], J. Lipták[1,2], E. Niemczura[3], Z. Mikulášek[4], M. Cabezas[1,2], M. Vítková[1,4], R. Karjalainen[1], and P. Kabáth[1]

[1] Astronomical Institute of the Czech Academy of Sciences, Fričova 298, CZ-25165 Ondřejov, Czech Republic
[2] Institute of Theoretical Physics, Faculty of Mathematics and Physics, Charles University, V Holešovičkách 2, 180 00 Praha 8, Czech Republic
[3] Instytut Astronomiczny, Uniwersytet Wrocławski, Kopernika 11, PL-51-622 Wrocław, Poland
[4] Department of Theoretical Physics and Astrophysics, Masaryk University, Kotlářská 2, CZ-61137 Brno, Czech Republic

Received 23 September 2024 / Accepted 8 April 2025

ABSTRACT

Context. The interplay between radiative diffusion, rotation, convection, and magnetism in metallic-line chemically peculiar stars is not yet fully understood. Recently, evidence has emerged that these effects can work together.
Aims. Our goal was to study the bright binary system 50 Dra, describe its orbit and components, and study additional variability.
Methods. We conducted our analysis using TESS short-cadence data and new high-resolution spectroscopic observations. We disentangled the spectra using KOREL and performed spectral synthesis with ATLAS9 and SYNTHE codes. The system was modelled using KOREL and PHOEBE2.4. We also employed SED fitting in ARIADNE and isochrone fitting using PARAM1.5 codes.
Results. Our findings indicate that the non-eclipsing system 50 Dra (with an inclination of 49.9(8) deg), which displays ellipsoidal brightness variations, consists of two nearly equal A-type stars with masses of $M_1 = 2.08(8)$ and $M_2 = 1.97(8)\,M_\odot$, and temperatures of 9800(100) and 9200(200) K, respectively. Our analysis also indicates that the system, with an orbital period of $P_{\rm orb} = 4.117719(2)$ days, is tidally relaxed with a circular orbit and synchronous rotation of the components. Furthermore, we discovered that both stars are metallic-line Am chemically peculiar stars with an underabundance of Sc and an overabundance of iron-peak and rare-earth elements. We identified additional variations with slightly higher frequency than the rotational frequency of the components that we interpret as prograde g-mode pulsations.
Conclusions. The system 50 Dra exhibits multiple co-existing phenomena and may have an impact on our understanding of chemical peculiarities and pulsations.

Key words. methods: data analysis – binaries: spectroscopic – stars: chemically peculiar – stars: rotation – stars: variables: general

1. Introduction

About a third of spectral A-type stars show a deficiency of He, Ca, and/or Sc an overabundance of iron-group and rare-earths metals (Abt 1981; Gray et al. 2016). These stars, which are mostly observed in spectral types earlier than F2 within a typical temperature range between 7250 and 8250 K (Gray et al. 2016; Qin et al. 2019), are termed metallic-line chemically peculiar (CP) stars, or AmFm stars. Their peculiar chemical compositions arise from atomic diffusion, which occurs in stars with stable outer layers that transfer energy through radiation (Michaud 1970). This condition is satisfied in slowly rotating stars ($<\simeq 100\,{\rm km\,s^{-1}}$) where rotational mixing is weak (Abt & Morrell 1995; Qin et al. 2021; Trust et al. 2020). It is not surprising that more than 70 % of AmFm stars are found in binary systems, particularly those with orbital periods shorter than 20 days (peaking around 5 days), where tidal effects slow the stars' rotation rates (Abt 1961; Abt & Levy 1985; Carquillat & Prieur 2007). Systems where both components are AmFm-type appear common, as evidenced by Catanzaro et al. (2024), who studied six eclipsing binaries with AmFm stars and found that four of these systems exhibit the AmFm peculiarity in both primary and secondary components.

Although He is expected to rapidly gravitationally settle in AmFm stars (Charbonneau & Michaud 1991), they were not expected to pulsate. However, Am stars exhibiting p-mode pulsations were documented prior to the availability of ultra-precise space data (Kurtz 1989). Current observations confirm that AmFm stars can pulsate as δ Sct, γ Dor, and hybrid pulsators (e.g. Balona et al. 2015; Smalley et al. 2017; Dürfeldt-Pedros et al. 2024). It was also discovered that insufficient He in the He II ionisation zone leads to pressure modes in δ Sct AmFm stars being excited either by the turbulent pressure mechanism in the hydrogen ionisation zone (Antoci et al. 2014; Smalley et al. 2017) or by a bump in the Rosseland mean opacity resulting from the discontinuous H-ionisation edge in bound-free opacity (Murphy et al. 2020).

It is generally assumed that rotationally induced variability can only be observed in CP stars with strong (kG), globally-organised magnetic fields that can stabilise abundance spots (Ap/Bp stars, Preston 1974). However, a recent investigation of an Ap star 45 Her with a magnetic field strength of only 100 G by Kochukhov et al. (2023) questioned the necessity of strong magnetic fields to stabilise spots. Furthermore, precise space observations revealed that CP stars without strong magnetic fields (HgMn and AmFm stars) and normal A-type stars also show rotation modulation (e.g. Balona 2011; Sikora et al.

⋆ Corresponding author: skarka@asu.cas.cz

2019; Kochukhov et al. 2021; Trust et al. 2020). The brightness variations in the non-magnetic A-stars are less regular than in magnetic CP stars and resemble the differential rotation and spot evolution observed in cool stars (e.g. Balona 2011; Blazère et al. 2020). This observational evidence, combined with the spot evolution in some HgMn stars (Kochukhov et al. 2007) and rotation periods of less than 1 day observed in some Am stars (Trust et al. 2020), challenges the requirement for stable and calm atmospheres in these stars[1].

The Fourier spectrum of many normal and AmFm stars shows a broad group of closely spaced peaks, often with a single peak or a very narrow group of unresolved peaks (Balona 2013; Balona et al. 2015; Trust et al. 2020; Henriksen et al. 2023a). Recent studies attribute the sharp peak (referred to as the 'spike') to surface rotational modulation connected with stellar spots and complex magnetic fields generated in the sub-surface convective layer (Antoci et al. 2025). The broad group of peaks (the 'hump') likely arises from either prograde g-modes (spike at lower frequency) or unresolved Rossby modes (spike at higher frequency). The Rossby modes are mechanically excited by deviated flows caused by stellar spots, mass outbursts, and by non-synchronous tidal forces (Saio et al. 2018).

Our study focuses on a 5.3-mag star, 50 Dra (basic parameters in Table 1), a double-line spectroscopic binary system. The binary nature of 50 Dra was first discovered by Harper (1919), who found an orbital period of 4.1175 days and estimated the basic parameters of the orbit. Skarka et al. (2022) classified this star as a ROTM|GDOR variable, suggesting variations connected with rotation and/or pulsations. We collected new spectroscopic observations over a century later and found almost the same orbital parameters as Harper (1919). However, combining our new spectroscopic observations with photometric data from the Transiting Exoplanet Survey Satellite (TESS) mission (Sect. 2, Ricker et al. 2015) revealed ellipsoidal and additional brightness variations (Sect. 3). This enabled us to determine the parameters of the system and both components (Sect. 4), and to identify both stars as metallic-line CP stars (Sect. 5). All features of 50 Dra are discussed in Sect. 6.

2. Observations

2.1. TESS photometry

We collected available data reduced by the TESS Science Processing Operations Centre (SPOC; Jenkins et al. 2016) and the Quick-Look Pipeline (QLP; Huang et al. 2020a,b) using LIGHTKURVE software (Lightkurve Collaboration 2018; Barentsen & Lightkurve Collaboration 2020) from the Mikulski Archive for Space Telescopes (MAST) archive. We extracted the pre-search data conditioning simple aperture photometry (PDCSAP) flux with long-term trends removed (Twicken et al. 2010) and transformed the normalised flux to magnitudes. The LIGHTKURVE software was also used to stitch data from different sectors together.

Data generated by various pipelines at varying cadences exhibit differences. The most reliable products are the 2-min short-cadence (SC) data sets from the Science Processing Operations Center (SPOC), as discussed by Skarka et al. (2022). The distinctions between the 50 Dra data products are illustrated in Fig. 1. The frequency spectra of the SPOC SC data exhibit the lowest noise levels and lack the artificial peak at 0.07 c/d (as seen in the QLP data). The distribution of SC data decreases

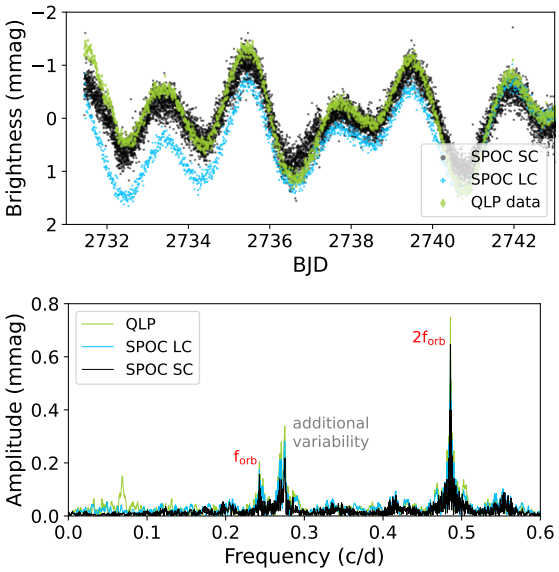

Fig. 1. Comparison of the available data products generated by different pipelines (top panel) and corresponding frequency spectra with labelled features (bottom panel).

the presence of artificial data peaks, such as those around the dominant frequency peak at 0.48 c/d. Consequently, we based our analysis on the 2-minute SPOC data. We acquired SPOC SC data from 28 sectors (14–26, 40–41, 47–58, 60, and 74), excluding data from Sector 25 due to its poor quality. We used a total of 440 166 observations at 2-min cadence, spanning almost 4.5 years (1629 days, from 2019–2024).

The contamination ratio of only 0.02% (Paegert et al. 2021) suggests no contamination of the 50 Dra light. The only possible contaminants are two bright stars located 20 and 34 arcmin away[2] and 17 additional faint stars (7.7–12.5 mag fainter than 50 Dra, see Table A.1) near 50 Dra, shown in Fig. 2. However, the two bright stars do not show signatures of variability similar to 50 Dra, and a custom aperture analysis around the faint, numbered stars in Fig. 2 rules out the possibility that any of the signals observed in 50 Dra originates from a different star.

2.2. Spectroscopy

We obtained 20 spectra of 50 Dra between February and July 2022 using the Ondřejov Echelle Spectrograph (OES) at the 2m Perek telescope (Ondřejov, Czech Republic). The spectrograph has a resolving power of $R = \lambda/\delta\lambda \approx 50\,000$ in the Hα region and covers a spectral range of 3800–9100 Å (Koubský et al. 2004; Kabáth et al. 2020). The spectra were processed and reduced using standard tasks in the IRAF package (Tody 1986), and cosmic-particle hits were eliminated using the DCR code (Pych 2004). The median S/N of the 600-second exposures in the Hα region was 150, with only four exposures having S/N slightly less than 100, and a few reaching S/N = 230.

[1] It is worth noting that the short period may arise from binarity that has not been addressed in Trust et al. (2020).

[2] HD 174257 (V = 7.53 mag) and HD 176795 (V = 6.71 mag).

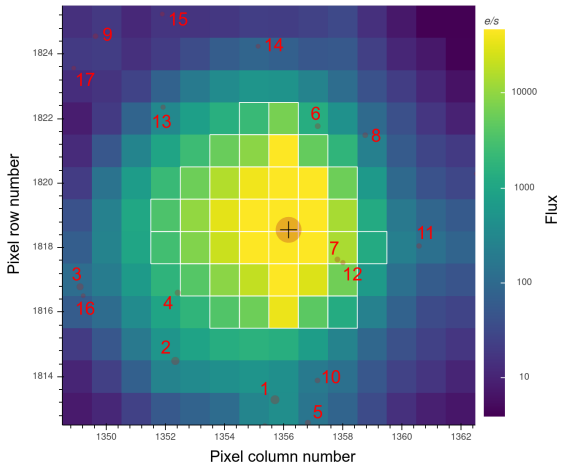

Fig. 2. Vicinity of 50 Dra showing the aperture mask in Sector 14 with identification of possible contaminants identified in Table A.1. The field size shown in the figure is approximately 4×4 arcmin.

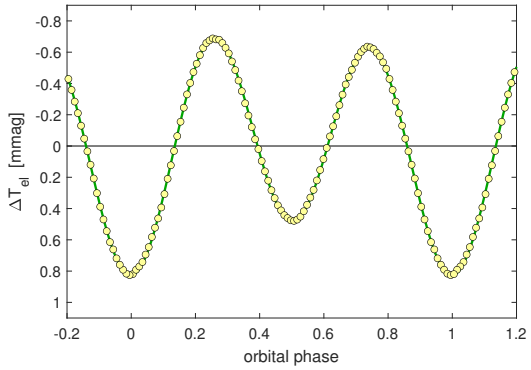

Fig. 3. TESS SC data of 50 Dra phase-folded with the orbital period. Each circle corresponds to the mean of 4400 individual TESS observations.

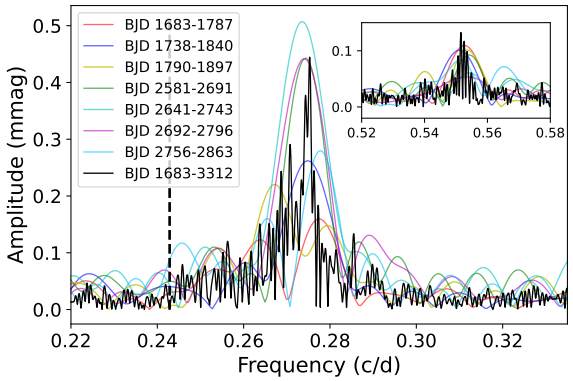

Fig. 4. Frequency spectrum centred around a group of peaks produced by additional variability from different data segments (coloured lines) and the full data set (black line). The amplitude of the frequency spectrum of the full dataset is multiplied by two for better readability. The black dashed line denotes the position of the orbital and rotational frequency.

3. Photometric variability

We observed the expected double-wave variations in the TESS SC light curve, with a period of $P_{\rm orb} = 4.117719(2)$ days (peaks labelled $f_{\rm orb}$ in Fig. 1). This period agrees with the orbital period derived from spectroscopic observations but is more precise due to the extended time span. As expected, a primary minimum occurs at the inferior conjunction of the binary components.

Given the short orbital period and the almost perfectly sinusoidal radial velocity (RV) curves of both components (within observational uncertainties) it is reasonable to assume that the trajectory of the binary star's components is nearly circular (see Sect. 4, Table 3 and Fig. 7). As a result, the light curve of this non-eclipsing binary, $F_{\rm ell(}{}_{t)}$, can be well approximated by a simple trigonometric polynomial model:

$$F_{\rm ell}(t) = \overline{m} + \sum_{k=1}^{3} A_k \cos(2\pi k\vartheta) - A_4 \sin(2\pi\vartheta), \quad \vartheta = \frac{t - M_0}{P_{\rm orb}}, \quad (1)$$

where t is the BJD timestamp and M_0 is the reference time for the start of the phase that we set at the moment of the inferior conjunction (the time of the deeper minimum). The phase function ($\vartheta(t)$) is the sum of the number of orbits completed by the system since the passage through the basic inferior conjunction and the fractional orbital phase $\varphi = {\rm Frac}(\vartheta)$. The coefficients of the model are denoted as A_1, A_2, A_3, A_4, and $\overline{m}$. The binned data along with the model are shown in Fig. 3.

Symmetrical terms of the ellipsoidal variability correspond to the effects of tidal deformation and reflection, while the antisymmetrical term, which causes the uneven heights of maxima, results from Doppler beaming (e.g. Zucker et al. 2007). The parameters of the model with Eq. (1) are in Table 2.

After removing variability related to the orbital period $P_{\rm orb} = 4.117719$ days, a complex, unresolved variability around 0.27 and 0.55 c/d persists in the frequency spectrum (see Fig. 1 and 4). Since the group of peaks with higher frequencies is in the region of harmonics and combination peaks of the lower frequencies, we assume that the peaks have a common nature. As shown in Fig. 4, which shows the frequency spectra of approximately 100-day segments, the variation changes over time. We discuss possible explanations for this additional variability in Sect. 6. Apart from the ellipsoidal variability peaks and the unresolved peaks around 0.27 and 0.55 c/d, we did not find any other significant frequencies.

4. System parameters

4.1. Spectral energy distribution

We used photometry across 12 filters spanning visual to infrared wavelengths (Table A.2) and fitted the spectral energy distribution (SED) with ARIADNE (Vines & Jenkins 2022). This code uses SED fitting methods and *Gaia* distances. It then combines results via Bayesian model averaging to derive basic stellar parameters such as $T_{\rm eff}$, $\log g$, iron abundance [Fe/H], extinction, and stellar radius.

The SED fitting results are shown in Fig. 5, with derived values listed in Table 1 (labelled 'SED' in the column 'Source'). The results are provided for reference only, since 50 Dra is not a single star. However, this exercise illustrates the reliability of the literature-derived stellar parameters when considering 50 Dra

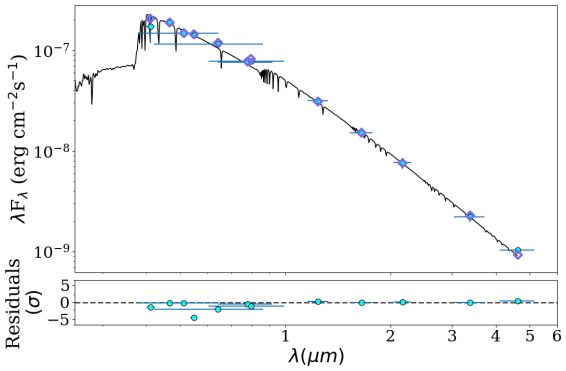

Fig. 5. Spectral energy distribution (SED) derived from photometric observations (Table A.2) using ARIADNE.

as a single object. The temperature $T_{\rm eff}$ = 9123 K, [Fe/H] = –0.07 dex, and $\log g$ = 3.90 are within uncertainties with the catalogue values, particularly the excellent agreement in $T_{\rm eff}$ with the value of Paegert et al. (2021). The largest discrepancy is in the iron abundance, which is around 0.3 dex lower than the [Fe / H] values from Gaia Collaboration (2023) and from our spectroscopic analysis (see Sect. 4). Thus, the [Fe/H] form of the SED is less reliable than that of other methods. We adopt the radius R_* = 2.91(9) $R_\odot$, derived using ARIADNE under the single star assumption, to derive the radii of the components in Sect. 4.4. This is possible because, as demonstrated by the spectral synthesis (see Sect. 5) the stars have similar temperatures (in the range 9000−10 000 K). This results in their SEDs being nearly scaled versions of each other in the visual and infrared bands used to derive R_*, with a better approximation at longer wavelengths. We note that binary SED fitting alone fails to converge to a well-defined solution, even using the priors on temperature from spectra, due to degeneracies between the component radii. In case of equal temperatures, we obtain only the constraint $R_*^2 = R_1^2 + R_2^2$.

4.2. Spectra disentanglement

Since 50 Dra is a double-lined spectroscopic binary (SB2) system, variations in the spectral line positions of both components are distinct and apparent at first glance (see Fig. 6). The movement of some of the prominent spectral lines during orbital motion is best demonstrated by the trail plots in the lower panel of Fig. 6. We performed Fourier spectral disentangling using the KOREL code (Hadrava 1995, 2004), which performs simultaneous decomposition of spectra and solution of orbital parameters. We fixed the orbital period P = 4.117719 days, as it was precisely determined from ellipsoidal variations in photometric data spanning almost 4.5 years (Sect. 3).

We performed the Fourier spectral disentangling in 41 spectral regions with a typical width of 140 Å. An example of the final disentangled spectra of both components around the Mg I 5167–5183 Å triplet is shown in the upper panel of Fig. 6. KOREL also derives RVs and provides a model of the orbit (see Sect. 4.3 and Table 3). To ensure consistency, we retained only 25 spectral regions with a sufficient number of spectral lines. The RV values for both components are listed in Table A.3 together with their errors, calculated as the standard deviation of the values from the individual segments.

Table 1. Basic characteristics of 50 Dra.

HD 175286, TIC 424391564, *Gaia* DR3 2268467486545969792		
ID	Value	Source
RA_{J2000} (^{hh}:^{mm}:^{ss})	18:46:22.24	1
Dec_{J2000} ($^\circ$:′:″)	+75:26:02.24	1
Tycho V_T (mag)	5.358(1)	2
Tycho B_T (mag)	5.409(14)	2
TESS T (mag)	5.345 (7)	3
Gaia G (mag)	5.357(3)	4
$\mu_\alpha \cos\delta$ (mas yr^{-1})	17.06(14)	4
μ_δ (mas yr^{-1})	70.39(15)	4
Parallax (mas)	11.42(11)	4
γ (km s^{-1})	–8.79(49)	5
	–7.8	6
	–8.8(2.8)	7
$T_{\rm eff}$ (K)	9150(142)	3
	9572^{+128}_{-297}	4
	9130^{+290}_{-262}	SED
[Fe/H] (dex)	$0.22^{+0.21}_{-0.14}$	4
	$-0.07^{+0.21}_{-0.23}$	SED
$\log g$ (cm s^{-2})	3.97(67)	3
	$3.935^{+0.024}_{-0.028}$	4
	$3.90^{+0.33}_{-0.33}$	SED

Notes. Effective temperature $T_{\rm eff}$ and surface gravity $\log g$ corresponds with the assumption of a single star. References: 1 – Gaia Collaboration (2021), 2 – Høg et al. (2000), 3 – Paegert et al. (2021), 4 – Gaia Collaboration (2023), 5 – Harper (1919), 6 – Wilson (1953), 7 – Gontcharov (2006), SED – this work (spectra energy distribution fitting).

Table 2. Model parameters of the ellipsoidal variations.

Ephemeris	Parameters
M_0 = 2 459 365.9508(2)	A_1 = 0.172 8(5) mmag
$P_{\rm orb}$ = $4^{\rm d}.117\,719(2)$	A_2 = 0.652 9(4) mmag
	A_3 = 0.002 9(4) mmag
$\rm ampl_{eff}$ = 1.35 mmag	A_4 = 0.029 6(5) mmag

4.3. Orbital parameters

We determined the orbital parameters (time of periastron passage T_0, eccentricity e, argument of pericentre ω, semi-amplitudes of radial velocities K_1, K_2, and mass ratio $q = M_2/M_1$) using KOREL'S disentangling process, solving the orbit simultaneously across all disentangled regions. The values in Table 3, which are calculated as the average values of all solutions in 25 spectral regions, indicate a circular orbit (e is almost zero) with large semi-amplitudes of the RV curves ($K_1 \approx 79$ km s^{-1}, $K_2 \approx 83$ km s^{-1}). The similarity in semi-amplitudes, and thus the mass ratio $q \approx 0.95$, show that both components have almost equal masses (see Fig. 7). Systems with $q \simeq 1$ components are commonly observed among AmFm binaries, consistent with the findings of Carquillat & Prieur (2007), who found that six out of 12 of their SB2 systems had $q > 0.9$. Notably, all of our values are consistent with those estimated over a century ago by Harper (1919).

The only discrepancy between our results and the values in the literature is the systemic velocity γ, where our value

Table 3. Parameters of the binary system.

	KOREL	H19		PARAM 1.5	PHOEBE 2.4
T_0	2459654.241(4)		M_1 ($M_\odot$)	$2.39^{+0.27}_{-0.15}$	2.08(8)
e	0.0021(3)	0.012(9)	R_1 ($R_\odot$)	$2.13^{+0.80}_{-0.32}$	2.06(9)
ω (deg)	94.85(2)		$(\log g)_1$ (cm s^{-2})	$4.16^{+0.23}_{-0.11}$	4.13(5)
K_1 (km s^{-1})	78.93(2)	79.12(97)	M_2 ($M_\odot$)	$2.21^{+0.15}_{-0.13}$	1.97(8)
K_2 (km s^{-1})	82.96(20)	83.9(97)	R_2 ($R_\odot$)	$2.34^{+0.35}_{-0.30}$	1.99(9)
$q(M_2/M_1)$	0.951(2)	0.947	$(\log g)_2$ (cm s^{-2})	$4.04^{+0.10}_{-0.10}$	4.13(5)
$a \sin i$ ($R_\odot$)		13.3	$a \sin i$ ($R_\odot$)		13.184(26)
i (deg)			i (deg)		49.9(8)

Notes. H19 is the reference to Harper (1919).

($\gamma = -6.53(9)$ km s^{-1}) is about 1-2 km s^{-1} higher than previous estimates (see Table 1). We did not identify any problem in our analysis that could explain the difference. Since all of the previous values are based on low-resolution spectroscopy and/or historical photographic plates, we assume that our new value is more reliable than those published previously.

4.4. Characteristics of the system components

To estimate stellar parameters, we used the Bayesian fitting tool PARAM 1.5[3] (da Silva et al. 2006; Rodrigues et al. 2014, 2017). The code uses a new version of PARSEC (Bressan et al. 2012) evolutionary tracks and isochrones that include the effects of rotation, improvements in nuclear reaction networks, and other effects (Nguyen et al. 2022). Since 50 Dra is not a single star, we derived individual observed magnitudes for each component.

If we assume the mass ratio $q \approx 0.951$ and the mass-luminosity relation $L \simeq M^{4.329}$ for the main-sequence stars in the 1.05–2.4 $M_\odot$ range (based on 275 well measured stars, Eker et al. 2018), we derive the flux ratio $F_{\rm Prim}/F_{\rm Sec} = 0.951^{-4.329} = 1.243$. After transformation into magnitudes, we obtain $V_{\rm Prim} = 5.997$ mag and $V_{\rm Sec} = 6.238$ mag by assuming the total magnitude of the system is $V_T = 5.358$ mag (Høg et al. 2000). We used the calculated V magnitudes, $T_{\rm eff}$, $\log g$, and [Fe/H] from Table 4, and the *Gaia* DR3 parallax from Table 1 as input parameters for PARAM 1.5. Although these are only rough estimates, the resulting values (see Table 3) are all within errors consistent with results from binary star modelling and spectral analysis (Sect. 5).

As an alternative and more appropriate way to derive system parameters without using stellar evolution models, we used the light-curve model, the SED fit, and the radial velocities. We used PHOEBE 2.4 (Conroy et al. 2020) to run the binary model. Since Doppler beaming, apparent in our light curve, is not currently implemented in PHOEBE 2.4, and the use of SED is quite convoluted, we directly computed radii and temperatures.

The Doppler beaming amplitude ΔF is given by

$$\frac{\Delta F}{F} = \frac{1}{c}\frac{\beta_1 K_1 F_1 - \beta_2 K_2 F_2}{F_1 + F_2}, \quad (2)$$

where c is the speed of light and β_1, β_2 are Doppler beaming coefficients of the stars. The relative beaming amplitude, $\frac{\Delta F}{F}$, taken with respect to the total flux of the binary components, $F = F_1 + F_2$, can easily be converted from the magnitude value A_4 in Table 2 corresponding to the expansion in Eq. (1). Using the radial velocity amplitudes K_1 and K_2 from Sect. 4.3 and beaming coefficients $\beta_1 = 2.01(5)$ and $\beta_2 = 2.09(5)$, derived by interpolation of tables by Claret et al. (2020) for the TESS passband, we get the passband relative fluxes $F_1/(F_1 + F_2) = 0.547(9)$ and $F_2/(F_1 + F_2) = 0.453(9)$. Next, we used PHOEBE to derive the relation between the flux and temperature ratios for stars with

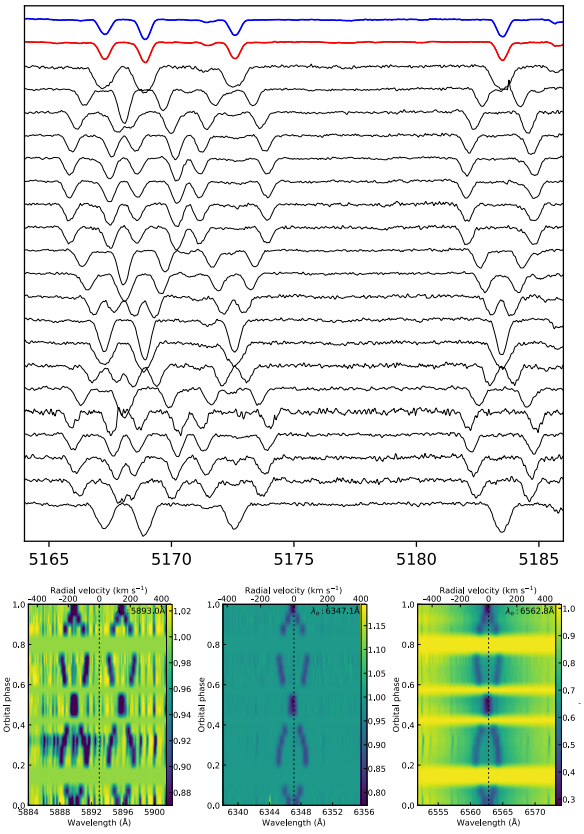

Fig. 6. Top: Observed spectra in different orbital phases around the Mg I 5167–5183 Å triplet and Fe II 5169 Å lines. The mean disentangled spectra for the primary and secondary components are shown in blue and red, respectively. Bottom: Trails of Na D, Si II, and Hα lines (from left to right) showing the variation of the position of the lines of both components during the orbital cycle. The relative intensity of the lines is also indicated.

[3] http://stev.oapd.inaf.it/cgi-bin/param

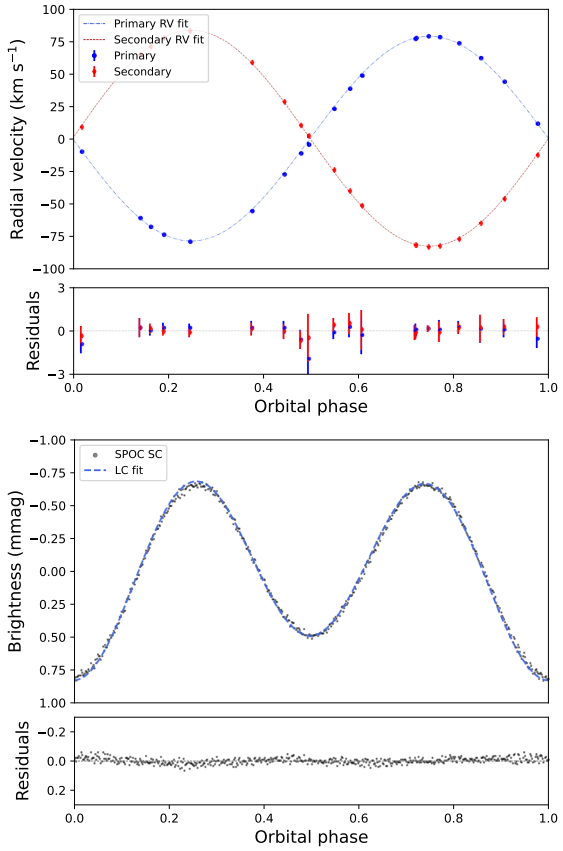

Fig. 7. Radial velocity curve of both components with the best fit (upper panel) and the light curve with the best fit (bottom panel). The photometric points are binned to produce 500 points per orbital phase.

the same radius $R_1 = R_2 = 2\,R_\odot$ in the TESS passband. Using the range $T_2/T_1 \in (0.90, 1.00)$ and the primary star temperature $T_1 = 9800\,K$ we derive a linear relation between the two. After incorporating the surface area ratio, we obtain the final relation:

$$F_2/F_1 = \left(-0.88 + 1.88\frac{T_2}{T_1}\right)\left(\frac{R_2}{R_1}\right)^2 . \quad (3)$$

To obtain the radii themselves, we used the SED result for R_*. In the long wavelength limit (far IR) under the Rayleigh-Jeans approximation it should hold

$$R_1^2 T_1 + R_2^2 T_2 = R_*^2 T_* , \quad (4)$$

where R_*, and T_* are the stellar radius and effective temperature derived under the single star assumption in Sect. 4.1. Using the effective temperatures of stars $T_1 = 9800(100)$ K and $T_2 = 9200(200)$ K derived from spectra (see Sect. 5) we get the radii $R_1 = 2.06(9)$ and $R_2 = 1.99(9)$.

Next, we fit the ellipsoidal variation using PHOEBE to determine the inclination of the system. We used PHOENIX atmospheric models by Husser et al. (2013) to obtain passband luminosities and limb-darkening coefficients. We set bolometric gravity brightening coefficients of both stars $b_1 = b_2 = 1.0$ and bolometric reflection coefficients to $a_1 = a_2 = 1.0$, valid for stars with radiative atmospheres above $T_1 = 8000$ K (see Claret 2003). Sampling the derived radii-temperature distributions yields an inclination of $i = 49.9(8)$ deg. This allows us to derive the semi-major axis of the system and the masses of the components from the radial velocity fit. The best fit (shown in Fig. 7) gives values shown in the final column of Table 3. All of the parameters obtained with PHOEBE are consistent with the results of other routines and methods.

5. Spectral synthesis and abundances

Before spectral analysis, we scaled the disentangled spectra of both components assuming a flux ratio of $F_1/F_2 = 1.243$ (based on empirical formulae from Eker et al. 2018), yielding $F_1 = 0.555\,F_{tot}$ and $F_2 = 0.445\,F_{tot}$, which are in agreement with flux ratios derived from Doppler beaming amplitudes (Sect. 4.4). We used the spectrum synthesis method to analyse the spectra of both stars. This method allows for the simultaneous determination of parameters that influence stellar spectra and involves minimising the deviation between the theoretical and observed spectra. The synthetic spectrum depends on stellar parameters including effective temperature ($T_{\rm eff}$), surface gravity ($\log g$), microturbulence ($V_{\rm mic}$), projected rotational velocity ($V \sin i$), and relative abundances of elements ($\log N$(El)), where 'El' denotes the individual element. All of these parameters are correlated.

All atmospheric models were computed with the line-blanketed, local thermodynamical equilibrium (LTE) ATLAS9 code, while synthetic spectra were computed with the SYNTHE code (Kurucz 2005). Both codes were adapted for GNU/Linux by Sbordone (2005). Stellar line identification and abundance analysis over the entire observed spectral range were performed based on the line list from the Fiorella Castelli website[4]. The solar abundances were adopted from Asplund et al. (2005).

In our method, the effective temperature, surface gravity, and microturbulence were determined through line analysis of neutral and ionised iron. We adjusted $T_{\rm eff}$, $\log g$, and $V_{\rm mic}$ by comparing the abundances determined from Fe I and Fe II lines. First, we adjusted $V_{\rm mic}$ until no correlation was observed between iron abundances and line depths for the Fe I lines. Next, we modified $T_{\rm eff}$ until there was no trend in the abundance versus excitation potential for the Fe I lines. The surface gravity was then determined by fitting the Fe II and Fe I lines, ensuring the same iron abundances from the lines of both ions. Using the derived $T_{\rm eff}$, $\log g$, and $V_{\rm mic}$, we calculated the abundances. The final results are presented in Table 4. The chemical abundance uncertainties in Table 4 represent the standard deviations derived from the analysis of multiple spectral lines per element or uncertainties resulting from the steps of the atmospheric model grid.

The derived atmospheric parameters and chemical abundances are influenced by errors from several sources, including assumptions taken into account to build an atmospheric model, the adopted atomic data, and spectra normalisation. A detailed discussion of possible uncertainties of the parameters obtained is provided in Niemczura et al. (2015) and Niemczura et al. (2017). Figure 8 compares the observed and theoretical spectra calculated for the final parameters.

The effective temperatures of both components ($T_{\rm eff1} = 9800(100)$ K and $T_{\rm eff2} = 9200(200)$ K) and their surface gravities ($(\log g)_1 = 4.1(1)$ and $(\log g)_2 = 4.0(1)$ cm s^{-2}) suggest that both stars are of A0-A3 V spectral types. Both system components are slow-rotators with $v \sin i = 19(1)$ km s^{-1}.

We estimated abundances for 29 elements (see Table 4). The number of lines used for the abundance estimation is

[4] https://wwwuser.oats.inaf.it/fiorella.castelli/

Table 4. Parameters of the components and their abundances from the spectral synthesis.

		Star 1			Star 2		
$T_{\rm eff}$ (K)		9800(100)			9200(200)		
$\log g$ (cm s^{-2})		4.1(2)			4.0(1)		
$V_{\rm mic}$ (km s^{-1})		0.5(3)			0.5(3)		
$v \sin i$ (km s^{-1})		19(1)			19(1)		
El	Nr	$\log \epsilon$	σ	Nr	$\log \epsilon$	σ	$\log \epsilon$ (Sun)
C	15	8.17	0.25	15	8.12	0.24	8.43
N	4	8.08	0.35	7	8.17	0.16	7.83
O	8	8.52	0.18	6	8.82	0.18	8.69
Ne	–	–	–	1	9.07	–	7.93
Na	4	6.88	0.22	1	6.28	–	6.24
Mg	9	7.46	0.23	8	7.24	0.06	7.60
Al	2	6.42	–	3	6.38	0.11	6.45
Si	11	7.50	0.23	15	7.55	0.26	7.51
P	1	6.26	–	2	6.36	–	5.41
S	9	7.75	0.19	12	7.66	0.17	7.12
Ca	12	6.28	0.10	13	6.03	0.14	6.34
Sc	5	2.51	0.11	7	2.33	0.38	3.15
Ti	42	5.14	0.12	39	4.94	0.15	4.95
V	8	4.43	0.06	8	4.56	0.31	3.93
Cr	55	6.09	0.13	66	5.93	0.16	5.64
Mn	16	5.76	0.14	24	5.65	0.12	5.43
Fe	207	7.71	0.09	206	7.58	0.10	7.50
Co	1	5.43	–	4	5.63	0.24	4.99
Ni	34	6.85	0.11	44	6.69	0.14	6.22
Cu	2	4.89	–	2	4.64	–	4.19
Zn	1	5.51	–	2	5.14	–	4.56
Sr	1	3.89	–	2	3.47	–	2.87
Y	6	3.15	0.09	11	3.07	0.15	2.21
Zr	5	3.68	0.19	16	3.40	0.10	2.58
Ba	4	3.59	0.04	3	3.27	–	2.18
La				1	2.37	–	1.10
Ce	1	3.17	–	7	2.54	0.20	1.58
Nd	1	2.62	–	2	2.33	–	1.42
Sm				1	1.95	–	0.96

Notes. The 'Nr' denotes the number of lines used to calculate abundance (including blends), $\log \epsilon$ denotes the average abundances (on the scale in which $\log \epsilon$(H) = 12), σ denotes the standard deviation in cases where the fit was based on more than three lines, $\log \epsilon$ (Sun) denotes the solar abundance (Asplund et al. 2009).

given in columns denoted as 'Nr'. The Fe abundance is the most robust measurement, based on 207 and 206 spectral lines for the primary and secondary components, respectively. The Fe abundances differ slightly between components ([Fe/H]$_{\rm prim}$ = 0.21(9) and [Fe/H]$_{\rm sec}$ = 0.08(10)) but are consistent within their errors. Both [Fe/H] values are in line with the catalogue value (Gaia Collaboration 2023) but are 0.3 dex higher than the SED-fitting results (Sect. 4). The abundances of iron-peak and rare-earth elements, combined with slow rotation, indicate chemical peculiarity in both components, as discussed in Sect. 6.3.

6. Discussion

6.1. Rotation

Slow to moderate rotation is critical for chemical peculiarity. In AmFm stars, the rotation rate should not exceed around 120 km s^{-1} (Abt & Moyd 1973; Michaud et al. 1983). The rotation velocity of the components, $v_{\rm rot,1,2} = v \sin i / \sin i \approx 24.8$ km s^{-1} (see Table 3), is well below this limit and is typical for AmFm stars (see the distribution of rotational velocities in Royer et al. 2007; Trust et al. 2020; Qin et al. 2021; Niemczura et al. 2017).

Using the values of $R_{1,2}$, $(v \sin i)_{1,2}$, and i from Table 3 (and their uncertainties), we calculate the rotational frequencies of both components $f_{\rm rot,1,2}$, and their errors. We determine the rotation period by solving the standard relation (e.g. Preston 1971)

$$f_{\rm rot} = \frac{v \sin i}{50.6 R_* \sin i}, \quad (5)$$

and use the propagation of errors law. We derive rotational frequencies of $f_{1,\rm rot}$ = 0.238(17) and $f_{2,\rm rot}$ = 0.246(17) c/d, consistent with the orbital frequency $f_{\rm orb}$ = 0.2428529(1) c/d. This suggests that the value of the inclination is well-established and that the system is relaxed with a circularised orbit and synchronous rotation of the components. The assumption of circular orbit and synchronously rotating components is further reinforced by the following angular momentum investigation.

The tidal equilibrium of the system is only possible if the total angular momentum, $L_{\rm tot}$ (a sum of the orbital and spin

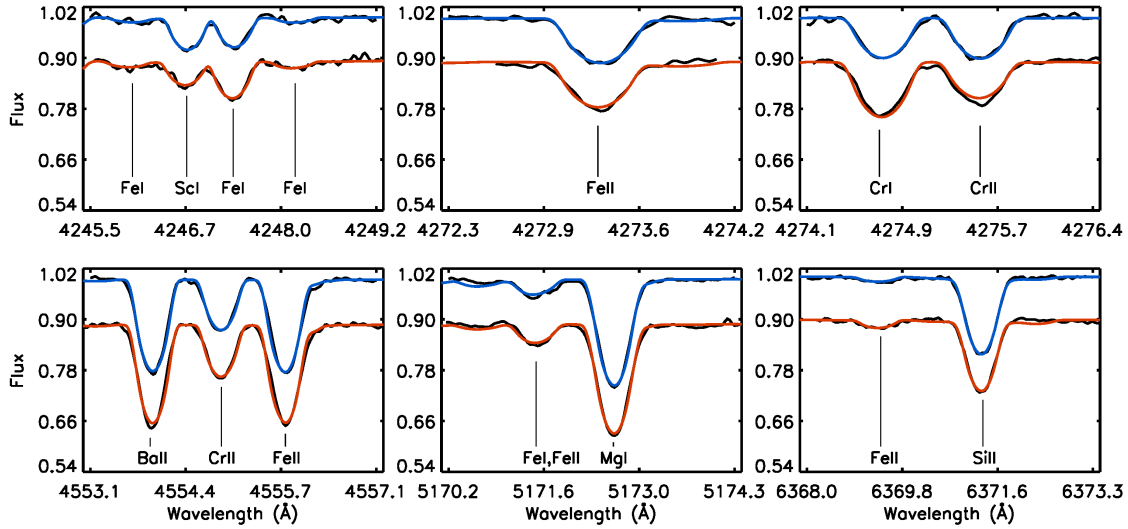

Fig. 8. Comparison of the observed (black lines) and theoretical spectra calculated with final parameters. Star 1 is represented by the blue line, and Star 2 by the red line. The spectra of Star 2 were shifted by subtracting a value of 0.1 from the flux.

momenta), exceeds the critical momentum, $L_{\rm crit}$, calculated as per Ogilvie (2014):

$$L_{\rm crit} = 4I(GM)^{1/2}\left(\frac{\mu}{3I}\right)^{3/4}, \quad (6)$$

where $M = M_1 + M_2$ is the total mass of the stars (values from PHOEBE in Table 3), $I = I_1 + I_2$ is the total spin momentum of inertia of the stars, and $\mu = M_1 M_2/(M_1 + M_2)$. The spin moment of inertia of the stars was calculated as $I = \beta^2 M_* R_*^2$ with M_* and R_* from Table 3 and $\beta = 0.218$ for stars with $M = 2\,M_\odot$ from Claret & Gimenez (1989).

The total angular momentum of the system, $L_{\rm tot}$, is given by:

$$L_{\rm tot} = L_{\rm orb} + L_{\rm spin} = L_{\rm orb} + I_1\Omega_1 + I_2\Omega_2 \quad (7)$$

and is dominated by the orbital angular momentum, $L_{\rm orb}$, that can be expressed as

$$L_{\rm orb} = \frac{GM_1M_2\left(1-e^2\right)^{1/2}}{\Omega a}, \quad (8)$$

where $\Omega = 2\pi f_{\rm orb}\,{\rm rad\,s^{-1}}$ is the angular velocity. If we assume that the spin angular velocity of the stars is equal to the orbital angular velocity (the calculated rotational frequencies match the orbital frequency), then $L_{\rm orb} \approx 380 L_{\rm spin}$. The total angular momentum, $L_{\rm tot} \sim 2.5 L_{\rm crit}$, indicates that the system is in tidal equilibrium, while $L_{\rm orb} \gg 3L_{\rm spin}$ indicates that the system is relaxed with a stable tidal equilibrium resulting in a circular orbit and synchronous rotation of the components (Hut 1980; Ogilvie 2014). Carquillat & Prieur (2007) identified a circularisation cut-off period of 5.6(5) days ($f_{\rm orb} \geq 0.179$ c/d) for AmFm stars. All observational indices support the synchronous rotation of 50 Dra components with an orbital frequency of 0.243 c/d.

6.2. Additional variability

Since both components are almost equal, assigning the additional variability (manifesting as a group of peaks in the frequency spectra; Figs. 1 and 4) to either star is challenging. The unresolved frequency patterns suggest that it results from stochastic semi-regular or unresolved regular variability. In cold stars, such variations can be associated with magnetic activity, cold spots, their finite life span, and differential surface rotation. Although not expected in A-type stars (including AmFm stars), rotational variability analogous to cold stars likely connected with spots has been reported (e.g. Balona 2011; Sikora et al. 2019; Trust et al. 2020).

Stellar spots in cold stars are linked to local magnetic fields. Cantiello & Braithwaite (2019) demonstrated that spots in A-type stars can be induced by local magnetic fields generated by convection in thin sub-surface zones due to high opacity and/or low adiabatic gradient in the ionisation zones of H, He, and/or Fe. Weak magnetic fields have been detected in a few AmFm stars (e.g. Blazère et al. 2016a,b). In particular, the 50 Dra components resemble Sirius A, which is also an AmFm star, where a very weak magnetic field of 0.2 ± 0.1 G was detected (Petit et al. 2011), suggesting that this mechanism could operate in 50 Dra. However, the spot scenario is less likely because the group of peaks has a higher frequency than the rotational frequency (see Sect. 6.1) and is distinct from it (see Fig. 4). Such behaviour would require spots confined to higher latitudes (avoiding areas close to the equator) and polar regions rotating faster than equatorial regions. However, latitudinal differential rotation in the context of binarities remains poorly understood. The centre of the power hump is only about 10 % higher than the value of $f_{2,\rm rot}$, indicating that differential rotation may still be a plausible explanation that cannot be fully ruled out.

The group of frequencies (hump) may originate from unresolved prograde g-modes at frequencies higher than the rotational frequency. Similar features have been reported by Saio et al. (2018) and Henriksen et al. (2023a,b). For 50 Dra, the difference between the hump and the rotational frequency is only around 0.03 c/d, while the calculation for a star with two solar masses by Henriksen et al. (2023b) suggests a frequency separation of about 0.2 c/d. However, 50 Dra is about 2500 K hotter than their model star and its rotation rate is about four times lower. The g-mode explanation for the hump

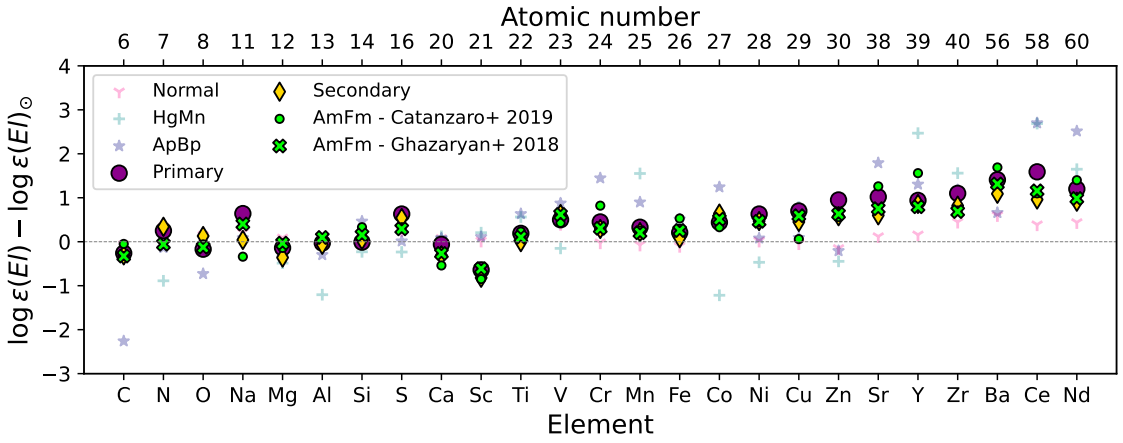

Fig. 9. Comparison of the mean element abundances of different classes of chemically peculiar stars (Ghazaryan et al. 2018; Catanzaro et al. 2019), normal stars (Niemczura et al. 2017) and 50 Dra components (magenta circles and yellow diamonds). The abundances of both stars of 50 Dra follow the AmFm abundances (green crosses and circles).

in 50 Dra requires detailed modelling, as g-mode excitation – as seen in γ Dor stars – is not expected and rarely observed at these temperatures (Guzik et al. 2000; Dupret et al. 2005; Dürfeldt-Pedros et al. 2024).

6.3. Chemical peculiarity

To assess the chemical peculiarity of 50 Dra components, we calculated average abundances of CP stars from the catalogue of Ghazaryan et al. (2018) and compared them with those of both components listed in Table 4. The abundances of particular elements in the stars AmFm (118 stars), HgMn (112 stars), and ApBp (188 stars) have typical uncertainties of 0.35, 0.65 and 0.60 dex, respectively. For stars with normal abundances, we used the sample of 33 stars from Niemczura et al. (2017) with a typical uncertainty of the abundance value of 0.39 dex. We also plotted the mean element abundances of 62 Am stars from Catanzaro et al. (2019, their table 3).

Comparison of catalogue values with abundances of 50 Dra components listed in Table 4, shows that both stars follow the sequence of AmFm stars (Fig. 9), with low abundance of Sc and overabundant heavy and rare-earth elements. We note that the mean values of the AmFm stars from Ghazaryan et al. (2018) differ from those of Catanzaro et al. (2019), increasing the range of possible values for the AmFm stars.

Previous studies have shown that more than 70 % of AmFm stars reside in binary systems (e.g. Abt & Levy 1985; Carquillat & Prieur 2007). In addition, AmFm stars tend to appear in tight binaries with periods under 20 days (peaking near 5 days) (Carquillat & Prieur 2007). It is believed that the tidal forces in binary systems play a crucial role in slowing down the rotation of these stars, enabling atomic diffusion and the emergence of the chemical peculiarity observed in AmFm stars. In this context, 50 Dra is considered a typical representative of this category of CP stars.

Am stars predominantly exhibit temperatures between 7250 and 8250 K, peaking at 7750 K (Qin et al. 2019). From their collection of 9372 Am stars, Qin et al. (2019) found that only 32 stars have temperatures higher than 9000 K and only five were hotter than 9500 K. However, Catanzaro et al. (2019) identified that 15 of their 62 Am sample stars have temperatures above 9500 K, based on SED fitting. The components of 50 Dra thus represent a small group of hot Am stars.

7. Conclusions

We analysed 20 high-resolution spectra from the OES spectrograph (Koubský et al. 2004; Kabáth et al. 2020) together with photometric data from TESS (Ricker et al. 2015) to investigate 50 Dra. We modelled the radial velocity curve and photometric data, revealing that the system consists of two intermediate-mass stars with nearly equal masses close to 2 $M_\odot$ (q = 0.951). The system exhibits an orbital period of 4.117719(2) days and an inclination of i = 49.9(8) deg, displaying ellipsoidal variations. Our investigation shows that both components are slow rotators ($v \sin i$ = 19(1) km s^{-1}) in synchronous rotation with the orbital period.

Based on the analysis of separated spectra and comparison with catalogue values, it was determined that both stars in the system are metallic-line AmFm CP stars with temperatures of 9800 and 9200 K. The high temperatures indicate that the components of 50 Dra belong to a less common group of AmFm stars with temperatures above 9000 K. Beyond the effects of binarity, such as ellipsoidal variation, reflection effect, and beaming, the only feature detected in the frequency spectrum was the hump at 0.275 c/d. As the most probable explanation of this structure, we assume the presence of prograde g-modes. No signs of p-mode pulsations, which are rare in this temperature region (Dürfeldt-Pedros et al. 2024), or other signs of variability were found. We were unable to assign the hump feature to either component due to their near-identical properties.

Acknowledgements. We thank the referee for useful comments that helped to improved the manuscript. MS is grateful to T. van Reeth for the discussion about the nature of the additional variations and to P. Gajdoš for reading the manuscript. We would like to thank the observers for their work. MS acknowledges the support by Inter-transfer grant no LTT-20015. PK acknowledges the funding from ESA PRODEX PEA 4000127913. The calculations have been partly carried out using resources provided by the Wrocław Centre for Networking and Supercomputing (http://www.wcss.pl), Grant No 214. This paper includes data collected with the TESS mission and with the Perek telescope at the Astronomical Institute of the Czech Academy of Sciences in Ondřejov. Funding for the TESS mission is provided by the NASA Explorer Program. Funding for the TESS

Asteroseismic Science Operations Centre is provided by the Danish National Research Foundation (Grant agreement no.: DNRF106), ESA PRODEX (PEA 4000119301) and Stellar Astrophysics Centre (SAC) at Aarhus University. We thank the TESS team and staff and TASC/TASOC for their support of the present work. We also thank the TASC WG4 team for their contribution to the selection of targets for 2-minute observations. The TESS data were obtained from the MAST data archive at the Space Telescope Science Institute (STScI). This research made use of NASA's Astrophysics Data System Bibliographic Services, and of the SIMBAD database, operated at CDS, Strasbourg, France.

References

Abt, H. A. 1961, ApJS, 6, 37
Abt, H. A. 1981, ApJS, 45, 437
Abt, H. A., & Levy, S. G. 1985, ApJS, 59, 229
Abt, H. A., & Morrell, N. I. 1995, ApJS, 99, 135
Abt, H. A., & Moyd, K. I. 1973, ApJ, 182, 809
Antoci, V., Cunha, M., Houdek, G., et al. 2014, ApJ, 796, 118
Antoci, V., Cantiello, M., Khalack, V., et al. 2025, A&A, 697, A111
Asplund, M., Grevesse, N., & Sauval, A. J. 2005, ASP Conf. Ser., 336, 25
Asplund, M., Grevesse, N., Sauval, A. J., & Scott, P. 2009, ARA&A, 47, 481
Balona, L. A. 2011, MNRAS, 415, 1691
Balona, L. A. 2013, MNRAS, 431, 2240
Balona, L. A., Baran, A. S., Daszyńska-Daszkiewicz, J., & De Cat, P. 2015, MNRAS, 451, 1445
Blazère, A., Neiner, C., & Petit, P. 2016a, MNRAS, 459, L81
Blazère, A., Petit, P., Lignières, F., et al. 2016b, A&A, 586, A97
Blazère, A., Petit, P., Neiner, C., et al. 2020, MNRAS, 492, 5794
Bressan, A., Marigo, P., Girardi, L., et al. 2012, MNRAS, 427, 127
Cantiello, M., & Braithwaite, J. 2019, ApJ, 883, 106
Carquillat, J. M., & Prieur, J. L. 2007, MNRAS, 380, 1064
Catanzaro, G., Busà, I., Gangi, M., et al. 2019, MNRAS, 484, 2530
Catanzaro, G., Frasca, A., Alonso-Santiago, J., & Colombo, C. 2024, A&A, 685, A133
Charbonneau, P., & Michaud, G. 1991, ApJ, 370, 693
Claret, A. 2003, A&A, 406, 623
Claret, A., & Gimenez, A. 1989, A&AS, 81, 37
Claret, A., Cukanovaite, E., Burdge, K., et al. 2020, A&A, 641, A157
Conroy, K. E., Kochoska, A., Hey, D., et al. 2020, ApJS, 250, 34
Cutri, R. M., Skrutskie, M. F., van Dyk, S., et al. 2003, VizieR On-line Data Catalog: II/246
Cutri, R. M., Wright, E. L., Conrow, T., et al. 2021, VizieR On-line Data Catalog: II/328
da Silva, L., Girardi, L., Pasquini, L., et al. 2006, A&A, 458, 609
Dupret, M. A., Grigahcène, A., Garrido, R., Gabriel, M., & Scuflaire, R. 2005, A&A, 435, 927
Dürfeldt-Pedros, O., Antoci, V., Smalley, B., et al. 2024, A&A, 690, A104
Eker, Z., Bakış, V., Bilir, S., et al. 2018, MNRAS, 479, 5491
Gaia Collaboration (Brown, A. G. A., et al.) 2018, A&A, 616, A1
Gaia Collaboration (Brown, A. G. A., et al.) 2021, A&A, 649, A1
Gaia Collaboration (Vallenari, A., et al.) 2023, A&A, 674, A1
Ghazaryan, S., Alecian, G., & Hakobyan, A. A. 2018, MNRAS, 480, 2953
Gontcharov, G. A. 2006, Astron. Lett., 32, 759
Gray, R. O., Corbally, C. J., De Cat, P., et al. 2016, AJ, 151, 13
Guzik, J. A., Kaye, A. B., Bradley, P. A., Cox, A. N., & Neuforge, C. 2000, ApJ, 542, L57
Hadrava, P. 1995, A&AS, 114, 393
Hadrava, P. 2004, Publ. Astron. Inst. Czechoslovak Acad. Sci., 92, 15
Harper, W. E. 1919, JRASC, 13, 236
Henriksen, A. I., Antoci, V., Saio, H., et al. 2023a, MNRAS, 520, 216
Henriksen, A. I., Antoci, V., Saio, H., et al. 2023b, MNRAS, 524, 4196
Høg, E., Fabricius, C., Makarov, V. V., et al. 2000, A&A, 355, L27
Huang, C. X., Vanderburg, A., Pál, A., et al. 2020a, Res. Notes Am. Astron. Soc., 4, 204
Huang, C. X., Vanderburg, A., Pál, A., et al. 2020b, Res. Notes Am. Astron. Soc., 4, 206
Husser, T.-O., Wende-von Berg, S., Dreizler, S., et al. 2013, A&A, 553, A6
Hut, P. 1980, A&A, 92, 167
Jenkins, J. M., Twicken, J. D., McCauliff, S., et al. 2016, SPIE Conf Ser, 9913, 99133E
Kabáth, P., Skarka, M., Sabotta, S., et al. 2020, PASP, 132, 035002
Kochukhov, O., Adelman, S. J., Gulliver, A. F., & Piskunov, N. 2007, Nat. Phys., 3, 526
Kochukhov, O., Khalack, V., Kobzar, O., et al. 2021, MNRAS, 506, 5328
Kochukhov, O., Gürsoytrak Mutlay, H., Amarsi, A. M., et al. 2023, MNRAS, 521, 3480
Koubský, P., Mayer, P., Čáp, J., et al. 2004, Publ. Astron. Inst. Czechoslovak Academy Sci., 92, 37
Kurtz, D. W. 1989, MNRAS, 238, 1077
Kurucz, R. L. 2005, Mem. Soc. Astron. It. Suppl., 8, 14
Lightkurve Collaboration (Cardoso, J. V. d. M., et al.) 2018, Astrophysics Source Code Library [record ascl: 1812.013]
Barentsen, G., & Lightkurve Collaboration 2020, Am. Astron. Soc. Meeting Abstr., 235, 409.04
Michaud, G. 1970, ApJ, 160, 641
Michaud, G., Tarasick, D., Charland, Y., & Pelletier, C. 1983, ApJ, 269, 239
Murphy, S. J., Saio, H., Takada-Hidai, M., et al. 2020, MNRAS, 498, 4272
Nguyen, C. T., Costa, G., Girardi, L., et al. 2022, A&A, 665, A126
Niemczura, E., Murphy, S. J., Smalley, B., et al. 2015, MNRAS, 450, 2764
Niemczura, E., Polińska, M., Murphy, S. J., et al. 2017, MNRAS, 470, 2870
Ogilvie, G. I. 2014, ARA&A, 52, 171
Paegert, M., Stassun, K. G., Collins, K. A., et al. 2021, ArXiv e-prints [arXiv:2108.04778]
Paunzen, E. 2015, A&A, 580, A23
Petit, P., Lignières, F., Aurière, M., et al. 2011, A&A, 532, L13
Preston, G. W. 1971, PASP, 83, 571
Preston, G. W. 1974, ARA&A, 12, 257
Pych, W. 2004, PASP, 116, 148
Qin, L., Luo, A. L., Hou, W., et al. 2019, ApJS, 242, 13
Qin, L., Luo, A. L., Hou, W., et al. 2021, AJ, 162, 32
Ricker, G. R., Winn, J. N., Vanderspek, R., et al. 2015, J. Astron. Telescopes Instrum. Syst., 1, 014003
Rodrigues, T. S., Girardi, L., Miglio, A., et al. 2014, MNRAS, 445, 2758
Rodrigues, T. S., Bossini, D., Miglio, A., et al. 2017, MNRAS, 467, 1433
Royer, F., Zorec, J., & Gómez, A. E. 2007, A&A, 463, 671
Saio, H., Kurtz, D. W., Murphy, S. J., Antoci, V. L., & Lee, U. 2018, MNRAS, 474, 2774
Sbordone, L. 2005, Mem. Soc. Astron. It. Suppl., 8, 61
Sikora, J., David-Uraz, A., Chowdhury, S., et al. 2019, MNRAS, 487, 4695
Skarka, M., Žák, J., Fedurco, M., et al. 2022, A&A, 666, A142
Smalley, B., Antoci, V., Holdsworth, D. L., et al. 2017, MNRAS, 465, 2662
Tody, D. 1986, SPIE Conf. Ser., 627, 733
Trust, O., Jurua, E., De Cat, P., & Joshi, S. 2020, MNRAS, 492, 3143
Twicken, J. D., Chandrasekaran, H., Jenkins, J. M., et al. 2010, SPIE Conf. Ser., 7740, 77401U
Vines, J. I., & Jenkins, J. S. 2022, MNRAS, 513, 2719
Wilson, R. E. 1953, General catalogue of stellar radial velocities (Washington D.C.: Carnegie Institute Washington Publication)
Zucker, S., Mazeh, T., & Alexander, T. 2007, ApJ, 670, 1326

Table A.1. Stars in the vicinity of 50 Dra shown in Fig. 2.

NR	*Gaia* DR3 ID	G	B-R
1	2268466696271988736	13.047	0.9704
2	2268467349107014400	13.72	0.971
3	2268467383466749184	14.873	0.951
4	2268467349107013760	15.786	1.3158
5	2268466627552513024	16.034	1.0765
6	2268467894567507072	16.153	1.1483
7	TIC 335965559	16.331	-
8	2268467898862831360	16.407	0.9278
9	2268467795783608832	16.5	1.4393
10	2268466661912250752	16.529	1.8639
11	2268467074229113344	16.703	1.0081
12	TIC 335965560	17.059	-
13	2268467727064133248	17.088	1.0404
14	2268467928927245952	17.624	0.8851
15	2268467757127995264	17.681	1.0049
16	2268467379171426048	17.767	1.2799
17	2268467688408453248	17.856	2.0393

Notes. Data from Gaia Collaboration (2023)

Table A.2. Magnitudes used for SED fitting.

Filter	Magnitude	Uncertainty	Ref
STROMGREN *v*	5.598	0.013	1
STROMGREN *b*	5.392	0.006	1
GaiaDR2v2 *BP*	5.371	0.003	2
STROMGREN *y*	5.369	0.001	1
GaiaDR2v2 *G*	5.357	0.003	2
GaiaDR2v2 *RP*	5.303	0.006	2
TESS *T*	5.345	0.007	3
2MASS *J*	5.219	0.018	4
2MASS *H*	5.233	0.031	4
2MASS *Ks*	5.206	0.018	4
WISE RSR *W1*	5.249	0.188	5
WISE RSR *W2*	5.092	0.071	5

Notes. References: 1 – Paunzen (2015), 2 – Gaia Collaboration (2018), 3 – Paegert et al. (2021), 4 – Cutri et al. (2003), 5 – Cutri et al. (2021)

Appendix A: Supporting material

Table A.3. Radial velocities of both components in km s^{-1}.

BJD	RV_1	σ_{RV_1}	RV_2	σ_{RV_2}
2459623.2165	-10.95	0.65	10.45	0.57
2459624.2168	77.53	0.48	-81.65	0.45
2459625.2641	11.68	0.67	-12.41	0.54
2459630.2691	-73.43	0.34	77.75	0.35
2459638.3844	-67.18	0.38	71.13	0.38
2459639.5434	-26.94	0.51	28.70	0.46
2459640.6760	77.22	0.36	-81.54	0.41
2459641.4470	44.24	0.55	-46.18	0.65
2459646.5317	-60.81	0.67	64.68	0.46
2459647.4978	-55.29	0.46	58.77	0.43
2459648.4501	48.68	1.35	-51.43	0.67
2459652.4616	38.66	0.71	-39.85	0.84
2459653.4062	73.58	0.38	-76.96	0.41
2459658.3811	-9.75	0.67	9.12	0.60
2459659.3145	-78.72	0.33	83.21	0.39
2459660.3422	-4.29	1.62	2.26	0.56
2459661.3819	78.90	0.23	-82.76	0.34
2459722.3264	23.24	0.47	-24.11	0.72
2459764.4223	78.18	0.68	-82.31	0.62
2459789.4843	61.93	0.95	-64.85	0.51